1986

Studies On A Fluorinated Alkoxy-phosphino Ligand

Craig Duvall Montgomery

CANADIAN THESES

THÈSES CANADIENNES

NOTICE

The quality of this microfiche is heavily dependent upon the quality of the original thesis submitted for microfilming. Every effort has been made to ensure the highest quality of reproduction possible.

If pages are missing, contact the university which granted the degree.

Some pages may have indistinct print especially if the original pages were typed with a poor typewriter ribbon or if the university sent us an inferior photocopy.

Previously copyrighted materials (journal articles, published tests, etc.) are not filmed.

Reproduction in full or in part of this film is governed by the Canadian Copyright Act, R.S.C. 1970, c. C-30.

AVIS

La qualité de cette microfiche dépend grandement de la de la thèse soumise au microfilmage. Nous avons tout fa assurer une qualité supérieure de reproduction.

S'il manque des pages, veuillez communiquer avec l' sité qui a conféré le grade.

La qualité d'impression de certaines pages peut lai désirer, surtout si les pages originales ont été dactylogra à l'aide d'un ruban usé ou si l'université nous a fait p une photocopie de qualité inférieure.

Les documents qui font déjà l'objet d'un droit d'auteur (de revue, examens publiés, etc.) ne sont pas microf

La reproduction, même partielle, de ce microfilm est s à la Loi canadienne sur le droit d'auteur, SRC 1970, c

THIS DISSERTATION HAS BEEN MICROFILMED EXACTLY AS RECEIVED

LA THÈSE A ÉTÉ MICROFILMÉE TELLE QUE NOUS L'AVONS REÇUE

Cana

CANADIAN THESES

THÈSES CANADIENNES

NOTICE

The quality of this microfiche is heavily dependent upon the quality of the original thesis submitted for microfilming. Every effort has been made to ensure the highest quality of reproduction possible.

If pages are missing, contact the university which granted the degree.

Some pages may have indistinct print especially if the original pages were typed with a poor typewriter ribbon or if the university sent us an inferior photocopy.

Previously copyrighted materials (journal articles, published tests, etc.) are not filmed.

Reproduction in full or in part of this film is governed by the Canadian Copyright Act, R.S.C. 1970, c. C-30.

AVIS

La qualité de cette microfiche dépend grandement de l
de la thèse soumise au microfilmage. Nous avons tout
assurer une qualité supérieure de reproduction.

S'il manque des pages, veuillez communiquer avec
sité qui a conféré le grade

La qualité d'impression de certaines pages peut l
désirer, surtout si les pages originales ont été dactylog
à l'aide d'un ruban usé ou si l'université nous a fait
une photocopie de qualité inférieure

Les documents qui font déjà l'objet d'un droit d'auteur
de revue, examens publiés, etc.) ne sont pas micro

La reproduction, même partielle, de ce microfilm est
à la Loi canadienne sur le droit d'auteur, SRC 1970,

THIS DISSERTATION
HAS BEEN MICROFILMED
EXACTLY AS RECEIVED

LA THÈSE A ÉTÉ
MICROFILMÉE TELLE QUE
NOUS L'AVONS REÇUE

Can

STUDIES ON A FLUORINATED ALKOXY-PHOSPHINO LIGAND

by

Craig Duvall Montgomery

Department of Chemistry

Submitted in partial fulfillment
of the requirements for the degree of
Doctor of Philosophy

Faculty of Graduate Studies
The University of Western Ontario
London, Ontario

May 1986

ISBN 0-315-33003-1

ABSTRACT

The synthesis and coordination chemistry of a fluorinated alkoxy-phosphino hybrid ligand is described. The fluorinated alcohol $Ph_2PCH_2C(CF_3)_2OH$, HL^1, is readily deprotonated in solution giving a bidentate, uninegative ligand, $[L^1]$, containing both hard and soft donors, the alkoxide and phosphine respectively. Alternately the ligand in its protonated form, HL^1, can serve as monodentate phosphine ligand. The ligand coordinates, as a chelate, to both hard (Rh^{3+}, Co^{2+}, Ni^{2+}) and soft (Cu^+, Pt^{2+}, Pd^{2+}, Pt^{4+}) metals. In the case of platinum, a variety of complexes were prepared: cis- and trans-$[Pt(HL^1)_2Cl_2]$, $[Pt(L^1)_2]$, cis- and trans-$[Pt(HL^1)(L^1)Cl]$, $[Pt(PR_3)(L^1)Cl]$ (where PR_3 = PPh_3, PPh_2Me, $PPhMe_2$, or PMe_3), $[Pt(HL^1)(L^1)CH_3]$ and the Pt^{4+} complex $[Pt(L^1)_2Cl_2]$. The preferred geometry of these complexes depends on a combination of electronic and steric factors and the latter factors were investigated further by two crystal structure determinations, those of trans-$[Pt(HL^1)_2Cl_2]$ and cis-$[Pt(L^1)_2]$. The monodentate ligand HL^1 is sterically demanding because of the bulky fluorinated alcohol group. For this reason, a trans-geometry is preferred for $[Pt(HL^1)_2Cl_2]$. The steric interactions are lessened considerably for the bidentate ligand L^1 and as a result a geometry with cis-phosphines is preferred for $[Pt(L^1)_2]$, $[Pt(L^1)_2Cl_2]$, $[Pt(HL^1)(L^1)Cl]$ and

$[Pt(PR_3)(L^1)Cl]$.

The palladium complex $[Pd(L^1)_2]$ can be made to react with $[Pd(PhCN)_2Cl_2]$ giving a chloro-bridged dimer, $[Pd_2(L^1)_2(\mu\text{-}Cl_2]$, which could then be cleaved with a variety of ligands, L' giving $[Pd(L')(L^1)Cl]$ (L' = PR_3, SMe_2, py). A crystal structure determination of one such cleavage product, cis-$[Pd(PPh_2Me)(L^1)Cl]$, was carried out, and the results indicated that the fluorinated alkoxide has a greater cis-influence than a chloride ligand.

The complex $[Ni(L^1)_2]$ exists in solution as a mixture of cis- and trans-isomers in a solvent- and temperature-dependent equilibrium. Thermodynamic data for this isomerization were determined using variable-temperature ^{31}P NMR. Kinetic data were also determined and an intramolecular mechanism through a tetrahedral intermediate was proposed. The crystal structure of $[Ni(L^1)_2]$ was also determined. The phosphino groups are trans-disposed in square-planar geometry, and a weak interaction between trifluoromethyl groups and the metal ion appears to be responsible for the colour change observed on crystallization.

to Beverly

Let not the wise man glory in his wisdom, neither let the mighty man glory in his might, let not the rich man glory in his riches, but let him that glorieth glory in this, that he understandeth and knoweth me, that I am the LORD ...

Jeremiah 9:23,24

ACKNOWLEDGEMENTS

I owe a great debt of thanks, first of all, to my supervisor Dr. Willis. His expert guidance was, of course, crucial but beyond that, his graciousness, patience and unique sense of humour made my time at U.W.O. all the more enjoyable. Also I wish to thank Dr. Payne, under whose guidance the X-ray structure determinations in this thesis were done.

A number of other people in the department were of great assistance. In particular, Susan Wilson and Val Richardson ran numerous NMR spectra while Janice Miller expertly typed my thesis.

I thank all my fellow students for friendships gained; I think especially of René Boeré and Brian Lloyd.

Finally I thank my wife Beverly, without whose faithful love and support this endeavour would certainly not have been possible.

TABLE OF CONTENTS

Page

List of Tables

List of Figures

Chapter 1

Introduction

1.1 Hybrid Ligands

A hybrid ligand may be defined as a multidentate ligand having more than one type of donor atom which can coordinate to a metal. Perhaps the best-studied hybrid ligands are the Schiff bases, complexes of which have been known for over a hundred years.[1] These ligands are formed on reaction of an aldehyde with a primary amine. If the aldehyde compound bears a second functional group, a hybrid ligand may be formed as in the case of bis(salicycl-aldehyde)ethylenediimine (1-1).[2]

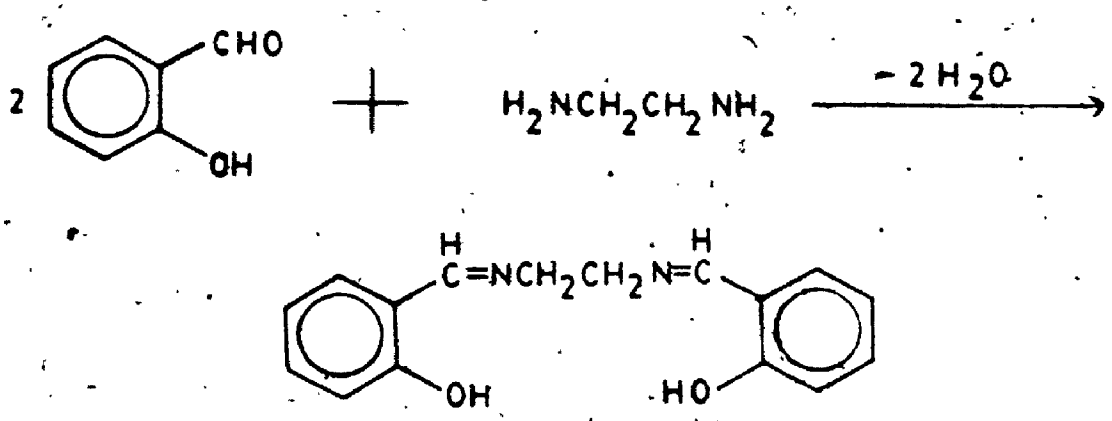

1-1

A more recent trend in studies of hybrid ligands has been towards the design of ligands combining "hard" and "soft" donor groups in a single molecule.

The division of acids and bases into such groups first originated with Ahrland, Chatt and Davies,[3] who divided metal ions into two classes. Class a) consisted of those metals which formed more stable complexes with the first

ligand atom in each group from the periodic table while class b) consisted of those which formed more stable complexes with the second or subsequent members of the group.

Pearson[4] noted that the factor which seems to determine into which class an acid or base goes is polarizability; class a) acids and bases tend to be small, often highly charged, electronegative, and unpolarizable while class b) consists of larger, more electropositive, polarizable, species. It was then possible to classify every conceivable acid or base as "hard" (class a) or "soft" (class b). A partial listing is given in Table 1.1.

As a general rule, hard bases prefer to coordinate to hard acids and soft bases prefer to coordinate to soft acids.

There have been a few possible explanations put forward for the observed hard-soft rule.[4] The first is that of the ionic-covalent theory; hard acids and bases both favour ionic bonding because of their higher charge to size ratio and low polarizability, while soft acids and bases would both favour covalent bonding due to their high polarizability. Therefore the strongest bonding, ionic or covalent, would exist between a hard acid and base or a soft acid and base.

Such an arrangement would also lead to stronger π-bonding, since both hard acids and soft bases would tend to be π-electron acceptors while soft acids and hard bases

Table 1.1. Classification of Bases and Acids

Hard Acids	Hard Bases
H^+, Li^+, Na^+, K^+	H_2O, OH^-, F^-, $CH_3CO_2^-$, Cl^-
Fe^{3+}, Co^{3+}, VO^{2+}, Ti^{4+}	CO_3^{2-}, NO_3^-, NH_3, RNH_2, RO^-
Borderline Acids	**Borderline Bases**
Fe^{2+}, Co^{2+}, Ni^{2+}, Cu^{2+}, Zn^{2+}, Rh^{3+}, Ir^{3+}, Ru^{3+}, Pb^{2+}	C_5H_5N, N_2, NO_2^-, Br^-, SO_3^{2-}
Soft Acids	**Soft Bases**
Pd^{2+}, Pt^{2+}, Pt^{4+}, Cu^+ Ag^+, Au^+	R^-, C_2H_4, C_6H_6, CN^-, RNC, CO, SCN^-, R_3P, R_3As, R_2S, RSH, RS^-, I^-

tend to be π-electron donors.

The final theory used to explain the hard-soft rule involves Van der Waals' forces. Since these stabilizing forces increase with polarizability, they might help to stabilize a bond between a soft acid and a soft base.

Hybrid ligands, particularly those having both a hard and soft base, are able to coordinate to metals in a number of different modes. These different coordination modes are illustrated in 1-2 through 1-6 for hybrid ligands with donor-groups X and Y. Such a ligand can serve as a monodentate ligand coordinating to a metal through either X or Y (1-2 and 1-3 respectively) depending on the nature of the metal and the donor group. Alternatively, it can behave as a bidentate ligand forming an unsymmetrical chelate ring (1-4). A bridging coordination mode is also possible, giving a homonuclear (1-5) or heteronuclear (1-6) dimer.

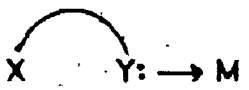

1-2

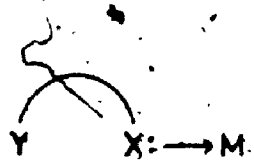

1-3

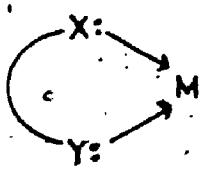

1-4

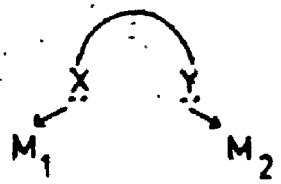

1-5 $M_1 = M_2$
1-6 $M_1 \neq M_2$

The intent of this work is to continue along this trend in hybrid ligand chemistry and prepare a ligand which combines a soft phosphino donor with a hard fluorinated alkoxide donor.

1.2 Fluorinated Alkoxides

Fluorinated alkoxides, like their unfluorinated analogs, are hard bases and as a result, their coordination chemistry is dominated by complexes formed with hard, strongly oxophilic, metals.

Primary and secondary fluorinated alcohols are unstable, as they tend to eliminate HF to give a fluorinated carbonyl compound. Ionic derivatives of these alcohols can be prepared by reaction of alkali metal fluorides with perfluorinated acid fluorides or ketones.[5,6]

$$R_FCOF + MF_{(s)} \rightleftharpoons M^+[R_FCF_2O]^-$$

$$CF_3COCF_3 + MF_{(s)} \rightleftharpoons M^+[(CF_3)_2CFO]^-$$

(R = F, CF_3 or C_2F_5; M = Cs, Rb, K)

However these ionic derivatives are likewise unstable as they eliminate F^-.[6]

Covalent alkoxides can be prepared from tertiary fluorinated alcohols however, because of their greater stability. For example, perfluoro-t-butanol forms stable

complexes with strongly oxophilic metals such as oxomolybdenum(VI)[7] and uranium(V)[8].

Two effects are observed on substitution of fluorine for hydrogen in a tertiary alcohol. First of all, the acidity of the alcohol increases markedly. For example, perfluoro-t-butanol has a pK_a value of 5.4[9] compared with 20.0 for tertiary-butanol. As a result, fluorinated alcohols are readily deprotonated in basic media. Secondly, while unfluorinated alkoxides show a strong tendency to bridge between metal centres in complexes, fluorinated alkoxides are exclusively monodentate in metal complexes. No example of a bridging fluorinated alkoxide exists.

While the second effect may be in part due to the bulky, sterically demanding nature of the fluorinated groups bonded to oxygen, the primary reason for both effects is the same. Fluorine is the most electronegative element and therefore the fluorinated groups withdraw electron density from the oxygen, thereby decreasing its nucleophilicity. This then has the effect of both increasing the acidity of the alcohol and reducing the coordinating ability of the alkoxide.

The stability of complexes of fluorinated alkoxides may be enhanced through the use of bidentate, chelating, alkoxides. Perhaps the most common example is the diol, perfluoropinacol, $HOC(CF_3)_2C(CF_3)_2OH$, which readily coordinates as the dianion, PFP^{2-}, to give metal complexes

$[M(PFP)_2]^{2-}$ (M = Ni^{2+}, Cu^{2+}, Zn^{2+}) or $[Fe(PFP)_3]^{3-}$.[10,11] The perfluoropinacol dianion can also stabilize metals in high oxidation states because of its stability against oxidation.[12]

The increased stability associated with the use of bidentate fluorinated alkoxides also allows for the expansion of the number of metal complexes prepared to include those of softer transition metals. For example, $[Pt(PFP)(PR_3)_2]$ and $[Pt(PFP)(SR_2)_2]$ have been prepared.[13]

Hybrid ligands have been synthesized, incorporating a fluorinated alkoxide along with some other donor group. Schiff-base type ligands having a fluorinated alkoxide group have been prepared by template synthesis. These include macrocyclic and chelating ligands such as 1-7[14] and 1-8[15] respectively.

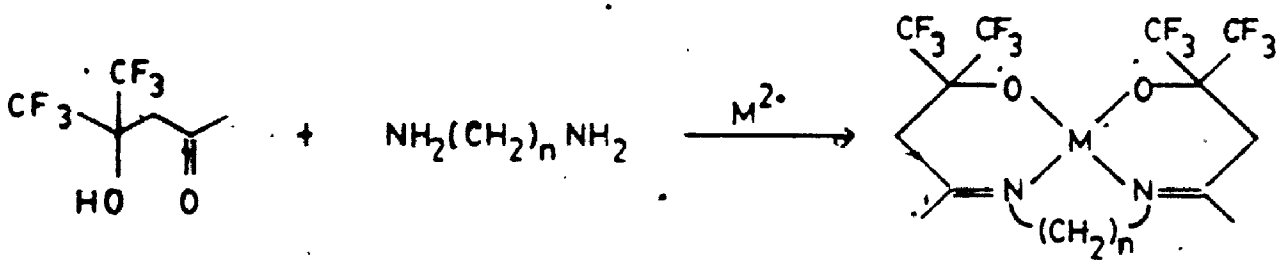

(n=2,3 ; M=Ni, Cu)

1-7

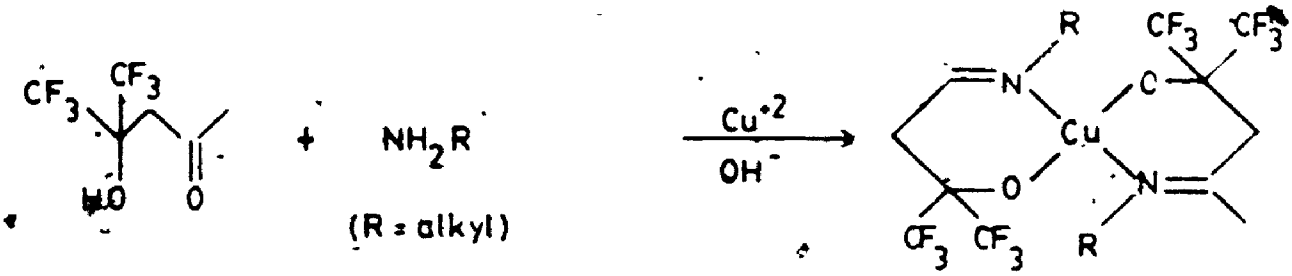

1-8

Iminoalkoxy bidentate ligands such as those in 1-8 have been hydrogenated to the corresponding alcohols by $LiAlH_4$. Complexes of the aminoalkoxy ligands could then be prepared also.[16]

More recently, fluorinated alkoxy hybrid ligands with a class b base as the second donor group have been studied. Specifically, a soft thioether group is combined with the hard fluorinated alkoxide in 1-9 and 1-10.[17,18]

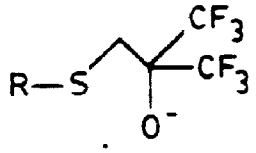

1-9

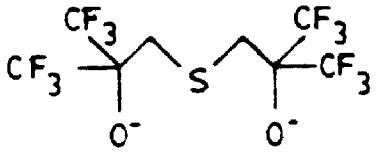

1-10

The thioether group does allow the ligand 1-9 to chelate to softer metals such as Pd^{2+} and Pt^{2+}, but the ligand will not coordinate to hard metals.[17] Alternatively 1-10 forms complexes with Co^{2+}, Cu^{2+} and Ni^{2+}[18] but not with the softer metals.

Clearly a hybrid ligand of this type would be more useful if it contained, as the soft donor, one which would coordinate more strongly and to a wider variety of metals than the thioether group. A study of such a ligand, containing a hard fluorinated alkoxy group and a diarylphosphino group, is the subject of this thesis.

I.3 Phosphine-Containing Hybrid Ligands

Considerable interest has been shown recently in the

coordination chemistry of functional phosphines. Such species contain some functional group in addition to a phosphino group, and as a result can serve as a bidentate hybrid ligand. For example, Meek et al[19] prepared functional phosphines where the second donor group can be an amino, arsino, ether or thioether group. These ligands were prepared from various primary or secondary phosphines, using free-radical addition of P-H across the C = C double bond of vinyl or allyl compounds.

Functional phosphine ligands have been applied widely. Balch et al[20] used the functional phosphine, 2-(diphenylphosphino)pyridine, 1-11, to prepare binuclear metal complexes, both heteronuclear, 1-12, and homonuclear, 1-13.

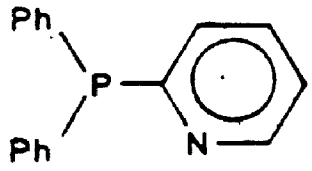

1-11

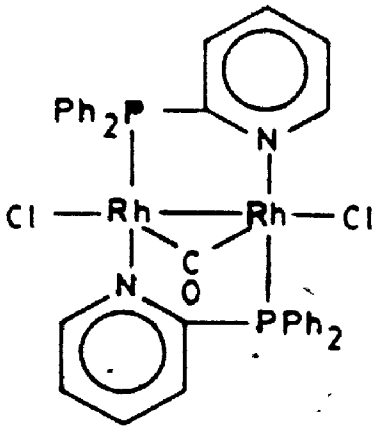

1-12

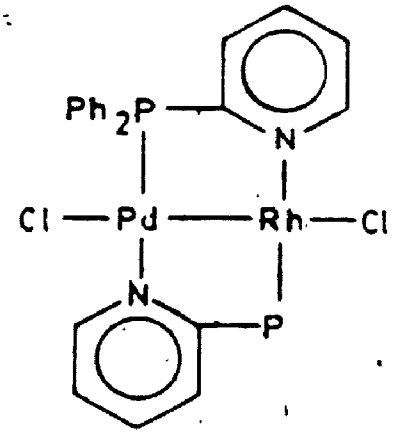

1-13

The precursor compound to these binuclear complexes is one where the hybrid phosphine ligand serves as a monodentate ligand coordinating to Rh(I) through the phosphorus.

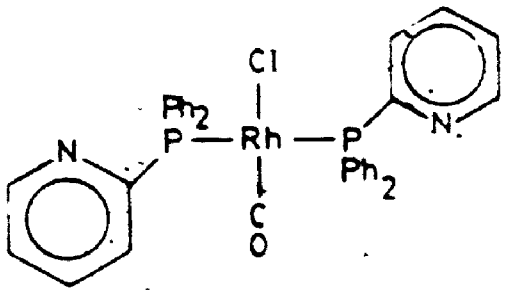

1-14

Alternately, there are numerous examples of complexes featuring a hybrid phosphino ligand appearing as an unsymmetrical chelate. The iridium(I) complex, 1-15, was prepared by D.M. Roundhill et al.[21]

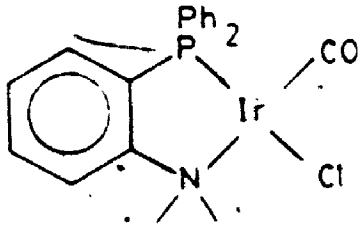

1-15

The ligand whose preparation and coordination chemistry is described in this thesis is a functional phosphine, or hybrid ligand containing a phosphino group and a fluorinated alkoxy group. There have been other examples of phosphino ligands containing a second oxygen donor function. The nature of the oxygen donor varies, and examples include ethers, aldehydes, ketones, esters, phenoxides and carboxylic acids.

Dombek[22] prepared complexes of phosphino-ethers. Heating complexes 1-16 in 2 methoxyethanol yielded a cyclometalated derivative 1-17.

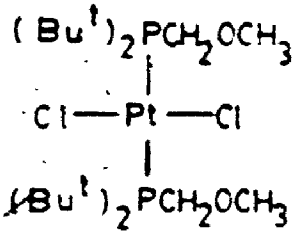

1-16

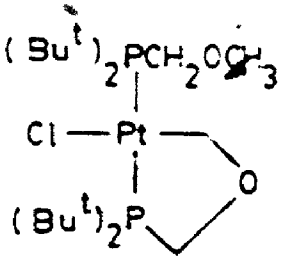

1-17

$[IrCl(COT)_2]_2$ also reacts with $Bu^t_2PCH_2OCH_3$ and CO to give the iridium(III) carbonyl hydride 1-18.

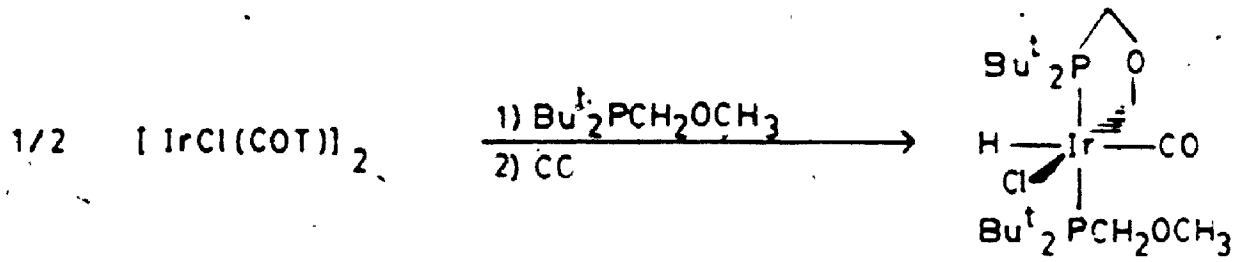

1-18

Anderson[23] was interested in preparing low-valent complexes of bidentate ligands having one strong and one weak donor. The weak donor should readily dissociate, leaving a vacant site for an organic substrate. Phosphino-ether hybrid ligands were employed in preparing complexes of Pt(II). The ether function of 1-19 could indeed be replaced on the metal by another neutral ligand to give the cationic complex, 1-20.

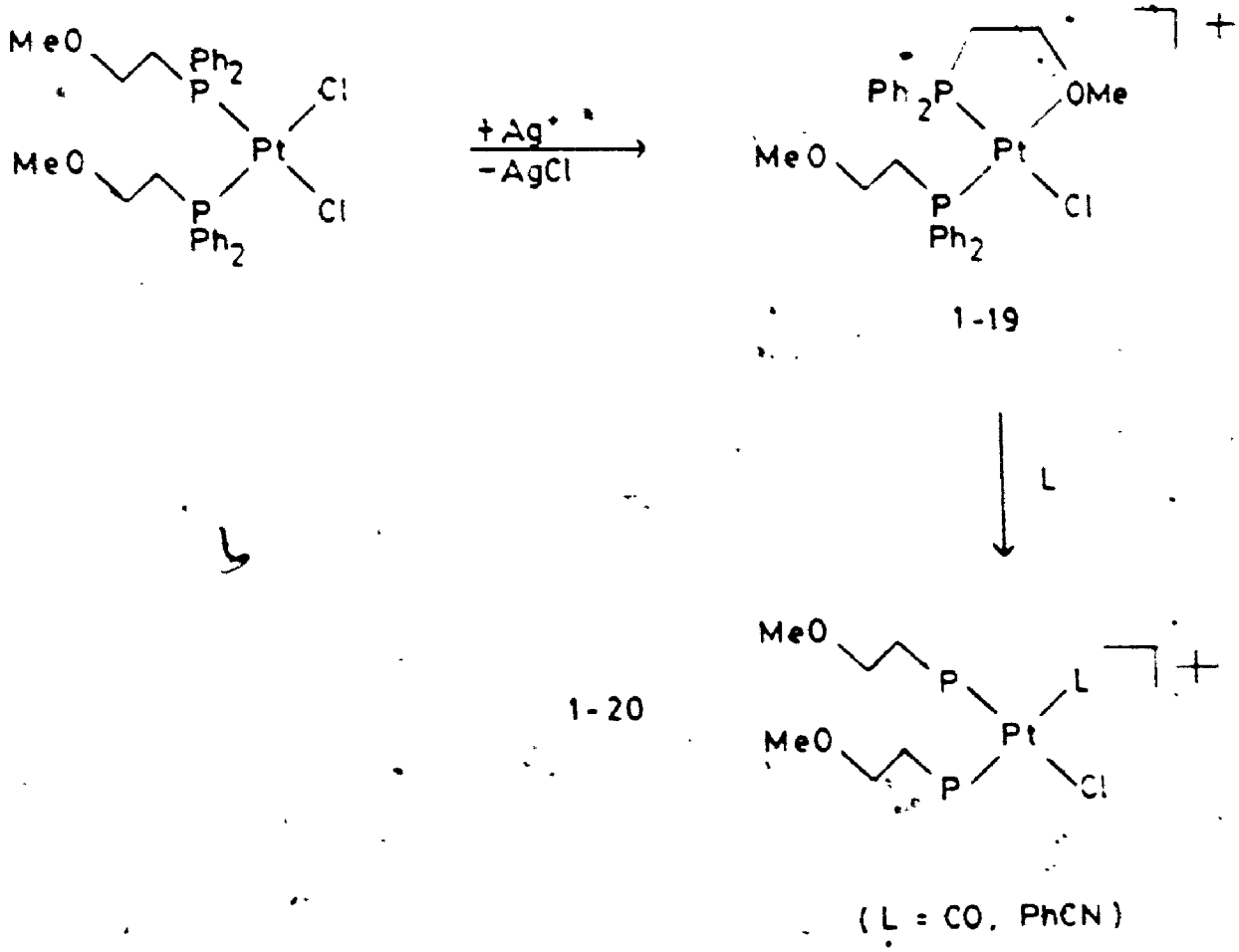

Likewise Rauchfuss[24] employed bidentate phosphino-ether ligands to make complexes which were referred to as "hemilabile". Dichlorobis(o-(diphenylphosphino)anisole) ruthenium(II), 1-21, reacts at room temperature with CO to give the fluxional complex 1-22 and the all-trans 1-23. At high temperatures, 1-21 reacts with CO to give the cis-complex 1-24, which can be converted photochemically to a mixture of 1-22 and 1-23.

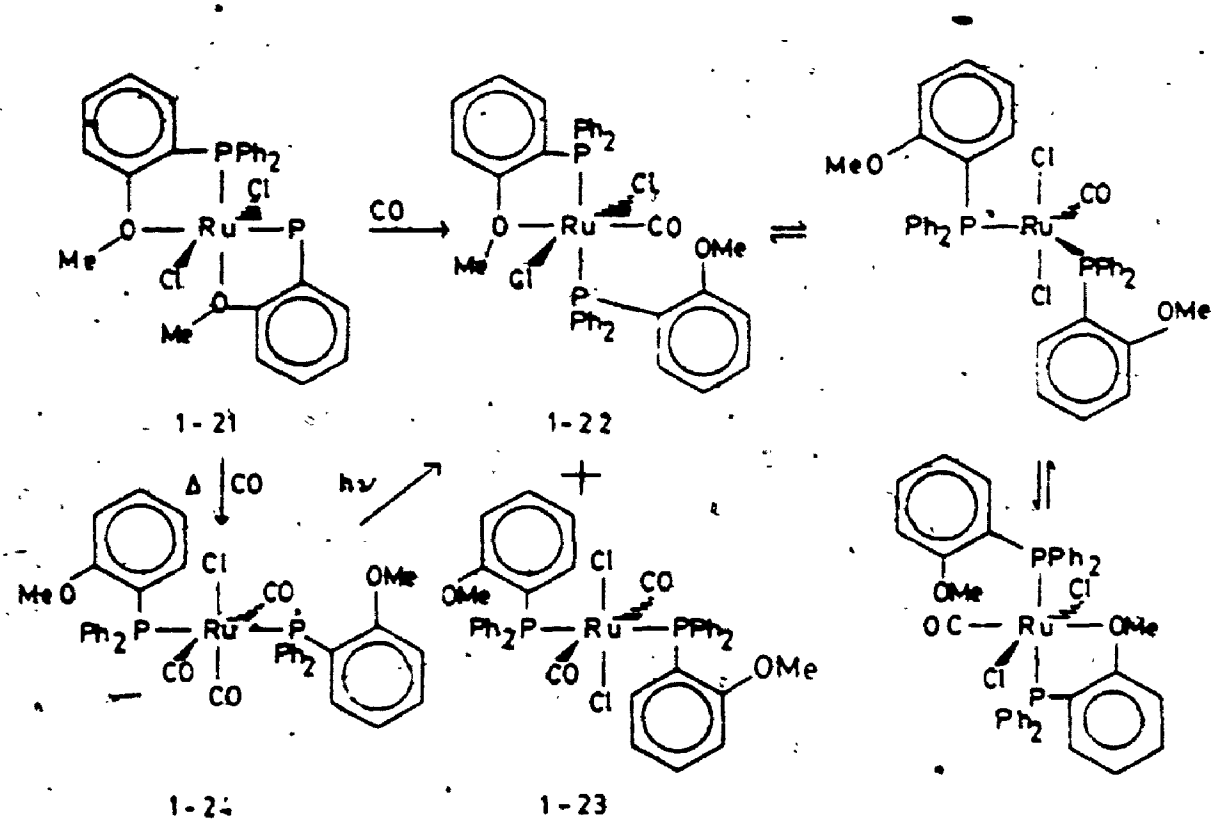

Bernard L. Shaw[25] compared the rate of oxidative addition for the phosphino-ether complexes, trans-[IrCl(CO)(PMe_2(O-$MeOC_6H_4$))$_2$] and trans-[IrCl(CO)(PMe_2(p-$MeOC_6H_4$))$_2$] with that for trans-[IrCl(CO)(PMe_2Ph)$_2$]. The PMe_2(o-$MeOC_6H_4$) complex reacted much faster than the other two due to a direct electronic interaction between the oxygen and the iridium, thus increasing the nucleophilicity of the iridium and lowering the activation energy for the oxidative addition.

The methoxyphenylphosphino ligands also reacted with Pt(II) halides to give complexes of the type PtX_2L_2 where L = PMe_2(2-methoxyphenyl), PPh_2(2-methoxyphenyl),

PPh_2(2-ethoxyphenyl), PBu^tMe(2-methoxyphenyl and PBu^t_2(2-methoxyphenyl)[26]. In these complexes, the P,O hybrid ligand serves as a monodentate ligand coordinated only through the phosphorus. However on heating, the complexes were converted to O-metallated chelates by demethylation. The resulting chelating ligand may be considered a phosphino-phenoxide. O'Flynn and McDonald[27] later determined the x-ray crystal structure of the bis O-metallated complex, $[Pt(Ph_2PC_6H_2O)_2]$.

The O-metallation reaction was favoured by very strong heating or heating in a polar solvent and is believed to occur via a four-centre transition state.[26]

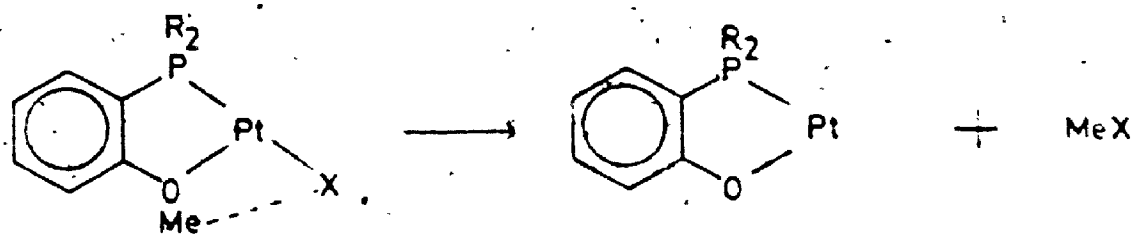

Alternatively heating in a polar solvent such as xylene favours C-metallation by deprotonation of the methyl or ethyl group.

Complexes of phosphino-phenoxide ligands were also prepared using phosphino-phenol ligands.[28] The complexes $[M(Ph_2PC_6H_4OH)_2Cl_2]$ (M = Pd or Pt) have been prepared and readily lose HCl to give the bischelate complex $[M(Ph_2PC_6H_4O)_2]$. The phosphino-phenol ligand $Bu^t_2PC_6H_4OH$ has been used to prepare complexes $[M(Bu^t_2PC_6H_4O)_2]$ (M =

Co, Ni, Pd, Pt).

Treatment of cis-[Pt($Ph_2PC_6H_4O$)$_2$] with Na[BH_4] causes one ring to open, resulting in the Pt(II) hydride, [PtH($Ph_2PC_6H_4O$)($Ph_2PC_6H_4OH$)]. Ring-opening can occur likewise on reaction of the complex with excess MeLi to give [$PtCH_3$($Ph_2PC_6H_4O$)($Ph_2PC_6H_4OH$)]. The hydride when reacted with acetic anhydride gives the acetyl complex [Pt(COMe)($Ph_2PC_6H_4O$)($Ph_2PC_6H_4O_2CMe$)].

The reactions of phosphino-ethers with Rh(I) and Rh(III) have also been investigated by Shaw et al.[29] The ligand PMe_2(2-methoxyphenyl) reacts with $Rh_2Cl_2(CO)_4$ to give trans-[RhCl(CO){PMe_2(2-$MeOC_6H_4$)}$_2$]. Like the Ir(I) analogue, these complexes undergo rapid oxidative addition, more rapidly than when PMe_2Ph is substituted for PMe_2(2-$MeOC_6H_4$). As in the iridium case, an electronic interaction between the oxygen and the rhodium could increase the nucleophilicity of the metal and cause the observed effect on the rate of oxidative addition. Rh(III) in the form of $RhCl_3 \cdot 3H_2O$ reacts with PMe_2(2-$MeOC_6H_4$) to give the tris chelate [Rh($PMe_2C_6H_4O$)$_3$]. Alternatively when reacted with PBu^t_2(2-$MeOC_6H_4O$), Rh(III) is reduced to the Rh(II) species [Rh($PBu^t_2C_6H_4O$)$_2$].

Likewise an iridium(II) complex has been prepared,[30] however in this case the method involved oxidation of an iridium(I) complex.

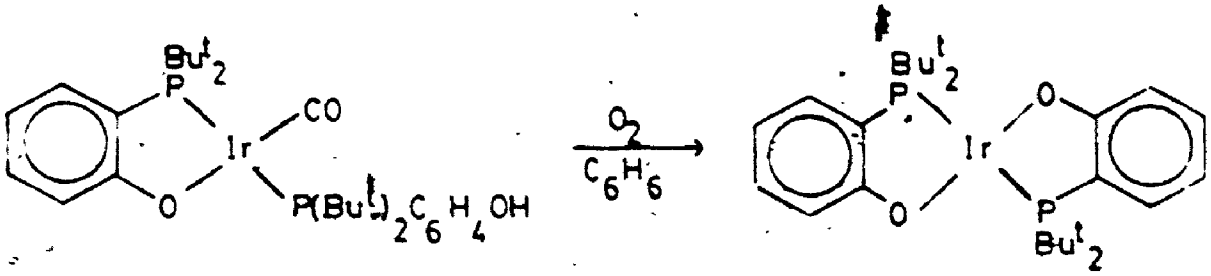

The iridium(II) species can be further oxidized with hydrogen to an Ir(III) hydride, 1-25, which is also the product of the reaction of $IrCl_3.3H_2O$ and $P(Bu^t)_2(C_6H_4OH)$ in isopropyl alcohol.

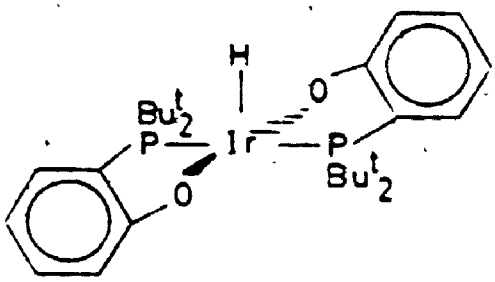

1-25

A benzene solution of the iridium(II) species in air slowly forms another five-coordinate Ir(III) complex, I-26. In this case the complex is a purple C-metallated [illegible]ne.

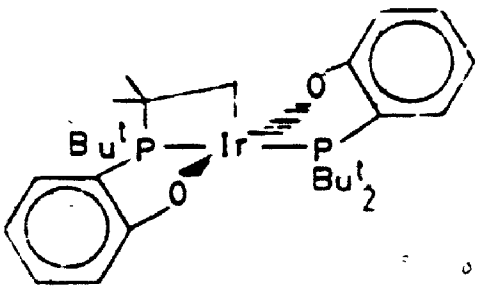

1-26

This represents the first example of internal metallation of a tertiary butyl group. Likely an iridium-oxygen species is first formed which then loses the hydrogen as H_2O or H_2O_2. In benzene, carbon monoxide rapidly fills the vacant sixth coordination site in 1-25 and 1-26.

Shaw was able to prepare more unusual iridium complexes using dimethoxyphenylphosphines, specifically (2,6-dimethoxyphenyl)- and (2,3-dimethoxyphenyl)-di-t-butylphosphine.[31] Again a five-coordinate Ir(III) complex 1-27 was synthesized which can be reduced in solution to an iridium(II) complex 1-28 and subsequently converted back to the Ir(III) species by treatment with $NaBH_4$. The hydride, 1-27, reversibly takes up small molecules such as carbon monoxide and pyridine. The iridium(II) species takes up O_2 reversibly as well as CO and NO to give 1-29, 1-30 and 1-31 respectively. In air, a solution of 1-29 or 1-30 slowly converts to the C-metalated species 1-32. The complex 1-32 reversibly takes up small molecules and a crystal structure was obtained of one product, 1-33 where L = MeNC. The various interconversions of this system are summarized in Scheme 1.1.

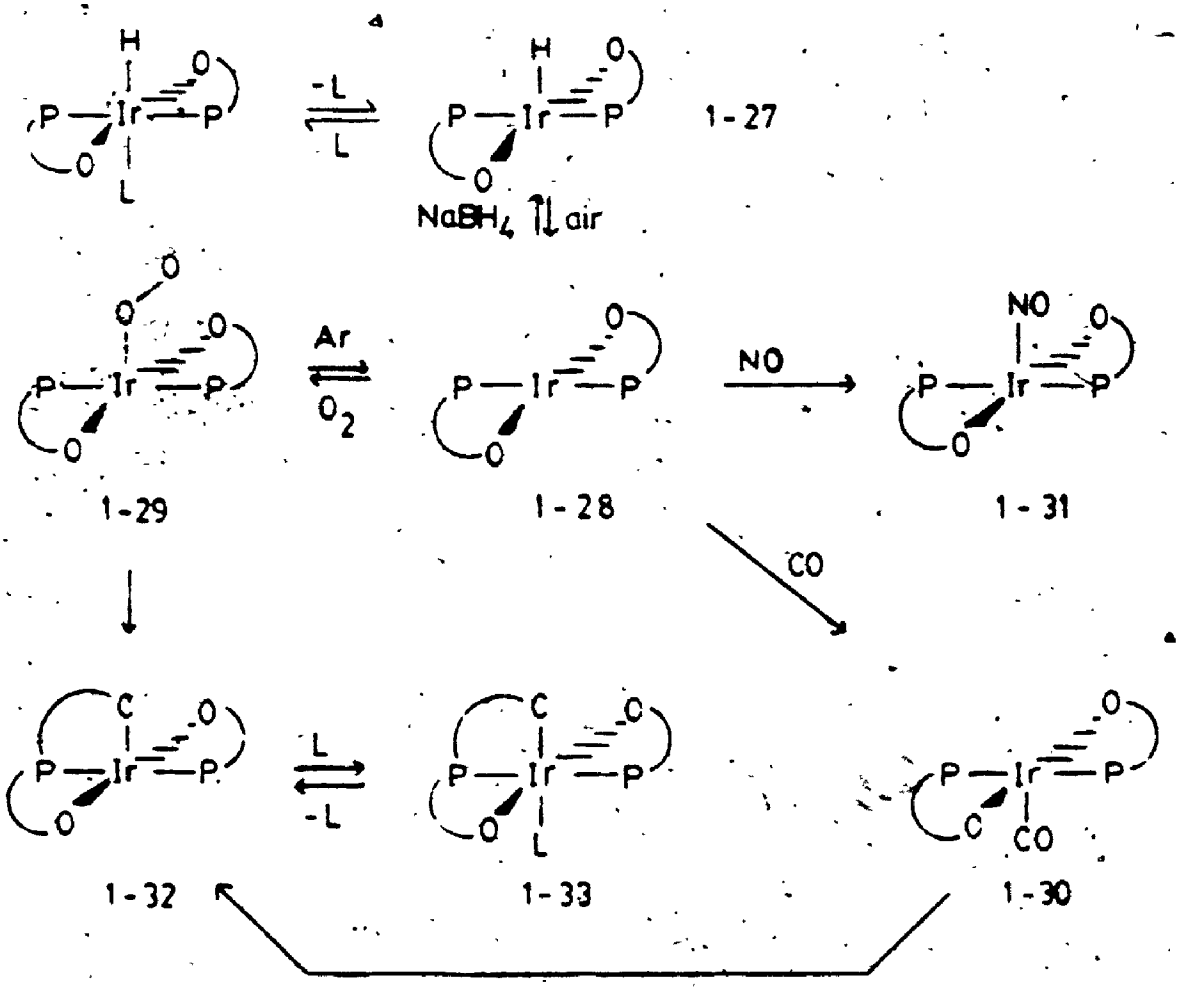

SCHEME 1-1

Not only can an ether group or phenoxide be used as the oxygen donor group in a phosphorus-oxygen hybrid ligand, but carbonyl groups can also be employed. Rauchfuss[32] also made complexes of a bidentate phosphino-aldehyde 1-34, with Pt(II), Ir(I), Ir(III) and Ru(II) to give 1-35, 1-36, 1-37 and 1-38 respectively.

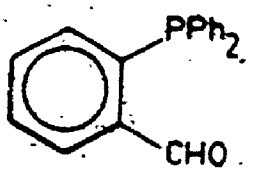

1 - 34

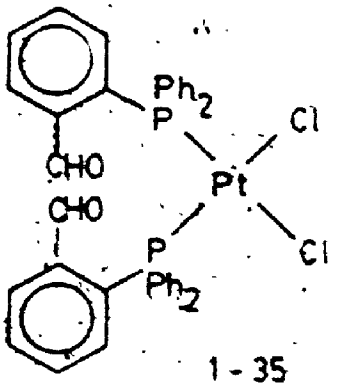

1 - 35

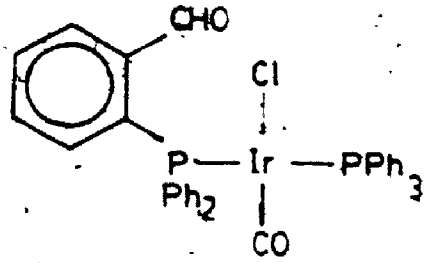

1 - 36

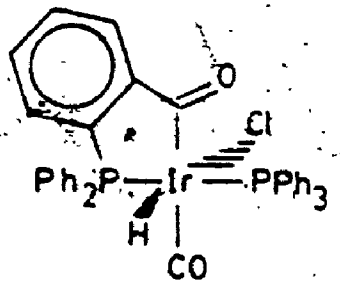

1 - 37

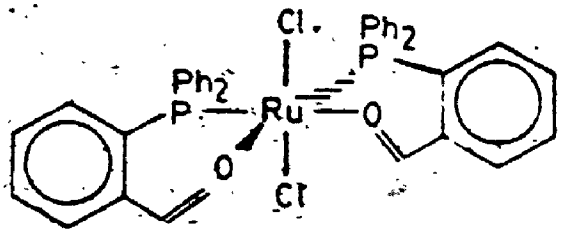

1 - 38

On heating, 1-35 eliminates HCl to give a metal acyl complex, while 1-38 yields cis,cis,trans-$RuCl_2(CO)_2(PPh_3)_2$. Complex 1-36 was not isolated but is the intermediate on oxidative addition of the ligand to Ir(I).

SCHEME 1.2

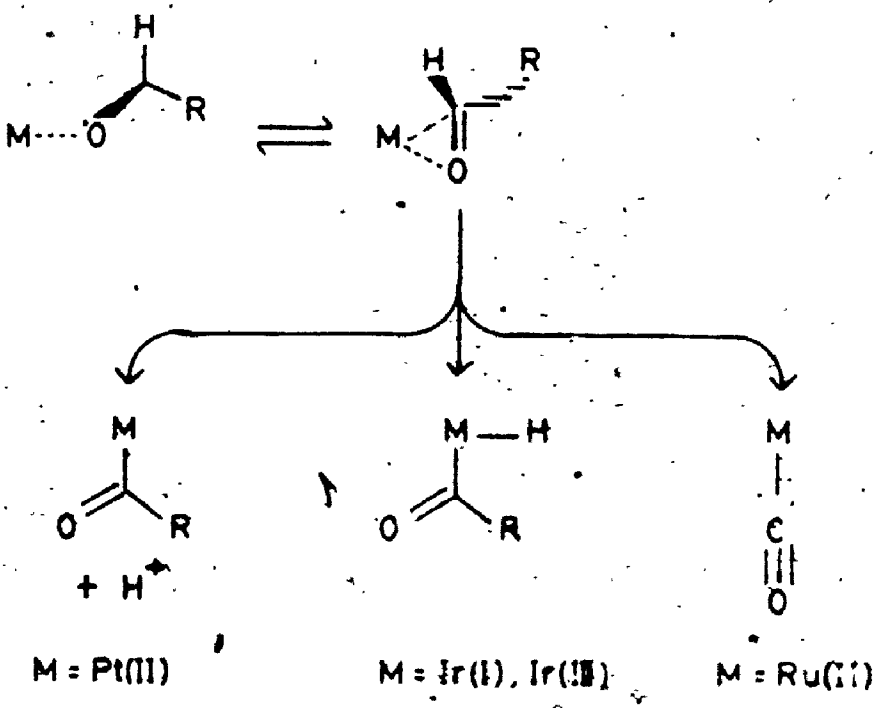

Rauchfuss proposed the formation of a π-bonded carbonyl to explain the different reactions of the transition metal-aldehydes as in Scheme 1.2.

Shaw studied β-ketophosphine complexes of rhodium and iridium.[33] The ligands $But_2PCH_2C(O)Ph$ and $But_2PCH_2(O)But$ could coordinate through the phosphorus alone as a unidentate ligand, through the phosphorus and the keto-group as a neutral bidentate ligand or, by deprotonation, through the phosphorus and the oxygen of an enolate group as a bidentate uninegative ion. These three possible modes of coordination are shown as 1-39, 1-40 and 1-41 respectively.

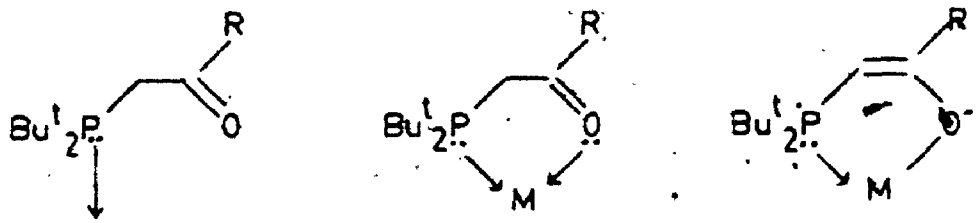

1-39 1-40 1-41

When treated with $[RhCl(CO)_2]_2$, both ligands give complexes of the type trans-$[RhCl(CO)\{But_2PCH_2C(O)R\}_2]$, 1-42, where the β-ketophosphines are coordinated through the phosphorus only. Ring closure involving one phosphine, by deprotonation to yield the enolate complex, is incurred on treatment of these Rh(I) complexes with sodium methoxide.

The deprotonation can be reversed with hydrogen chloride. A bischelate, 1-44, where one chelating ligand is a neutral β-ketophosphine and the second is a uninegative enolate ion, is the product of the reaction of the ligand with the metal trihalides. For 1-44, when M = Rh, treatment with sodium methoxide brings about reduction to the rhodium (II) bischelate 1-45, whereas when M = Ir, treatment with sodium ethoxide gives the Ir(III) hydride 1-46. These hydrides are capable of reversible uptake of CO to fill the vacant sixth site.

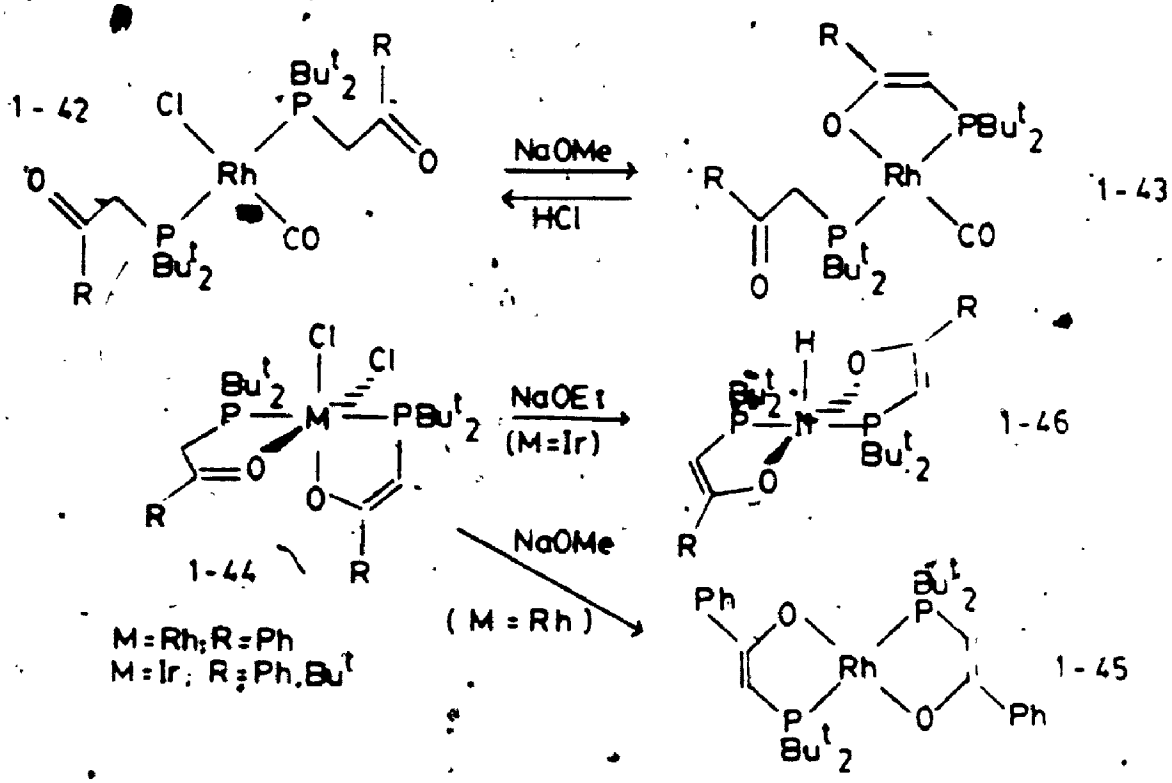

These β-ketophosphine hybrid ligands also form complexes with the divalent metals of the nickel triad.[34] The reaction with nickel(II) chloride proceeds to give the bischelate complex, trans-$[Ni(Bu^t_2PCH = C(O)R)_2]$, while the reaction with $MCl_2(PhCN)_2$ (where M = Pd, Pt) gives the complexes trans-$[MCl_2(Bu^t_2PCH_2C(O)R)]$. Ring closure to

give the bischelate complex occurs by deprotonation with sodium 2-methoxyethoxide.

Carty et al[170] prepared palladium complexes of β-ketophosphines by mild hydrolysis of acetylenes held proximate to a metal by a coordinated phosphines. Starting from cis-$[PdCl_2(Ph_2P{=}CCF_3)_2]$, a mixture of products was obtained including $[\overline{Pd(Ph_2PCH{=}C(O)CF_3}\}_2]$, $[\overline{PdCl(Ph_2PCH{=}C(O)CF_3}\}(PPh_2(OH))]$ and $[\overline{PdCl(Ph_2PCH{=}C(O)CF_3}\}(PPh_2(OEt))]$. Likewise Shaw[171] made some rhodium and iridium complexes containing a bidentate β-ketophosphine by attack of an alkoxide on coordinated $PBu^t_2(C{\equiv}CPh)$.

Esters, more specifically acetates, have also been combined with phosphino groups in a P,O hybrid ligand. Shaw prepared complexes of platinum, palladium and rhodium with the phosphine esters $Bu^t_2(P(CH_2)_nCO_2Et$, n = 1, 2 or 3.[35] Reaction of $Bu^t_2PCH_2CO_2Et$ with $MCl_2(PhCN)_2$ (M = Pt,Pd) gave $MCl_2(Bu^t_2PCH_2CO_2Et)_2$. Treatment with NaI for the complex where M = Pt gave the O-metallated species $[\overline{PtI(Bu^t_2PCH_2C(O)O}\}(Bu^t_2PCH_2CO_2Et)]$ which in turn gave the bischelate when reacted with $[CH_3CO_2]Na$ in 2-methoxyethanol. The complex $[\overline{PtI(Bu^t_2PCH_2C(O)O}\}(Bu^t_2PCH_2C(O)OEt)]$ can also be reduced with $NaBH_4$ to $[\overline{PtH(Bu^t_2PCH_2C(O)O}\}(Bu^t_2PCH_2C(O)OEt)]$. For the ligands where n = 2 or 3, it was possible to make chlorobridged dimers $[PtCl_2(Bu^t_2P(CH_2)_nC(O)OEt)]_2$, along with $[PdCl_2(Bu^t_2P(CH_2)_3C(O)OEt)]_2$. The platinum dimer undergoes

C-metallation in the case where n = 3 when heated in toluene to give $[PtCl\{Bu^t_2PCH_2CH_2CHC(O)OEt\}]_2$ which can subsequently be cleaved by PPh_3 yielding trans-$[PtCl\{Bu^t_2PCH_2CH_2CHC(O)OEt\}(PPh_3)]$.

A six-coordinate rhodium (III) species $[RhCl_2\{Bu^t_2PCH_2C(O)OEt\}_2]^+$ was synthesized and converted using $Na[BH_4]$ to the six-coordinate dihydride $[RhH_2(BH_4)\{Bu^t_2PCH_2C(O)OEt\}_2]$. This complex has been assigned a structure having trans-phosphine ligands and cis-hydrido ligands trans to a bidentate tetrahydroborate ligands. Reaction of $RhCl_3 \cdot 3H_2O$ with the ligands having n = 2 or 3 gave rhodium (II) species, trans-$[RhCl_2\{Bu^t_2P(CH_2)_nC(O)OEt\}_2]$.

Braunstein also investigated the coordination properties of ethyl (diphenylphosphino)acetate.[36] This ligand forms complexes with Pd(II) where the phosphinoacetate acts as a monodentate ligand coordinated through phosphorus only, 1-47 or as a bidentate neutral ligand 1-48. In addition, the carbanion of the ligand, prepared by reacting the acetate with $LiN(c\text{-}C_6H_{11})(i\text{-}Pr)$, can be reacted with the dinuclear complex $[Pd(dmba)Cl]_2$ (dmba = dimethylbenzylamine). A Pd/ligand anion ratio of 2/1 yields the dinuclear complex [dmba)Pd(μ-Cl)(μ-$Ph_2PCHC(O)OEt$)Pd(dmba], 1-49, while a 1/1 ratio yields the mononuclear $[Pd(Pd_2PCHC(O)OEt\}(dmba)]$, 1-50. The complex 1-50 reversibly takes CO_2 to give $\{Pd\{Ph_2PC(CO_2Et)$-$C(O)OH\}(dmba)]$ 1-51, in what is the first known example of

reversible CO_2 fixation fully characterized by X-ray structural determination.

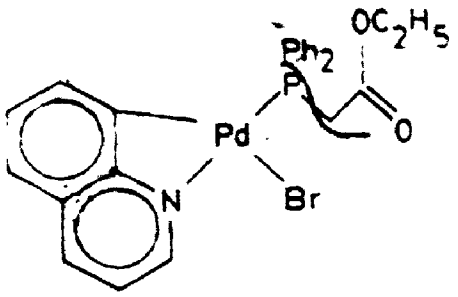

1-47

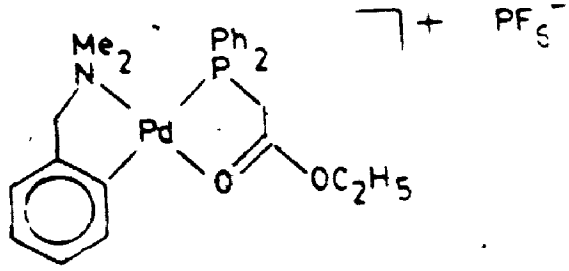

1-48

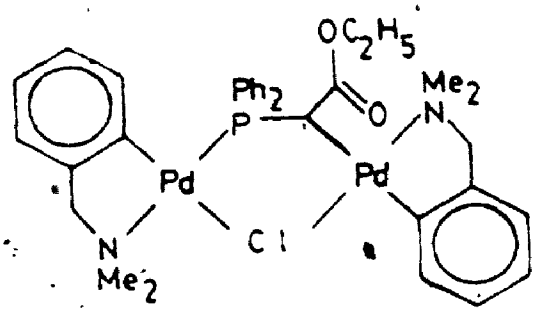

1-

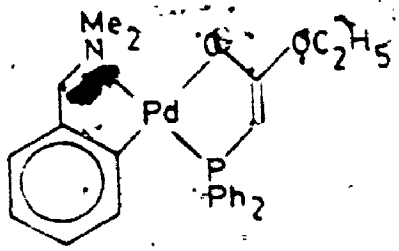

1-50

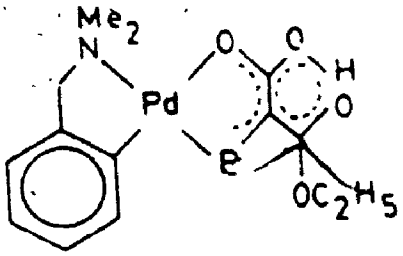

1-51

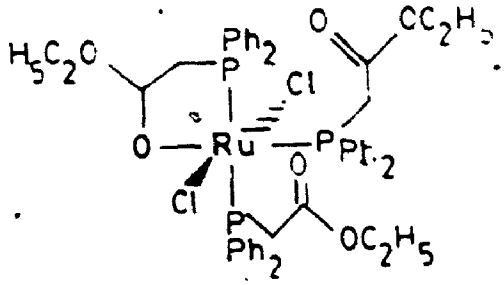

1-52

Complexes of ethyl (diphenylphosphino)acetate with Rh(III) and Ru(II) have also been made.[37] Displacement of a single nitrile ligand of $RuCl_3(o\text{-}CH_3C_6H_4CN)_3$ by the ligand gives trans,trans,trans-$RuCl_2(O\text{-}CH_3C_6H_4CN)_2$ $(Ph_2PCH_2C(O)Et)_2$ in which the ligands coordinate as a monodentate phosphine. Reaction in hot ethanol of $RuCl_3$ and the ligand gives the Ru(II) complex trans-$[RuCl_2\{Ph_2PCH_2C(O)OEt\}(Ph_2PCH_2C(O)OEt)_2]$ 1-52. The complex 1-52 will take up CO to give trans,trans,trans-

$[RuCl_2(CO)_2\{Ph_2PCH_2C(O)OEt\}_2]$ where the phosphines are monodentate. A single coordinated carbon monoxide can then be reversibly lost as one of the acetate groups coordinates to the metal to give a bidentate phosphino-acetate. The ease with which CO replaces the coordinated O-donor group in these complexes again illustrates the "hemilabile" nature of these ligands and their potential in catalysis.

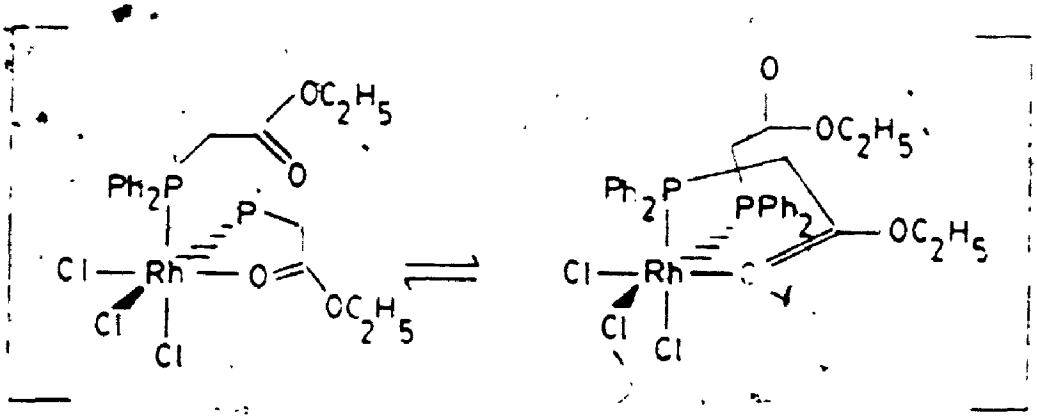

1-53

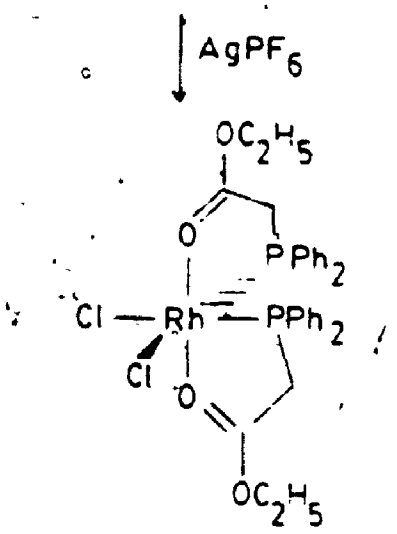

1-54

With Rh(III), the ligand forms $[RhCl_3(Ph_2PCH_2C(O)OEt)(Ph_2PCH_2C(O)OEt)]$, 1-53, a stereodynamic molecule in which the monodentate and bidentate ligands exchange roles. Addition of $AgPF_6$ converts a monodentate ligand into a bidentate one, yielding 1-54.

As mentioned earlier, hybrid ligands potentially can exhibit a number of different coordination modes. Two of the less common modes of coordination are illustrated by a phosphorus-oxygen hybrid ligand where a sulphonate group serves as the O-donor.[38] A dinuclear complex, 1-55, with a bridging $\{Ph_2P(m\text{-}C_6H_4SO_3)\}^-$ has been synthesized. This complex reacts with methyl cyanide yielding the O-coordinated complex 1-56.

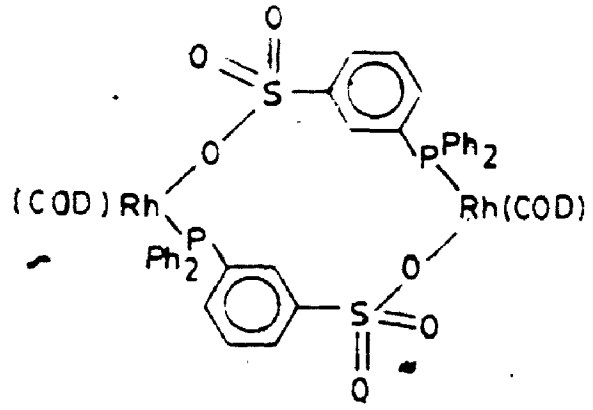

1-55

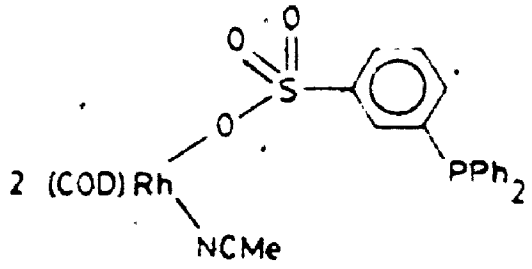

1-56

Podlahova has extensively studied ligands combining a phosphino group with a carboxylic acid. (Diphenylphosphino)acetic acid coordinates with Ni(II) to give the tetrahedral bischelate $[Ni(Ph_2PCH_2C(O)O)_2]$ and the trans-square-planar complexes $[NiX_2(Ph_2PCH_2COOH)_2]$ where X = Cl, Br, I, SCN.[39] A crystal structure was determined for

the palladium analog, trans-$[PdBr_2(Ph_2PCH_2COOH)_2]$.[40] With Pt(II),[41] three types of complex were formed, $[PtX_2(Ph_2PCH_2COOH)_2]$, $[PtX\{Ph_2PCH_2C(O)O\}(Ph_2PCH_2COOH)]$ and $[Pt\{Ph_2PCH_2C(O)O\}_2]$. The complex formed was determined by the nature of X, the acidity of the solvent and solvent polarity. All of these complexes are cis.

Rh(I) complexes, $[Rh(CO)X(Ph_2PCH_2COOH)_3]$ and $[Rh(CO)\{Ph_2PCH_2C(O)O\}(Ph_2PCH_2COOH)_2]$, were prepared.[42] These complexes proved to be reactive and readily undergo oxidative addition.

In addition, a number of potentially multidentate ligands were studied by Podlahová. Nickel(II) complexes were formed with ethane-1,2-bis-(phenylphosphino-ethanoic acid) including the six-coordinate complexes 1-57[47] and a five-coordinate complex 1-58.[44]

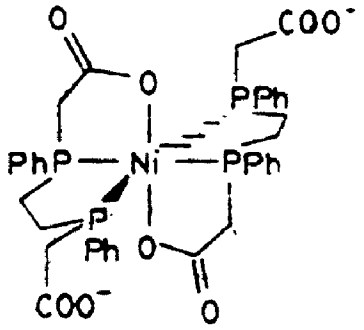

1-57

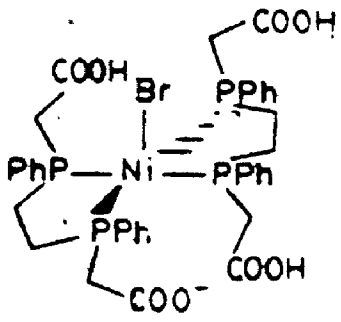

1-58

Also ethylphosphinediacetic acid was prepared and shown to prefer to coordinate to soft metals.[45]

Gervais et al[46] synthesized a zirconum complex having two $Ph_2PCH_2COO^-$ ligands by an interesting method. Carbon

dioxide was inserted into the Zr(IV)-carbon bonds in $[Zr(cp)_2(CH_2PPh_2)_2]$ to give $[Zr(cp)_2(O_2CCH_2PPh_2)_2]$. Reduction of the complex with Na/Hg produced a Zr(III) species which could be examined using ESR. The ESR spectra indicated that the phosphino-acetate ligands are chelating with phosphorus and oxygen donors.

An attempt has been made in Table 1.2 to summarize some of the work that has already been done with P,O-donor hybrid ligands.

These examples of complexes of phosphorus-oxygen hybrid ligands help to illustrate some of the reasons for the interest in such species, and more specifically, in the system presented in this thesis.

First of all, these complexes exhibit some interesting structural features. Examples exist where the hybrid ligands coordinate: through oxygen, $[Rh(OS(O)_2C_6H_4PPh_2)(COD)(NCMe)]$ (1-56) or phosphorus, $[RhCl(CO)(Bu^t_2PCH_2C(O)C_6H_5)_2]$ (1-42), as monodentate ligands, as an unsymmetrical chelate $[Pt(Ph_2PCH_2C(O)O)_2]$, or as a bridging ligand in a dimeric complex, $[Rh(COD)(\mu\text{-}Ph_2P(C_6H_4SO_3))]_2$ (1-55). Also the presence of the phosphino group in a chelate ring stablizes the metal-oxygen bond for a number of less oxophilic metals such as Rh(I) and Pt(II). In some of the complexes, the metals were found to be in less common oxidation states as well, such as the Ir(II) complex $[Ir(Bu^t_2PC_6H_4O)_2]$.

Secondly these complexes show interesting reactivity.

Table 1.2 P,O Hybrid Ligands

O-donor group	Ligand Examples	Metals Coordinated To	Ref -
ether	$Bu_2^tPCH_2OCH_3$	$Pt^{2+}, Ir^{3+}, Ru^{2+}, Ir^+$	22,23,24
	$Ph_2P(CH_2)_2OCH_3$	$Rh^+, Rh^{3+}, Rh^{2+}, Ir^{2+}$	25,26,29
	$R_2P(O\text{-}C_6H_4OMe)$		
	R,=Ph_2,Me_2,Bu_2^t,		
	Bu^tMe		
phenoxide	$R_2P(O\text{-}C_6H_4O)^-$	$Pd^{2+}, Pt^{2+}, Ni^{2+}, Co^{2+}$	26,27,28
	R=Ph_2Bu^t	Ir^+, Ir^{3+}, Ir^{2+}	30,31
aldehyde	$Ph_2P(O\text{-}C_6H_4CHO)$	Pt^{2+}, Ir^+, Ir^{3+}	32
		Ru^{2+}	
ketone	$Bu_2^tPCH_2C(O)R$	$Rh^+, Rh^{3+}, Rh^{2+}, Ir^+$	33,34
	R=Ph,Bu^t	$Ir^{3+}, Ni^{2+}, Pd^{2+}, Pt^{2+}$	
esters	$Bu_2^tP(CH_2)_nCO_2Et$	$Pt^{2+}, Pd^{2+}, Rh^{3+}$	35,36,37
	n=1,2,3	Ru^{2+}	
	$Ph_2PCH_2CO_2Et$		
sulphonate	$Ph_2P(m\text{-}C_6H_4SO_3)^-$	Rh^+	38
carboxylic acid	$Ph_2PCH_2COO^-$	$Ni^{2+}, Pd^{2+}, Pt^{2+}$	39,40,41
		Rh^+, Zr^{4+}, Zr^{3+}	42,43,44, 45,46,47

Most importantly the "hemilabile" nature of the hard oxygen donor in some complexes of soft metals allows for the uptake of small molecules such as CO. Also the Ir(I) complex trans-[Ir(Cl)(CO){$Me_2P(O\text{-}MeOC_6H_4)$}$_2$] was considerably more labile towards oxidative addition than trans-[$IrCl(CO)(PMe_2Ph)_2$] because of the interaction between oxygen and metal.

The interesting reactivity of complexes of phosphorus-oxygen hybrid ligands has in fact resulted in their application as catalysts in some industrial processess. In the Shell ethylene oligomerization process[47] a Ni(II) complex of diphenylphosphinoacetic acid, 1-59, is used as a catalyst. This complex is prepared by reduction of a nickel salt in the presence of the phosphine-carboxylic acid.[48]

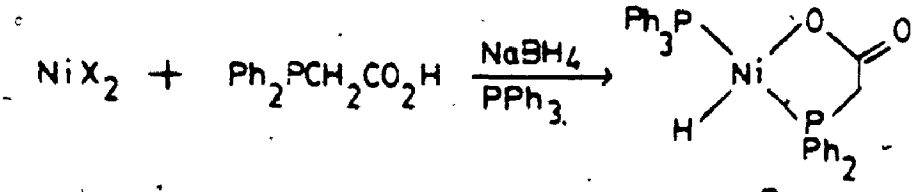

1-59

Typically, this catalyst is allowed to react with ethylene in ethylene glycol at about 100°C and 40 atm. pressure. The product of the reaction is a mixture of linear α-olefins. The readily marketable C_{10}-C_{18} olefins can be separated by distillation.

Complexes of phosphorus-oxygen hybrid ligands have also been applied in asymmetric catalytic synthesis as in the

Monsanto L-dopa synthesis.[49] In this process, hydrogenation of the prochiral olefin 1-60, a substituted cinnamic acid, yields L-dopa, a drug used in the treatment of Parkinsons' disease. The use of a chiral ligand, in this case a chelating phosphine with oxygen functional groups such as 1-61,[50] causes the olefin to bind to the catalyst in a preferred conformation. The active catalyst in the reaction is described as an octahedral Rh(III) species 1-62, where the phosphines are cis and the remaining four sites are in dynamic equilibrium with substrate, product, H_2, solvent and possibly vicinal methoxy groups.[50]

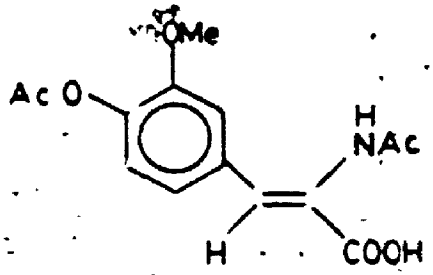

1-60

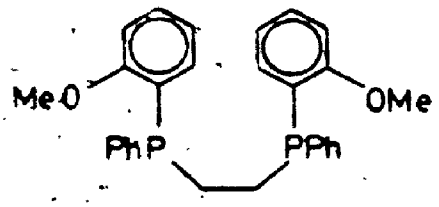

1-61

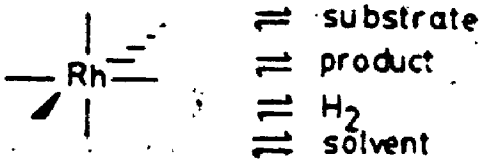

1-62

1.4 Scope of the Thesis

This thesis describes a detailed study on the coordination chemistry of a single compound; a novel hybrid ligand containing a phosphino group and a fluorinated alkoxide. Chapter 2 describes the synthesis of the ligand

itself, along with an overview of the complexes prepared from it. In chapter 3, the chemistry of the many complexes which the ligand forms with platinum(II) is discussed in more detail. X-ray crystal structures of two of the platinum(II) complexes discussed in chapter 3 are presented in chapter 4. In chapter 5, the chemistry of complexes formed by the ligand with palladium(II) are discussed, together with a crystal structure of one of the complexes. Chapter 6 contains a detailed study of a single nickel(II) complex of the ligand, including its crystal structure. In chapter 7, the experimental details of the preparation of all of the compounds discussed in the thesis are given. Finally, chapter 8 contains the thesis summary and conclusions.

Table 1.3 List of Abbreviations

H_2PFP	perfluoropinacol
COT	cyclo-octatetraene
Bu^t or t-Bu	tertiary butyl
Me	methyl
Ph	phenyl
Et	ethyl
Pr^i or i-Pr	iso-propyl
dmba	dimethylbenzylamine
cp	cyclopentadienyl
HFA	hexafluoroacetone
TMED	N,N,N',N'-tetramethylethylenediamine
THF	tetrahydrofuran
Py	pyridine
acac	acetylacetonate anion
hfac	hexafluoroacetylacetonate anion
tfac	trifluoroacetylacetonate anion
Bu^n or n-Bu	primary butyl
bipy	α,α'-bipyridyl
phen	ortho-phenanthroline
DMF	dimethylformamide
dppm	bis(diphenylphosphino)methane
dppp	bis(diphenylphosphino)propane
dppe or dpe	bis(diphenylphosphino)ethane
COD	cyclo-octadiene
etu	ethylenethiourea

Table 1.3 Continued

detu	N,N'-diethylthiourea
cyclam	1,4,8,11-tetraazacyclotetradecane
pdta	o-phenylenebis(di-p-tolylarsine)
pdpa	o-phenylenebis(diphenylarsine)
diarsine	o-phenylenebis(dimethylarsine)
2,3-lut	2,3-lutidine

Chapter 2

Preparation of the Ligand and its Complexes

2.1 Introduction

Hybrid ligands combining a tertiary phosphine and an oxygen donor group have attracted considerable attention. The combination of hard and soft donors has allowed these ligands to coordinate to a wide range of metals. A variety of modes of coordination have been exhibited by the P,O hybrid ligands in these complexes, while some of the metals exist in unusual oxidation states.

In addition, the complexes have displayed some interesting reactivity, including in some cases the "hemilabile" behaviour of the oxygen donor which allows for its displacement by small molecules. A number of industrial processes make use of the reactivity of these complexes by employing them as catalysts.

While many different functional groups have served as oxygen donors, no report has yet appeared of an alkoxide in combination with a phosphine. It was therefore the intention of this work to prepare a ligand combining a fluorinated alkoxide with a tertiary phosphine in order to extend both the chemistry of fluorinated alkoxides and that of P,O hybrid ligands.

2.2 Ligand Synthesis

2.2.1 Synthesis of HL^1

The carbonyl group of hexafluoroacetone is highly

electrophilic due to the strong electron withdrawing ability of the CF_3 groups.[51] As a result, the ketone would be expected to react readily with nucleophiles such as organolithium reagents, and such reactivity has been demonstrated in earlier studies of hexafluoroacetone.[52]

The product of such a reaction is a fluorinated tertiary alcohol, $RC(CF_3)_2OH$, where the R group can be alkyl or aromatic, fluorinated or unfluorinated.[53,54]

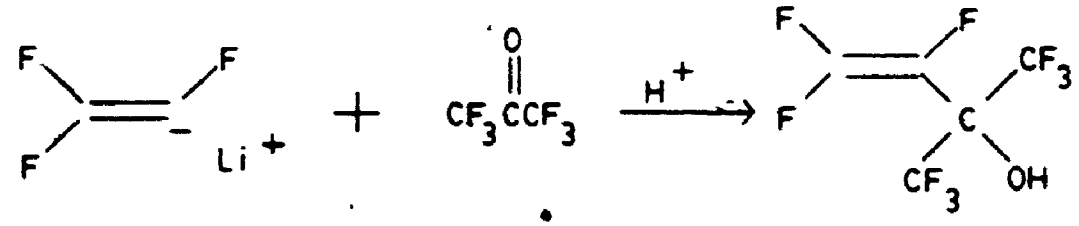

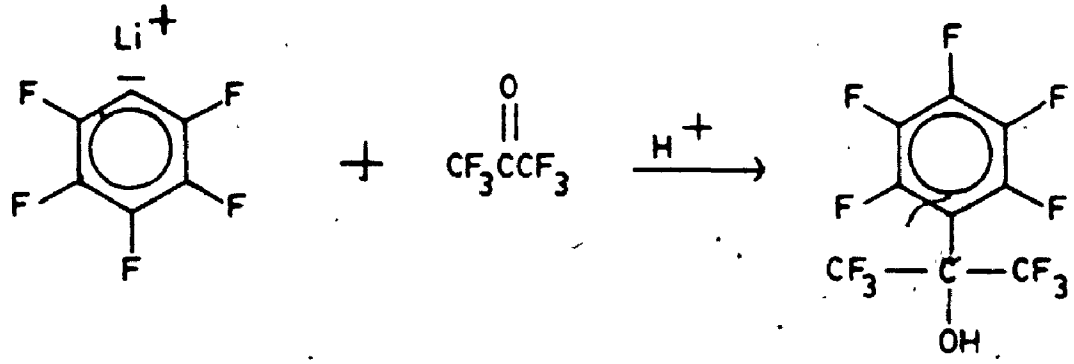

More recently, in such syntheses, the R group of the organolithium reagent has contained another functional group so that the product obtained is a potential hybrid ligand containing both a hard fluorinated alcohol and a second donor site. A number of fluorinated alcohol-thioethers have been so prepared.[17]

$$RSCH_3 + n\text{-}BuLi\cdot TMED \rightleftharpoons RSCH_2Li\cdot TMED + C_4H_{10}$$

$$RSCH_2Li + HFA \xrightarrow[2.\ H^+/H_2O\ 0°C]{1.\ \text{ether},\ -78°} RSCH_2C(CF_3)_2OH$$

R = Ph, CH_3, Bu^t

Attempts were made to extend this series of hybrid ligands to include other chalcogenoether species. However, while the reaction appears to proceed to the desired product, in the case of selenoethers,[55] workup to isolate the product was difficult.

Peterson was able to prepare a number of phosphinomethyllithium compounds.[56] Diphenylmethylphosphine was rapidly metallated at room temperature by the 1:1 complex of n-butyllithium and tetramethylethylenediamine (TMED), described by Eberhardt and Bute.[57] After two hours, the yield is 70% for the monometalated phosphine compared with 84% after one hour. This illustrates the problem of secondary metallation. Phosphorus-31 NMR and mass spectrometry were used to identify dimetalated products in the lithiation of dimethylphenylphosphine with t-butyllithium.[58] The initial step involves a selective lithiation of the methyl group followed by a non-selective second lithiation involving the second methyl group or the phenyl group.

The yields obtained for the lithiation of methyldiphenylphosphine with the n-butyllithium-TMED complex are considerably higher than those for metallation using t-butyllithium (36% after 312 hours).[59] The decreased reactivity using t-butyllithium has been attributed to

steric factors.

Methyldiphenylphosphine was chosen initially as the phosphine for the lithiation and subsequent reaction with hexafluoroacetone (HFA) for a number of reasons:

1) Peterson showed that the order of reactivity of the phosphines towards lithiation by the n-butyllithium TMED complex is Ph_2PMe > $PhPMe_2$ > $(C_{12}H_{25})PMe_2$.[56] That methyldiphenylphosphine is the most reactive would be expected since the greater electron-withdrawing effect of the aryl groups over the alkyl groups increases the ease with which the proton is removed. Also the aryl groups would have the effect of contracting the normally diffuse phosphorus d-orbitals[60] to give better overlap with the carbanion.
2) The tendency towards oxidation of the phosphine or the ligand product would also be lessened by the electronic effect of the phenyl groups.
3) Dimetallation is less of a problem with only one methyl group present.
4) Initially, one would desire to attempt the reaction with an achiral phosphine.
5) There is an abundance of complexes known with Ph_2PR ligands available for purposes of comparison.
6) Methyldiphenylphosphine is a readily available compound.

Meek et al[19] had used P-lithiated phosphines to prepare hybrid ligands.

$$PhPH_2 + n\text{-}BuLi \longrightarrow PhP(H)Li + n\text{-}BuH$$

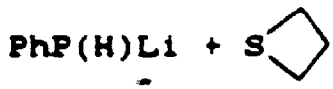

$$2PhP(H)CH_2CH_2CH_2S^-Li^+ + Br(CH_2)_3Br \rightarrow CH_2[CH_2S(CH_2)_3PPhH]_2$$

However, the use of lithiated phosphino methyl groups in hybrid ligand synthesis is not such a well-known route. It seemed likely that the reaction of such an intermediate with hexafluoroacetone should indeed lead to a compound containing a diarylphosphino group and a fluorinated alkoxide, and therefore this approach was used.

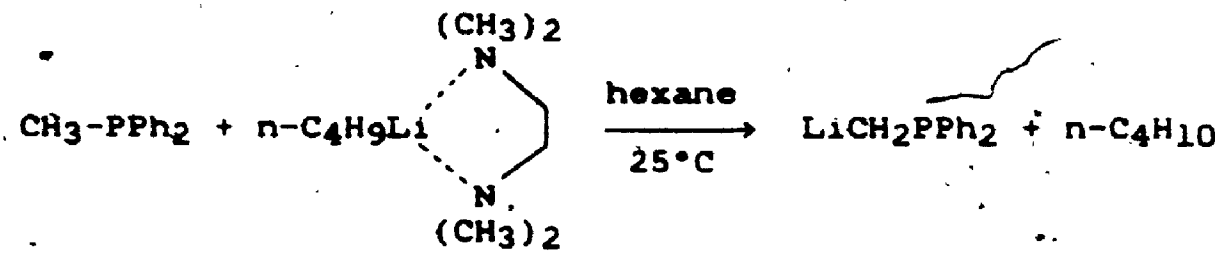

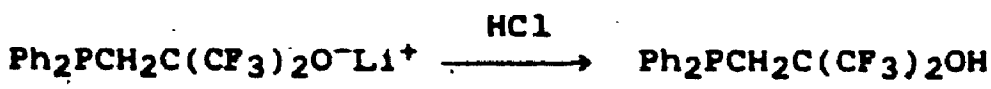

Because of the high reactivity of the lithiated phosphine, its reaction with hexafluoroacetone was rapid at -78°C.

Hexafluoroacetone is known to react with tertiary phosphines with reductive dimerization to give cyclic

phosphoranes, 2-1.[61]

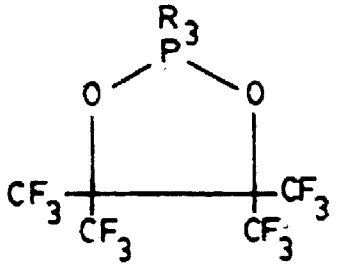

2-1

Although no spectroscopic evidence was found for the production of such a species in the ligand synthesis, the highest yield of ligand was obtained when only a slight excess (~3%) of HFA was used. Larger excesses resulted in lower yields.

The product of the synthesis, $Ph_2PCH_2(CF_3)_2OH$, HL^1, is a waxy, colourless, low-melting solid obtained in 52% yield. It shows little tendency to oxidize in air. The ^{31}P NMR spectrum shows a septet at -33.6 ppm due to coupling to the six equivalent fluorine nuclei. The value of $^4J(P,F)$ is 16.5 Hz. The NMR data are given in Table 2.1.

The major contaminant appeared in the ^1H NMR as a doublet at δ = 2.86 ppm and $^2J(P,H)$ = 11.8 Hz. The effect of oxidation of a tertiary phosphine on the methylene protons is to cause a downfield shift in the resonance position, along with a decrease in the $^2J(P,H)$ value. For example, the chemical shift of the methylene protons in $P(Et)_3$ is 1.27 ppm and $^2J(P,H)$ = 0.5 Hz.[62] On oxidation to $O{=}P(Et)_3$ however these values become 1.65 ppm and 11.9 Hz respectively.[63] The sign of $^2J(P,H)$ is believed to be

Table 2.1 NMR Data[a]

Compound	Solvent[b]	^1H (CH_2) δ ppm	$^2J(P,H)$ Hz	^{19}F (CF_3) δ ppm	$^4J(P,F)$ Hz	^{31}P δ ppm	Δδ[c] ppm
HL^1	C	2.83(d)	<1	-77.4(d)	16.5	-33.6	-
$HL^1(=O)$	C	2.86(d)	11.8	-	-	-	-
$HL^2(=O)$	C	2.54(d)[d]	12	-	-	-	-
$Cu(PPh_3)_2(L^1)$	C	2.85(d)	9.5	-77.8	6.8	-20.7[e]	+12.9
$K[Rh(L^1)_2Cl_2]$	A	3.80(d)	13	-77.4	-	+30.0[f]	+65.6

a at ambient temperatures

b C = $CDCl_3$; A = $(CD_3)_2CO$

c the coordination shift, $\Delta\delta = \delta_{coord} - \delta_{free}$

d CH_3 signal at 1.94 ppm (doublet) $^2J(P,H)$ = 13.5 Hz

e PPh_3 signal at -4.2 ppm (singlet)

f doublet, $^1J(Rh,P)$ = 115 Hz

negative for both $HL^1(=O)$ and the example, $O=PEt_3$, in keeping with the expected decrease in $^2J(P,H)$ on oxidation. This will be discussed further in chapter 3.3.7.

Therefore the contaminant was tentatively identified as the oxide of the ligand, $Ph_2P(=O)CH_2C(CF_3)_2OH$, $[HL^1(=O)]$.

2.2.2 Other Ligands

An obvious extension of this ligand synthesis would be to use as a starting material a prochiral phosphine. This was attempted using $PhPMe_2$ which, after lithiation and reaction with HFA, would be expected to give the chiral ligand $PhP(CH_3)CH_2C(CF_3)_2OH$. However by replacing the one phenyl group with a methyl group, the ease with which the starting material and final product can be oxidized is increased dramatically. As a result, when the synthesis is carried out using $PhPMe_2$ under the conditions used successfully with Ph_2PMe the only product obtained is the ligand oxide, $PhP(Me)(=O)CH_2C(CF_3)_2OH$ $[HL^2(=O)]$. The NMR data for this compound also appear in Table 2.1.

Clearly since Peterson was able to lithiate $PhPMe_2$ easily using n-butyllithium and TMED, then the preparation of the ligand is possible. However future attempts must be carried out under rigorously oxygen-free conditions.

2.3 Complexes of Co^{2+}, Cu^{2+}, Cu^{+} and Rh^{3+}

2.3.1 Introduction

The ligand L^1 contains a phosphino group and a fluorinated alkoxide and therefore serves primarily as a bidentate uninegative ligand coordinating through phosphorus and oxygen. The ability of the ligand to act as a monodentate donor will be shown in later chapters, however in this chapter the complexes will all involve L^1 as a bidentate ligand.

The general route to the bischelate complexes involves dissolving the metal dichloride in an appropriate solvent, usually ethanol, adding the ligand in the protonated form followed by base in the form of a standardized ethanolic solution of KOH.

$$MCl_2 + 2HL^1 + 2KOH \longrightarrow \left[\begin{array}{c} Ph_2 \\ P \\ M \\ O \end{array}\!\!\begin{array}{l} \\ \\ \\ CF_3 \\ CF_3 \end{array}\right]_2 + 2KCl$$

The KCl was removed and workup of the solution produced the tetracoordinate bischelate complexes.

In the case of Cu(I), $[Cu(PPh_3)_3Cl]$ was used as the starting material and addition of one equivalent of HL^1 with base displaced a triphenylphosphine ligand and a chloride ligand.

$$Cu(PPh_3)_3Cl + HL^1 + KOH \longrightarrow Cu(L^1)(PPh_3)_2 + KCl + PPh_3$$

$RhCl_3 \cdot 3H_2O$ was used as a starting material for the Rh(III) complex.

$$RhCl_3 + 2HL^1 + 2KOH \longrightarrow K[Rh(L^1)_2Cl_2] + KCl$$

In each case the complex was characterized by elemental analysis (Table 7.1) and mass spectrometry (Table 7.2). Infrared spectroscopy was used primarily to confirm the presence of L^1 in the complex by detection of the strong C-F stretching mode at ~1200 cm^{-1}. NMR data for the complexes and HL^1 appear in Table 2.1, for those cases which are diamagnetic. Visible spectral data appear in Table 2.2.

2.3.2 $Co(L^1)_2$

A complex was prepared by reacting $CoCl_2 \cdot 6H_2O$ with two equivalents of ligand in ethanol. Mass spectrometry along with elemental analysis were used to characterize the complex as $[Co(Ph_2PCH_2C(CF_3)_2O)]$. However the compound as expected was paramagnetic and therefore NMR methods could not be applied to it.

Four-coordinate Co(II) can exist either in a tetrahedral or square planar geometry. The d-electron configuration of cobalt(II) causes the ligand field stabilization energy to favour octahedral stereochemistry over tetrahedral to a lesser extent than for any other d-electron configuration. As a result, tetrahedral complexes of

Table 2.2 Visible Spectra

Compound	Solvent	Absorption Maxima ^{a} (cm^{-1})
$Co(L^1)_2$	CH_2Cl_2	24600 (179) 202000 (70)
"	Py	22,100(76) 16,300 (26)
$Cu(L^1{=}O)_2$	$(CH_3)_2CO$	14,500 (58)
$K[Rh(L^1)_2Cl_2]$	$(CH_3)_2CO$	23000 (380)

Co(II) are more numerous than those of other d^1–d^9 transition metal ions.

Complexes of the type CoL_2X_2 having two monodentate anionic ligands, such as Cl^-, Br^-, I^-, OH^- and SCN^- and two neutral monodentate ligands are tetrahedral.[64] Complexes having two bidentate anionic ligands such as L^1, can be either tetrahedral, as in the case with bulky β-diketonate anions (2-2)[64] or square planar as in the case with dimethylglyoximate (2-3).[64]

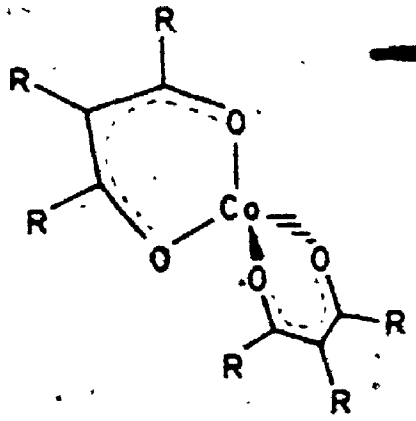

2-2

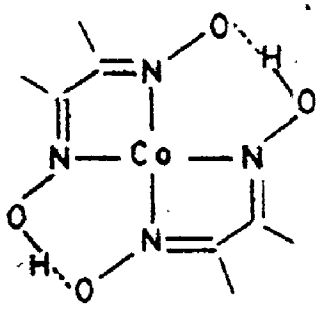

2-3

Since it is only by the introduction of chelating ligands that deviation from tetrahedral geometry is observed for four-coordinate Co(II) complexes, it appears that the combination of electronic factors and steric interactions favour tetrahedral geometry. Only for reasons of minimization of ring strain energy for certain bidentate ligands is square-planar geometry observed.

For tetrahedral Co(II) the most common colours are blue and green. The dominant band in the visible spectrum is

from 14,000 to 18,000 cm^{-1} with an extinction coefficient of 15,000 or greater.[65]

Square-planar complexes of Co(II) exhibit a band near 20,000 cm^{-1} (ϵ = 300 l cm^{-1} $mole^{-1}$).[74] Examples of visible spectra for tetrahedral and square-planar Co(II) complexes are given in Tables 2.3 and 2.4 respectively.

$Co(L^1)_2$ is orange-red in colour and displays an absorption band at 24,600 cm^{-1} (ϵ = 179 cm^{-1} mol^{-1}) (see Fig. 2.1). It has therefore been assigned a square-planar geometry. In support of this, when pyridine is added to a solution containing $[Co(L^1)_2]$, a green complex is obtained which is consistent with coordination of the pyridine to the square-planar complex to give a five-coordinate or six-coordinate complex. Since no six-coordinate complex of Ni(II) or Cu(II) of a fluorinated alkoxide has been prepared (presumably because of the steric bulk of the CF_3 groups), it can be assumed that the complex with pyridine is also five-coordinate.

Because of the lower extinction coefficient of the absorption band for $[Co(L^1)_2]$, it is believed that the complex is in the more symmetrical trans-square-planar geometry. This is consistent with the solid-state structure of $[Ni(L^1)_2]$ which will be discussed in chapter 6.

2.3.3 Attempt to Prepare $Cu(L^1)_2$

Since it was possible to prepare the complex

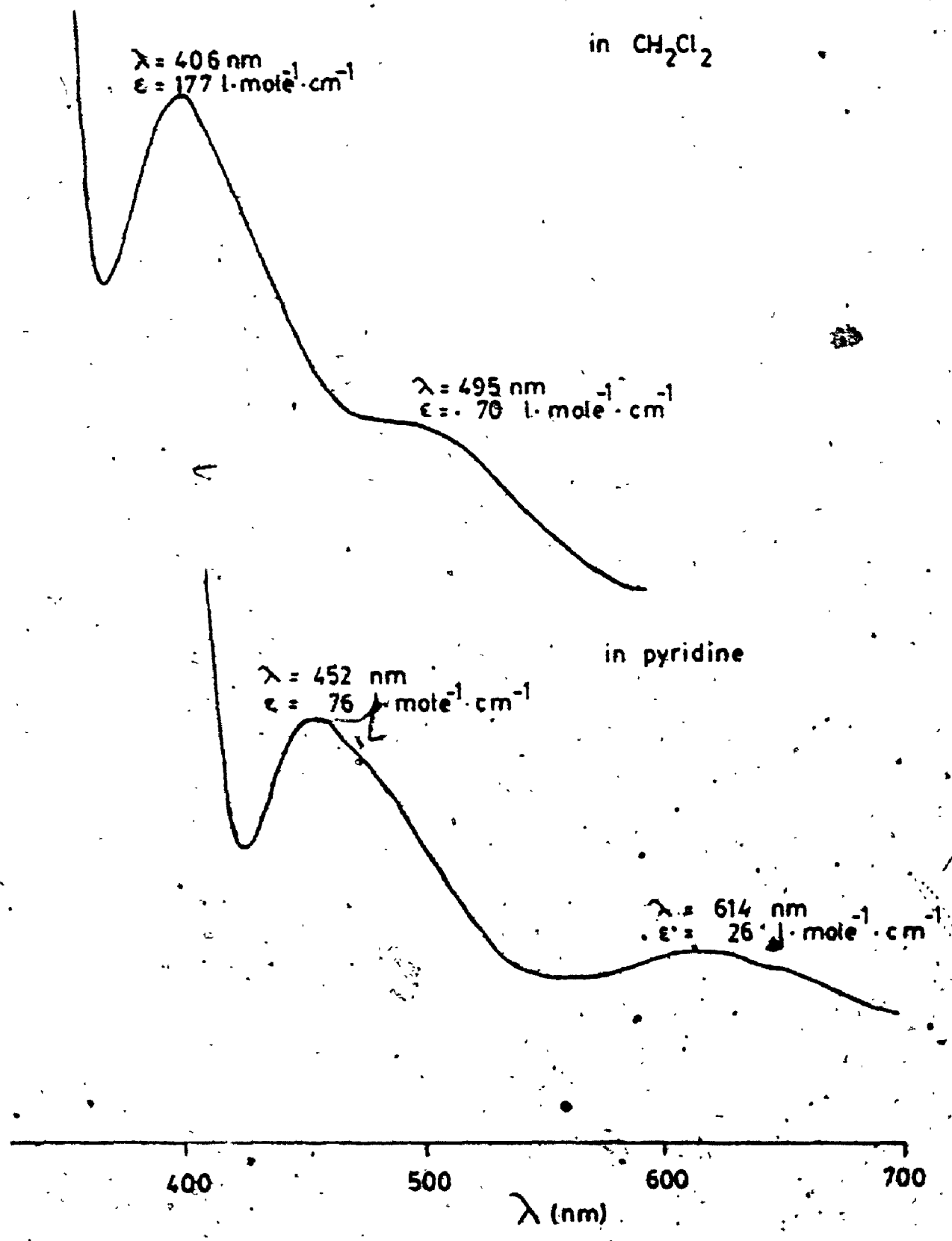

Figure 2.1 Visible spectra of $\{Co(L^1)_2\}$

Table 2.3 Visible Spectra of Tetrahedral Cobalt(II) Complexes

Complex	$^4T_1(F)$	$^4T_1(P)$	Ref
$Co(PPh_3)_2Cl_2$	6400,8000	13600,15800,16700	66
$Co(Ph_3AsO)_4^{2+}$	6490 (72)	16670 (395),17300	67
$Co(Ph_3AsO)_2Cl_2$	5240(60),5780(65)	14810(536),16000	68
$Co(TMED)Cl_2$	6000,7250	15400,17200	69
$Co(4\text{-}EtPY)_2BR_2$	9265 (71)	16690 (502)	70
$Co(NH_3)_4^{2+}$	5900($^4T_2$) 10000($^4T_1$)	16000,18000,19200	71

Table 2.4 Visible Spectra of Square-Planar Cobalt(II) Complexes.

Complex	Absorption Bands	Ref
Co(trans[1,4]diene)	6300(35),22400(130), 29800(2500)CT	72
$Co(acac)_2(-)pn$	3970(96),4300,4870,5550(16), 8500(20),20,600(1100),22000, 26800(6500)	73
$Co(aba)_2(-)pn$	5100(18),6250(22),6900, 11,050(73),11,900,16,670(370) 18,900(5000)	73

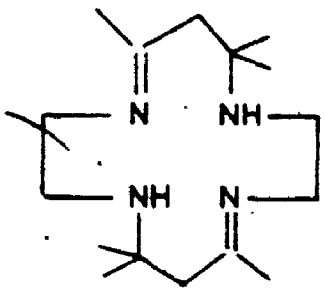

trans [1,4] diene

$(acac)_2(-)pn$ (diketone Schiff base)

$(aba)_2(-)pn$ (diketone Schiff base)

$Co(L^1)_2$, it seemed likely that L^1 would also coordinate to the equally hard transition-metal ion, Cu(II). The affinity of Co^{2+}, Ni^{2+}, Cu^{2+} towards oxygen donors such as fluorinated alkoxides is well-known.[75] However attempts to prepare the bis-complex of Cu(II) by the same method as with Co(II) were unsuccessful. Discolouration of the solution resulted and workup produced a blue complex which was identified by mass spectrometry and by elemental analysis as the copper complex of the ligand oxide $Ph_2P(=O)CH_2C(CF_3)_2O^-$.

Oxidation of phosphines by Cu(II) is well-known process. Copper(II) chloride oxidizes both triethyl- and triphenyl-phosphine resulting in a variety of oxidation products. For the reaction with triethylphosphine,[76] the fundamental oxidation-reaction process is:

$$(C_2H_5)_3P + 2CuCl_2 \rightarrow (C_2H_5)_3PCl_2 + 2CuCl.$$

However, these products can react with each other to give products including $[CuCl(Et_3P)_n]$ (n = 1,3). The reaction products for the oxidation of PPh_3 with $CuCl_2$ in acetone vary depending on the ratio of reactants. A 1:1 ratio results in Ph_3PO,[b] $[CuCl_2(Ph_3PO)_2]$, $[CuCl_2(Ph_3PO)\cdot 2H_2O]$ and $[Cu_4OCl_6(Ph_3PO)_4]$, while a 1:4 copper:phosphine ratio produces copper(I) complexes $[CuCl(PPh_3)_3]$ and $[CuCl(PPh_3)_2]$.[77] So it is not uncommon for the oxidized phosphine to coordinate to remaining Cu(II) as occurred in

the reaction of L^1.

Unlike copper(I), there are very few examples of copper(II) tertiary phosphine complexes. Among the few that are known are those with fluorinated acetylacetonate anion ligands such as $Cu(hfac)_2L$ and $Cu(tfac)_2L$ (where hfac = hexafluoroacetylacetonate anion, tfac = trifluoroacetylacetonate anion and L = Ph_3P, $MePh_2P$, Me_2PhP, Et_3P, $Bu^n{}_3P$).[78]

Since, with very few exceptions, neutral copper(II) complexes having a chelating ligand are square-planar in their coordination geometry, this is assumed to be the case also for $[Cu(L^1{=}O)_2]$. It is the strong Jahn-Teller distortion accompanying a d^9 configuration which makes square-planar geometry so common for Cu(II) complexes. The blue colour of $[Cu(L^1{=}O)_2]$ in the solid state is typical of square-planar Cu(II). However when taken up into solution, the initial blue colour changes with time to green, presumably as the complex becomes five-coordinate. This is seen in both donor solvents (acetone, pyridine) and with non-donor solvents ($CHCl_3$, CH_2Cl_2) suggesting that the complex in the absence of a donor solvent picks up a molecule of water in the fifth coordination site.

2.3.4 $Cu(PPh_3)_2L^1$

Since the attempt to make a Cu(II) phosphine complex was not successful, an attempt was made to synthesize a phosphine complex with the softer Cu(I) metal ion. It was

hoped that the presence of the phosphorus in the chelate ring, along with the chelate effect itself, would help to stabilize the bond from oxygen to Cu(I).

There are few examples of Cu(I) alkoxides[79,80,81] known; those that have been prepared are accessible via two general routes:

$$CuCl + LiOR \rightarrow LiCl + CuOR$$

$$(CuMe)_n + nROH \rightarrow nCuOR + nCH_4$$

The copper(I) phosphine halide complexes, $CuXL_m$, are numerous and have been the subject of considerable study because of the various possible structures available to them. Trimethylphosphine complexes of copper(I) can be: tetrameric, $[CuCl(PMe_3)]_4$; dimeric, $[CuCl(PMe_3)_2]_2$; monomeric, $[CuCl(PMe_3)_3]$ and possibly ionic $[Cu(PMe_3)_4]Cl$.[82]

The monomeric tetrahedral complex $CuCl(PPh_3)_3$ was used as the starting material for the reaction with HL^1. By adding an excess of HL^1 followed by KOH, it was hoped that L^1 would replace a PPh_3 and a chloride ion in the complex. This substitution proved successful, resulting in the complex $[Cu(L^1)(PPh_3)_2]$, 2-4.

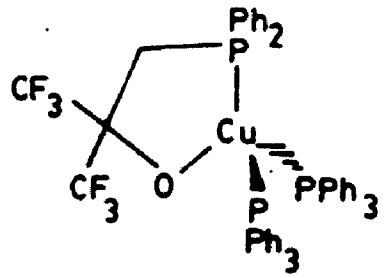

2-4

The ^{31}P NMR spectrum of the complex (see Table 2.1) showed two signals at -4.2 and -20.7 ppm due to the triphenylphosphine and L^1 respectively. As expected the ratio of the area under the signals obtained by integration was ~2/1.

Surprisingly, the two signals in the proton-decoupled ^{31}P NMR spectra both appeared as singlets; there was no observed coupling between the triphenylphosphine phosphorus nuclei and that of L^1, even when a sample was cooled down to 0°C. On the other hand, the ^{1}H and ^{19}F NMR spectra showed coupling of the phosphorus nucleus in L^1 to both the methylene protons and the fluorine nuclei of 9.5 Hz and 6.8 Hz respectively. These couplings are of two and four bonds respectively and their appearance makes the absence of any $^{2}J(P_A,P_B)$ type coupling to be all that much more surprising.

A possible explanation is that the triphenylphosphine ligands are involved in a process of rapid exchange with free triphenylphosphine in solution. Such a phenomenon is not unknown for Cu(I) phosphine complexes. Lippard and Mayerle[83] used osmometry to measure the extent of dissociation of complexes of the type, $[(PPh_{3-n}Me_n)_3CuX]$ (n = 0,1,2; S = Cl, Br, I). It was found that the extent of dissociation followed the order $[(PPh_3)_3CuX] > [(PPh_2Me)_3CuX] \approx [(PPhMe_2)_3CuX]$ thus eliminating the possibility of ligand basicity being the major factor determining the stabilites. Were basicity the predominant governing factor, then one would expect $[(PPh_2Me)_3CuX]$ to

be less stable than $[(PPhMe_2)_3CuX]$. It would seem that the stabilities are controlled by steric factors rather than electronic factors. The solid state structure of $[(PPh_2Me)_3CuCl]$ shows the methyl groups directed towards the chloride.[84] If this structure persists in solution, then substitution of a phenyl for a methyl group in each phosphine should lead to a considerable increase in L-L and L-Cl interactions, decreasing complex stability, while substitution of methyl for phenyl should have little effect. Such an argument does explain the observed stabilities. In addition tricyclohexylphosphine, a very basic but sterically demanding phosphine, does not form a complex of the type $[L_3CuX]$.

Returning to the complex $[(PPh_3)_2CuL^1]$, one would expect the bidentate ligand L^1, with two aryl groups bonded to phosphorus along with the two bulky CF_3 groups in the chelate ring backbone, to be a very sterically demanding ligand. This is supported by the experimental observation that dissociation of the triphenylphosphines occurs even at 0°C.

What is also unusual about the ^{31}P NMR data for this complex is the value of $\Delta\delta$, the coordination shift, which for L^1 is smaller here than for any other complex prepared in this study. The coordination shift represents the difference in chemical shift of the coordinated phosphine and the free phosphine.

$\Delta\delta$ = (δ complex - δ free ligand)

The value of the coordination shift for the phosphorus nucleus in L^1 is +12.9 ppm in comparison with values up to 74.2 ppm for other complexes presented here.

There are two possible explanations for this observation. First of all, Cu(I) is a much more electron-rich metal than the other metals [(Pt(II), Pd(II), Ni(II), Rh(III)] in complexes of this study where large values of $\Delta\delta$ were obtained. Coordination of a phosphine to an electron rich d^{10} metal would be expected to result in weaker metal-phosphine bonding and considerably less deshielding than in a more electron-deficient metal centre. This is seen by comparing $\Delta\delta$ for PEt_3 in $[Cu(PEt_3)_3Cl]$ (+4.8 ppm)[85] with the value in the complex trans-$[Pd(PEt_3)_2Cl_2]$ (+37.3 ppm).[86] Also the value of $\Delta\delta$ for the triphenylphosphine in $[Cu(PPh_3)_2L^1]$ appears to be considerably less than in trans-$[Pt(PPh_3)_2Cl_2]$ (+26.0) or cis-$[Pt(PPh_3)_2Cl_2]$ (+19.4 ppm).[87] However the value of $\Delta\delta$ for the PPh_3 in $[CuL^1(PPh_3)_2]$ is not known precisely. Since fast exchange of triphenylphosphine between complex and solution is being proposed to explain the lack of ^{31}P-^{31}P coupling, yet no free triphenylphosphine signal is observed, then the ^{31}PNMR signal at -4.2 ppm must be viewed as an average of the two signals due to coordinated and free triphenylphosphine.

A second possible explanation of this low value of $\Delta\delta$

concerns the ring contribution to the coordination shift in chelating phosphines. The value of Δ_R may be obtained as the difference between $\Delta\delta$ for a cis-substituted bisphosphine complex and $\Delta\delta$ for an equivalent phosphine in a chelate complex. Garrou showed that the ring contribution leads to a deshielding of the phosphorus by 21-33 ppm in 5-membered rings but only by 2-25 ppm in 4-6 membered rings.[88]

Presumably this phenomenon where ΔR is maximized in 5-membered rings reflects a dependence of ΔR on the bite angle of the chelating ligand. Therefore as the molecular geometry is changed from square-planar or octahedral to tetrahedral, as in the case of $[Cu(PPh_3)_2L^1]$, the bite angle of L^1 is forced to increase and one might expect an accompanying decrease in ΔR and hence $\Delta\delta$.

2.3.5 $K[Rh(L^1)_2Cl_2]$

An anionic Rh(III) complex was prepared by the reaction of an excess of HL^1 with $RhCl_3 \cdot 3H_2O$ and the appropriate amount of KOH. Elemental analysis and mass spectrometry were used to determine the molecular formula as $K[Rh(L^1)_2Cl_2]$.

For such a complex there are five different possible geometrical isomers, three of which are chiral. Since the ^{31}P NMR spectrum of the complex shows only one signal at +32.0 ppm with $^1J(P,Rh)$ = 115 Hz then one can eliminate those geometries with inequivalent phosphorus nuclei and

geometries with mutually trans phosphorus nuclei. That is, both phosphorus nuclei must be trans to Cl^- or both trans to $-C(CF_3)_2O^-$ rather than trans to each other. In complexes of the type mer-$[RhCl_3(PR_3)_3]$, values of $^1J(P,Rh)$ are in the range 111-115 Hz for P trans to Cl^- but 83-86 Hz for P trans to another phosphine.[89]

The anionic complex therefore displays cis phosphines, and either cis chlorides and trans alkoxides, 2-6, or trans chlorides and cis alkoxides, 2-7.

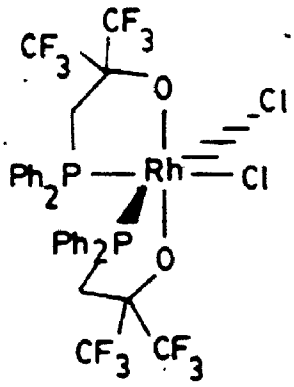

2-6

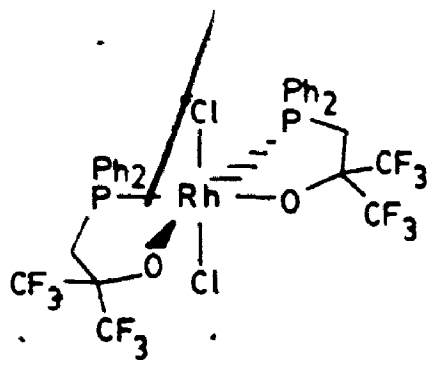

2-7

If the chlorides are cis, as in 2-6, then the complex is chiral while the geometry 2-7 has a mirror plane in the P_2O_2 plane and is therefore achiral. Both ^{31}P and ^{19}F spectra run in a chiral solvent, ethyl l-lactate, still showed only one signal. While it may be that the difference in the chemical shifts of the two enantiomers in a chiral solvent is too small to resolve, the evidence would suggest that the chlorines are mutually trans. The complex has therefore been assigned the geometry 2-7.

Such a geometry is consistent with that assigned to

$[Ru(O\text{-}Ph_2PC_6H_4CHO)_2Cl_2]$ and $[Ru(O\text{-}Ph_2PC_6H_4OCH_3)_2Cl_2]$.[24] The geometry of the former was determined by IR spectroscopy, which indicated that the chlorines were mutually trans, and ^1H NMR, which showed a "filled in doublet" virtual coupling pattern for the formyl protons, characteristic of coupling to a trans phosphorus nucleus. The second complex was characterized by X-ray crystallography studies. Both of these complexes possess a $Cl_2P_2O_2$ donor set on Ru(II) which is, of course, isoelectronic with Rh(III). Therefore the geometry of these complexes helps to confirm the proposed geometry of the Rh(III) complex in this study.

2.4 Other Complexes of L^1

In addition to the complexes already discussed, a number of complexes were prepared using the metals of the nickel triad: Ni, Pd and Pt. For each metal a bischelate complex, $M(L^1)_2$ was prepared. In the case of Pt and Pd these two complexes displayed extensive chemical behaviour and therefore they will be discussed in more detail in chapters 3 and 4 (for Pt) and 5 (for Pd). In the case of Ni, only the bischelate complex was prepared. However, this complex displayed some very interesting properties both in solution and in the solid state and it is discussed at length in chapter 6.

It is clear from this discussion of the range of complexes and the metals to which L^1 will coordinate that the ligand is indeed highly versatile. The combination of the phosphino group with the fluorinated alkoxide succeeds in causing the ligand to coordinate to metals of soft character (Pt^{2+}, Cu^{+}, Pd^{2+}) as well as those which are harder and more oxophilic (Co^{2+}, Ni^{2+} and Rh^{3+}).

Chapter 3

Platinum Complexes of HL^1

3.1 Introduction

Tertiary phosphine complexes of platinum(II) are numerous. The simplest examples are the bisphosphine complexes $[Pt(PR_3)_2X_2]$, prepared by reaction of the phosphine with the tetrachloroplatinate anion.[183] For phosphines containing alkyl groups lower than n-butyl, the ionic complex $[Pt(PR_3)_4]^{2+}$ $[PtCl_4]^{2-}$ is first formed, which then slowly converts to $[Pt(PR_3)_2Cl_2]$.[183] Although the cis-isomers have long been known to be the thermodynamically-favoured form, trans isomers have also been isolated because of the inert nature of platinum(II).[216] In a few cases involving sterically-demanding phosphines, the trans-isomer is thermodynamically favoured.[219]

The dimeric halogen-bridged complexes $[(PR_3)(X)Pt(\mu\text{-}X)_2Pt(X)(PR_3)]$ are much more difficult to prepare than their palladium analogues. The synthesis involves fusing together the monomer $[Pt(PR_3)_2X_2]$ with the platinum dihalide and as a result is dependent on the products and reactants having a high degree of thermal stability.[217,218]

Alkoxide complexes for both platinum(II) and palladium(II) are quite rare, due to the hard nature of alkoxides. The first non-fluorinated alkoxides of platinum(II) were prepared by oxidative addition of primary

alcohols to cyclohexyne complexes of platinum(0);[220,221] a typical product of the oxidative addition reaction would be $[Pt(OCH_3)(C_6H_9)(dppe)]$.

Methoxy complexes of platinum(II) could also be prepared by the metathesis of $[PtRCl(PPh_3)_2]$ with NaOMe where R = $-C_6H_5$, $-CH=CCl_2$, $-CCl=CCl_2$.[222] Both cis- and trans-isomers were prepared. Similar methoxy complexes, prepared by metathesis, were found to readily undergo hydrolysis with water and insertion of CO, COS, CS_2 and SO_2.[223]

Fluorinated alkoxides form complexes with platinum(II) when bidentate ligands such as perfluoropinacol, (PFP), are used in conjunction with soft coligands. For example, $[Pt(PFP)(PR_3)_2]$ and $[Pt(PFP)(SR_2)_2]$ have been prepared. Platinum(0) complexes such as $L_4Pt(0)$ react with HFA to give three-membered cyclic alkoxides, $[L_2\overline{PtC(CF_3)_2O}]$.[172,224] A second molecule of hexafluoroacetone can be incorporated to give $[L^2\overline{PtC(CF_3)_2O(CF_3)_2O}]$. The gem-diol, $(CF_3)_2C(OH)_2$, can also be used to prepare $[(R_3P_2\overline{PtOC(CF_3)_2O})]$ which contains a four-membered, di-alkoxide ring.[225]

Since Pt(IV) like Pt(II) is a soft acid, there are very few known Pt(IV) alkoxides. In 1958, the complex $[PtMe_3(OMe)]_4$ was reported but not fully characterized.[243] The only fully-characterized platinum(IV) alkoxides prior to this study were prepared by Monaghan and Puddephatt.[244,245] Oxidative addition of alcohols

(methanol, ethanol and isopropanol) to electron-rich platinum(II) complexes gave the platinum(IV) species, 3-1

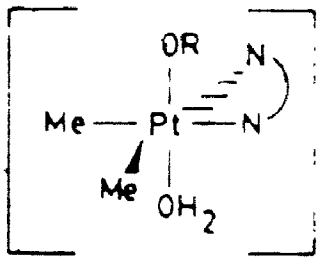

3-1

$\overset{\frown}{N\ N}$ = bipy or phen

R = Me, Et or i-Pr

By incorporating a soft donor group such as a thioether into a bidentate ligand together with a fluorinated alkoxide, it has proved possible to prepare platinum(II) alkoxide complexes.[17] This chapter will deal with further attempts to synthesis platinum(II) and platinum(IV) alkoxides by this method; the ligand HL^1 will be used to extend the chemistry of the Pt-O bond.

3.2 Synthesis of the Complexes

All of the complexes prepared in this study were characterized using elemental analysis (Table 7.1). Mass spectra were also obtained for each compound, and the results are given in Table 7.2. Infrared spectra were used to confirm the presence of L^1 in the complexes by the appearance of an intense band in the 1160 to 1190 cm^{-1}

region due to C-P stretching.

The range of platinum(II) complexes of HL^1 numbered I through VIII and their various methods of synthesis and interconversion are best illustrated by Scheme 3.1.

The compound $[Pt(L^1)_2]$, I, was prepared by the same method as that used for $[Co(L^1)_2]$ in chapter 2 as well as $[Pd(L^1)_2]$ and $[Ni(L^1)_2]$ in chapters 5 and 6 respectively. The appropriate amount of ethanolic KOH was added to a solution containing $PtCl_2$ and two equivalents of HL^1 in DMF. The product was a white solid, cis-$[Pt(L^1)_2]$, where both the ligands are ionized and chelating.

It was of interest to investigate further the chemical properties of such a complex, containing the ligand L^1. When chlorine gas was bubbled through a solution of $[Pt(L^1)_2]$ in benzene a yellow solid was obtained, which was characterized as the Pt(IV) complex $[Pt(L^1)_2Cl_2]$, VIII. However, this complex was of limited stability in solution and reverted to $[Pt(L^1)_2]$ with time. Attempts were made to prepare more Pt(IV) alkoxides by using other potential oxidizing agents (Br_2, CH_3I) but no success was achieved.

When HCl gas was bubbled through a solution of $[Pt(L^1)_2]$ in benzene the product obtained was not a Pt(IV) species resulting from oxidative addition, but rather the complex cis-$[Pt(HL^1)(L^1)Cl]$, IV. In this complex, one of the chelating ligands has been protonated at the oxygen to give a unidentate phosphine with the alcohol uncoordinated. The fourth coordination site has been

occupied by the chloride ion.

If an excess of HCl gas is bubbled through the $[Pt(L^1)_2]$ solution, both alkoxides are protonated and the product is cis-$[Pt(HL^1)_2Cl_2]$, II. This can be converted to cis-$[Pt(HL^1)(L^1)Cl]$, IV, by dissolving the compound in DMF. In fact, the compound cis-$[Pt(HL^1)_2Cl_2]$ was found to be quite unstable in solution; it would with time convert back to cis-$[Pt(HL^1)(L^1)Cl]$ even in a non-basic solvent such as CH_2Cl_2. The second alkoxide can likewise be deprotonated by treating cis-$[Pt(HL^1)(L^1)Cl]$ in DMF with one equivalent of ethanolic KOH to give cis-$[Pt(L^1)_2]$. Similarly, treatment of cis-$[Pt(HL^1)_2Cl_2]$ with two equivalents of KOH yields $[Pt(L^1)_2]$. However if only one equivalent of KOH is used in an attempt to stop at cis-$[Pt(HL^1)(L^1)Cl]$, then disproportionation occurs to give a 50% yield of $[Pt(L^1)_2]$.

Attempts to prepare complexes of the type $[M(PR_3)(L^1)Cl]$, where M = Pt(II) or Pd(II), by displacing a molecule of PR_3 and a chloride ion from $[M(PR_3)_2Cl_2]$ with L^1 were unsuccessful, leading to disproportionation to $[M(L^1)_2]$ instead. In the case of Pd(II), the dimer $[(L^1)Pd(\mu\text{-}Cl)_2Pd(L^1)]$ could be synthesized and subsequently cleaved with PR_3 to give $[Pd(PR_3)(L^1)Cl]$. However, due to the more inert nature of Pt(II), it was not possible to prepare the analogous platinum dimer.

With the isolation of cis-$[Pt(HL^1)(L^1)Cl]$, a route to $[Pt(PR_3)(L^1)Cl]$ complexes, VI, became available. The

monodentate phosphine. HL^1, could be replaced by another monodentate phosphine, PR_3. This was done using PPh_3, PPh_2Me, $PPhMe_2$ and PMe_3 to give the appropriate mixed ligand complexes, all with cis-phosphines.

The complex cis-$[Pt(HL^1)(L^1)Cl]$ can be prepared directly by the reaction of an excess of HL^1 with $PtCl_2$ in DMF. The solvent alone is sufficiently basic to cause ring closure. If this same reaction is carried out with $PtCl_2$ as the excess reagent, then the trans isomer, trans-$[Pt(HL^1)(L^1)Cl]$, V, is formed.

The complex trans-$[Pt(HL^1)(L^1)Cl]$ can be converted to the cis-isomer by dissolution in DMF along with excess ligand, HL^1. Also treatment of the trans isomer with PR_3 yields cis-$[Pt(PR_3)(L^1)Cl]$. As with the cis-isomer, treatment of trans-$[Pt(HL^1)(L^1)Cl]$ with KOH causes the uncoordinated alcohol to be deprotonated giving a second chelate ring and the product cis-$[Pt(L^1)_2]$. Also like the cis-isomer, treatment of trans-$[Pt(HL^1)(L^1)Cl]$ with HCl causes the second chelate ring to open up to give $[Pt(HL^1)_2Cl_2]$ which in this case however has a trans geometry, III.

Trans-$[Pt(HL^1)_2Cl_2]$, III, can be prepared directly from $PtCl_2$ by dissolving the metal dichloride in CH_3CN with two equivalents of HL^1. As with the cis isomer, addition of two equivalents of KOH causes both rings to close to give cis-$[Pt(L^1)_2]$. Also like the cis-isomer, the ring closure can be stopped half-way giving trans-$[Pt(HL^1)(L^1)Cl]$ by

dissolving the complex in DMF. However unlike the cis-isomer, trans-[$Pt(HL^1)_2Cl_2$] is stable in non-basic media. Heating a solution of trans-$Pt(HL^1)_2Cl_2$ in DMF, however, results in ring-closure and subsequent displacement of the remaining monodentate HL^1 by DMF. The products were not isolated, but were characterized by ^{31}P NMR as cis- and trans-[$Pt(DMF)(L^1)Cl$].

Attempts were made to convert cis-[$Pt(HL^1)_2Cl_2$] to the trans isomer by the same method as the trans → cis-[$Pt(HL^1)(L^1)Cl$] conversion; that is, by adding excess HL^1. No reaction occurred at 25°, and with heating, ring closure to give cis-[$Pt(HL^1)(L^1)Cl$] was observed instead of the desired reaction.

Attempts were also made to prepare the complex cis-[$Pt(HL^1)_2(CH_3)_2$]. It was thought that this synthesis might be achieved by the addition of four equivalents of HL^1 to a solution containing the dimer, [$(CH_3)_2Pt(\mu$-$SMe_2)_2Pt(CH_3)_2$]. However, the product of such a reaction is trans-[$Pt(HL^1)(L^1)(CH_3)$], VII. The same product was obtained when [$Pt(COD)(CH_3)_2$] was treated with two equivalents of HL^1.

The possibility of binding the uncoordinated alcohols in trans-[$Pt(HL^1)_2CL_2$] to an oxophilic centre, to give a bridging L^1 ligand, was also investigated. Oxophilic reagents used included [$Ti(cp)_2Cl_2$], $Si(CH_3)_2Cl_2$, and $OSn(Bu)_2$. The only product obtained in each case was trans-[$Pt(HL^1)(L^1)Cl$], V.

All of these platinum complexes of HL^1, outlined in Scheme 3.1, have been investigated further using ^1H, ^{19}F and proton-decoupled ^{31}P NMR. The results of these studies are discussed in chapter 3.3.

3.3 NMR Studies

The results of the $(^1H)^{31}P$ NMR studies are given in Table 3.1 while Table 3.2 contains the ^1H and ^{19}F NMR results. Since the structural assignments are tied so closely to the interpretation of the NMR data, the following discussion will also deal with the structures of the complexes.

3.3.1 $[Pt(L^1)_2]$

A single resonance appeared in the (^1H) ^{31}P NMR spectrum of $[Pt(L^1)_2]$ at +17.3 ppm with satellites due to coupling to ^{195}Pt ($^1J(Pt,P)$ = 3517 Hz). The methylene protons in L^1 produced a signal in the ^1H NMR spectrum at 3.38 ppm with coupling to ^{31}P ($^2J(P,H)$ = 12 Hz) and ^{195}Pt ($^3J(Pt,H)$ = 14 Hz). As a result, the methylene proton signal appeared as a filled-in doublet. The ^{19}F NMR spectrum contained a single resonance, indicating that the two CF_3 groups in each chelate ring are equivalent on the NMR time scale.

It is not difficult to determine the geometry of these platinum complexes of HL^1 from the value of $^1J(Pt,P)$. Spin-spin coupling is always transmitted via electron

Table 3.1. ^{31}P NMR Data on Platinum Complexes [7]

Compound [solvent][a]		P_A[b]			P_B			$^2J(P_A,P_B)$
		δ ppm	$\Delta\delta$[c] ppm	^1J(Pt,P) Hz	δ ppm	$\Delta\delta$ ppm	^1J(Pt,P) Hz	Hz
I cis-$Pt(L^1)_2$	[C]	17.3	+50.9	3517	—	—	—	—
II cis-$PtCl_2(HL^1)_2$	[A]	—	—	—	2.0		3755	
III trans-$PtCl_2(HL^1)_2$	[C]	—	—	—	3.2	36.8	2574	—
	[A]	—	—	—	3.0	36.6	2610	—
IV cis-$PtCl(L^1)(HL^1)$	[A]	30.4	64.0	3819	-6.3	+27.3	3410	14.4
V trans-$PtCl(L^1)(HL^1)$	[C]	28.9	62.5	2707	+7.1	40.7	2580	463
	[A]	29.0	62.6	2854	+6.7	40.3	2720	459
VIa cis-$PtCl(L^1)(PPh_3)$	[D]	29.7	63.3	3808	-1.9	4.1	3423	14.3
VIb cis-$PtCl(L^1)(PPh_2Me)$	[D]	32.2	65.8	3805	-14.4	13.6	3326	15.6
VIc cis-$PtCl(L^1)(PPhMe_2)$	[D]	31.5	65.1	3818	-28.5	18.5	3242	16.7
VId cis-$PtCl(L^1)(PMe_3)$	[D]	32.2	65.8	3852	-35.4	26.6	3157	16.8
VII trans-$PtMe(L^1)(HL^1)$	[C]	37.0	70.6	3263	+16.7	50.3	3125	444
VIII $PtCl_2(L^1)_2$	[A]	2.4	36.0	2206	—	—	—	—
	[D]	3.8	37.4	2226	—	—	—	—

[a] A = $(CD_3)_2CO$; C = $CDCl_3$; D = CD_2Cl_2

[b] P_A is the phosphorus atom in the chelate ring throughout.

[c] the coordination shift, $\Delta\delta = \delta(\text{coord}) - \delta(\text{free})$

Table 3.2 ^{1}H and ^{19}F NMR Data on Platinum Complexes[a]

Compound (solvent)[a]		$^{1}H(CH_3)$			$^{1}H(CH_2)$			$^{19}F(CF_3)$		
		δ ppm	$^{2}J(P,H)$ Hz	$^{3}J(Pt,H)$ Hz	δ ppm	$^{2}J(P,H)$ Hz	$^{3}J(Pt,H)$ Hz	δ ppm	$^{4}J(P,F)$ Hz	$^{4}J(Pt,F)$ Hz
I	cis $Pt(L^1)_2$	[C]	—	—		3.33	12	14	76.3		11
II	cis $PtCl_2(HL^1)_2$	[C]	—	—	—	3.25	12.1	27	76.3		
III	trans $PtCl_2(HL^1)_2$	[A]	—	—		3.31	6.3[b]	25.4	76.0		
IV	cis $PtCl(L^1)(HL^1)$	[A]				3.79	11.3	20.9	76.4	2.3	11 (chelate)
						3.15	11.3	18.0	76.7		(non chelate)
V	trans $PtCl(L^1)(HL^1)$	[A]				3.42	12.4[c]	21	76.2		(chelate)
						3.14	11.9		75.2		(non chelate)
VIa	cis $PtCl(L^1)(PPh_3)$	[D]				3.07	11.7	19.6	77.1	3.3	5.4
VIb	cis-$PtCl(L^1)(PPh_2Me)$	[D]	1.88	11.0[d]	35.2	3.09	11.7	18.8	77.2	1.8	
VIc	cis $PtCl(L^1)(PPhMe_2)$	[D]	1.63	11.1	34.3	3.11	11.5	17.6	77.3	6.1	
VId	cis-$PtCl(L^1)(PMe_3)$	[D]	1.26	11.5	33.5	3.09	11.9	23.6	77.2	3.1	
VII	trans $PtMe(L^1)(HL^1)$	[C]	0.11	7.3.5.7	88	3.19	11.1[e]	40.0	77.3	-	(chelate)
						2.79	11.1	27.6	76.8	-	(non chelate)
VIII	$PtCl_2(L^1)_2$	[D]				3.98	13.7	10	74.3		

[a] A = $(CD_3)_2CO$; C = $CDCl_3$; D = CD_2Cl_2

[b] apparent J value in triplet, see text

[c] $^{4}J(Pt,H)$ = 8.2 Hz

[d] $^{4}J(Pt,H)$ = 13.1 Hz

[e] $^{4}J(Pt,H)$ = 8.66 Hz

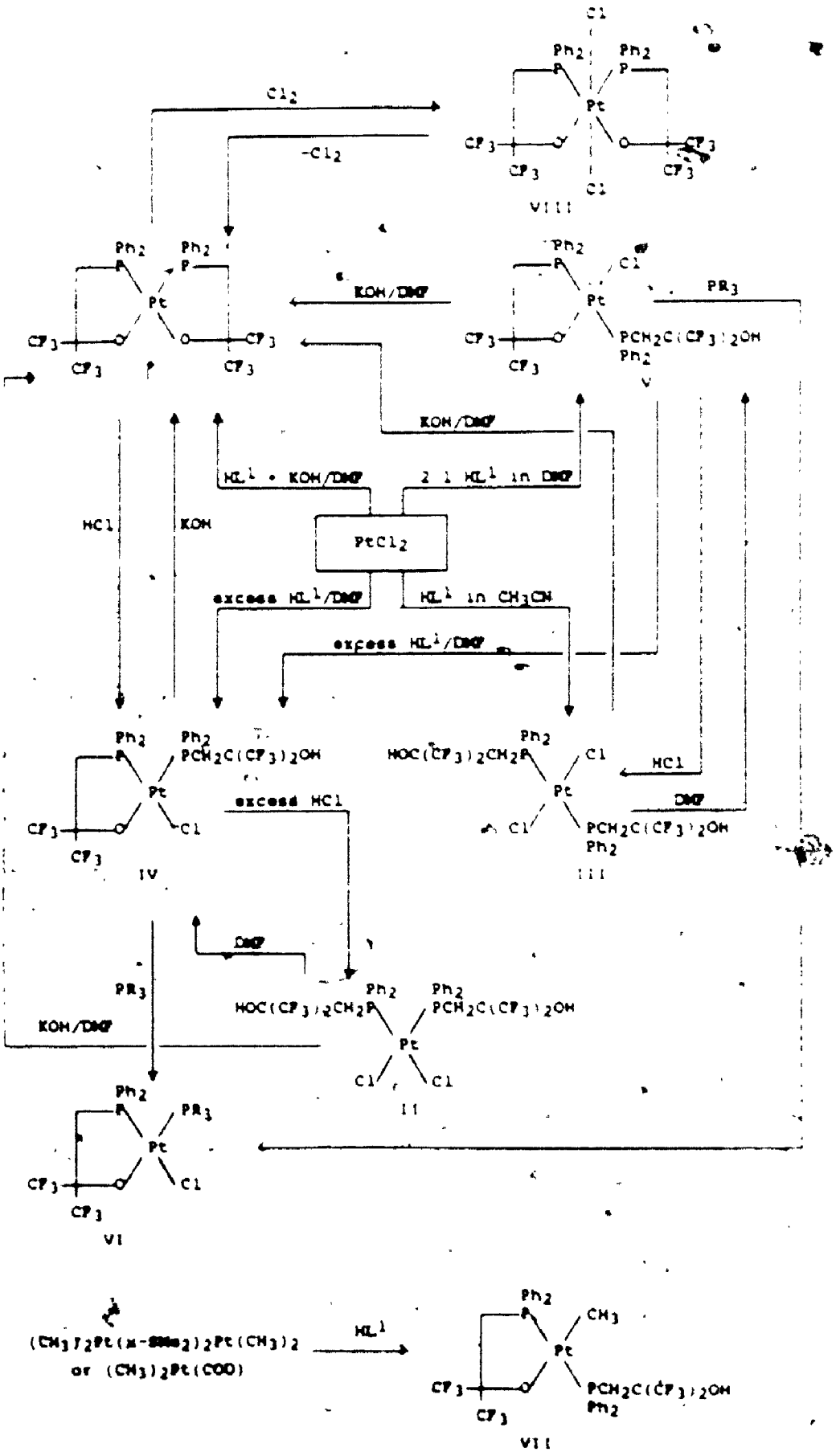

Scheme 1 1 Synthesis of some Pt Complexes of $PPh_2CH_2C(CF_3)_2OH$ (HL^1)

density in the molecule. The metal-phosphorus bond consists of a σ and a π contribution; the extent of π-bonding being dependent on the nature and oxidation state of the metal as well as the coligands. However only the σ-bonding affects the value of $^1J(Pt,P)$; equations describing $^1J(M,P)$ make no provision for the direct influence of π-bonding. The σ-bond strength is in turn dependent on the trans-influence of the ligand in the trans position.

As a result, the value of $^1J(Pt,P)$ in complexes of the type $[Pt(PR_3)_2X_2]$ is considerably higher for the cis-isomer, when the phosphines are trans to ligands of low trans-influence, than for the trans-isomer. Table 3.3 lists $^1J(Pt,P)$ values for a number of cis- and trans-$[Pt(PR_3)_2Cl_2]$ compounds. Typically, $^1J(Pt,P)$ values for phosphorus trans to chloride are in the range 3500-3700 Hz while for phosphorus trans to phosphorus the values are in the range 2400-2500 Hz. The value of $^1J(Pt,P)$ for $[Pt(L^1)_2]$ is 3517 Hz and therefore the complex has been assigned a cis-geometry.

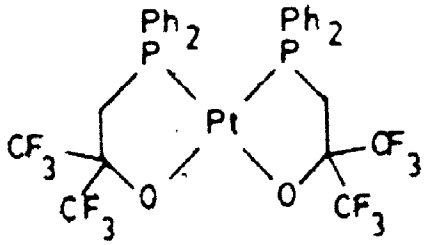

The cis-geometry is not unexpected for a platinum(II) complex with this combination of hard alkoxide and soft phosphino ligands. Electronic factors favouring the cis geometry dominate the trans-favouring steric factors. Thus, the cis isomers of $[Pt(PR_3)_2X_2]$ complexes are the thermodynamically favoured form for all but a few examples with very bulky phosphines.[109,219]

Originally, the relative thermodynamic stability of the cis-isomers was attributed to the effect of π-bonding. Two π-acceptor ligands, such as phosphines, in mutually trans positions will compete for electron density in the same d_π-orbital on the metal, thus destabilizing the complex. However, the π acceptor or σ donor properties of the ligands appear to have little significance. Rather, the preference for a cis-geometry in these complexes mainly is due to Pearson's antisymbiotic effect,[110] not π-bonding.

Soft ligands such as phosphino groups have a large trans influence, and therefore two mutually trans soft ligands on a soft metal will have a destabilizing effect on the complex. It is advantageous to have a hard, ionic ligand with a low trans influence trans to the softer ligand; this behaviour is called antisymbiosis. Since the trans influence is primarily due to strong covalent bonding, antisymbiosis should not be expected to be significant for harder metals such as Ni(II).

Antisymbiosis will be used to help in explaining the stereochemical preferences of complexes of soft metals

throughout this thesis. Alternately, steric effects favour a trans geometry and this conflict will be noted along with the diminishing significance of antisymbiosis as the metal centre becomes harder.

3.3.2 Cis- and trans-$[Pt(HL^1)_2Cl_2]$

The two geometrical isomers of $[Pt(HL^1)_2Cl_2]$, II and III, can be distinguished by ^{31}P NMR spectra as with other complexes of the type $[Pt(PR_3)_2Cl_2]$. The patterns of the spectra for both isomers were identical, a single resonance with satellites due to coupling to ^{195}Pt nuclei. The position of the signal was shifted slightly further, (δ = 2.0 ppm for the cis-isomer, 3.0 ppm for the trans-isomer) and the value of $^1J(Pt,P)$ was considerably greater for the cis-isomer (3755 Hz) than for the trans-isomer (2610 Hz). These values of $^1J(Pt,P)$ are consistent with cis- and trans-isomers of a $[Pt(PR_3)_2Cl_2]$ complex.

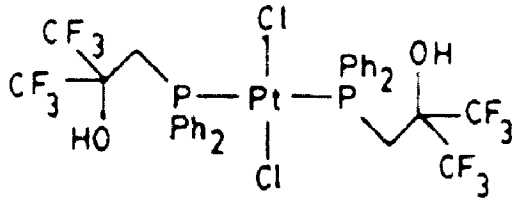

trans

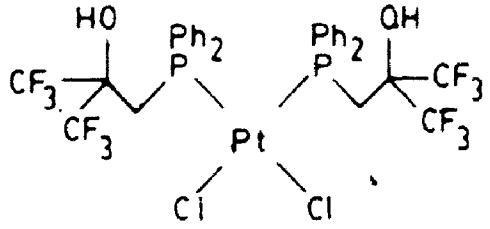

cis

The ^{19}F NMR spectra for the two compounds are virtually indistinguishable with each spectrum consisting of a single resonance, at -76.3 ppm for the cis-isomer and -76.0 for the trans isomer.

The two isomers are easily distinguished by ^{1}H NMR as well. The signal due to the methylene protons appears as a doublet, with satellites in the case of the cis-isomer due to coupling to ^{31}P and ^{195}Pt as expected. The signal appears at 3.16 ppm and the values of $^{2}J(P,H)$ and $^{3}J(Pt,H)$ are 12.6 and 27 Hz respectively. However, the appearance of the methylene proton signal for the trans-isomer is quite different. Rather than the expected doublet, the signal appears as a triplet as if the two phosphorus nuclei are magnetically equivalent. This phenomenon, known as virtual coupling, is not uncommon for trans-$[Pt(PR_3)_2Cl_2]$ complexes. It is seen as a limiting case in such $X_nAA'X'_n$ spin systems when $|J(A,A')| >> |J_{AX} - J_{AX'}|$. For this reason it is much more common for trans-square-planar complexes than for the cis-isomers. Virtual coupling will be discussed in more detail in chapter 6, including some warnings concerning assignment of stereochemistry based solely on the appearance of a virtual triplet. However, for isomers of a $[Pt(PR_3)_2Cl_2]$ complex, when one isomer displays a virtual triplet in the NMR spectrum while the other does not, the assignment of geometry is unambiguous. The ^{31}P NMR spectra were, of course, available to confirm the assignment in this case.

Since both isomers have been isolated, it is of interest to determine which isomer is the thermodynamically favoured species. Generally, as mentioned in the chapter

the thermodynamically-favoured isomer as a result of antisymbiosis. It is usually possible to convert the kinetically favoured trans-isomer to the cis-isomer. This reaction is catalyzed by excess phosphine and is thus considered to proceed via a five-coordinate intermediate.

In this case we speculated that the trans-isomer was actually favoured thermodynamically, due to the considerable steric demands of HL^1. Therefore attempts to interconvert the two isomers were made in the direction cis → trans. However, as mentioned in chapter 3.2, instead of isomerization, ring-closure occurred to produce cis-$[Pt(HL^1)(L^1)Cl]$. In fact, cis-$[Pt(HL^1)_2Cl_2]$ proved unstable even during attempts to recrystallize a sample, as cis-$[Pt(HL^1)(L^1)Cl]$ was again produced. This relative instability of the cis-isomer seemed to support the proposal that the trans-isomer is actually the thermodynamically-favoured isomer. The cis-isomer is the kinetically-favoured isomer on addition of HCl to cis-$[Pt(HL^1)(L^1)Cl]$ or cis-$[Pt(L^1)_2]$. However when excess HL^1 is added to a solution of $PtCl_2$ in CH_3CN, one would expect the product to be the thermodynamically-favoured isomer since the excess ligand should catalyze the isomerization should any of the less-favoured isomer form. Indeed under such conditions the trans-isomer is the only product.

Since antisymbiosis would still favour the cis-isomer over the trans-, then the relative stability of the

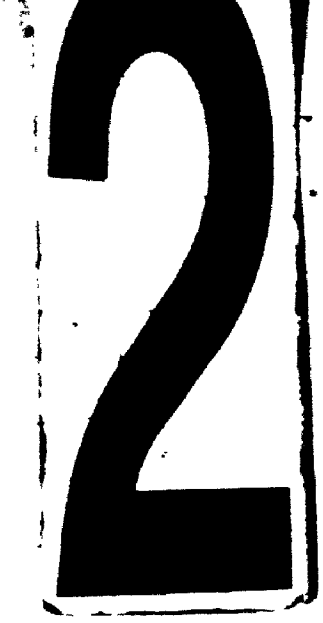

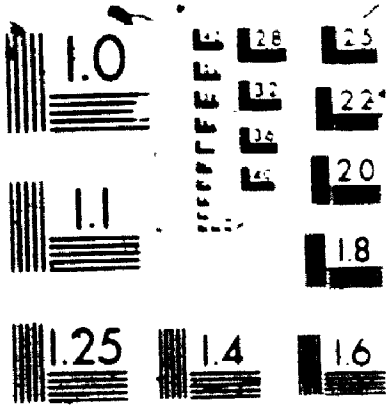

ligand. Unlike the cis-isomer, the trans-isomer is stable during recrystallization, and we were able to investigate the steric demands of monodentate HL^1 through an X-ray structure determination of trans-$[Pt(HL^1)_2Cl_2]$. This crystal structure analysis will be presented in chapter 4.

For a number of types of phosphine complex, including cis- and trans-$[Pt(PR_3)_2Cl_2]$ complexes, a linear relationship between the chemical shift of the free phosphine and the coordination chemical shift, $\Delta\delta$, has been observed.[214] The coordination chemical shift, $\Delta\delta$, is the difference in chemical shift between the complex and that of the free ligand.

$$\Delta\delta = (\delta_{complex} - \delta_{free\ phosphine})$$

For cis- and trans-$[Pt(PR_3)_2Cl_2]$ complexes the slope and intercepts have been determined,[126] using 16 complexes for the trans- and 14 complexes for the cis-isomer

$$\Delta\delta = A \cdot \delta + B$$

For trans-$[Pt(PR_3)Cl_2]$ $A = -0.481 \pm 0.023$ $B = 21.41 \pm 0.55$

cis-$[Pt(PR_3)Cl_2]$ $A = -0.326 \pm 0.070$ $B = 18.83 \pm 1.82$

These two functions have been plotted out in Fig. 3.1 along with all the cis- and trans-$[Pt(PR_3)_2Cl_2]$ complexes from Tables 3.3 and 3.4. In addition cis- and trans-$[Pt(HL^1)_2Cl_2]$ have been added to the plots in Fig. 3.1 to show how well these complexes adhere to the linear relationship.

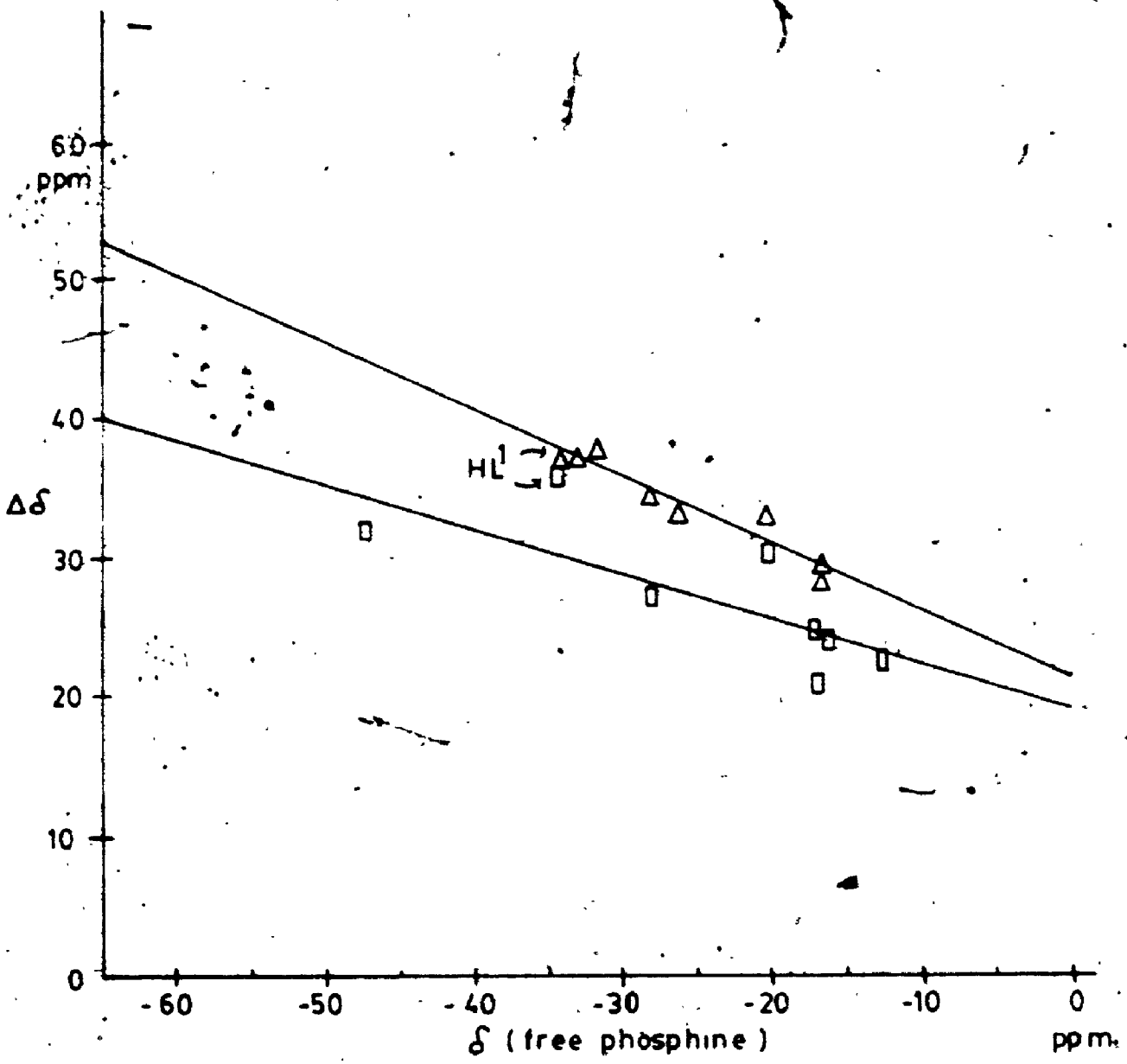

Figure 3.1 Plot of coordination shift vs δ(free ligand) for cis- and trans-$[Pt(PR_3)_2Cl_2]$

Δ = trans ▯ = cis

Table 3.3 ^{31}P NMR Data for cis-$[Pt(PR_3)_2Cl_2]$ Complexes.

PR_3	Chemical Shift (ppm, vs H_3PO_4) Free Ligand	Complex	$\Delta\delta$ (ppm)	$^1J(Pt,P)$ (Hz)	Ref
PMe_3	-62	-24.0	38	3480	211, 212
PMe_2Ph	-46.9	-15.2	31.7	3549	226
$PMePh_2$	-28.1	-1.2	26.9	3616	226
PPh_3	-5.9	14.3	20.2	3617	87, 227
PEt_3	-20.4	9.6	30.0	3520	226
PEt_2Ph	-17.1	3.3	20.4	3530	226
$PEtPh_2$	-12.5	9.8	22.3	3640	226
PPr_3^n	-33.0	-0.2	32.8	3530	226
PPr_3^nPh	-27.7	-2.7	25.0	3561	226
$PPr_2^nPh_2$	-17.6	6.9	24.5	3639	226
PBu_3^n	-32.3	1.2	23.9	3551	226
PBu_2^nPh	-26.2	-2.3	23.9	3551	226
PBu^nPh_2	-17.1	7.0	24.1	3641	226

Table 3.4 ^{31}P NMR Data for trans-$[Pt(PR_3)_2Cl_2]$ Complexes

PR_3	Chemical Shift (ppm, vs H_3PO_4) Free Ligand	Complex	$\Delta\delta$ (ppm)	$^1J(Pt,P)$ (Hz)	Ref
PMe_3	-62.	-15.8	46.2	2379	211, 227
PPh_3	-5.9	20.1	26.0	2637	87, 212
PEt_3	-20.4	12.3	32.7	2400	226
PEt_2Ph	-17.1	11.3	28.4	2482	226
PPr^n_2Ph	-27.7	6.3	34.0	2463	226
PBu^n_3	-32.3	5.1	37.4	2392	226
PBu^n_2Ph	-26.2	6.5	32.7	2462	226
PBu^nPh_2	-17.1	12.0	29.1	2531	226

While the linearity of the relationship is purely empirical, the observation that those phosphines whose NMR resonance appears furthest downfield in the free ligand have the smallest downfield coordination shift would be predicted on the basis of theory. Phosphines with strongly electron-withdrawing substituents, such as PPh_3, should as free ligands have strongly deshielded ^{31}P nuclei and thus downfield ^{31}P NMR resonances. Because of the effect of the substituents, these phosphines should also be poor σ-donors but good π-acceptors. Therefore, the deshielding effect of coordination and hence Δδ, should be smallest for such a phosphine.

By observing where HL^1 fits into the plots one may conclude what sort of σ-donor/π-acceptor properties the ligand displays. The upfield chemical shift and high coordination shift of HL^1 suggest that it is a strong σ-donor and weak π-acceptor as a monodentate phosphine. The resonance of the free ligand is even further upfield than PMe_3 as well as all the PPh_2R-type phosphines in Tables 3.3 and 3.4. The alkyl groups in the phosphines of Tables 3.3 and 3.4 are all straight-chain. However even compared to $Ph_2PCH_2C(CH_3)_3$,[228] the ^{31}P resonance of free HL^1 is further upfield. The ^{31}P resonance of HL^1 is almost as far upfield as that of Ph_2PH (-41.1 ppm).[229]

The electron-withdrawing CF_3 groups of HL^1 are sufficiently far removed from the phosphorus atom that they do not deshield the phosphorus nucleus. Instead, the

$-CH_2C(CF_3)_2OH$ group causes the monodentate phosphine, HL^1, to be a very strong σ-donor.

This strong σ-donor ability of HL^1 seems to be evident from the values of $^1J(Pt,P)$ for the two isomers of the platinum complex. In both cases, the values are slightly above the range of values exhibited by those complexes in Tables 3.3 and 3.4. However such data should be interpreted with caution. While it was previously noted that the values of coupling constants are directly affected by σ-bonding only, nevertheless π-bonding does have a synergic effect on coupling. That is, as the metal-phosphorus π-bonding is increased, the σ-bond strength increases as a result. This synergic effect has been used to explain the unexpected decrease in $^1J(M,P)$ as the σ-donor ability increases in going from a complex of PPh_3 through to an analogous complex of PR_3 (where R is an alkyl groups).[230]

The value of $^1J(Pt,P)$ in cis-$[Pt(HL^1)_2Cl_2]$ can also be used to determine the relative size of the trans influence of a fluorinated alkoxide, by comparison with $^1J(Pt,P)$ in cis-$[Pt(L^1)_2]$. These two complexes are highly analogous. In cis-$[Pt(L^1)_2]$ when the phosphino groups are trans to a fluorinated alkoxide, the value of $^1J(Pt,P)$ is 3517 Hz compared with 3755 Hz for cis-$[Pt(HL^1)_2Cl_2]$ when the phosphino groups are trans to chloride. This suggests that the destabilizing trans influence of a fluorinated alkoxide is greater than that of a chloride ion.

It might be argued that not only is the trans ligand changing in going from cis-$[Pt(HL^1)_2Cl_2]$ to cis-$[Pt(L^1)_2]$ but the phosphino group is also being incorporated into a chelate ring. While it is true that this chelation may affect the value of $^1J(Pt,P)$, it will be shown using the complex trans-$[Pt(HL^1)(L^1)Cl]$ in section 3.3.3 that the effect of chelation is actually to increase the value of the coupling. Therefore the difference between the destabilizing trans influence of fluorinated alkoxide and a chloride may be greater than that originally suggested by the relative $^1J(Pt,P)$ values in cis-$[Pt(L^1)_2]$ and cis-$[Pt(HL^1)_2Cl_2]$.

These results serve to confirm an earlier report[17] that the trans influence of a fluorinated alkoxide is greater than that of a chloride. It was suggested that the electron-withdrawing nature of the CF_3 groups causes the fluorinated alkoxide to be a strong σ-acceptor ligand. As a result electron density is withdrawn from the bond trans to it, thus weakening the bond.

3.3.3 Cis- and trans-$[Pt(HL^1)(L^1)Cl]$

Both cis- and trans-isomers of the complex, $[Pt(HL^1)(L^1)Cl]$, IV and V, with one chelating ligand and one monodentate HL^1 ligand, were isolated as well. Again the two isomers are easily distinguished by NMR and visible spectroscopy. The trans-isomer is yellow while the cis-isomer is colourless.

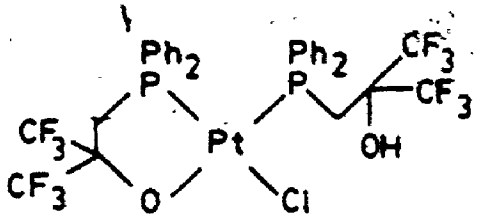

cis

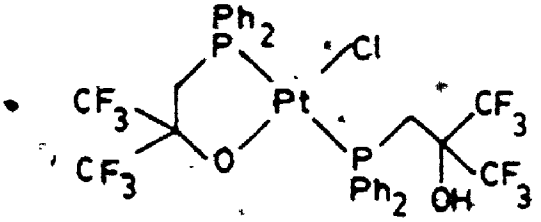

trans

The two inequivalent phosphorus nuclei in each isomer represent an AB spin system. As a result, the ^{31}P NMR spectrum of each isomer displays two resonances, each split into a doublet by the phosphorus-phosphorus coupling. In addition, each phosphorus nucleus is coupled to the ^{195}Pt nucleus ($I=\frac{1}{2}$) resulting in satellites. The values of $^{1}J(Pt,P)$ are again consistent with cis and trans isomers. In the cis-isomer, where the two phosphino groups are trans to a chloride and an alkoxide, $^{1}J(Pt,P_A)$ = 3819 Hz and $^{1}J(Pt,P_B)$ = 3410 Hz (P_A is used throughout to refer to the phosphorus atom in the chelate ring, while P_B refers to the phosphorus atom in the monodentate ligand). However in the trans-isomer $^{1}J(Pt,P_A)$ = 2854 Hz and $^{1}J(Pt,P_B)$ = 2720 Hz.

The value of $^{2}J(P,P)$ can also be used to distinguish between cis- and trans-isomers of $[Pt(PR_3)_2X_2]$ complexes, $^{2}J(P,P)_{trans} > {}^{2}J(P,P)$ cis. Consistent with this, $^{2}J(P_A,P_B)$ = 14.4 Hz for the cis-isomer of $[Pt(HL^1)(L^1)Cl]$ while for the trans isomer, $^{2}J(P_A,P_B)$ = 459 Hz.

The ^{1}H NMR spectra of the two isomers each display two methylene proton resonances due to the chelating and

monodentate ligands. Each signal appears as a doublet, due to coupling to the ^{31}P nuclei, with ^{195}Pt satellites. As with the $^{1}J(Pt,P)$ values, the $^{2}J(P,H)$ and $^{3}J(Pt,H)$ couplings are smaller in the trans-isomer than in the cis- because of the greater trans influence of a phosphino group over that of a chloride or alkoxide. This trend is well-known; for example in $[Pt(PMe_3)_3Cl]NO_3$, $^{3}J(Pt,H)$ and $^{2}J(P,H)$ are smaller for the mutually trans phosphino groups than for the phosphino group trans to the chloride ion.[231]

No coupling was observed in the ^{19}F NMR spectra of the trans-isomer for either the chelating or monodentate ligand. For the cis-isomer, one of the two signals showed coupling, to both the ^{31}P and ^{195}Pt nuclei. Coupling to the ^{19}F nuclei is also seen in the $[Pt(PR_3)(L^1)Cl]$ complexes where the fluorine atoms are all in a chelate ring. Therefore, the upfield resonance at -76.7 for the $[Pt(HL^1)(L^1)Cl]$ complex which shows coupling ($^{4}J(P,F)$ = 2.3 Hz, $^{4}J(Pt,F)$ = 11 Hz) has been assigned to the CF_3 groups in the chelate ring, while the downfield resonance is assigned to those in the monodentate ligand.

The NMR data for these two compounds illustrate the effect of chelation on coupling constants and chemical shifts, specifically $^{1}J(Pt,P)$ and $\delta^{31}P$. It was noted that $^{4}J(P,F)$ coupling is observed only in the chelating ligand of cis-$[Pt(HL^1)(L^1)Cl]$. In addition, the two phosphorus nuclei in trans-$[Pt(HL^1)(L^1)Cl]$ may be used to observe the effect on $^{1}J(Pt,P)$ of incorporation of the phosphorus into

a chelate ring; the chelate ring is the only difference between the environments of the two phosphorus nuclei in this compound. In acetone solution, the value of $^1J(Pt,P)$ increases from 2720 to 2854 Hz on chelation. The effect of chelate ring size has previously been illustrated using [Pt(diphosphine)Cl_2] complexes[236] and the order of increasing $^1J(Pt,P)$ values is dppm (3098 Hz) < dppp (3420 Hz) < 2 $PMePh_2$ (3616 Hz) ~ dppe (3618 Hz).

Platinum-phosphorus coupling constants are considered to be dominated by the Fermi-contact term.[237]

$$^1J(Pt,P) \propto \alpha_{Pt}^2 \alpha_P^2 [S_{Pt(6s)}(0)][S_{P(3s)}(0)]/\Delta E.$$

In this equation, α_x^2 is the s character of the bonding orbital of x, $S_{x(ns)}(0)$ is the density of the ns orbital of x at the nucleus and ΔE is the singlet-triplet excitation energy. The variation in $^1J(Pt,P)$ with ring size is presumably due to changes in α^2_{Pt} and α^2_P which are in turn dependent on the bond angles; the electronic factors change little from chelate to chelate as the phosphorus substituents do not change significantly. This would explain why the most pronounced effect appears for the highly-strained four-membered ring. In the case of trans-[Pt(HL^1)(L^1)Cl], the effect of chelation appears to be to alter the bond angles about the phosphorus and platinum nuclei such that the s character of the bonding orbitals and hence $^1J(Pt,P)$ increase.

Likewise the chemical shift of the phosphorus nuclei is affected by chelation. This was mentioned briefly in

chapter 2.3.4 in the discussion of the $[Cu(PPh_3)_2(L^1)]$ complex. A "ring contribution", Δ_R, to the chemical shift has previously been noted[88] where Δ_R equals the difference between $\Delta\delta$ for a cis-bisphosphine complex and $\Delta\delta$ for an equivalent phosphorus in a chelate complex. The ring contribution was greatest, deshielding the phosphorus nucleus by 21-33 ppm in five-membered rings, compared with 2-25 ppm in four- and six-membered rings. Again, trans-$[Pt(HL^1)(L^1)Cl]$ likely gives the best estimate of Δ_R for L^1 as in this complex the trans ligand remains constant for the chelating and monodentate ligands. The value of Δ_R for L^1 is 22.3 ppm, obtained from trans-$[Pt(HL^1)(L^1)Cl]$ in acetone solution. However, as yet no explanation has been given for the phenomenon of the ring contribution to $\Delta\delta$.

It is again of interest to compare the relative stabilities for the two geometrical isomers. The cis-isomer is formed when an excess of HL^1 is added to a solution of $PtCl_2$ in DMF, while a less than stoichiometric amount of HL^1 yielded the trans-isomers. Addition of excess HL^1 to a solution of the trans-isomer catalyzed the isomerization to the cis-isomer. These observations are consistent with observations of most $[Pt(PR_3)_2Cl_2]$ complexes, where the cis-isomer is thermodynamically-favoured while the trans-isomer is kinetically-favoured and the trans → cis inteconversion is catalyzed by PR_3.

In the case of $[Pt(HL^1)_2Cl_2]$, the trans isomer was considered to be the thermodynamically-preferred isomer and

the cis-isomer was very unstable. The great steric bulk of the HL^1 ligand is dominant over the effect of antisymbiosis. For the bischelate, $[Pt(L^1)_2]$, only the cis-isomer is observed because of antisymbiosis. In the intermediate case of $[Pt(HL^1)(L^1)Cl]$, where one ligand is bidentate and one is monodentate, both isomers are observed but the cis-isomer is favoured. As one of the monodentate ligands of $[Pt(HL^1)Cl_2]$ becomes a bidentate ligand in $[Pt(HL^1)(L^1)Cl]$, the steric interactions are lessened enough so that antisymbiosis dominates and can direct the complex towards the cis-isomer.

In the system reported by Anderson and Kumar,[23] a complex having one bidentate and one monodentate P,O ligand was prepared by partial ring closure of the complex with two monodentate ligands

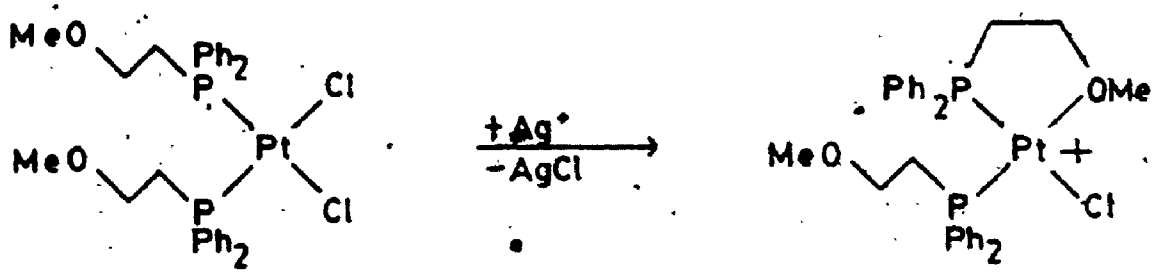

Only the cis-isomer was observed as the product. The bismonodentate complex was also only observed with a cis-geometry. This suggests that the CF_3 groups in HL^1 do possess considerable steric bulk, making the trans-isomer of $[Pt(HL^1)_2Cl_2]$ more favourable. Substitution of CO for Cl^- in cis-$[Pt(Ph_2PCH_2CH_2OMe)_2Cl_2]$ gives trans-$[Pt(Ph_2PCH_2CH_2OMe)_2(CO)Cl]$[23]. However this is consistent

with the effect of antisymbiosis, as CO has a greater trans influence than phosphines.

3.3.4 [Pt(PR$_3$)(L^1)Cl] Complexes

Substitution of PR$_3$ for the monodentate ligand, HL^1, in either cis- or trans-[Pt(HL^1)(L^1)Cl] yields [Pt(PR$_3$)(L^1)Cl], VI. The phosphines were always found to be cis in these compounds, the geometry again being readily established by ^{31}P NMR.

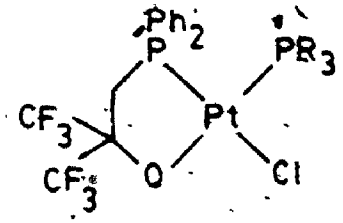

The ^{31}P NMR spectra have the appearance of a first-order AB pattern with ^{195}Pt satellites similar to that of cis-[Pt(HL^1)(L^1)Cl]. Again ^{1}J(Pt,P) is greater for the phosphine trans to the chloride than for that trans to a fluorinated alkoxide. The values of ^{1}J(Pt,P) for the monodentate phosphine increases from 3157 Hz in the case of PMe$_3$ to 3423 Hz in the case of PPh$_3$. This increase in ^{1}J(Pt,P) surprisingly parallels a decrease in σ-donor ability. However, as mentioned previously this is seen in cis-[Pt(PR$_3$)$_2$Cl$_2$] complexes (see Table 3.3) and has been explained by the synergic effect of increasing π-bonding on ^{1}J(Pt,P). For the bidentate phosphine, ^{1}J(Pt,P) values decrease from 3852 Hz in the case of PMe$_3$ to 3808 Hz in the

case of PPh_3. This trend is also surprising in light of the cis-influence series reported by Allen and Sze.[168]

$$PPh_3 > PPh_2Me > PPhMe_2 > PMe_3$$

This observation further illustrates the need for caution when interpreting $^1J(Pt,P)$ values in terms of σ-donor abilities or cis- and trans-influences alone. The secondary synergic effect of π-bonding is also important.

A linear relationship exists between Δδ of the monodentate phosphine and the chemical shift for the free phosphines for the $[Pt(PR_3)(L^1)Cl]$ complexes, as in the case of the $[Pt(PR_3)_2Cl_2]$ complexes. This relationship is illustrated in Fig. 3.2. The coordination shift increases with increasing σ-donor ability.

The values of Δδ are considerably greater for the ligand L^1, ranging from 63.3 to 65.8 ppm. These values are quite comparable to those of bidentate L^1 in cis- and trans-$[Pt(HL^1)(L^1)Cl]$. The ring contribution is again responsible for Δδ being much greater in the bidentate phosphine than in the monodentate phosphines.

The ^1H and ^{19}F NMR data are recorded in Table 3.2.

Assignment of geometry was made using the values of $^1J(Pt,P)$ and $^2J(P_A,P_B)$. It is not surprising that only the cis-isomers are observed, since the cis-isomer of $[Pt(HL^1)(L^1)Cl]$ is thermodynamically favoured even with the more sterically demanding phosphine HL^1 present. Therefore the cis-isomer is sure to be favoured for $[Pt(PR_3)(L^1)Cl]$

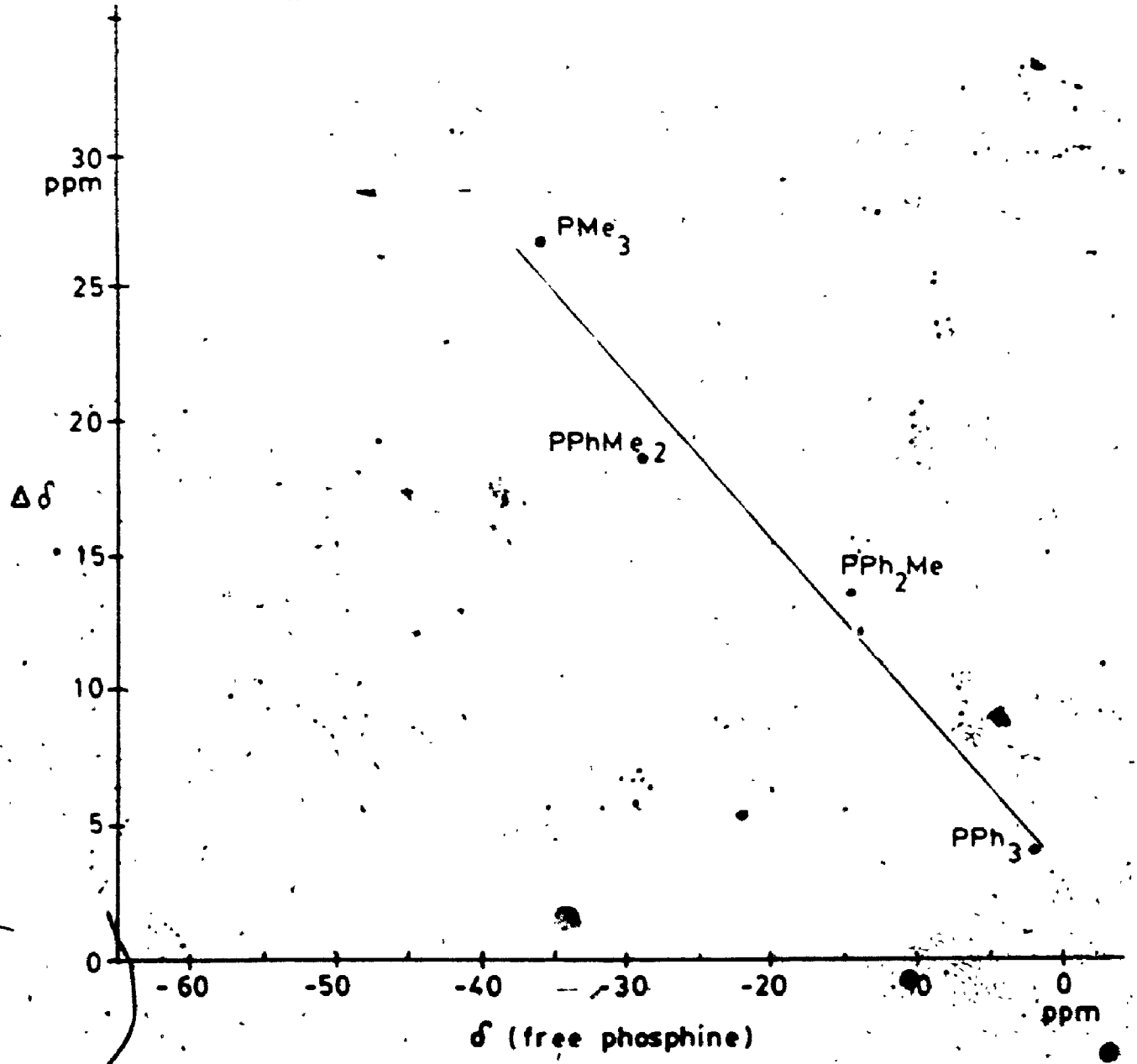

Figure 3.2 Plot of coordination shift vs. δ(free) for $[Pt(PR_3)(L^1)Cl]$ complexes

complexes (where PR_3 = PPh_3, PPh_2Me, $PPhMe_2$, PMe_3). Furthermore, since the method of preparation of these complexes involved displacement of HL^1 with PR_3, none of the trans-isomer would be expected as the excess phosphine would catalyze the isomerization to the favoured cis-isomer.

3.3.5 $[Pt(HL^1)(L^1)Me]$

Attempts to prepare cis-$[Pt(HL^1)_2(CH_3)_2]$ by addition of the appropriate amount of HL^1 to a solution containing $[(CH_3)_2Pt(\mu\text{-}SMe_2)_2Pt(CH_3)_2]$ or $[Pt(COD)(CH_3)_2]$ instead yielded $[Pt(HL^1)(L^1)(Me)]$, VII. The dimethyl species was of interest as it was thought that the strength of the Pt-CH_3 bond might cause the HL^1 ligands to bridge rather than chelate in the presence of another oxophilic metal.

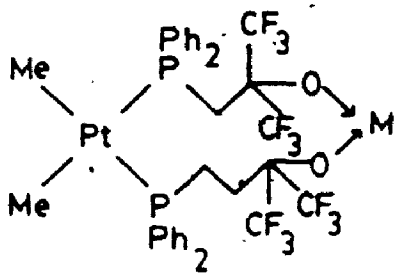

The ^{31}P NMR spectrum displayed two signals from the two inequivalent phosphines. The two resonances are coupled to give an AB pattern with ^{195}Pt satellites. The $^2J(P_A,P_B)$ value of 444 Hz suggested that the phosphorus atoms were mutually trans. This was confirmed by comparison of the $^1J(Pt,P)$ values, 3263 Hz for the chelating phosphine and 3125 Hz for the monodentate phosphine, with those of $[Pt(PEt_3)_2MeX]$ compounds. In the case of the

trans-isomers, $^1J(Pt,P)$ for these complexes range from 2595 Hz for X = CN^- to 2925 Hz for X = ONO_2^-; when X = Cl^-, $^1J(Pt,P)$ is 2821 Hz. Alternatively for the cis-isomers the values ranges from 1686 to 1856 Hz for the phosphorus nuclei trans to CH_3 and from 3878 Hz to 4179 Hz, for the phosphorus nucleus cis with respect to CH_3.[238] When X = Cl^- in the cis isomer, the $^1J(Pt,P)$ values are 1719 Hz and 4179 Hz respectively. The values of $^1J(Pt,P)$ for $[Pt(HL^1)(L^1)(CH_3)]$ compare favourably with the range of values for mutually trans phosphines if one bears in mind that HL^1 and L^1 are strong σ-donors through the phosphorus and as a result the $^1J(Pt,P)$ values for these ligands are slightly higher than expected.

It may seem surprising that the cis-isomer of $[Pt(HL^1)(L^1)Cl]$ is the low-energy geometric isomer yet only the trans-isomer of $[Pt(HL^1)(L^1)(CH_3)]$ is observed. However this may be explained in terms of the very strong trans influence of the methyl group, greater than that of the phosphine ligands. Thus the effect of antisymbiosis, as well as steric factors, is to favour the isomer with CH_3 trans to the lower trans influence alkoxide.

It is of interest to compare the ^{31}P NMR spectrum of trans-$[Pt(HL^1)(L^1)Cl]$ with that of trans-$[Pt(HL^1)(L^1)(CH_3)]$ since the complexes are identical but for the substitution of methyl for chloride trans to the alkoxide and cis to the phosphines. For both the chelating and monodentate phosphines, $^1J(Pt,P)$ is greater for the methyl complex than

for the chloride complex. This is consistent with the high stabilizing cis-influence of the methyl group. Bennett et al[241,242] among others noted that a ligand with a high destabilizing trans-influence, such as a methyl group, will have the effect of strengthening bonding to groups in cis-positions.

In the ^{1}H NMR spectrum, signals appear due to the methylene protons in both the bidentate and monodentate phosphine ligands as well as the methyl protons. The downfield methylene signal corresponding to the chelating ligand is coupled to both phosphorus nuclei as well as to ^{195}Pt. The monodentate phosphorus lies upfield and shows coupling only to the phosphorus nucleus located two bonds away as well as to ^{195}Pt. Like the chelating phosphine, the methyl proton signal is split into a doublet of doublets with satellites, by coupling to the two inequivalent phosphorus nuclei and ^{195}Pt. The ^{19}F NMR shows only two uncoupled signals due to the CF_3 groups in the bidentate and monodentate ligands.

The value of $^{2}J(Pt,H)$ for the methyl group trans to the fluorinated alkoxide is 88 Hz. A tabulation of $^{2}J(Pt,H)$ values for trans-$[Pt(PR_3)_2(CH_3)X]$ complexes,[215] shows that the values range up to 88 Hz for X groups of low trans influence. For trans-$[Pt(PPhMe_2)(CH_3)X]$[240] $^{2}J(Pt,H)$ is 81 Hz. These data would seem to suggest that the fluorinated alkoxide ligand actually has a lower trans influence than the halides. However, this may be due to the presence of

different phosphine coligands.

The proposal that fluorinated alkoxides have a greater trans influence than halides was based initially on comparisons of $^1J(Pt,P)$ values in $[Pt(PR_3)_2(PFP)]$ complexes with those of analogous $[Pt(PR_3)_2X_2]$ complexes.[17] Comparisons of $^1J(Pt,P)$ values of complexes in this study have confirmed this trans-influence order.

3.3.6 $[Pt(L^1)_2Cl_2]$

The Pt(IV) complex, VIII, prepared by oxidative addition of Cl_2 to $Pt(L^1)_2$, is one among a very short list of known Pt(IV) alkoxides.[244,245]

The ^{31}P NMR spectrum displayed a single resonance at 3.8 ppm in CD_2Cl_2 with ^{195}Pt satellites showing $^1J(Pt,P)$ coupling of 2226 Hz. This is consistent with the well-known observation that, for complexes of comparable ligands, $^1J(Pt(IV),P) < {}^1J(Pt(II),P) < {}^1J(Pt(0),P)$.[246] A decrease in polarizability of the platinum-phosphorus bond is accompanied by a decrease in $^1J(Pt,P)$.

The single ^{31}P signal indicates equivalent phosphines. Likewise the ^{19}F NMR exhibits a single uncoupled resonance at -74.7 ppm and the ^1H NMR spectrum has but one signal for the methylene protons. The methylene proton resonance appears as a filled-in doublet similar to that of $Pt(L^1)_2$, due to coupling to ^{31}P and ^{195}Pt. The value of $^1J(Pt,P)$ when compared to $^1J(Pt,P)$ values for analogous Pt(IV) complexes[247] indicates that the phosphines are trans to

ligands of weak trans-influence, and consequently are mutually cis.

As in the case of the Rh(III) complex discussed in chapter 2.3.5, there are two possible geometries for this octahedral Pt(IV) complex which are consistent with the NMR results. The chloride ligands could either be cis or trans, with the phosphines being in each case mutually cis and equivalent. The two possible geometries are shown as 3-2 and 3-3.

Species 3-2 would be chiral and therefore a ^{31}P spectrum of $[Pt(L^1)_2Cl_2]$ was run in a chiral solvent, (ethyl L-(+)-lactate). No splitting in the ^{31}P resonance was observed indicating that the complex is achiral and has the geometry of 3-3.

As a check on this assignment, the complex was allowed to react with ethanolic $AgNO_3$. It has been observed previously that the high trans-effect of the phosphino groups would labilize chloride ions trans to the phosphine and immediate precipitation of AgCl occurs. If however the chloride ions are mutually trans, then precipitation occurs slowly.[263,264] When $[Pt(L^1)_2Cl_2]$ was reacted with

ethanolic $AgNO_3$, the precipitation of AgCl took place over several hours.

Based on these two pieces of experimental evidence the geometry of 3-3 has been tentatively assigned to $[Pt(L^1)_2Cl_2]$.

3.3.7 Signs of $^2J(P,H)$ and $^4J(P,F)$

The changes in the couplings from phosphorus to other nuclei in the ligand which occur on complexation, deserve comment. In the free ligand, the coupling from phosphorus to fluorine, $^4J(P,F)$ is 16.5 Hz while the coupling to the methylene protons $^2J(P,H)$ is too small to be observed. However in the metal complexes, the situation is reversed as $^4J(P,F)$ is not detected in $[Pt(L^1)_2]$, $[Pt(HL^1)_2Cl_2]$, trans-$[Pt(HL^1)(L^1)Cl]$ or in the monodentate ligand HL^1 in cis-$[Pt(HL^1)(L^1)Cl]$. The value of $^2J(P,H)$ on the other hand becomes 12 Hz in cis-$[Pt(L^1)_2]$ and 11.3 Hz in both the chelating and monodentate ligands of cis-$[Pt(HL^1)(L^1)Cl]$. These same effects are seen in other metal complexes in this study.

These trends may be rationalized by assuming that the two coupling constants in the complexes, $^4J(P,F)$ and $^2J(P,H)$ are opposite in sign, with $^4J(P,F)$ being positive. Such a reversal in $^2J(P,H)$ couplings has long been recognized,[232] along with the observation that small or zero values of $^2J(P,H)$ may result from cancellation of terms of different sign.[233] For example, $^2J(P,H)$ is +2.8

Hz in $(CH_3)_3P$ but decreases to values of -7 to -8 Hz in complexes $[(CH_3)_3PM(CO)_5]$ (M = Cr, Mo, W).[234] With the phosphine $CH_3P(CF_3)_2$, both hydrogen and fluorine are present and $^2J(P,H)$ decreases from +4.4 to -6.8 Hz and $^2J(P,F)$ decreases from 74.5 to 70.0 Hz on coordination to $Cr(CO)_5$.[234] Likewise, $^2J(P,H)$ is -0.5 Hz in $(CH_3CH_2)_3P$[233] and undetected (<1.0 Hz) in $CH_3CH_2PPh_2$[100] but in the complex $[(CH_3CH_2PPh_2)Cr(CO)_5]$, $|^2J(P,H)|$ is 7.0 Hz.[235] This coupling is almost certainly negative in sign. The assignment of signs as such to these coupling constants is to be consistent with the general trend that coupling constants decrease as electron density is removed from the phosphorus atom by oxidation or coordination.[233]

The value of $^2J(P,H)$ in the free ligand, HL^1, is 2.4 Hz, and by analogy with the similar phosphines discussed above, the sign of $^2J(P,H)$ has been assigned as positive. The values of $^2J(P,H)$ for the platinum complexes discussed here are then actually negative. The value of $^4J(P,P)$ is likewise positive in the free ligand and decreases on coordination.

Throughout this study, the changes in coupling constants from ^{31}P to ^1H and ^{19}F do not correlate exactly with each other or with the coordination shift for the ^{31}P resonance. However, this is not very surprising because of the additional effects of chelation and the variety of coordinaton geometries of the different metal complexes, on the coupling constants.

3.4 Reaction Mechanisms

It is possible to propose a mechanistic scheme to explain the various interconversions and isomerizations that occur in this system of platinum complexes of HL^1. In doing so, two assumptions will first be made:

1) All intermediates in these substitution reactions are five-coordinate trigonal bipyramidal species, as has been proposed for such reactions of platinum(II) complexes.[248]
2) Groups that are mutually trans in the product of the substitution reactions assume axial positions in the trigonal bipyramidal intermediates. This is also consistent with the observation that stereochemistry about the platinum is maintained during substitution reactions.[248]

With these two assumptions in mind, Scheme 3.2 is presented to illustrate a possible mechanism for the substitution reactions.

The initial reaction of $PtCl_2$ with HL^1 involves coordination of the phosphino groups to give $[Pt(HL^1)_2Cl_2]$, III, which can be isolated from the non-basic solvent acetonitrile. However in more basic media such as DMF, one of the dangling fluorinated alcohols is deprotonated giving IIIa of Scheme 3.2. This alkoxide can now coordinate to

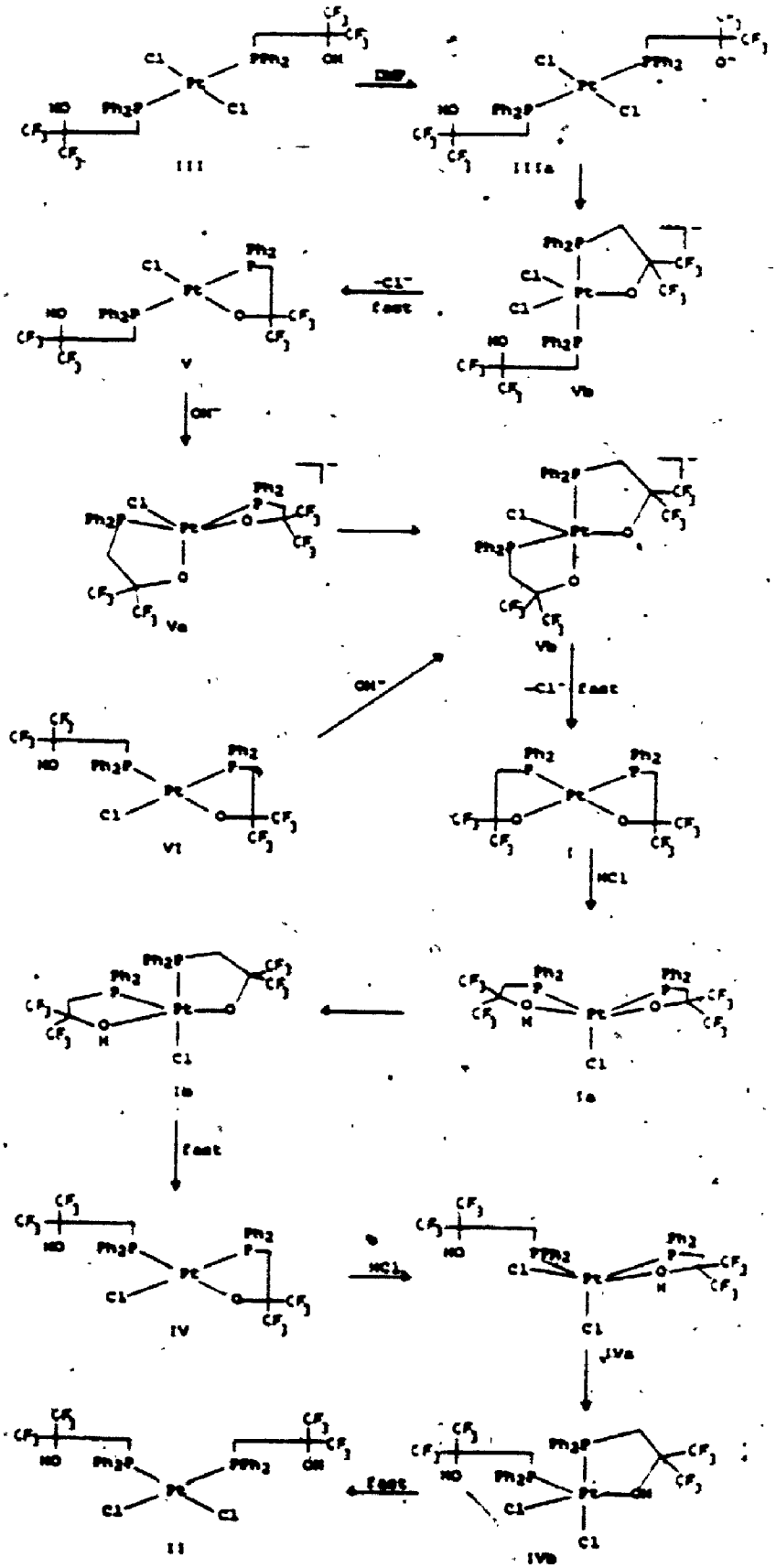

Scheme 3.2. Mechanisms of interconversion of complexes.

the platinum atom to give a trigonal bipyramidal anionic intermediate, IIIb, with the phosphines in the axial positions. Rapid loss of chloride ion from IIIb yields trans-[Pt(HL^1)(L^1)Cl], V.

Addition of OH^- to a solution containing V results in deprotonation of the second fluorinated alcohol, which can then coordinate apically, giving a distorted square-pyramidal anionic species Va. The species Va rearranges to a trigonal bipyramid with one phosphino group and one alkoxide in the axial positions, Vb. Again, rapid loss of chloride ion from such an intermediate would yield the observed product, cis-[Pt(L^1)$_2$], I.

Likewise addition of OH^- to a solution of cis-[Pt(HL^1)(L^1)Cl], IV, produces cis-[Pt(L^1)$_2$]. In this case the square-pyramidal species would have cis, basal, phosphines (not shown in Scheme 3.2). This species could then rearrange to Vb and lose chloride ion to give I.

Continuing on through Scheme 3.2, one can now by addition of HCl cause ring-opening substitution reactions to take place. Addition of HCl to I gives the square-pyramidal species Ia where the chloride ion assumes the apical position and H^+ attacks the coordinated alkoxides. Rearrangement of Ia gives the trigonal bipyramidal Ib with an axial phosphine and chloride ion. The alcohol can then dissociate from the metal centre giving cis-[Pt(HL^1)(L^1)Cl], IV.

Attack on IV by another molecule of HCl gives the square-pyramidal species IVa. This species can rearrange to a trigonal bipyramidal, IVb, and dissociate the second fluorinated alcohol to give cis-$[Pt(HL^1)_2Cl_2]$, II.

The failure of attempts to make the dimethylated analog of II, cis-$[Pt(HL^1)_2(CH_3)_2]$ was most likely due to the high trans-influence of all four ligands, resulting in destabilization of the complex. Instead, partial ring closure occurs giving trans-$[Pt(HL^1)(L^1)(CH_3)]$, VII. Hydrogen chloride and other protonic acids attack platinum methyl compounds by addition-elimination mechanism.[249] First, a platinum(IV) species is formed by oxidative addition, then elimination of CH_4 occurs yielding the platinum(II) product. It seems likely that a similar mechanism is in operation here, involving the six-coordinate, platinum(IV) intermediate $[Pt(HL^1)(H)(L^1)(CH_3)_2]$.

Scheme 3.3 summarizes the proposed mechanistic scheme for reactions with phosphines of the platinum(II) complexes, specifically cis- and trans-$[Pt(HL^1)(L^1)Cl]$. These reactions are of two types: conversion to cis-$[Pt(PR_3)(L^1)Cl]$, or isomerization of trans- to cis-$[Pt(HL^1)(L^1)Cl]$ catalyzed by free ligand, HL^1. The trans-isomer of $[Pt(L^1)_2]$ was never observed, nor was cis- to trans-isomerization of $[Pt(HL^1)_2Cl_2]$, the cis-isomer preferring ring closure to isomerization.

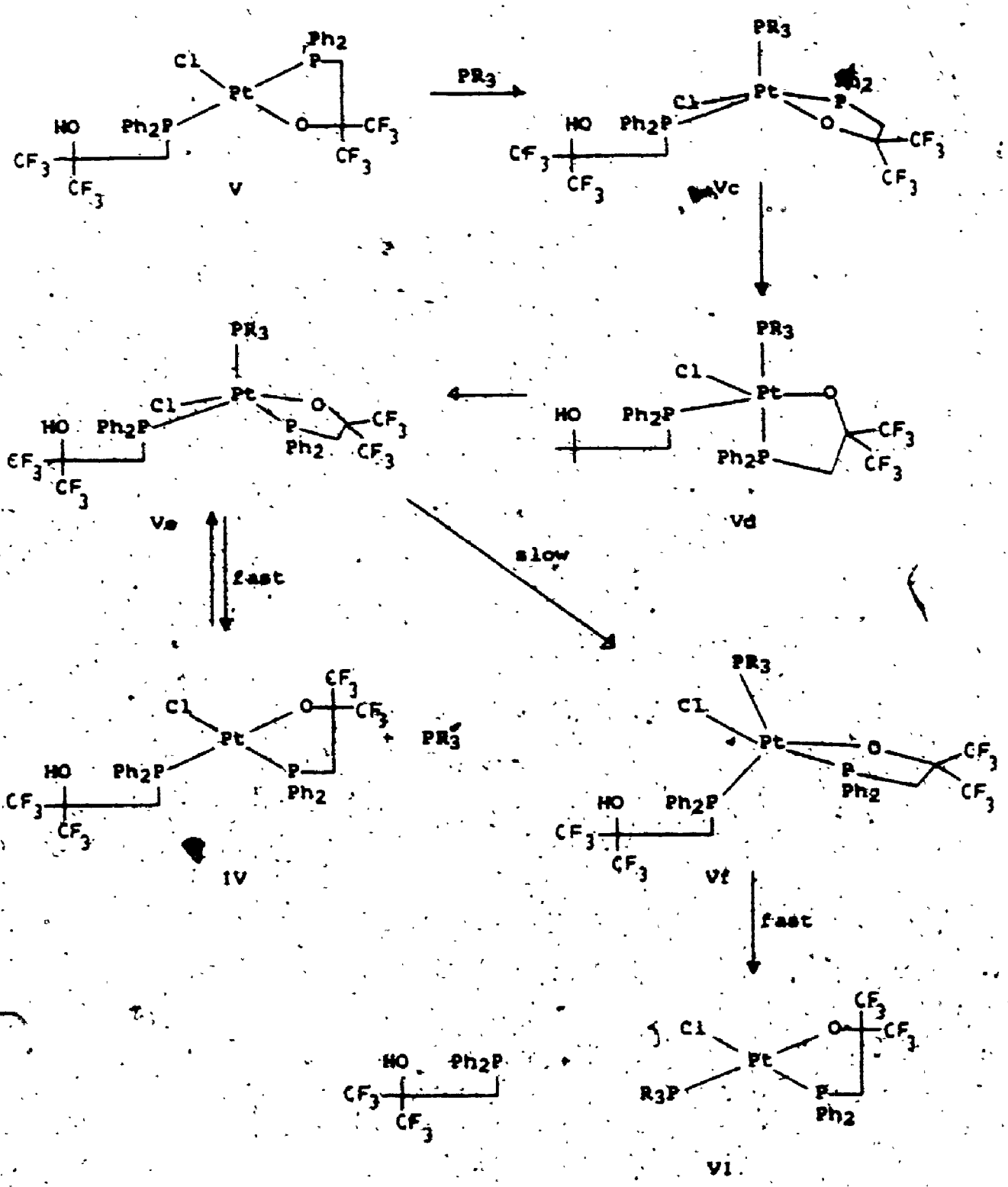

Scheme 3.3. Mechanisms of Isomerisation and Phosphine Exchange

It has previously been shown that isomerization of platinum(II) phosphine complexes is catalyzed by excess phosphine, suggesting again a five-coordinate intermediate.[248] The use of a different incoming phosphine leads to isomerization <u>without</u> phosphine exchange, showing that the catalyzing phosphine ligands occupies a unique position in the intermediate.[250] This also suggests that the trans → cis isomerization of $[Pt(HL^1)(L^1)Cl]$ occurs rapidly by a mechanism independent of the catalyzing phosphine, while the substitution of PR_3 for HL^1 occurs by a subsequent slower reaction.

Scheme 3.3 illustrates that the first step in the mechanism is coordination of the phosphine PR_3 to give a square-pyramidal species, with PR_3 in the unique apical position. This can then rearrange through the trigonal-bipyramidal intermediate, Vd, with axial chelating phosphine and PR_3 groups to Ve, another square-pyramidal intermediate with an apical PR_3 group; only in this case the basal phosphino groups are cis. A rapid dissociative equilibrium now results in formation of the cis-isomer of $[Pt(HL^1)(L^1)Cl]$.

Alternatively, to account for phosphine exchange, Ve may slowly rearrange to Vf, a trigonal-bipyramidal intermediate with an axial chloride ion and chelating phosphine. Rapid loss of the monodentate ligand HL^1, from an equatorial position then gives the phosphine exchange product cis-$[Pt(PR_3)(L^1)Cl]$, VI, where PR_3 = PPh_3, PPh_2Me,

$PPhMe_2$, PMe_3.

Consideration of this mechanism suggests why the cis-trans isomerization of $[Pt(HL^1)_2Cl_2]$ was never observed; the great steric interactions between three monodentate HL^1 ligands would certainly destabilize the five-coordinate intermediate $[Pt(HL^1)_3Cl_2]$.

Finally, the stereochemistry of these mechanistic schemes are consistent with some general observations:

1) The chelating ligand assumes an axial-equatorial arrangement in each trigonal-bipyramidal intermediate (except Ib where the fluorinated alcohol is about to dissociate). This is consistent with the known bite angle of bidentate L^1, which, as will be discussed in chapter 4, has values of 85.2(2)° and 82.7(2)° in cis-$[Pt(L^1)_2]$.

2) In these trigonal-bipyramidal intermediates, the phosphino group of L^1 assumes the axial position and the alkoxide takes up the equatorial position. This is consistent with the fact that Pt-P bond lengths are longer than Pt-O bonds. Furthermore this is consistent with the suggestion that for pentacoordinate d^8 transition metal complexes, a trigonal-bipyramidal structure with the acceptor ligands (more electronegative) in the equatorial position and the donor ligands (more electropositive) in the axial positions, is preferred.[251] In the case of $Pt(L^1)_2$, antisymbiosis causes the

cis isomer to be favoured. Therefore, it is necessary for one of the chelate rings in 2b to have an axial fluorinated alkoxide so that loss of equatorial Cl^- yields cis-$[Pt(L^1)_2]$ rather than the trans isomer.

3) Likewise in Scheme 3.3, the chelating ligands assumes an axial-equatorial arrangement in the intermediates with the phosphine in the axial position.

Therefore, these two possible mechanistic schemes are consistent with the associative mechanism via trigonal-bipyramidal intermediates proposed for such substitution, phosphine catalyzed isomerization, and phosphine exchange reactions of platinum(II) compounds. The stereochemistry of the intermediates are consistent with: the bite angle of L^1, the preference of penta-coordinate platinum(II) compounds for trigonal-bipyramidal structures with electropositive substituents in the axial positions, the return to square-planar products by equatorial ligand dissociation, the axial ligands in the trigonal-bipyramidal intermediate becoming mutually-trans ligands in the square-planar product.

The chemistry of the ligand HL^1 with platinum(II) complexes will be compared with that of palladium(II) and nickel(II) in the thesis summary in chapter 8.

Chapter 4

The Crystal Structures of Two Platinum(II) Complexes of HL^1

4.1 Introduction

In the previous chapter the platinum(II) complexes of the ligand HL^1 were discussed. For two of these complexes, $[Pt(HL^1)_2Cl_2]$ and $[Pt(HL^1)(L^1)Cl]$, both cis- and trans-isomers of the complex were isolated; in the case of $[Pt(HL^1)_2Cl_2]$, the trans-isomer appears to be thermodynamically-favoured.

It is well-known that for complexes of the type $[Pt(PR_3)_2Cl_2]$, the effect of antisymbiosis is to favour the cis-isomer. Indeed, because the fluorinated alkoxide is a hard ligand like the chloride ion, the complex $[Pt(L^1)_2]$ is observed only as the cis-isomer. However, the fact that both isomers are observed for $[Pt(HL^1)(L^1)Cl]$ and $[Pt(HL^1)_2Cl_2]$, with the trans-isomer being favoured in the case of the later, suggests that a subtle interplay of steric and electronic factors exists.

It would seem that, when HL^1 acts as a monodentate phosphine, its steric bulk is responsible for stabilizing the trans-isomer of $[Pt(HL^1)_2Cl_2]$. In order to investigate the steric demands of monodentate HL^1 and bidentate L^1 and to better understand the relative importance of the steric and electronic effects in these complexes, two x-ray crystal structures were determined. The compounds

investigated were trans-$[Pt(HL^1)_2Cl_2]$, 4-1, and cis-$[Pt(L^1)_2]$, 4-2.

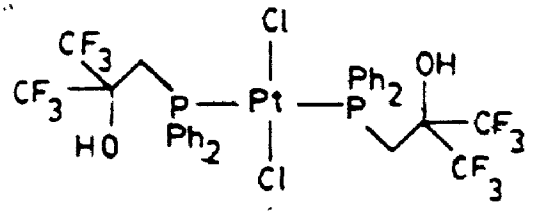

4-1

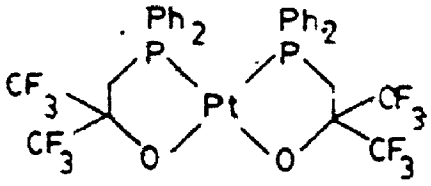

4-2

This chapter describes the results of this study and the structures of these two compounds.

4.2 Experimental

The crystals of $[Pt(HL^1)_2Cl_2]$, 4-1, were grown by slow evaporation of a solution in $CHCl_3$/acetone, while the $[Pt(L^1)_2]$ crystals, 4-2, were obtained from a solution of $CHCl_3$.

Preliminary photographic analysis was carried out for both compounds. In each case, a suitable crystal was chosen and precession photographs of the hk0, hkl, 0kl, 1kl layers were obtained along with Weissenberg photographs of the h0l and h1l layers. These photographs showed that both crystals belong to the monoclinic crystal system, having Laue symmetry 2/m.

For 4-1, systematic absences were observed when h+l is odd for the h0l class of reflections and when k is odd for the 0k0 class of reflection. The interpretations of these systematic absences are a (010) glide plane with component a/2 + c/2 and a [010] screw axis with component b/2

respectively.

For 4-2, the systematic absences occurred when l is odd for the hOl class of reflections and when k is odd for the OkO class of reflections. These absences indicated a (010) glide plane with component c/2 and a [010] screw axis with component b/2 respectively.

The space groups for 4-1 and 4-2 were thus uniquely determined to be $P2_1/n$, a non-standard setting of $P2_1/c$, and $P2_1/c$ - C^5_{2h}- No. 14[132] respectively. Both of these space groups are centrosymmetric. The interpretations of the systematic absences for these two structures are summarized in Tables 4.1 and 4.2.

At this point, the crystal density was determined in each case, using the method of neutral buoyancy in cyclohexane and 1,2-dibromoethane. The density of 4-1 was determined to be 1.848(1) g/cm^3. Using the lattice constants obtained by photographic analysis (a =16.95(7)Å, b = 10.3(1)Å, c = 10.3(1)Å, $\alpha = \gamma = 90°$, $\beta = 90.5°$) the number of formula weights per unit cell was calculated as 2.002. A value of Z = 2 then yields a calculated density of 1.846 g/cm^3, very close to the measured value.

There are therefore two formula weights of $[Pt(HL^1)_2Cl_2]$ per unit cell. Since the symmetry elements of this centrosymmetric space group determine that there be four equivalent positions, the platinum atom must lie on a centre of inversion in the unit cell.

The density of 4-2 was determined to be 1.882(1)

Table 4.1 Summary of Systematic Absences for 4-1.

Class of Reflection	Condition for Non-extinction	Interpretation	Symbol
hOl	h + l = 2n	(101) glide plane component a/2 + c/2	n
0k0	K = 2n	[010] screw axis, component b/2	2_1

Table 4.2 Summary of Systematic Absences for 4-2.

Class of Reflection	Condition for Non-extinction	Interpretation	Symbol
hOl	l = 2n	(010) glide plane, component c/2	c
0k0	k = 2n	[010] screw axis, component b/2	2_1

g/cm^3. Calculations using the photographic cell constants (a = 20.04(4)Å, b = 10.13(2)Å, c = 19.51(1)Å, $\alpha = \gamma = 90°$, β = 109.7°) yielded a value of 4.57(3) for the number of formula weights per unit cell. If alternately the formula weight was considered to consist of both a molecule of $[Pt(L^1)_2]$ and a molecule of $CHCl_3$, then the number of formula weights per unit cell would be calculated as 4.05(2). Therefore for 4-2, there are four molecules of $[Pt(L^1)_2]$ and four molecules of $CHCl_3$ per unit cell. This result is not surprising because it had previously been observed that, with time, the crystals become opaque and appear to lose solvent molecules from the lattice.

A single crystal was chosen for each structure for data collection. In the case of 4-1, the crystal was yellow with ten faces, the longest dimension being approximately 0.60 mm. The crystal was mounted on a glass fibre with the fibre approximately parallel to the long axis.

The crystals of 4-2 on the other hand were flat needles with each end capped by two faces. It was therefore necessary to cut the crystal in order that it be more equi-dimensional. A cut was made perpendicular to the long dimension of the needle near one end so that a plate with seven sides was obtained. The longest dimension of the crystal was from the cut face to the edge where the two faces meet capping one end; this distance was measured as 0.260 mm. The glass fibre was glued to the crystal on the cut face.

For both 4-1 and 4-2, the goniometer head with the glass fibre and crystal was mounted on an Enraf-Nonius CAD4F computer-controlled kappa axis diffractometer. Both the preliminary examination and data collection were performed with MoKα radiation (λ = 0.71073 Å).

A polaroid photograph was obtained and 20 intense reflections were chosen from it. The crystal was centred using one of these reflections. The reflections were all centred, then a least-squares indexing and fitting procedure of these 20 reflections provided the lattice constants and cell volume.

Omega scans of three intense reflections along each of the three axes were obtained as a check on crystal quality. For 4-1, the reflections chosen were (200), (020) and (00$\bar{2}$) and the widths at half height for the scans were 0.177°, 0.198° and 0.156° respectively. Likewise for 4-2, scans of reflections (200), (040) and (002) had widths of 0.115°, 0.125° and 0.094° respectively. These omega scans indicate good crystal quality in both cases.

By collecting data in the range 32° $\leq 2\theta \leq$ 40° for 4-1 and 32° $\leq 2\theta \leq$ 38° for 4-2, it was possible to choose some intense high angle reflections for further least-squares refinement of the lattice constants. For 4-1, 20 reflections with 31.90° $\leq 2\theta \leq$ 37.30° were used while for 4-2, 19 reflections were chosen with 32.04° $\leq 2\theta \leq$ 39.80°.

The final unit cell dimensions, which were arrived at after a number of cycles of least-squares refinement, are

given in Table 4.3.

The data for structure 4-1 were collected in two shells: $0° \leq 2\theta \leq 50°$ and $50° \leq 2\theta \leq 60°$. However for 4-2 only one shell was collected, having $0° \leq 2\theta \leq 45°$, because as noted earlier the crystals appeared to lose solvent with time. In both cases MoKα radiation was used. For 4-1, the data collected were in the range $-23 \leq h \leq 23$, $-1 \leq k \leq 14$, $0 \leq \ell \leq 14$, while for 4-2, the data were in the range, $-21 \leq h \leq 21$, $-10 \leq k \leq 0$, $0 \leq \ell \leq 21$.

A total of 6057 reflections were measured for 4-1 of which 5200 were unique and not systematically absent. For 4-2, a total to 5161 reflections were measured with 4860 unique and not systematically absent data. Processing of the data was done in both cases using the program BEGIN.[133] The processing included a correction for back ground counts, scanning rate, the Lorentz effect and polarization. The actual formulae used for the correction were:

$$I_{raw} = \frac{20.1166 \times ATN}{NPI} \times (C - RxB)$$

where ATN = attenuator factor

C = total count

R = ratio of scan time to background counting time

B = total background count

NPI = ratio of fastest possible scan time to scan rate for the measurement

and $F_{OBS} = \sqrt{I_{raw}/L_p}$

where L_p = Lorentz-Polarization Factor and is dependent on

the relative positions of the monochromater and tube mount and on the mosaicity of the monochromator graphite crystal.

In each case, four reflections were chosen, and the intensity of each reflection was measured every three hours as a check for intensity decay. For 4-1, the four standards were (00$\bar{2}$), (200), (0$\bar{2}$0) and (004); the total change in intensity of these four standards over the 135.0 hours of exposure time was actually a gain of 1.29%. Therefore, a correction was not considered necessary. On the other hand, the four standards for 4-2, (0$\bar{2}\bar{2}$), (002), (040) and (200) showed an overall loss in intensity of 5.3% over 86.0 hours of exposure time. Therefore the program DECAY was used to apply a linear correction for intensity loss due to crystal decay in the case of structure 4-2.

Each data crystal was examined on a two-circle goniometer. For each face, the ϕ and ρ angular settings which placed the face in a reflecting position were measured. These values, when compared with values calculated by the program CRYSTL[133] for various possible faces, allow for the identification of each crystal face. The dimensions of the crystals were measured on a microscope equipped with a filar eyepiece.

The data crystal of compound 4-1 has 10 faces: (1$\bar{1}$0), (2$\bar{1}$1), (2$\bar{1}\bar{1}$), ($\bar{2}\bar{1}\bar{1}$), ($\bar{2}\bar{1}\bar{1}$), ($\bar{1}$01) and (10$\bar{1}$). For 4-2, the data crystal had 7 faces including the cut face: (100), (001), (1$\bar{1}$0), ($\bar{1}\bar{1}$0) and the indices of the cut face were estimated as (010). ORTEP drawings of the two data

crystals appear in Fig. 4.1 and 4-2.

Having obtained descriptions of the data crystals, it was possible to correct the data for differential absorption. This was carried out by the program, ABSCOR[133] which uses Gaussian numerical methods.

In each case the range chosen over which the data was collected meant that some of the data were related by symmetry and could be averaged. The averaging is done by the program PAINT.[133] For 4-1, the agreement factors using observed and accepted reflections were 1.9% based on intensity and 1.8% based on F_{obs} before the absorption correction and 1.4% and 1.5% respectively after the absorption correction. For 4-2, the agreement factors were 2.4% and 2.1% respectively before the absorption correction and 1.8% after the correction. The fact that the agreement was better after the correction in each case suggests that the crystal descriptions used for the absorption correction were reasonable. Also the low value of the factors suggest that the measurement of the reflection intensities was reasonably precise.

The crystal data and the conditions for data collection are summarized in Table 4.3.

4.3 Structure Solution and Refinement

Both structures were solved using the package of programs called the Structure Determination Package[133] or SDP-Plus of Enraf-Nonius along with several U.W.O. programs

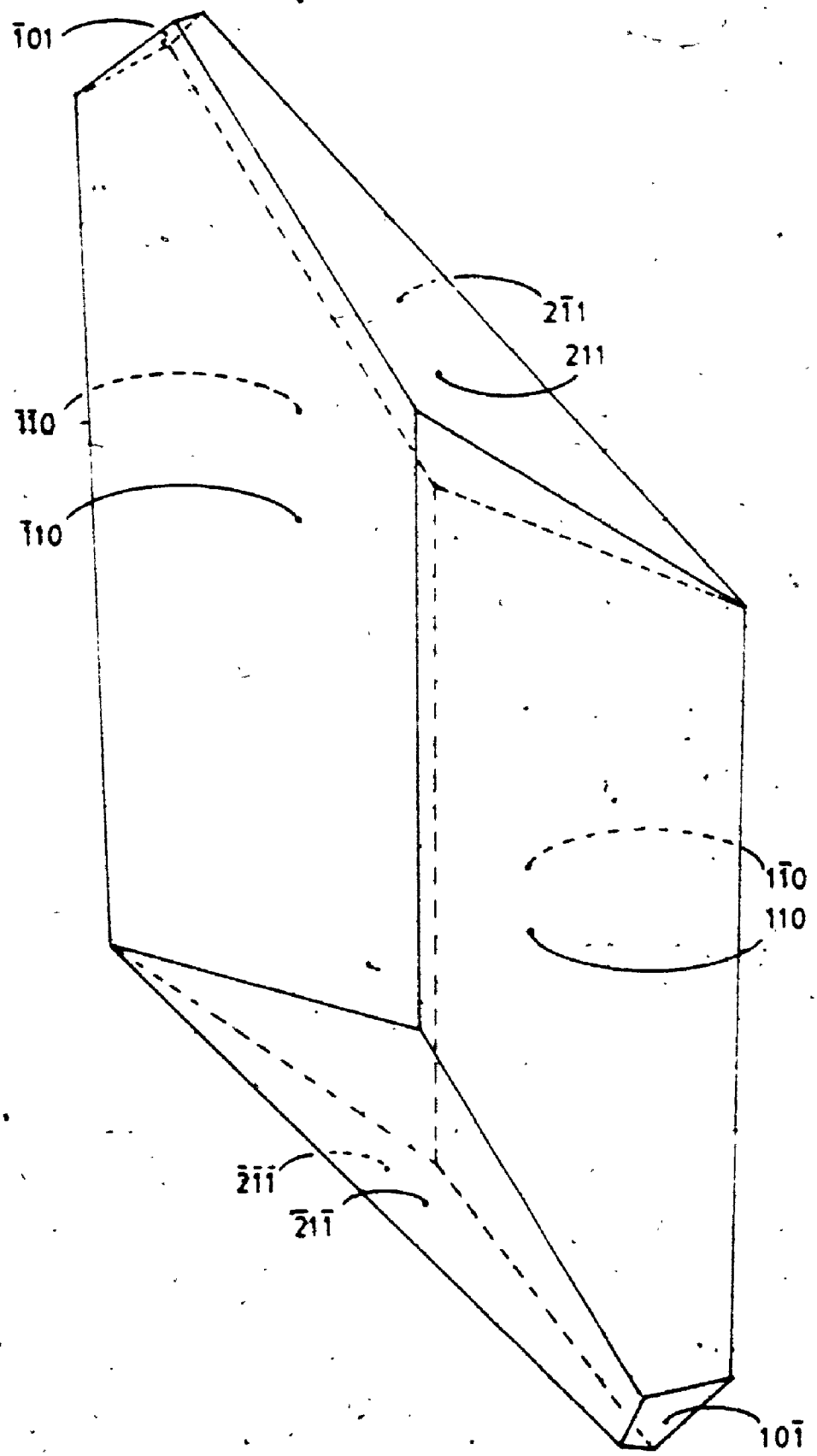

Figure 4.1 Drawing of data crystal for 4-1

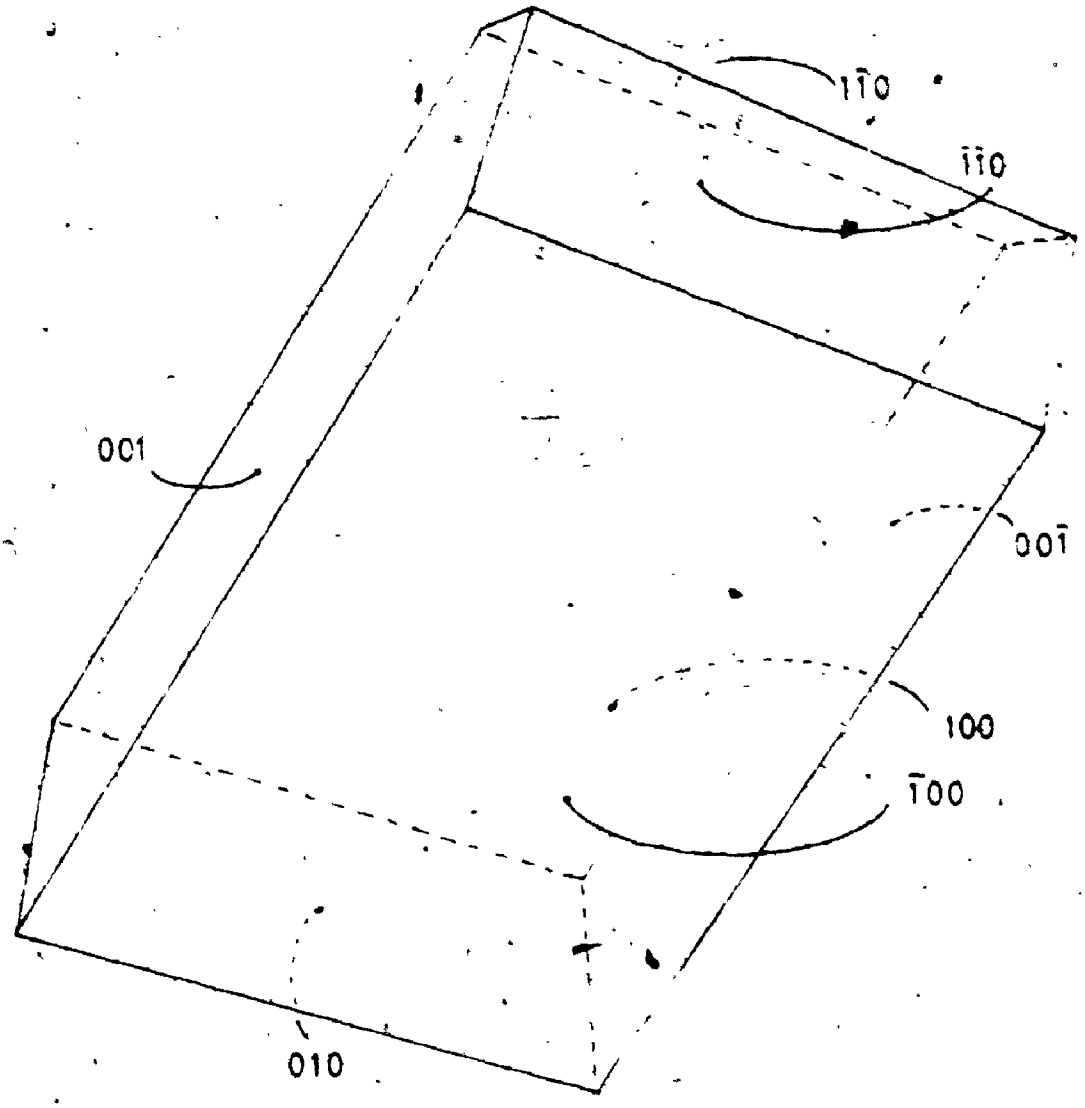

Figure 4.2 Drawing of data crystal for 4-2

Table 4.3 Crystal Data and Experimental Conditions

	4-1	4-2
Chemical Formula	$C_{32}H_{26}Cl_2F_{12}O_2P_2Pt$	$C_{33}H_{25}Cl_3F_{12}O_2P_2Pt$
Formula Weight	999.49	1044.94
Crystal System	Monoclinic	Monoclinic
Laue Symmetry	2/m	2/m
Space Group	$P2_1/n$	$P2_1/c$ No. 14
a (Å)	16.934(2)	20.036(3)
b (Å)	10.320(1)	10.133(1)
c (Å)	10.198(2)	19.517(3)
β	90.32(1)°	109.69(1)°
Cell Volume (Å^3)	1782.2(9)	3731(2)
Temperature (°C)	22	22
Obsvd. Density (g/cm^3)	1.848(1)	1.882
Calcd. Density (g/cm^3)	1.846	1.860
Crystal Volume (mm^3)	.00683	.00241
Diffractometer	Enraf-Nonius CAD4F	Enraf-Nonius CAD4F
Radiation	Mo Kα	Mo Kα
Monochromator	Graphite	Graphite
Wavelength (Å)	0.71073	0.71073
Absorption Coefficient (cm^{-1})	43.07	41.89
Absorption Correction	Gaussian, ABSCOR	Gaussian, ABSCOR
Gaussian Grid	10 x 6 x 26	8 x 15 x 12
Maximum Transmission Factor	0.6762	0.7430
Minimum Transmission Factor	0.4603	0.5497

Table 4.3 (Continued)

	4-1	4-2
Detector Vertical Aperture (mm)	4.00	4.00
Detector Horizontal Aperture (mm)	5.0 + 0.35 tan θ	5.0 + 0.35 tan θ
Crystal-Detector Dist. (mm)	205	205
Take-off Angle (deg)	2.5	2.5
Scan mode	ω/2θ	ω/2θ
Scan speed (deg. min^{-1})	1.1 - 3.3	1.3 - 3.3
Scan width (deg.)	0.80 + 0.35 tan θ	0.70 + 0.35 tan θ
Backgrounds	25% above and below calc. scan width	25% above and below calc. scan width
Data Collected	$-23 \leq h \leq 23$ $-1 \leq k \leq 14$ $0 \leq l \leq 14$	$-21 \leq h \leq 21$ $-10 \leq k \leq 0$ $0 \leq l \leq 21$
2θ Range	$0° \leq 2\theta \leq 60°$	$0° \leq 2\theta \leq 45°$
Standards	(002), (200), (020), (004)	$(0\bar{2}2)$, (002), (040), (200)
Change in Intensity	+1.2%	-5.3%
No. of Refl. Collected	6057	5161
No. averaged	1042	246
% agreement	1.4 on intensity 1.5 on F_{obs}	1.8 on intensity 1.8 on F_{obs}
No. Refl. in Final Cycle	3234	3030
Cutoff for Final Cycle	$F_o > 3\sigma F_o$	$F_o > 3\sigma F_o$
Number of Var. in Final Cycle	232	313
Final R	3.1	3.4
Final Weighted R	3.9	4.5

(see Appendix 1) on a PDP-11/23+ computer.

4.3.1 Structure 4.1

Earlier calculations involving the unit cell constants and the observed crystal density indicated that Z = 2, that is that there are two formula weights of $[Pt(HL^1)_2Cl_2]$ per unit cell. Also, the space group was shown to be $P2_1/n$, a non-standard setting of $P2_1/c$ with four equivalent positions. The molecule must then lie in a special position, on a symmetry element, since the number of formula weights per unit cell is only two.

For the space group, $P2_1/n$, the equivalent positions are: (x,y,z), $(\frac{1}{2}+x,\frac{1}{2}-y,\frac{1}{2}+z)$, $(\bar{x},\bar{y},\bar{z})$ and $(-\frac{1}{2}-x,-\frac{1}{2}+y,-\frac{1}{2}-z)$. The positions (x,y,z) and $(\bar{x},\bar{y},\bar{z})$ are related by an inversion centre, as are $(\frac{1}{2}+x,\frac{1}{2}-y,\frac{1}{2}+z)$ and $(-\frac{1}{2}-x,-\frac{1}{2}+y,-\frac{1}{2}-z)$. In the case of 4-1, the molecule must be lying on a special position, an inversion centre and must itself possess a centre of inversion. Therefore the complex 4-1 has a trans-geometry in the solid-state as well as in solution, with the inversion centre, the platinum atom, lying on an inversion centre in the unit cell.

If one platinum atom lies in the special positon $(0,0,0)$, then the other platinum atom lies in the special position $(\frac{1}{2},\frac{1}{2},\frac{1}{2})$. Similarly, it is possible that the two platinum positions are $(\frac{1}{2},0,0)$ and $(0,\frac{1}{2},\frac{1}{2})$ or $(0,0,\frac{1}{2})$ and $(\frac{1}{2},\frac{1}{2},0)$ or $(\frac{1}{2},0,\frac{1}{2})$ and $(0,\frac{1}{2},0)$. All four possibilities differ only in the choice of the origin.

A combination of direct methods and the Patterson method was used to locate the heavy atoms. SDP-Plus contains a series of programs called MULTAN11/82, which make up a direct-methods route to structure solutions. The phase determination of MULTAN11/82 makes use of the tangent formula of Karle and Kauptman[252] and each solution is assigned a figure of merit which expresses the probability of that phase determination being correct. An E-map can be produced for each phase determination.

E-maps were obtained for the three most probable solutions of MULTAN's phase determination. In the case of the E-map of the most probable solution, the three most intense peaks were:

1. (0.0959, 0.1244, 0.1001)
2. (0.9561, 0.1694, 0.8697)
3. (0.0000, 0.0000, 0.0000)

The E-maps of the next two most likely solutions were very similar. The special position (0,0,0) was chosen for the platinum atom.

A Patterson map was also obtained which showed, as expected, the most intense vector as (0.5, 0.5, 0.5) due to the platinum-platinum vector. In addition the next most intense vector was (0.0996, 0.13887, 0.1094), having a length of 2.473 Å. This is a reasonable length for a Pt-Cl bond length and if this vector is added to the platinum

position, the position generated is very close to that of position 1 in the E-map.

The fifth most intense vector in the Patterson map was (0.0488, 0.1660, 0.1094) with a length of 2.203 Å, not unreasonable for a Pt-P bond length. As the symmetry of a Patterson map is the Laue symmetry, 2/m in this case, then the vector (0.0488, 0.1660, 0.1094) is related to the vectors (0.0488, -0.1660, 0.1094) (-0.0488, -0.1660, -0.1094), (-0.0488, 0.1660, 0.1094). When (-0.0488, 0.1660, -0.1094) is added to the platinum position, the resulting position is very close to peak 2 in the E-map.

Therefore a likely solution would have the platinum atom at (0,0,0), the chlorine atom at (0.0959, 0.1244, 0.1010) and the phosphorus atom at (0.0488, -0.1660, 0.1094). By using the program SEARCH[133] with these three positions, it was quickly shown that such a solution would have a P-Pt-Cl bond angle of 87°, a reasonable value.

The standard determination proceeded assuming these positions for the Pt, Cl and P atoms. After two cycles of block-diagonal least-squares refinement, the positions had not shifted by much. However when a difference Fourier synthesis was then calculated it showed a number of peaks around the Cl but nothing around the P, indicating the positions were correct but the chlorine and phosphorus labels had to be switched. Once this change was made, the remaining non-hydrogen atoms were located using successive difference-Fourier syntheses. In between Fourier

syntheses, two cycles of block-diagonal least-squares refinement of the model would be run.

Once all the non-hydrogen atoms had been located, the refinement proceeded using full-matrix least-squares cycles, minimizing the function $\Sigma\omega(|F_o|-|F_c|)^2$ where ω is the weighting factor. The scattering factors used were those of Cromer and Waber.[135] Anomalous dispersion effects were included in the structure factor calculations.[253] The values of $\Delta f'$ were those of Cromer and were used for Pt, Cl, P, O, F and C atoms.[137]

Having found and refined all 26 non-hydrogen atoms, a difference Fourier was run in order to locate the hydrogen atoms. All 13 hydrogen atoms were found in the difference Fourier ranging from 0.642 e^-/A^3 as the fifth most intense peak to 0.495 e^-/A^3 as the twenty-third most intense peak. Subsequent cycles of least-squares refinement included the hydrogen atoms in idealized positions in the structure factor calculations. The scattering factors for hydrogen were those of Stewart, Davidson and Simpson.[136]

The final cycle of full-matrix least-squares refinement involved 232 variables (anisotropic thermal parameters of the platinum atom, positional parameters and anisotropic thermal parameters for the remaining 25 non-hydrogen atoms and an overall scale factor). It converged with unweighted and weighted R factors of 3.1% and 3.9% respectively. The largest parameter shift/error was 0.04 for one of the anisotropic thermal parameters of the platinum atom. The

estimated standard deviation on an observation of unit weight was 1.041. There were 3234 reflections used in the final cycle for which $F_o > 3\sigma F_o$. The value of P, an experimental instability factor used to downweight intense reflections, was 0.05.

The program CORCOE[133] was used to calculate correlation coefficients. There were ten correlation coefficients greater than 0.50, with the largest being 0.576 involving the scale factor and an anisotropic thermal parameter of the platinum atom.

The program PERFACT produced plots of $\omega(|F_o|-|F_c|)$ versus $|F_o|$, reflection order in data collection, $\sin\theta/\lambda$ and various classes of indices. These plots showed no unusual trends.

A final difference-Fourier synthesis was calculated and the highest peak had a height of 0.871 e^-/A^3 with an error of 0.08 e^-/A^3 based on F. It was most closely associated with the platinum atom, being 0.867 A removed. It was of no chemical significance.

The shortest Pt-Pt bond distance was 10.20 A. The shortest intermolecular distance was 2.54 A between the alcohol hydrogen and HC(25) at (x,y,z-1). There were no intermolecular distances under 3.0 A which did not involve hydrogen atoms. The shortest non-bonding intramolecular distance was 1.5513 A between H(1)C(1) and H(2)C(1). The shortest distance not involving hydrogen atoms was 2.109(7) A betwen F(1) and F(3). Therefore no unusually short

non-bonding contacts, either intra- or intermolecular, were detected.

The final positional and thermal parameters for structure 4-1 are given in Appendix 2.

4.3.2 Structure 4-2

In the case of structure 4.2, the number of formula weights per unit cell was determined to be four and the space group was shown to be $P2_1/c$ which has four equivalent positions. Therefore the molecule was not lying in a special position. Since the structure contains a platinum atom and the next heaviest atom is phosphorus, the position of the platinum atom could be determined by the heavy atom method.

An origin-removed Patterson synthesis was calculated and from it the platinum atom position was determined to be (0.2451, 0.223, -0.25). The remaining 52 non-hydrogen atoms were located using successive difference-Fourier syntheses.

After all the non-hydrogen atoms had been located, the refinement made use of full-matrix least-squares cycles in place of block-diagonal refinement. Again the scattering factors were those of Cromer and Waber.[135] Anomalous dispersion was included in the calculation of structure factors with $\Delta f'$ values of Cromer[137] being used for Pt, Cl, P, O, F and C atoms.

In addition, for structure 4-2, a molecule of

chloroform was included in the formula weight. There were no problems in locating and refining the four non-hydrogen atoms of the chloroform.

After having found and refined the 53 non-hydrogen atoms, a difference Fourier was calculated and used to locate the hydrogens. All 25 hydrogens were located, ranging in intensity from 0.713 to 0.271 e^-/A^3. The hydrogen atoms were then included in the structure factor calculations of subsequent refinements, using the scattering factors of Stewart, Davidson and Simpson[136] and assuming idealized geometry.

The final cycle of full-matrix least-squares refinement included 313 variables (positional and anisotropic thermal parameters for Pt, Cl, O, P and F atoms, positional and isotropic thermal parameters for C atoms and an overall scale factor) and 3030 reflections for which $F_o > 3\sigma F_o$. A value of 0.07 was chosen for P when weighting the data. The largest shift/error was 0.01 for positional parameters of four carbon atoms. The model converged with final unweighted and weighted R factors of 3.4% and 4.5% respectively. The estimated standard deviation on an observation of unit weight was 0.997.

Correlation coefficients were calculated and there were 22 coefficients greater than 0.50. The largest was 0.797 between two anistropic thermal parameters of a single fluorine atom.

Again plots of $\omega(|F_o|-|F_c|)$ versus $|F_o|$, reflection

order in data collection, $\sin\theta/\lambda$ and various classes of indices, produced by the program PERFACT, showed no unusual trends.

A final difference Fourier was calculated and the largest peak had a height of 0.902 e^-/A^3. It was most closely associated with the platinum atom, being 0.985 A removed, but of no chemical significance.

The shortest intramolecular non-bonding distance, excluding hydrogens, was 2.07(1) A from F(4) to F(6). The shortest intermolecular distance was 2.504(8) from F(2) to HC(36) at $(x, \frac{1}{2}+y, -\frac{1}{2}-z)$. The closest approach of the solvent molecule of the complex is 2.922(5) A between Cl(3) and HC(22) at $(1-x, y, z)$. Therefore there were no unusual short non-bonding contact distances.

The final positional and thermal parameters are given in Appendix 2.

4.4 Structure Descriptions

4.4.1 Structure 4.1.

An ORTEP drawing of structure 4.1 appears in Fig. 4.3, showing the stereochemical arrangement of the molecule. Selected bond lengths and angles appear in Table 4.4.

The coordination geometry about the platinum was confirmed to be trans-square-planar. In fact, because the platinum atom serves as a centre of symmetry, the P-Pt-P and Cl-Pt-Cl angles are constrained to be 180° and the

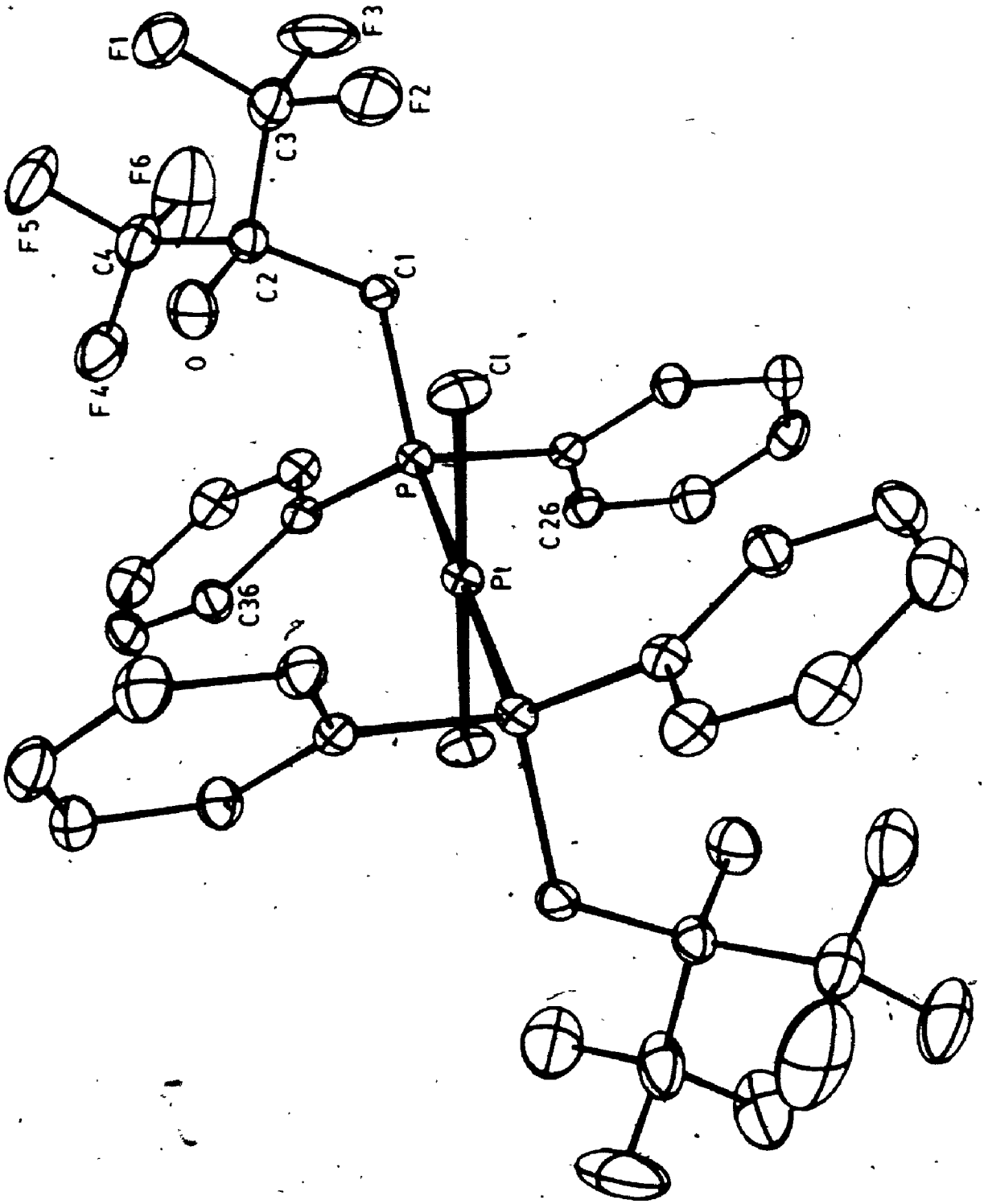

Figure 4.3 ORTEP drawing of 4-1

Table 4.4 Selected Bond Lengths and Angles for 4-1.

Bond Lengths (Å)		Bond Angles (deg)	
Pt - P	2.319(1)	Cl-Pt-P	87.25(5)
Pt-Cl	2.303(1)	Pt-P-C(31)	118.8(2)
P-C(1)	1.835(5)	Pt-P-C(21)	104.5(2)
P-C(21)	1.824(4)	Pt-P-Cl(1)	119.1(2)
P-C(31)	1.809(5)	C(1)-P-C(31)	105.2(2)
C(1)-C(2)	1.540(7)	C(1)-P-C(21)	99.7(2)
C(2)-O	1.388(7)	C(21)-P-C(31)	107.3(2)
C(2)-C(3)	1.508(9)	P-Cl(1)-C(2)	121.7(4)
C(2)-C(4)	1.555(8)	O-C(2)-C(4)	104.2(4)
C(3)-F(1)	1.306(9)	O-C(2)-C(3)	107.4(5)
C(3)-F(2)	1.344(9)	O-C(2)-C(1)	115.2(4)
C(3)-F(3)	1.343(9)	C(1)-C(2)-C(4)	112.7(4)
C(4)-F(4)	1.292(8)	C(1)-C(2)-C(3)	108.5(5)
C(4)-C(5)	1.303(8)	C(3)-C(2)-C(4)	108.6(5)

PtP_2Cl_2 fragment forms a plane. The only deviation from a square-planar configuration comes from the two differing P-Pt-Cl angles of 87.25(5)° and 92.75(5)°.

The comparison and averaging of bond lengths for all structures in this thesis demanded the application of statistical tests,[138] two of which are mentioned here. The χ^2 test is used to determine whether a group of m chemically equivalent bonds are in fact equivalent crystallographically and may then be averaged. This test involves the comparison of the standard deviation calculated for the group, with that based on the standard deviations of the atomic positions. Having calculated the ratio of these two standard deviations, one may determine, using tabulated values, the probability that m equivalent bonds would, by chance, have a value exceeding this ratio.

An average value can then be compared with known values for analogous structures. Here, the ratio of the difference between the two values (Δ) to the standard deviation for the two bond lengths (σ_ℓ where $\sigma_\ell = \sqrt{\sigma_1^2 + \sigma_2^2}$) is used. Again, tabulated values for $\lambda(=\Delta/\sigma_\ell)$ may be used to determine the probability, p, that the difference between the two bonds is significant. For $\lambda >$ 2.5 the difference is probably significant; for $2.5 > \lambda > 2$ the difference may be significant; for $2 > \lambda$ the difference is not significant.

There are three other reported structure of complexes of the type trans-$[Pt(PR_3)_2Cl_2]$: $[Pt\{P(C_6H_{11})_3\}_2Cl_2]$,[254]

$[Pt(PEt_3)_2Cl_2]$[255] and $[Pt(Bu^t_2P(CH_2)_{12}PBu^t_2)Cl_2]$.[256] The Pt-P bond lengths in these complexes are 2.337(2), 2.298(18) and 2.353(5) Å respectively. The Pt-P bond length in 4-I is 2.319(1) Å, which fits into the range for the comparable compounds.

It is significant that none of these values for Pt-P bond lengths approach that expected by summing the covalent radii of Pt and P (2.41 Å).[255] This has been interpreted as evidence of d_π-d_π bonding, from the nonbonding d orbitals on platinum to the empty d orbitals of the phosphorus.[254] Thus there would seem to be significant π-back bonding to the phosphorus in HL^1, even though it was suggested in chapter 3 that the phosphino group of HL^1 lies at the strong σ-donor end of the range of phosphine ligands. Consistent with this is the Pt-P bond length in $[Pt(PMe_3)_2I_2]$ of 2.315(4) Å;[257] this bond length has similarly been shortened, although PMe_3 is considered a strong σ-donor rather than a π-acceptor.

The average Pt(II)-P bond length for 22 structures having mutually trans phosphines of the type PR_nPh_{3-n} (R = alkyl, n = 0-3) is 2.302(1)Å.[258] While it is tempting to use Pt-P bond lengths in trans-$[Pt(PR_3)_2X_2]$ compounds to discuss the relative cis-influences of various X ligands, it appears there are other factors involved in determining the bond lengths. Steric interactions between ligands can cause lengthening of the Pt-P bond length.[259]

With the effect of steric interactions in mind, it is

of interest to note how the Pt-P bond length in 4-1 compares to those of the other trans-$[Pt(PR_3)_2Cl_2]$ complexes. It is less than that of the $[Pt(P(C_6H_{11})_3)_2Cl_2]$ structure but greater than that of the $[Pt(PEt_3)_2Cl_2]$ structure. This is consistent with the proposal that HL^1 is a bulky monodentate phosphine, more sterically demanding than PEt_3 but less so than $P(C_6H_{11})_3$.

The Pt-Cl bond length in 4-1 is 2.303(1) A. This also is comparable to previously-recorded values, as it lies between that of the PEt_3 complex (2.294(9) A) and that of the $P(C_6H_{11})_3$ complex (2.317(2) A). The ordering of the Pt-Cl bond lengths is also consistent with lengthening due to increasing steric interactions with the phosphine ligands.

The length of the C-O bond in 4-1 is 1.388(7) A. It has been noted previously that the C-O bond in a fluorinated alkoxide is shorter than expected for a normal carbon-oxygen single bond (1.43 A).[265] Indeed, this will be noted for the other structures in this work where the C-O bond lengths in the structures $[Pd(PPh_2Me)(L^1)Cl]$, $[Pt(L^1)_2]$ and $[Ni(L^1)_2]$ are 1.365(3) A, 1.370(7) A and 1.37(1) A. Previously the C-O bond length in a group of fluorinated alkoxide complexes was found to average 1.350(4) A compared with 1.41(4) A for non-fluorinated alkoxides.[55]

The length of the C-O bond in structure 4-1 is also less than for non-fluorinated alcohols having the structure

of 4-3.

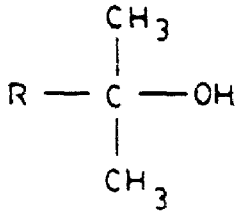

4-3

Typical values for the C-O bond length in these compounds include: 1.455(6) Å and 1.449(6) Å for 2,2'-(p-phenylene)-di-2-propanol,[266], 1.435(4) Å for pinacol,[267] 1.449(3) Å for 2,5-dimethyl-2,5-hexanediol tetrahydrate[268] and 1.422(3) Å for 2-hydroxy-2-methylpropanoic acid.[269] Therefore is is possible to order these different classes of compounds according to decreasing C-O bond length: non-fluorinated alcohols > non-fluorinated alkoxides > fluorinated alcohols > fluorinated alkoxides.

This is consistent with the reason previously given for the shortening of the C-O bond in fluorinated alkoxides.[55] As ligands, fluorinated alkoxides function as σ-acceptors. As a result, the metal-oxygen bond is highly polarized with the greater electron density on the oxygen. In order to remove some of this electron density, the oxygen forms a π-bond with the carbon. The σ-acceptor ability of the alkoxide and the π-bonding of the oxygen to the carbon is aided by the electron-withdrawing CF_3 groups on the carbon. However, in the case of the fluorinated alcohol, there is not as much electron-density on the oxygen drawn from the hydrogen as in the case of the metal-alkoxide

compounds. Therefore, the π-bonding to the carbon is less than in the alkoxides and hence the C-O bond is shortened but to a lesser extent than in the alkoxide complexes.

The possibility of the alcohol group in 4-1 being hydrogen-bonded to a chloride, fluorine or another alcohol either intra- or intermolecularly was investigated. However, a search around the hydrogen bonded to the oxygen showed no close approaches resembling hydrogen bonding. The atom, F(4), lies 2.407(4) Å removed from the hydrogen; the O-OH-F(4) angle is 91.9(3)°. Both the long distance and the angle suggest that no hydrogen-bonding is occurring here. Therefore, the fluorinated alcohol appears to be dangling free, and the trans-isomer is not stabilized by hydrogen-bonding, but rather a lessening of steric interactions appears to be the major factor.

4.4.2 Structure 4-2

An ORTEP drawing of structure 4-2 appears in Fig. 4.4 Table 4.5 contains selected bond distances and angles.

The coordination geometry of 4-2 is cis-square-planar. The least-squares plane through Pt,P(1),P(2),O(1) and O(2) is given in Table 4.6. The platinum atom lies on one side of the plane while the four donor atoms lie on the other side. As a result the geometry deviates slightly from planarity towards a pyramidal arrangement. The four least-squares planes through the phenyl rings appear in Table 4.6 also.

Figure 4.4 ORTEP drawing of 4-2

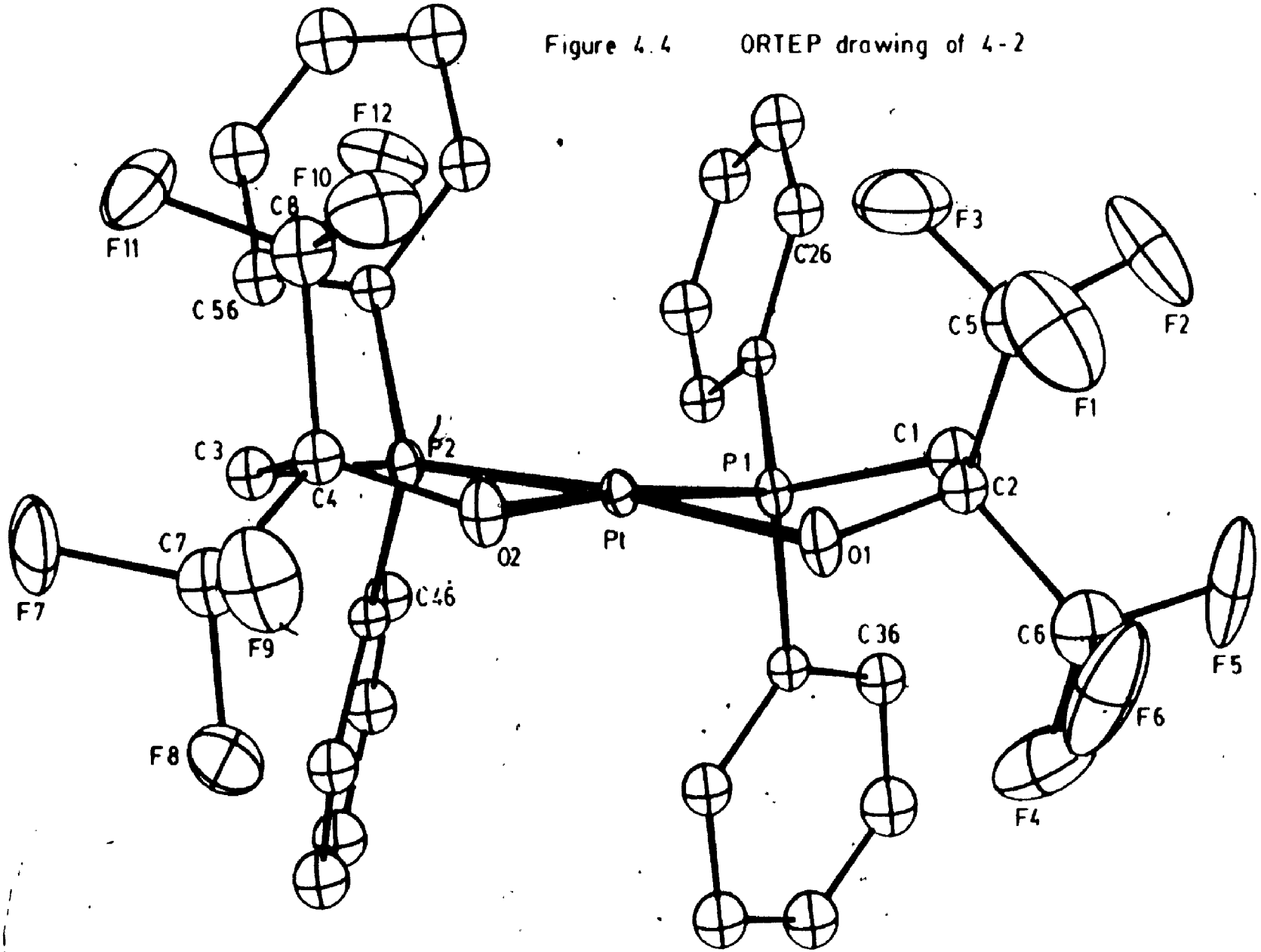

Table 4.5 Selected Bond Lengths and Angles for 4-2

Bond Distances (Å)

Pt-P(1)	2.210(3)	C(2)-C(5)	1.52(2)
Pt-P(2)	2.200(3)	C(2)-C(6)	1.51(1)
Pt-O(1)	2.030(6)	C(4)-C(7)	1.53(2)
Pt-O(2)	2.034(6)	C(4)-C(8)	1.55(1)
P(1)-C(1)	1.82(1)	C(5)-F(1)	1.32(2)
P(1)-C(21)	1.812(9)	C(5)-F(2)	1.32(2)
P(1)-C(31)	1.815(9)	C(5)-F(3)	1.31(1)
P(2)-C(3)	1.84(1)	C(6)-F(4)	1.31(2)
P(2)-C(41)	1.811(1)	C(6)-F(5)	1.34(2)
P(2)-C(51)	1.817(9)	C(6)-F(6)	1.31(2)
C(1)-C(2)	1.54(1)	C(7)-F(7)	1.34(1)
C(3)-C(4)	1.56(1)	C(7)-F(8)	1.35(1)
C(2)-O(1)	1.36(1)	C(7)-F(9)	1.32(1)
C(4)-O(2)	1.38(1)	C(8)-F(10)	1.32(1)
C(8)-F(11)	1.34(1)	C(8)-F(12)	1.31(1)

Bond Angles (deg)

P(1)-Pt-P(2)	103.72(9)	C(4)-O(2)-Pt	121.2(5)
P(1)-Pt-O(1)	82.7(2)	P(1)-C(1)-C(2)	111.8(8)
P(2)-Pt-O(2)	85.2(2)	P(2)-C(3)-C(4)	110.4(7)
O(1)-Pt-O(2)	88.2(3)	C(1)-C(2)-O(1)	114.0(8)
Pt-P(1)-C(1)	101.9(4)	C(3)-C(4)-O(2)	113.8(7)
Pt-P(2)-C(3)	103.1(3)	C(2)-O(1)-Pt	122.0(6)

Table 4.6 Least-Squares Planes in 4-2.

The equation of the plane is of the form Ax + By + Cz - D = 0

where A,B,C & D are constants and x,y & z are orthogonalized coordinates

Plane No	A	B	C	D	Atom	x	y	z	Distance	Esd
1	0.2235	0.0377	-0.9740	6.0127	----------Atoms in Plane----------					
					PT	6.6160	2.2160	-4.5203	-0.048	0.00(
					P1	5.2104	0.5673	-4.9589	0.003	0.002
					P2	8.0386	1.1919	-4.1910	0.022	0.002
					O1	4.9903	3.3640	-4.9217	0.023	0.006
					O2	7.6803	3.9300	-4.2586	0.001	0.006
					Chi Squared = 25109					
					----------Other Atoms----------					
					C1	3.6950	1.3760	-4.7158	-0.564	0.005
					C2	3.7183	2.9106	-4.7232	-0.472	0.008
					C3	9.7111	2.5838	-3.9218	0.075	0.009
					C4	8.9339	3.9120	-3.6877	-0.277	0.006
2	-0.8850	-0.2810	-0.3712	-2.8611	----------Atoms in Plane----------					
					C21	5.1620	-0.9297	-3.9389	-0.002	0.005
					C22	5.7434	-2.0818	-4.4082	0.000	0.011
					C23	6.7881	-3.2643	-3.6237	-0.002	0.012
					C24	6.2307	-3.1894	-2.3648	0.006	0.012
					C25	4.8802	-2.0428	-1.8818	-0.008	0.012
					C26	4.6283	-0.9076	-2.6557	0.006	0.011
					Chi Squared = 1					
					----------Other Atoms----------					
					P1	5.2104	0.5673	-4.9589	-0.069	0.00.
3	-0.6159	0.7522	-0.2344	-1.6702	----------Atoms in Plane----------					
					C31	5.2194	-0.0343	-6.6716	-0.006	0.01(
					C32	6.1375	0.4853	-7.5856	0.004	0.01
					C33	6.1441	0.0368	-8.9059	0.002	0.01:
					C34	5.2209	-0.8571	-9.3227	-0.005	0.01:
					C35	4.2816	-1.3507	-8.4666	0.002	0.01.
					C36	4.2660	-0.9380	-7.1068	0.003	0.01.
					Chi Squared = 1					

Table 4.6 Cont'd.

Plane No	A	B	C	D	Atom	x	y	z	Distance
					Other Atoms				
					P1	5 2104	0 5673	-4 9589	0 050
4	-0 9462	0 0385	-0 3213	-6 8405	Atoms in Plane				
					C41	9 1859	0 3193	-5 8478	-0 005
					C42	9 5782	1 0539	-6 7587	-0 007
					C43	9 9285	0 3898	-7 9393	0 013
					C44	9 9032	-0 9411	-7 9653	-0 006
					C45	9 5134	-1 6865	-6 9074	-0 006
					C46	9 1248	-1 0726	-5 7456	0 012
					Chi Squared =	4			
					Other Atoms				
					P2	8 5385	1 1919	-4 1910	0 157
5	-0 4222	-0 7598	-0 4945	-2 3871	Atoms in Plane				
					C51	8 7537	0 0661	-2 7811	0 016
					C52	7 7576	0 0118	-1 8185	0 002
					C53	7 9286	-0 7988	-0 8803	-0 017
					C54	9 0760	-1 5394	-0 5822	0 013
					C55	10 0772	-1 4921	-1 4956	0 006
					C56	9 9071	-0 6441	-2 5988	-0 021
					Chi Squared =	9			
					Other Atoms				
					P2	8 5385	1 1919	-4 1910	-0 050

Dihedral Angles Between Planes

Plane No	Plane No	Dihedral Angle
1	2	81 19 +- 0 26
1	3	83 16 +- 0 28
1	4	84 09 +- 0 26
1	5	69 98 +- 0 28
2	3	65 12 +- 0 35
2	4	18 94 +- 0 63
2	5	39 58 +- 0 54
3	4	46 61 +- 0 44
3	5	101 28 +- 0 31
4	5	58 06 +- 0 42

The four angles around the platinum also deviate from an ideal square-planar geometry. The P(1)-Pt-P(2) angle (103.72(9)°) is considerably greater than the O(1)-Pt-O(2) angle (88.2(3)°). Therefore the steric interactions between the phenyl groups is more signficant than those involving the CF_3 groups. In the chelating ligand, L^1, the CF_3 groups are removed far enough from the coordination sphere such that steric interactions are minimized. By comparison in structure 4-1, the fluorinated alcohol forms a very bulky substituent on the monodentate phosphine. The effect of chelation is to lessen the steric interactions to the extent that antisymbiosis, favouring the cis-geometry, now dominates.

The other two angles around the platinum, P(1)-Pt-O(1) and P(2)-Pt-O(2), represent the bite angle of the bidentate ligand, L^1, and are approximately equal, (82.7(2)° and 85.2(2)° respectively). The bite angles for L^1 in other structures in this study are: 84.36(6)° in $[Pd(PPh_2Me)(L^1)Cl]$, and 86.6(2)° and 87.1(2)° in $[Ni(L^1)_2]$. The angle would be expected to open up slightly as the size of the central metal decreases, as in the case of Ni(II).

Also given in Table 4.6 are the deviations of the carbon atoms in the chelate ring backbone from the least-squares coordination plane. The two chelate rings differ in conformation; ring(1), containing P(1) and O(1), is in an asymmetric envelope conformation with both carbon

atoms lying on one side of the plane while ring(2) is in an asymmetric skew conformation, with the two carbons lying on opposite sides of the plane. That both of these conformations are found in a single molecule would seem to suggest that the energy difference between the two conformations is quite small. The favoured conformation is likely determined by packing factors in the solid state, while rapid inversion occurs in solution. The torsional angles around each chelate ring are given in Table 4.7.

The two Pt-P bond lengths can be averaged to a weighted value of 2.203(3) Å. The shortening of the Pt-P bonds on substitution of a fluorinated alkoxide in 4-2 for a phosphino group in 4-1 in the trans position parallels the increase in the $^{1}J(Pt,P)$ coupling constant. Both trends result from the greater trans influence of the phosphino group over that of the fluorinated alkoxide.

There are a number of other structures reported of platinum(II) complexes with cis-P_2O_2 donor sets. The average Pt-P bond in 4-2 is shorter than that of any of these structures. However, caution must be used before interpreting these data in terms of a trans influence order for oxygen-donor ligands. As the phospine ligand is varied so are its electronic and steric properties which can also affect the bond length. For example, the Pt-P bond length in carbonatobis(tri-isopropylphosphine) platinum(II) is 2.262(7) Å[260] but when triphenylphosphine is substituted for tri-isopropylphosphine the bond length becomes 2.24

Table 4.7 Torsional Angles in 4-2

Atom 1	Atom 2	Atom 3	Atom 4	Angle	Atom 1	Atom 2	Atom 3	Atom 4	Angle
O1	Pt	P1	C1	-20 7	Pt	P2	C3	C4	13 1
O2	Pt	P2	C3	-0 1	Pt	O1	C2	C1	-22 6
P1	Pt	O1	C2	27 8	Pt	O2	C4	C3	28 8
P2	Pt	O2	C4	-16 2	P1	C1	C2	O1	0 7
Pt	P1	C1	C2	16 9	P2	C3	C4	O2	-25 9

A.[261] In addition, incorporation of the phosphine into a chelate ring, as in 4-2, will also affect the bond length.

One previously reported structure is quite analogous to 4-2, that of 2,2-bis(methyldiphenylphosphine)-4,4,6,6-tetrakis(trifluoromethyl)-1,3,5,2-trioxaplatinan, 4-4.

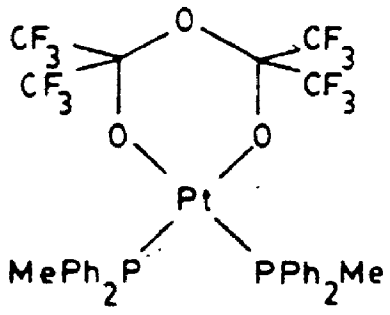

4-4

The Pt-P bond length in 4-4 is 2.223(9) A[262] which is comparable (λ = 2.1) to the value of 2.203(3) in 4-2.

The Pt-O bond lengths in 4-2 could also be averaged to a value of 2.032(4) A. In the analogous compound, 4-4, the bond length is 2.024(9) A. In a structure where triphenylphosphine is substituted for methyldiphenylphosphine in 4-4, the value is virtually identical to that of 4-2, 2.032(9) A.[262]

The C-O bond lengths were averaged to 1.370(7) A. Again, this is shorter than expected for a C-O single bond. It is also shorter than the C-O bond in a fluorinated alcohol of structure 4-1. This is again attributed to π-bonding from oxygen to carbon.

Other averaged values included the P-C(phenyl) bond length, 1.814(5) A, the P-C(methylene) bond length, 1.830(7) A and the C-C bond length, 1.550(7) A. These

values are reasonable by comparison to previously-recorded values in analogous structures.[260,262]

The aromatic C-C bonds in the phenyl rings had an average value of 1.387(6) A which is reasonable when compared to the value of 1.392 A used in rigid group refinement of phenyl rings.

The C-CF_3 bond lengths were averaged to 1.529(6) A which compares favourably with the average value of 1.53(1) in $Ni(L^1)_2$. Finally, it has been observed in previous structures involving fluorinated alkoxides, that the C-F bond lengths span a large range due to the thermal motion of the fluorine atoms. However, it was possible to average the C-F distances in 4-2, giving a value of 1.326(3) A. This agrees very well (λ = 0.24) with the mean value of 1.327(3) A for the C-F bonds in $[Pd(PPh_2Me)(L^1)Cl]$, another structure in this study with averaged C-F distances.

4.5 Steric Properties of Monodentate HL^1 and Bidentate L^1

The steric demands of HL^1 in trans-$[Pt(HL^1)_2Cl_2]$ and L^1 in $[Pt(L^1)_2]$ were investigated using the program, PROFILE.[276] This program calculates ligand profiles using crystallographic coordinates and van der Waals' radii. The ligand is "sliced" perpendicular to the metal-ligand bond and half-cone angles are calculated at intervals of theta degrees around the slice. For HL^1 and both L^1 ligands, the metal-ligand bond was sliced every 0.2 A from 0.2 A to 3.0 A from the metal and for each slice, a theta value of 10°

was used.

Cone angles were calculated using the same method as Ferguson, Roberts, Alyea and Kahn.[277] For each of the three phosphine substituents a maximum half-cone angle is calculated. An average half-cone angle is then calculated leading to a cone-angle, θ. In the case of HL^1 in trans $[Pt(HL^1)_2Cl_2]$, the results of the calculations of maximum half-cone angles are given in Table 4.8. The value of the cone angle is 159°.

A profile of HL^1 is shown in Fig. 4.5; the maximum half-cone angle is plotted as a function of θ. A radial plot, in Fig. 4.6 shows the ligand profile at a distance of 2.4 Å from the metal. The scale is in degrees and represents the half-cone angle. Both figures are labelled, showing the three different substituents.

Ferguson et al[277] used this method to calculate cone angles for a number of phosphines. The values obtained were comparable to those calculated by Tolman[278] using models. Therefore the cone angle of HL^1 has been compared with those of a number of other phosphines, as calculated by Tolman,[278] in Table 4.9.

These cone angles suggest that the fluorinated alcohol substituent is comparable in its steric bulk to a tertiary butyl or C_6F_5 group. The cone angles of $PPh_2(Bu^t)$ and $PPh_2(C_6F_5)$ are 157° and 158° respectively.

It is however of interest to note that the electronic properties of the ligand differ from that of $PPh_2(Bu^t)$.

Table 4.8 Cone Angle Data for HL^1.

Substituent	Maximum θ/2	Slice (Å)	Theta
$CH_2C(CF_3)_2OH$	80.32	0.60	120°
Ph(2)	76.68	0.80	260°
Ph(3)	81.95	0.40	60°

Table 4.9 Phosphine Cone Angles[278]

PR_3	θ (deg)
$PHPh_2$	128
$PMePh_2$	136
$PEtPh_2$	140
$PPh_2(Pr^i)$	150
$PPh_2(Bu^t)$	157
$PPh_2C_6F_5$	158
$PPh_2(CH_2C(CF_3)_2OH)$	159
PCy_3	170

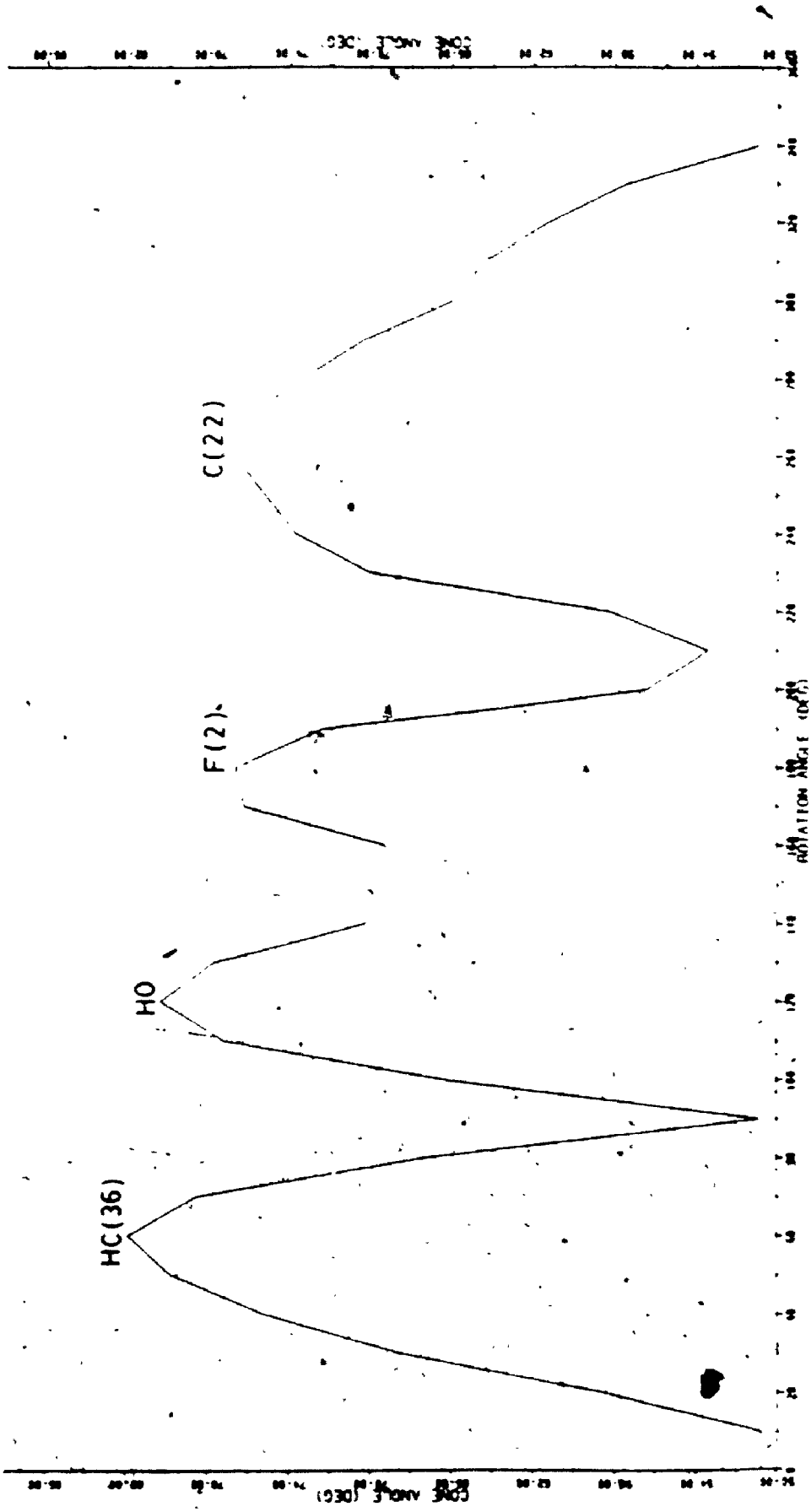

Figure 4.5 Profile of HL[1]

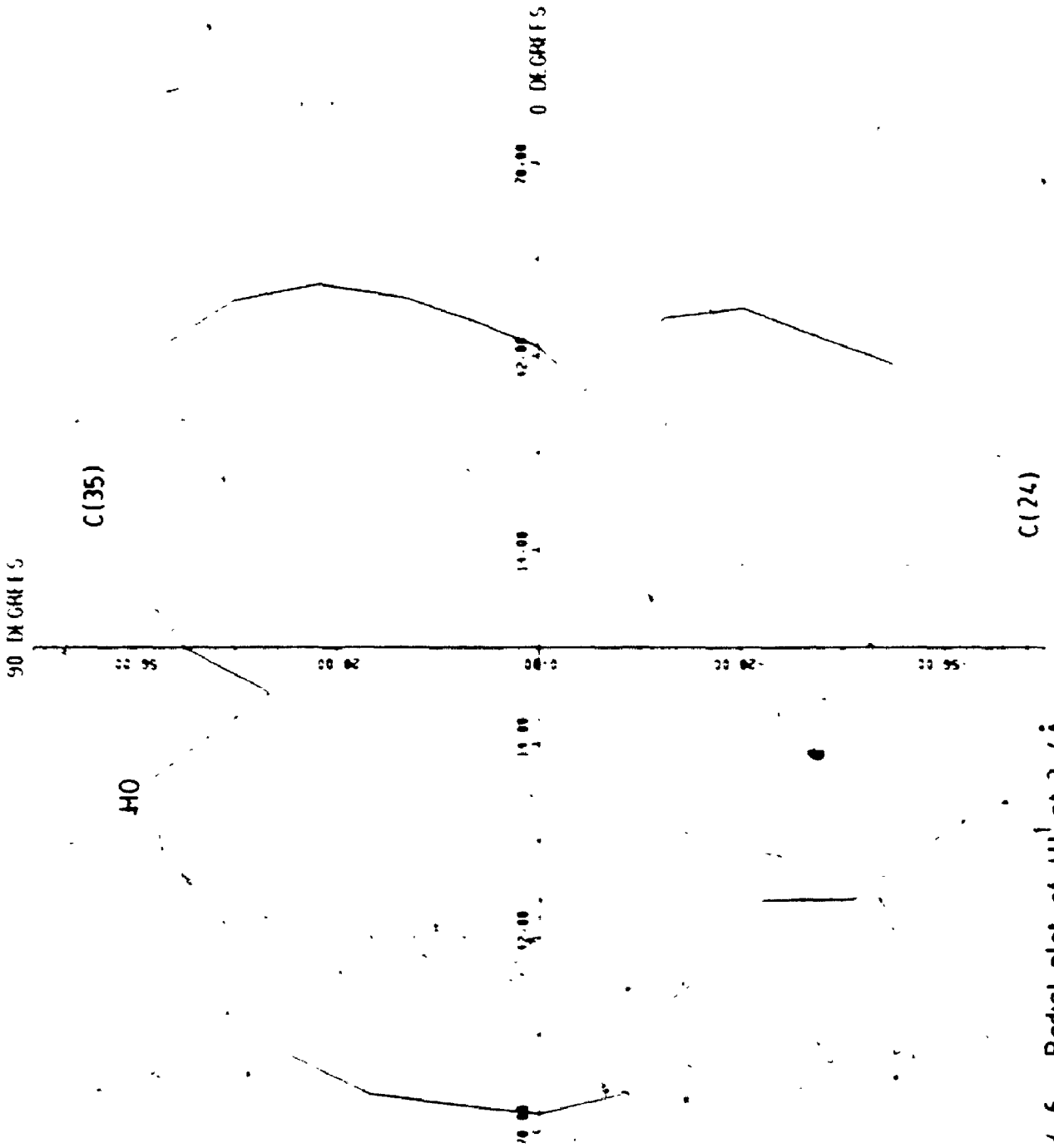

Figure 4.6 Radial plot of HL^1 at 2.4Å

Vincent et al[279] have suggested that, because the electronegativities of the substituents R in Ph_2PR compounds vary only a little,[280] steric effects are actually responsible for the wide range of ^{31}P chemical shift values. Indeed, a linear relationship between phosphine cone angle and ^{31}P chemical shift was shown to exist.[279]

This linear relationship exists for R = H, CH_3, C_2H_5, C_6H_5, i-C_3H_7 and t-C_4H_9, but appears to break down to R = $CH_2C(CF_3)_2OH$. While the cone angle of HL^1 is very close to that of Ph_2PBu^t, the ^{31}P chemical shift (-33.6 ppm) is much farther upfield, closer to that of Ph_2PH (-41.1 ppm).

Therefore, as a monodentate phosphine ligand, HL^1 resembles Ph_2PBu^t sterically with the fluorinated alcohol substituent being similar to a tertiary butyl group. However the ^{31}P NMR data suggest that no such similarity exists electronically. It is this large steric bulk of the fluorinated alcohol substituent that is believed to cause the trans-isomer to be thermodynamically favoured.

A cone angle is not so significant in the case of chelating ligands. Clearly, as the fluorinated alkoxide is bent back around to the metal to form a chelate, the steric interactions with the other ligand are reduced. As a result, cis-$[Pt(HL^1)(L^1)Cl]$ exists and is thermodynamically preferred over the trans isomer, while only the cis-isomer is known in the case of $[Pt(L^1)_2]$.

Ligand profiles of L^1 in cis-$[Pt(L^1)_2]$ were therefore

obtained, not to calculate cone angles, but rather to examine how the two chelates fit together on the platinum centre.

The profiles of the two ligands are shown in Cartesian plots (maximum half cone angle as a function of theta) in Figures 4.7 and 4.8. Figures 4.9 and 4.10 show the profiles, sliced 2.4 Å from the metal along the metal-phosphorus bond, as radial plots. On these plots, when theta is equal to 0°, the half-cone angle lies in the P, Pt, P plane.

There is no evidence from these plots that the cis-diphenylphosphino groups are meshed together, that is, that a phenyl ring on one phosphorus fits into a gap between the two phenyl rings on the other. In fact, no such gap between phenyl groups is apparent on either ligand; the two groups seem to form one smooth "surface".

The conclusion that the groups are not interlocked is not surprising. While the positions of the phenyl rings are somewhat dependent on chelate ring conformation and each phenyl ring is free to rotate about the phosphorus-carbon bond, movement of the phenyl rings is still very restricted. The chelate ring eliminates rotation about the platinum-phosphorus bond so the two groups are not free to take up an interlocking conformation.

Instead, the P-Pt-P angle opens up to 103.72(9)° to remove any unfavourable contacts between the two groups. It is clear from the ORTEP drawing that the CF_3 groups in

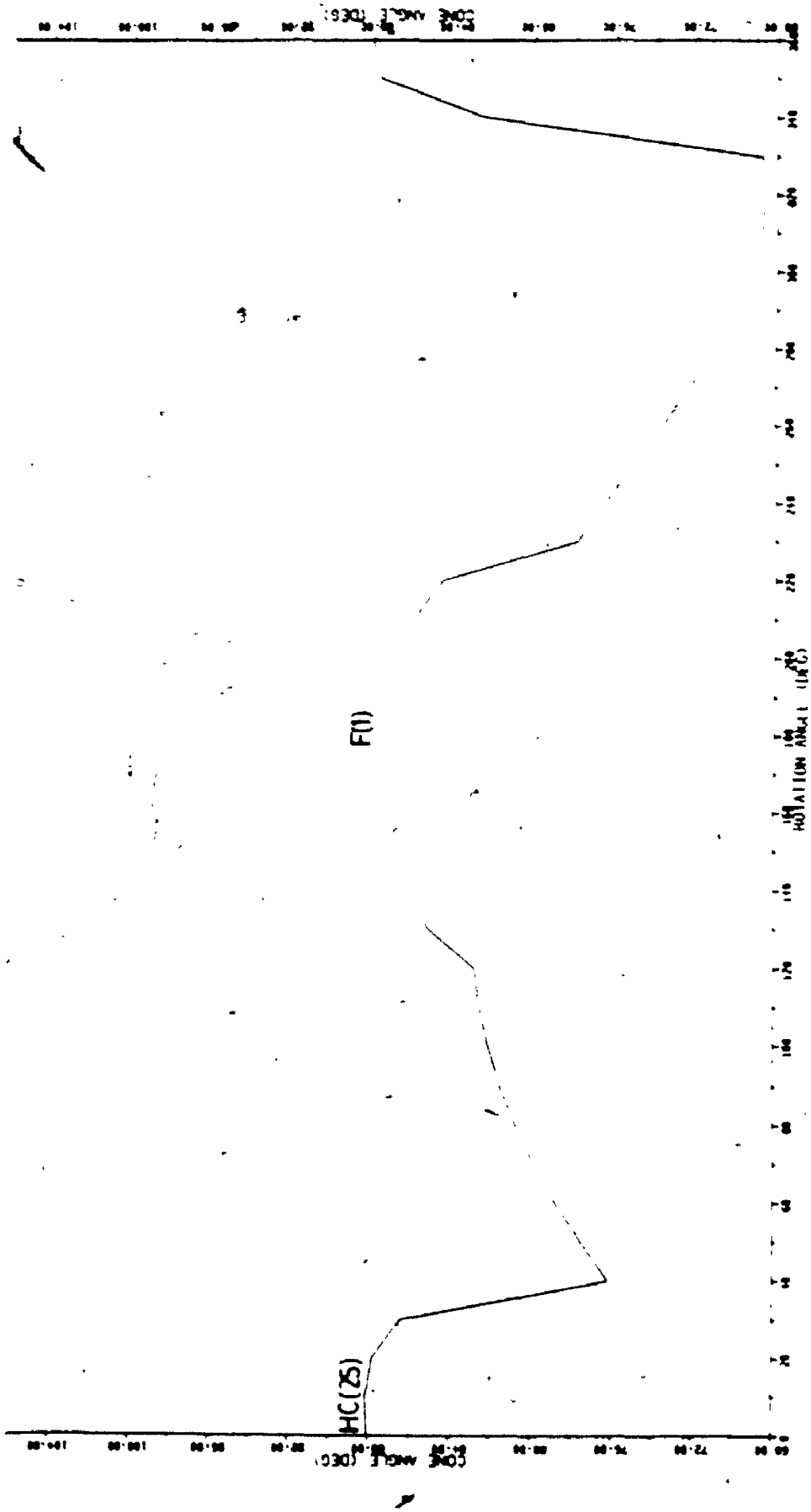

Figure 4.7 Profile of L^1 in $[Pt(L^1)_2]$, [P(1) O(1)]

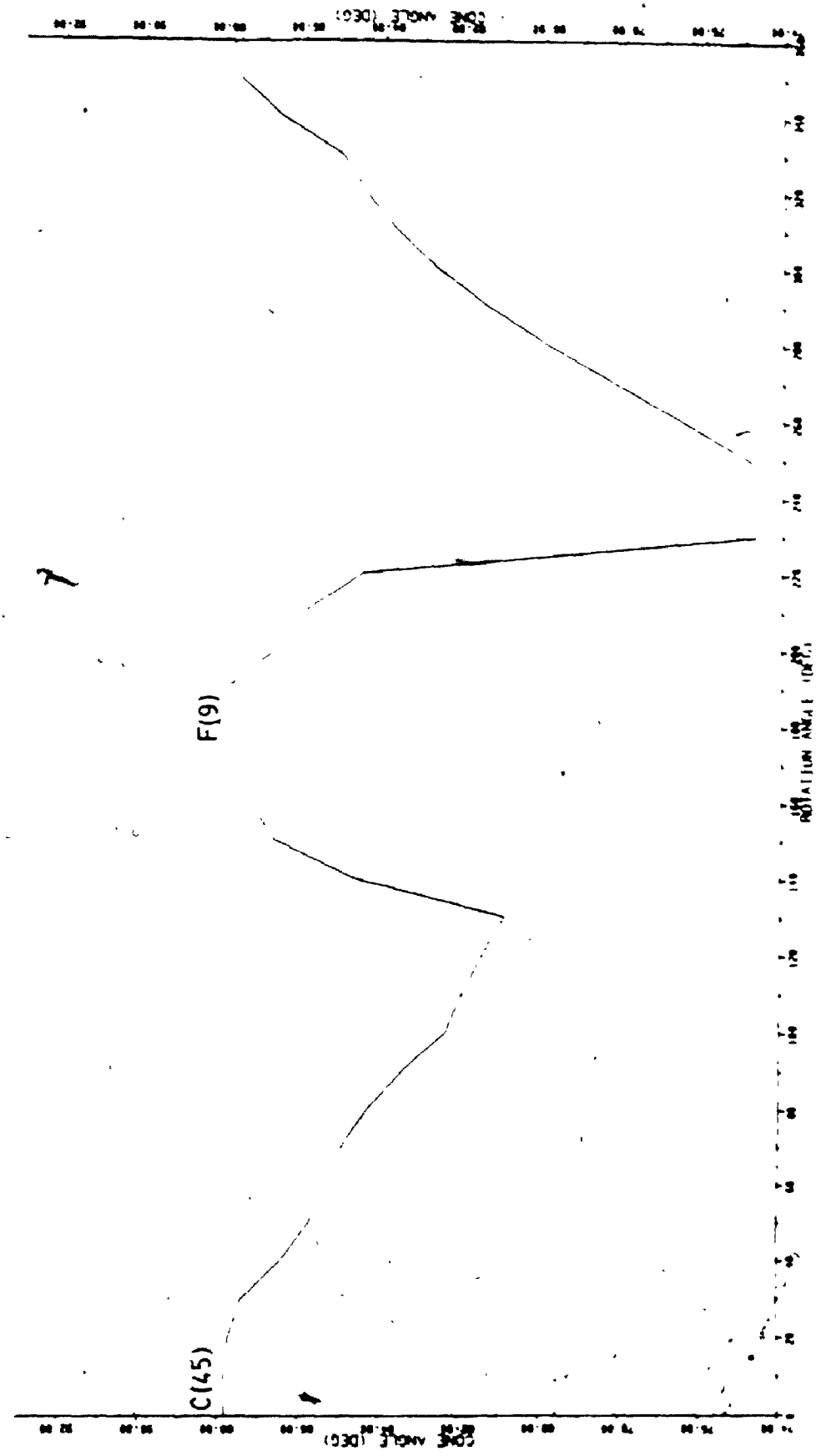

Figure 4.8 Profile of L^1 in $[Pt(L^1)_2]$, [P(2) O(2)]

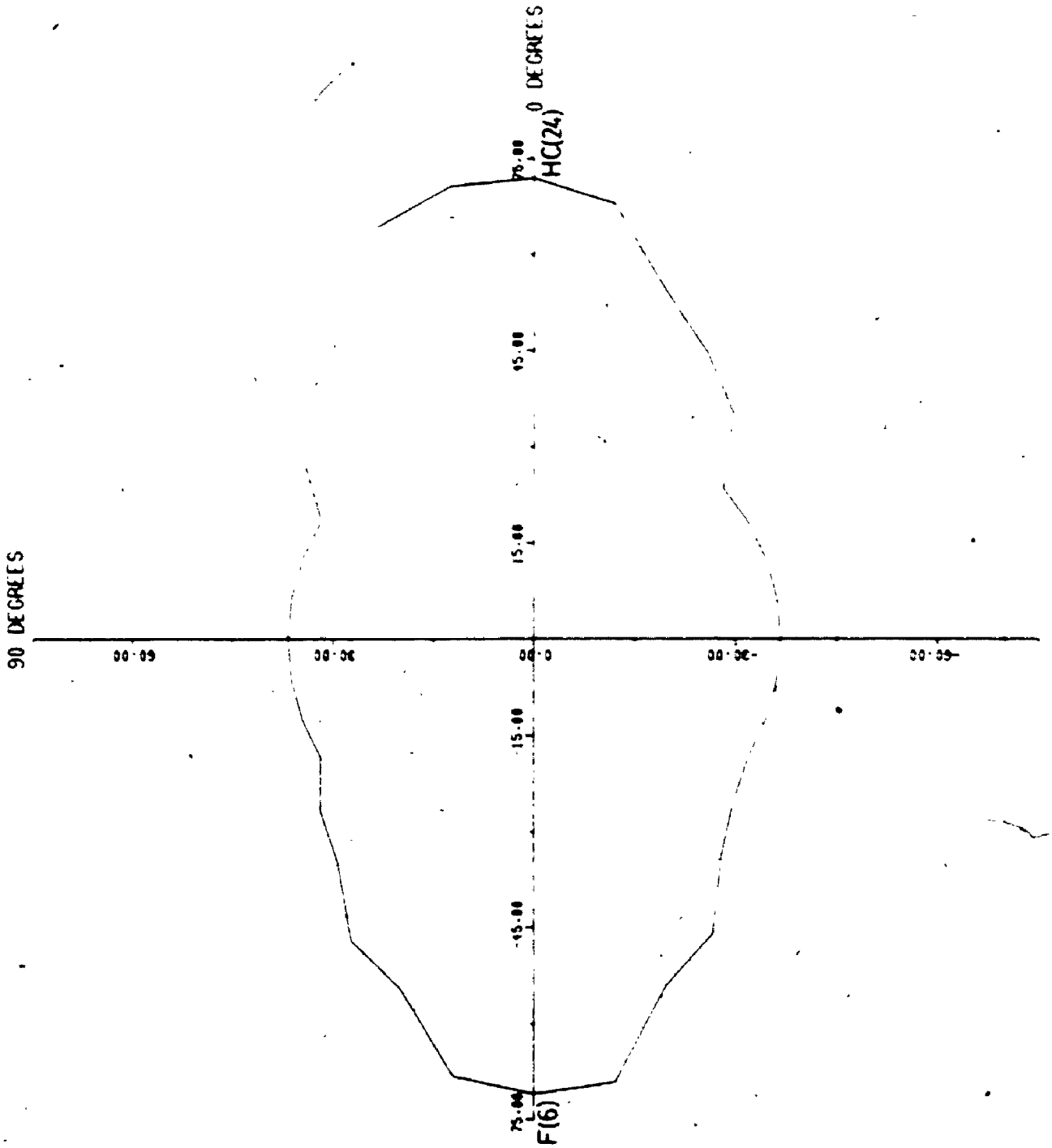

Figure 4.9 Radial plot of P(1) O(1) at 2.4Å

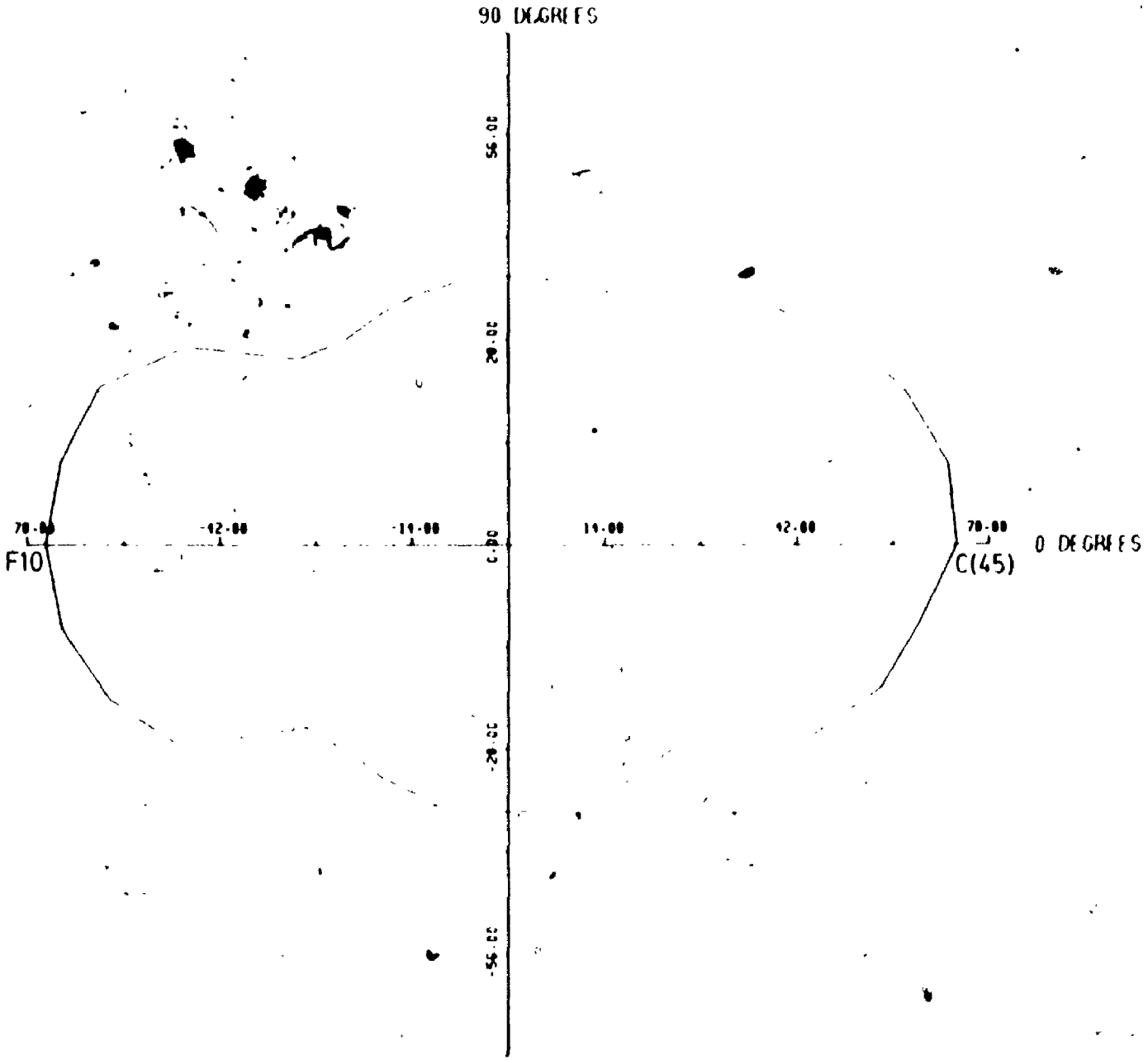

Figure 4.10 Radial plot of P(2) O(2) at 2.4Å

one chelate ring are far removed from those in the other. The O-Pt-O angle may then close down to 88.2(3)°. The bite angle of L^1 is also less than 90°.

In addition, the phenyl rings may rotate to minimize steric interactions. The angle formed by the planes of phenyl groups 2 and 5 on one side of the platinum atom is 39.6° while that between groups 3 and 4 on the other side of the chelate rings is 46.6°.

Therefore, HL^1 is a bulky ligand with a cone angle of 159° in trans-$[Pt(HL^1)_2Cl_2]$. However the steric bulk is lessened considerably in the case of the chelate L^1. The CF_3 groups are no longer positioned to add to steric interactions with other ligands and the chelate has a small bite angle (82.7(2)° and 85.2(2)° in $Pt(L^1)_2$). Therefore electronic rather than steric factors dominate in determining the geometry in platinum complexes of chelating L^1.

Chapter 5

Palladium Complexes of HL^1

5.1 Introduction

As tertiary phosphines are soft bases and palladium(II) is a soft acid, there are numerous palladium complexes with phosphine ligands. The complexes $[Pd(PR_3)_2X_2]$ are formed by reaction of the tertiary phosphine with $[PdX_4]^{2-}$ in solution.

These palladium(II) complexes with phosphine ligands were originally believed to be all trans[177], by analogy with the platinum complexes. The cis-isomers of the compounds, $[Pt(PR_3)_2X_2]$, had long been known to be the more thermodynamically stable, however the trans-isomers had been isolated in a number of cases presumably as the kinetically-favoured isomers due to the inert nature of platinum(II). Since the cis-isomers of platinum complexes are colourless, while the trans isomers are yellow,[177] and the initial palladium analogs were yellow with a low dipole moment in solution, the palladium complexes were assigned a trans geometry.

However, it was later found that the cis-isomers were more common than originally believed[121,178-182]. The compound, $[Pd(PPh(CH_3)_2)_2Cl_2]$, originally believed to be trans, was shown by X-ray crystallography to be cis in the solid state.[165] Thermodynamic studies[184] have subsequently shown some of these phosphine complexes to exist in

solution in an equilibrium involving both isomers. It appears that, like the platinum analogs, the cis isomers are favoured by the electronic factor of antisymbiosis, while steric factors favour the trans isomers. Solvation effects are also important in determining the position of the solution equilibrium.

The monomeric complexes, $[Pd(PR_3)_2X_2]$,[193] when refluxed in a solution containing the tetrahalopalladate(II) anion, form the dimeric halogen bridged palladium(II) complexes 5-1.

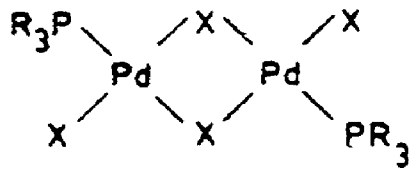

5-1

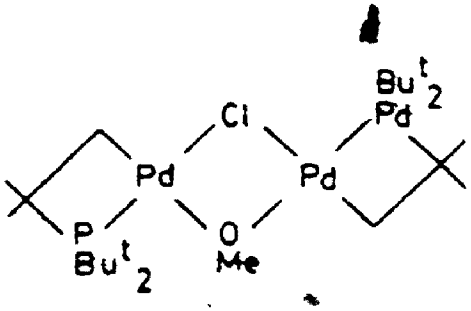

5-2

These complexes always have a trans[194] structure presumably because, in a cis-structure, the combined effect of two high trans-influence terminal phosphine ligands on a single bridging halide would destablize the complex.

Because of the hard nature of alkoxide ligands, it has only been recently that alkoxy-complexes of palladium(II) have been reported. In 1973, the methoxy complexes, cis- and trans-$[PdR(OMe)(PPh_3)_2]$ where R = C_6H_5, $-CH{=}CCl_2$, $-CCl{=}CCl_2$ were prepared by reaction of $PdRCl(PPh_3)_2$ with NaOMe.[187] In addition, the dinuclear compound 5-2 has been reported.[188]

More common are the fluorinated alkoxide complexes of

palladium(II). The unusual 3-membered ring complex, 5-3, was prepared by reaction of the zero-valent metal complex PdL_4 with hexafluoroacetone.[189]

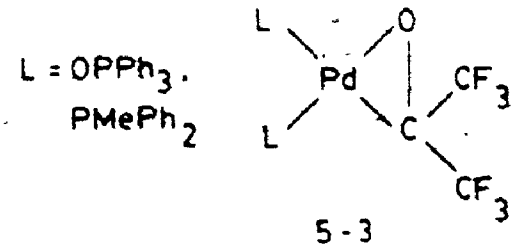

5-3

A second molecule of hexafluoroacetone will react with 5-3 to give $[L_2PdOC(CF_3)_2OC(CF_3)_2]$. Also Stone et al were able to prepare the complex $[Pd(PFP)(PEt_3)_2]$ by reaction of $[Pd(PEt_3)_2(CH_3)_2]$ with H_2PFP, perfluoropinacol.[189] The greater stability of palladium(II) alkoxides when chelating ligands are used allowed for the preparation of other complexes, $[Pd(PFP)L_2]$ where L is a soft coligand.[10] Alternatively the soft coligand has been incorporated into the chelating ligand to give hard-soft hybrid ligands which form palladium(II) alkoxide complexes.[190]

In this chapter, the chemistry of the hybrid ligand L^1 with Pd(II) will be examined. The bischelate complex $[Pd(L^1)_2]$ was prepared along with the complex $[Pd(HL^1)_2Cl_2]$ where each HL^1 functions as a monodentate phosphine ligand. A dimeric compound $[Pd(L^1)Cl]_2$ was prepared by the reaction of $[Pd(L^1)_2]$ with $[Pd(PhCN)_2Cl_2]$. Monomeric complexes, $[Pd(L^1)(L')Cl]$ were then obtained by cleavage of the dimer with L' where L' = PPh_3, PPh_2Me, $PPhMe_2$, PMe_3,

SMe_2 and py.

5.2 Characterization of Complexes

All complexes discussed in this chapter were characterized by elemental analysis; the analysis results are given in Table 7.1. Also in Table 7.2 the mass spectra data are given. In each case (with the exception of $[Pd(L^1)Cl(SMe_2)]$) the parent ion was seen, together with the loss of Cl and C_6H_5 in the case of the phosphine monomers or F in the case of the dimer. All monomers also exhibited loss of L' as well (except $[Pd(L^1)Cl(SMe_2)]$). Disproportionation giving $[Pd(L^1)_2]$ was evident in the mass spectrum of each of the monomers to varying degrees; in the case of $[Pd(L^1)Cl(SMe_2)]$, only disproportionation was seen. However, as no $[Pd(L^1)_2]$ was seen in the ^{31}P NMR studies, it seems that disproportionation was occurring only in the mass spectrometer.

In addition, the presence of L^1 in each complex was confirmed by the presence of a strong band in the infrared spectrum, in the region 1160-1190 cm^{-1} due to the C-F stretching mode. The far infrared spectrum of the dimer displayed peaks at 314 and 253 cm^{-1} corresponding to the bridging Pd-Cl vibrations. All ^{31}P, ^1H and ^{19}F NMR data are given in Table 5.1.

Table 5.1 NMR Data on Pd(II) Complexes[a]

Complex	CH_2		CF_3		CH_3[b]		P_A[c]		P_B[c]		
	δ	$^2J(P,H)$	δ	$^4J(P,F)$	δ	$^2J(P,H)$	δ	$\Delta\delta$[d]	δ	$\Delta\delta$[d]	$^2J(P_A,P_B)$
	ppm	Hz	ppm	Hz	ppm	Hz	ppm	ppm	ppm	ppm	Hz[e]
$Pd(HL^1)_2Cl_2$	3.53	4.3	-75.8	—	—	—	6.4	40.0	—	—	—
$Pd(L^1)_2$	3.47	12.5	-76.6	3.7	—	—	40.6	74.2	—	—	—
$[Pd(L^1)Cl]_2$	3.5	13	-76.1	4	—	—	47.35	81.0	—	—	—
$Pd(L^1)Cl(PPh_3)$	3.25	11.8	-77.1	3.5	—	—	50.09	83.7	26.52	32.4	5.3
$Pd(L^1)Cl(PPh_2Me)$	3.27	12.1	-77.2	2.8	1.92	11.1[f]	49.21	82.8	12.20	40.2	6.1
$Pd(L^1)Cl(PPhMe_2)$	3.25	12.0	-77.3	3.5	1.59	11.4[f]	48.76	82.4	-1.13	45.9	8.5
$Pd(L^1)Cl(PMe_3)$	3.32	12.1	-77.2	3.6	1.33	12.1	49.32	82.9	-6.96	55.0	8.4
$Pd(L^1)Cl(SMe_2)$	3.21	12.4	-77.2	4.0	2.39	—	43.0	76.6	—	—	—
$Pd(L^1)Cl(pyr)$	3.30	12.4	-77.0	3.6	[g]	—	42.5	76.1	—	—	—

[a] ambient temperature; solvent $CDCl_3$ or CD_2Cl_2

[b] CH_3-P or CH_3-S group.

[c] P_A is in the L^1 ligand; P_B is in the additional PR_3 ligand.

[d] the coordination shift: $\Delta\delta = \delta_{coord} - \delta_{free}$

[e] absolute values

[f] $^4J(P,H) \approx 1.3$ Hz.

[g] pyridine ^1H signals at 8.60 - 8.85 ppm.

5.3. Preparation of $[Pd(HL^1)_2Cl_2]$, $[Pd(L^1)_2]$ and their Structural Assignments

The palladium compound $[Pd(L^1)_2]$ was prepared by the reaction in $CHCl_3$ of $[Pd(PhCN)_2Cl_2]$ with two equivalents of the ligand, HL^1, and two equivalents of ethanolic KOH. The solution of $[Pd(PhCN)_2Cl_2]$ in $CHCl_3$, originally red, turns orange on addition of HL^1 and finally yellow after addition of the base. The final product, $[Pd(L^1)_2]$, was isolated as a white solid.

It was believed that the orange solution contained $[Pd(HL^1)_2Cl_2]$, which formed initially on addition of HL^1. This compound would be expected to have the phosphino groups of HL^1 coordinated to the palladium atom along with the chlorides while the fluorinated alcohols are dangling free, uncoordinated and unionized.

Work-up of the orange solution gave a yellow solid which was indeed characterized as $[Pd(HL^1)_2Cl_2]$. The proton-decoupled ^{31}P NMR showed a singlet at 6.36 ppm. The coordination chemical shift, $\Delta\delta$ for the ligand, HL^1, in this complex is then +40.0 ppm. This compares favourably with the values of $\Delta\delta$ in the platinum complexes for unidentate HL^1 coordinated through phosphorus only: these values ranged from +27.3 ppm to +40.7 ppm. The ^{19}F NMR shows a singlet at -75.8 ppm.

The appearance of the ^1H NMR spectrum is helpful in assigning the geometry of the complex, as the methylene protons appear at 3.53 ppm as a virtual triplet rather than

the expected doublet. Although the presence of a virtual triplet is not proof of a trans geometry, as will be discussed in chapter 6, it does indicate a high value of $J(A,A')/|J(A,X)-J(A,X')|$ in an $X_nAA'X'_n$ magnetic system such as this. For platinum and palladium bisphosphine complexes, this condition is usually fulfilled in trans complexes only; the values of $^2J(P,P')$ in trans-platinum(II) or palladium(II) bisphosphine complexes are considerably higher than in cis-complexes.

In addition, the colour of the complex is yellow. The cis-isomers of the complexes $[M(PR_3)_2X_2]$ (M = Pt or Pd) are colourless while the trans-isomers are yellow. Therefore on the basis of colour and the appearance of the virtual triplet in the ^1H NMR, the complex $[Pd(HL^1)_2Cl_2]$ has been assigned a trans geometry, 5-4.

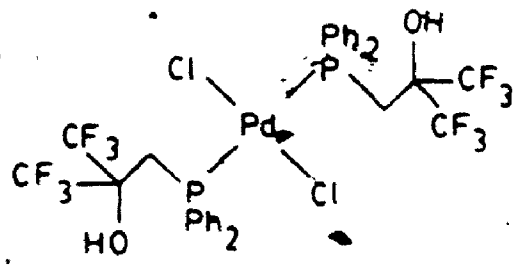

5-4

The observation that the trans geometry is preferred for this complex is not unexpected. For $[Pt(HL^1)_2Cl_2]$, both isomers were isolated, with the trans-isomer being the more thermodynamically favourable. The substitution of palladium for platinum would not be expected to change the thermodynamically-favoured isomer, as both platinum(II) and

palladium(II) are soft metal ions of approximately equal size.

Addition of two equivalents of KOH to an orange solution containing $[Pd(HL^1)_2Cl_2]$ causes the solution to turn yellow and work-up of this solution yields a white complex characterized as $[Pd(L^1)_2]$.

Unlike $[Pt(L^1)_2]$, the geometry of $[Pd(L^1)_2]$ cannot be easily established since there is not coupling from the phosphorus to the metal. In addition, the substitution of the fluorinated alkoxide for a chloride ion changes the spectral properties such that assignment of geometry can no longer be made on the basis of colour.

For this complex, the coordination shift, $\Delta\delta$, is therefore used to assign the geometry. The value of $\Delta\delta$ for $[Pd(L^1)_2]$ (74.2 ppm) is increased considerably from $[Pd(HL^1)_2Cl_2]$ (40.0 ppm). This is consistent with the platinum analogs, +36.0 ppm for trans-$[Pt(HL^1)_2Cl_2]$ and +50.9 for cis-$[Pt(L^1)_2]$. However, values of $\Delta\delta$ must be interpreted with caution because of the considerable variation in ^{31}P chemical shifts which occur when phosphines are incorporated into chelate rings of various sizes,[191] in addition to variation due to different metals.

The diphosphine complex, $[PdCl_2(Ph_2PCH_2CH_2PPh_2)]$, is comparable to $[Pd(L^1)_2]$ in that it contains phosphorus incorporated into a 5-membered ring. The coordination shift for this compound is 75.8 ppm,[192] almost identical to that of $[Pd(L^1)_2]$. Since the geometry of the phosphines in

$[PdCl_2(Ph_2PCH_2CH_2PPh_2)]$ is unambiguously cis, then the complex $[Pd(L^1)_2]$ has also been assigned a cis geometry.

Such an assignment is logical also, in light of the geometries of the analogous complexes of the other metals in the nickel triad; the complex $[Pt(L^1)_2]$ is cis while chapter 6 will reveal that $[Ni(L^1)_2]$ exists in solution as an equilibrium mixture involving both cis and trans isomers.

The electronic factors would favour the cis geometry for both $[Pd(L^1)_2]$ and $[Pd(HL^1)_2Cl_2]$, but the great steric bulk of the monodentate HL^1 ligands dominates and as a result the trans geometry is observed. The significance of the steric factors is lessened considerably in the case of the chelating L^1 ligand, such that in $[Pd(L^1)_2]$ the electronic factors dominate and the cis geometry is preferred. The mechanism by which the two complexes are interconverted is the same as for the platinum analogs, involving a five-coordinate intermediate.

5.4 The Chloro-bridged Dimer

A chloro-bridged dimer was prepared by refluxing a solution of $[Pd(L^1)_2]$ and $[Pd(PhCN)_2Cl_2]$ in chloroform. Work-up of this solution produced an orange solid characterized as $[Pd(L^1)Cl]_2$.

Although the geometry of the dimer has not been established, it has been assigned a trans configuration; 5-5

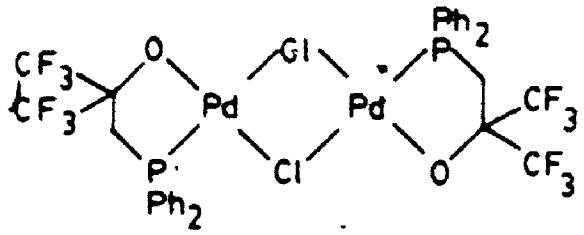

5-5

This assignment is made on the basis of the known geometries for complexes of the type $[(PR_3)ClPd(\mu\text{-}Cl)_2PdCl(PR_3)]$ which are all trans.[194]

These dimers, featuring terminal chlorides and monodentate tertiary phosphines, are prepared by reaction of the tetrahalopalladate anion with the monomeric phosphine complex $[Pd(PR_3)_2X_2]$.[193] It is this well-established route that is being followed in the synthesis of $[Pd(L^1)Cl]_2$. However, this route is not employed when the two terminal ligands on each palladium in the dimer are replaced by a chelating ligand; such compounds are generally prepared by the direct reaction of the bidentate ligand with $PdCl_2$.[195,196,197] This appears to be the first example of the displacement of a bidentate ligand from a bischelate in the formation of a chloride-bridged dinuclear palladium species.

Although there are numerous examples of chloro-bridged palladium dimers with terminal chelating ligands, the vast majority contain a metal-carbon bond. Of those that do not, none features a phosphorus atom as a donor atom in the chelate ring.

5.5 Cleavage of the Dimer with Monodentate Ligands

The halide-bridged dimers of platinum and palladium are readily cleaved by monodentate ligands to give monomeric complexes, $[M(PR_3)LCl_2]$.[210] The dimer $[Pd(L^1)Cl]_2$ was likewise cleaved by various ligands to give complexes of the type $[Pd(L^1)Cl(L')]$ where L' = PPh_3, PPh_2Me, $PPhMe_2$, PMe_3, py, SMe_2. This cleavage reaction provided a useful route to $[Pd(L^1)Cl(L')]$ type complexes. Previously, an attempt to prepare such mixed-ligand monomers by reacting L^1 with $[Pd(L')_2Cl_2]$ had resulted only in disproportionation.

5.5.1 $[Pd(L^1)Cl(PR_3)]$ Complexes

As mentioned in the introduction to chapter 5, complexes of the type $[Pd(PR_3)_2Cl_2]$ were originally thought to be invariably trans, but more recent studies show some examples of cis-trans isomerism.

Assignment of geometry for the four $[Pd(L^1)Cl(PR_3)]$ complexes was easily made. For each compound, the ^{31}P NMR spectrum exhibited two signals due to the two inequivalent phosphorus nuclei. Each signal was then split into a doublet due to coupling between the phosphorus nuclei. The value of $^2J(P_A,P_B)$ for the complexes ranged from 5.3 Hz for L' = PPh_3 to 8.5 Hz for L' = $PPhMe_2$. It is well-established that in bis(phosphine) complexes of palladium (II), phosphorus-phosphorus coupling is considerably greater in trans-isomers than in cis-isomers.

These values of $^2J(P_A,P_B)$ for the $[Pd(L^1)Cl(PR_3)]$ complexes indicate clearly that all are cis in the geometry of the phosphines.

The complexes $Pt(L^1)_2$ and $Pd(L^1)_2$, discussed previously, are both cis in solution, while $Ni(L^1)_2$ (chapter 6) is trans in the solid state but a solvent- and temperature-dependent mixture in solution. This difference may be ascribed to the greater importance of the antisymbiotic effect in complexes of softer metals.

Steric effects normally disfavour the cis geometry because of repulsion between bulky phosphines in the complexes, $[Pd(PR_3)_2X_2]$. In fact, in solution studies of cis-trans isomerism in these complexes done by Grim and Keiter[181] and by Redfield and Nelson,[184] no example was found of a complex that was exclusively cis. Yet, the trans isomers of the complexes, $[Pd(L^1)Cl(PR_3)]$, were never observed; the $[Pd(L^1)Cl(PR_3)]$ complexes are exclusively cis.

This stereochemical difference, observed on substitution of L^1 for a PR_3 and Cl^- in $[Pd(PR_3)_2Cl_2]$ compounds, is likely due to the effect of the chelate ring. The ligand, L^1, has a small bite angle which allows the P-Pd-P angle to open up more, minimizing the interaction between the phosphino groups. In the structure of $[Pd(L^1)Cl(PPh_2Me)]$, discussed later in this chapter, the P(1)-Pd-O angle is only 84.36(6)° while the P(1)-Pd-P(2) angle is 98.51(3)°.

The coordination shifts of the monodentate phosphines

are reported in Table 5.1. The values of the coordination shift increase as methyl groups are substituted for phenyl groups in the monodentate phosphines. This follows the usual trend that $\Delta\delta$ increases with increasing σ-donor power in the phosphine ligand. For the complexes $cis\text{-}PdCl_2(PPh_nMe_{3-n})$, the values of $\Delta\delta$ are 47.2[18], 53.3[18] and 60.1 ppm[211,212] for n = 2, 1 and 0 respectively. This trend in the value of $\Delta\delta$ for the complexes, $[Pd(L^1)Cl(PR_3)]$ is paralleled by an overall increase in the $^2J(P_A,P_B)$ value which should likewise depend on the σ-bond strength of the Pd-P bond.

One may compare the coordination shifts of the monodentate phosphines in the $[Pd(L^1)Cl(PR_3)]$ complexes with those of the analogous $cis\text{-}[PdCl_2(PR_3)_2]$ complexes. The value of $\Delta\delta$ is consistently 5-7 ppm less when the phosphine is trans to a fluorinated alkoxide than when trans to a chloride. The same trend is seen in the coordination shift of the chelating phosphine, which is 74.2 ppm in $cis\text{-}Pd(L^1)_2$, 81.0 ppm in $[Pd(L^1)Cl]_2$, and 82-84 ppm in $[Pd(L^1)Cl(PR_3)]$.

It has previously been argued that the trans-influence of a fluorinated alkoxide is greater than that of a chloride. The destabilizing trans-influence of the fluorinated alkoxide has been attributed to its ability as a good σ-acceptor to withdraw electron density from the M-L bond trans to it. On this argument, one would expect the substitution of a fluorinated alkoxide for a chloride trans

to a phosphine to have the effect of increasing the deshielding of the phosphorus nuclei and hence causing a greater value of Δδ. This is contrary to the observed result. Therefore, while it is tempting to use the Δδ data to compare the trans-influence of the alkoxide to that of a chloride ion, it does not appear that such a method of comparison is justifiable. Furthermore, the values of Δδ for the cis-complexes, $[Pd(PPh_nMe_{3-n})X_2]$, show no trend consistent with the relative trans-influences of Cl^-, Br^- and I^-.[213]

Instead, the difference in the values of Δδ between $[Pd(L^1)Cl(PR_3)]$ and $[Pd(PR_3)_2Cl_2]$ complexes may be due to the inability of the fluorinated alkoxide to function as a π-acceptor ligand. This would have the effect of strengthening the Pd→P π-bonding and hence the shielding of the phosphorus nucleus when the fluorinated alkoxide is in the trans position rather than the chloride.

It has been shown previously[213] that, in a number of systems, a linear relationship exists between the coordination chemical shift and the chemical shift of the free phosphine. Such a relationship exists for the $[Pd(L^1)Cl(PR_3)]$ complexes as well, as demonstrated in Fig. 5.1. It has been suggested[214] that the C-P-C angle in the phosphine is related to the s character of the lone electron pair on the phosphorus nucleus; the greater the C-P-C angle, the further downfield the ^{31}P resonance position is expected to appear. The degree to which the

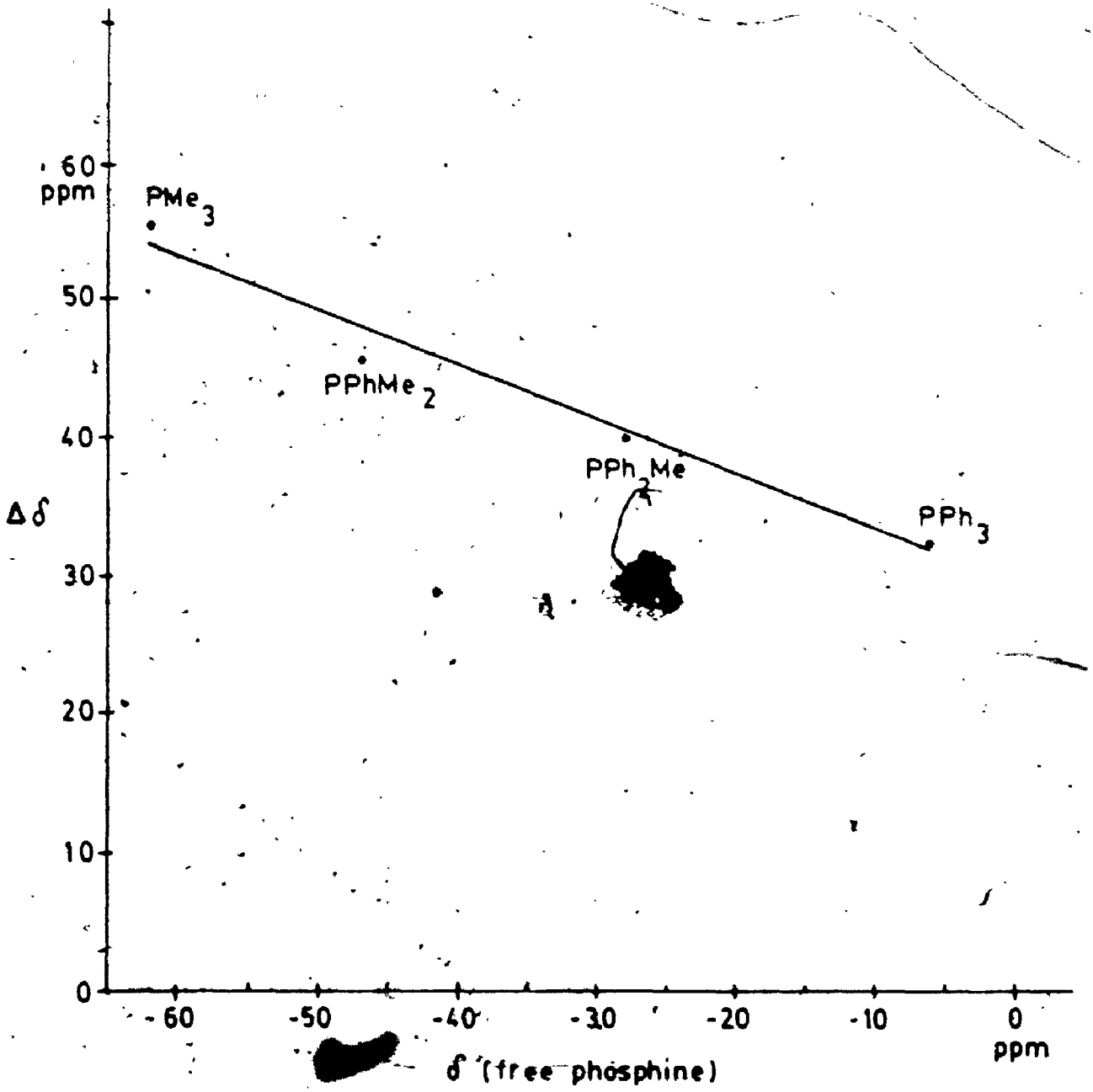

Figure 5.1 Plot of coordination shift vs. δ(free) for $[Pd(PR_3)(L^1)Cl]$ complexes

angle opens up on coordination is similarly related to the size of the coordination shift. The slope of the line in Fig. 5.1 suggests that the phosphorus with the smaller C-P-C angle (the upfield resonances) open up more on complexation to give a large coordination shift.

5.5.2 $[Pd(L^1)Cl(SMe_2)]$ and $[Pd(L^1)Cl(py)]$

The dimer, $[Pd(L^1)Cl]_2$, can also be cleaved using a thioether ligand or an amine. The products of the cleavage reaction are $[Pd(L^1)Cl(SMe_2)]$ and $[Pd(L^1)Cl(py)]$ respectively. However it is more difficult to assign the geometry of these complexes than with the phosphine cleavage products, because of the absence of $^2J(P_A,P_B)$ coupling. While the value of $\Delta\delta$ for the phosphine in L^1 was quite consistent for all the $[Pd(L^1)Cl(PR_3)]$ complexes (82.4 to 83.7 ppm), the values for $[Pd(L^1)Cl(SMe_2)]$ and $[Pd(L^1)Cl(py)]$ are considerably less (76.6 and 76.1 ppm respectively). The effect on the value of $\Delta\delta$ of substituting a thioether or pyridine for a phosphine in the cis position should be minimal. However if the thioether or pyridine were placed in the position trans to P_A, $\Delta\delta$ should decrease as both of these ligands have a greater trans influence that a chloride ion.[215] Also, complexes of the type $[PdCl_2(PR_3)L^*]$ where L^* is an N-donor ligand, prepared by cleavage of $[(PR_3)ClPd(\mu\text{-}Cl)_2PdCl(PR_3)]$ with L^*, are always trans.[214] Therefore the geometries of $[Pd(L^1)Cl(SMe_2)]$ and $[Pd(L^1)Cl(py)]$ have been tentatively

assigned as trans, as shown in 5-6 and 5-7 respectively.

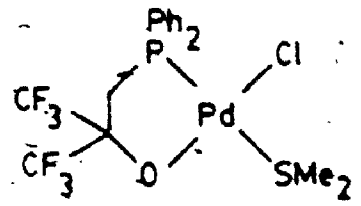

5-6

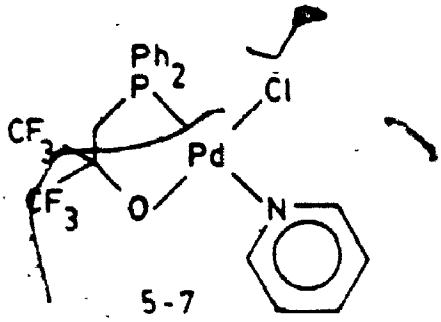

5-7

The difference in the stereochemical preference of these two complexes compared with the $[Pd(L^1)Cl(PR_3)]$ complexes, is probably due to the greater importance of the antisymbiotic effect in the latter where L' is a soft phosphine ligand. When the importance of antisymbiosis is reduced, steric effects predominate.

5.6 Crystal Structure of $[Pd(L^1)Cl(PMePh_2)]$

5.6.1 Experimental

The crystals of $[Pd(L^1)Cl(PMePh_2)]$ were grown by slow evaporation of a solution in $CHCl_3$/acetone, yielding yellow, hexagonal prisms. Preliminary photographic analysis was carried out and precession photographs of the hk0, hkl, h0l and h1l layers were obtained along with Weissenberg photographs of the 0kl and 1kl layers. These photographs showed that the crystal belonged to the monoclinic crystal system, having Laue symmetry 2/m.

Systematic absences were observed when l is odd for the h0l class of reflections and when k is odd for the 0k0 reflections. The interpretations of these systematic

absences are a (010) glide plane with component c/2 and a [010] screw axis with component b/2 respectively. The space group of the crystals is thus $P2_1/c$ - C^5_{2h} - No 14.[162] This is a centrosymmetric space group.

A crystal was chosen for data collection which had 8 faces with the approximate dimensions being 0.17 x 0.25 x 0.32 mm. This crystal was mounted on an Enraf-Nonius CAD4F computer controlled kappa axis diffractometer. Both the preliminary examination and the data collection were performed with Mo Kα radiation (λ = 0.71073 Å).

A polaroid photograph was obtained and from it 20 intense reflections were chosen and centred. The crystal was centred using one of these reflections, then a least-squares indexing and fitting procedure of these 20 reflections with $3.82 < 2\theta < 11.84$ provided the lattice constants and volume.

As a check on crystal quality, omega scans of three intense reflections along the three axes were done. For reflections (300), (002) and $(0\bar{2}0)$, the widths at half-height of the omega scans were 0.156°, 0.146° and 0.156° respectively, indicating good crystal quality.

Data collection for $32 < 2\theta < 40$ provided higher angle data from which 19 intense reflections were chosen, having $32.08 < 2\theta < 39.10$ for further least-squares refinement of the lattice constants and the orientation matrix.

The final lattice constants are given in Table 5.2. The density of the crystal was determined, by the flotation

method in a mixture of cyclohexane and 1,2-dibromoethane, to be 1.612(8) g/cm^3. This corresponds to 4 formula weights per unit cell. The X-ray formula weight, based on 4 formula weights per unit cell is then 708.3 compared with an expected value of 707.31 for $C_{29}H_{25}ClF_6OP_2Pd$.

The data were collected in two shells, $0 < 2\theta < 45$ and $45 < 2\theta < 50$ using Mo-Kα radiation. A total of 5927 reflections were collected of which 5085 were unique and not systematically absent. Processing of the data was done by the program BEGIN and included correction for background counts, scanning-rate, the Lorentz effect and polarization. Background estimates were made by extending the scans by 25% at each side. Four standard reflections, (231), (300), (020) and (006), were monitored every 3 hrs during the 124.4 hrs. for data collection. The average decay of these standards was 0.5%, so correction for intensity decay was not considered necessary.

The crystal faces were identified by optical goniometry. For each face, observed values of phi and rho on the two circle goniometer were compared with those predicted by the program CRYSTL.[133] In this way the eight crystal faces were identified as (200), (100), (00$\bar{1}$), (00$\bar{1}$), (01$\bar{1}$), (011), (011) and (01$\bar{1}$). An ORTEP[133] drawing of the crystal is shown in Figure 5-2 with the point of attachment of the glass fibre being approximately along the edge between the faces (100) and (011).

Once the crystal faces and dimensions had been

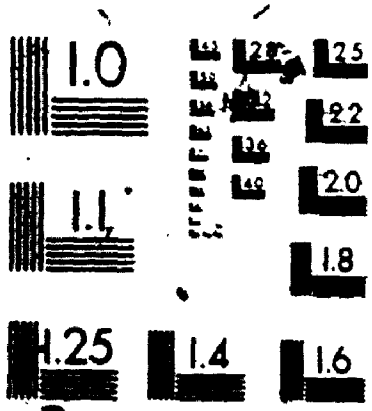

MICROCOPY RESOLUTION TEST CHART
NATIONAL BUREAU OF STANDARDS
STANDARD REFERENCE MATERIAL 1010a
(ANSI and ISO TEST CHART No. 2)

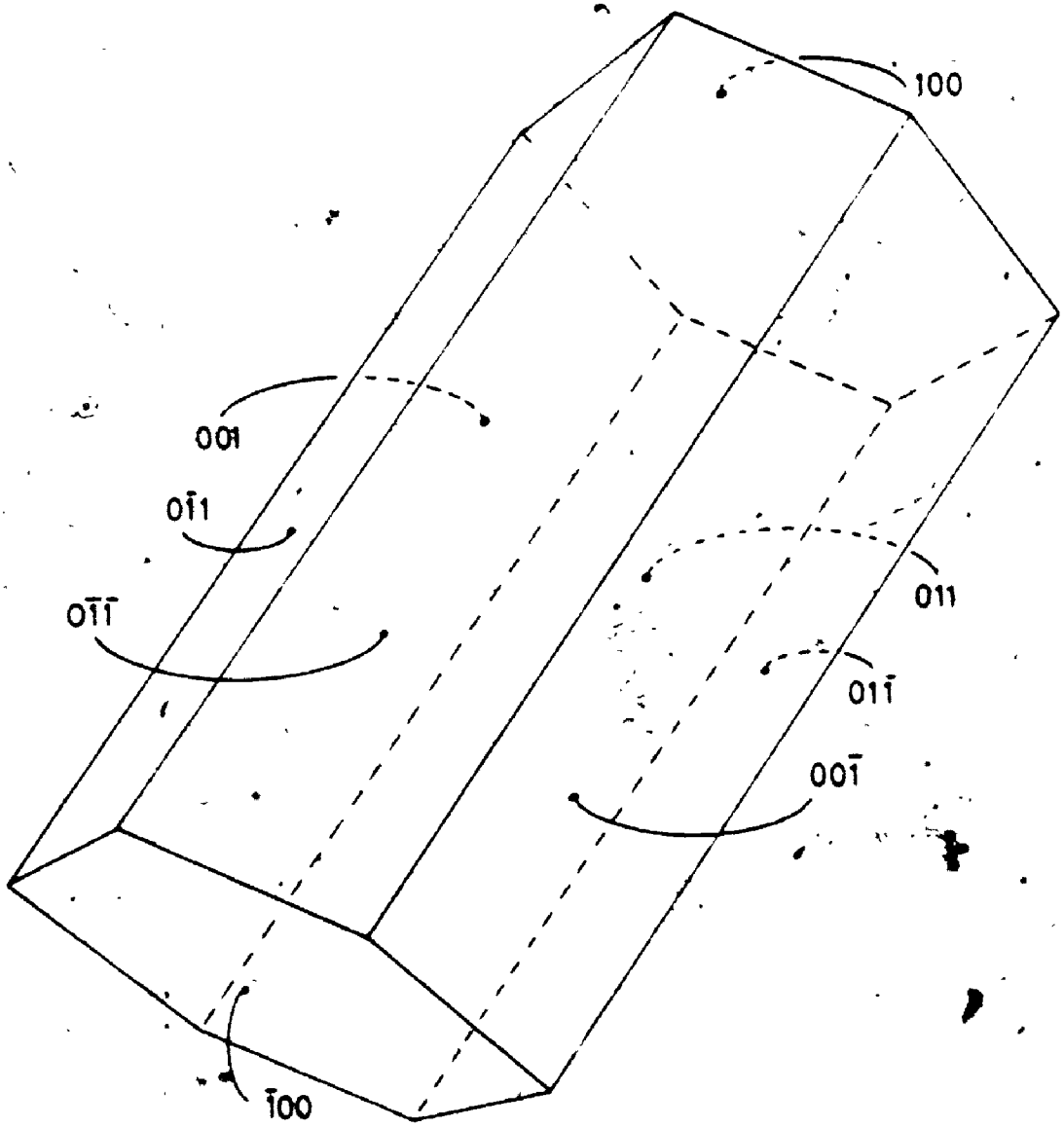

Figure 5.2 Drawing of data crystal for [Pd(PPh_2Me)(L^1)Cl]

described, a correction for differential absorption was possible. This was carried out using the program ABSCOR[133]. In this program, Gaussian numerical methods were applied.

The data collected were in the range $0 \leq h \leq 12$, $-17 \leq k \leq 0$, $-22 \leq l \leq 22$ and as a result, there were symmetry-related data collected. The program PAINT[133] was used to average the symmetry-related data. There were 1147 observed data averaged and the agreement factor was 1.5% based on intensity and 1.3% based on F_{obs}. Prior to the absorption correction the agreement factors were 1.6% and 1.3% respectively, which indicates that the absorption correction was effective in improving the precision of the data.

Table 5.2 contains the crystal data and the experimental conditions for the data collection.

5.6.2 Structure Determination and Refinement

All calculations in the structure determination and refinement were carried out on a PDP-11/23+ computer. The programs used in the determination and refinement were from the Structure Determination Package[133] along with several U.W.O. programs (see Appendix 1).

The structure was solved using the heavy atom method; the position of the palladium atom was determined from a three-dimensional Patterson synthesis. The remaining 39 non-hydrogen atoms were located using successive

Table 5.2 Crystal Data and Experimental Conditions for [Pd(PPh_2Me)(L^1)Cl].

compound	$C_{29}H_{28}ClF_6OP_2Pd$
formular weight	707.31
space group	monoclinic $P2_1/c$ No. 14
unit cell dimensions (Å)	a = 10.821(1) b = 14.600(1) c = 18.674(2) β = 101.25(1)°
cell volume (Å³)	2893(1)
temperature (°C)	19 ± 1
Z, F(000) electrons	4, 1416
Density (g cm⁻³) (obsvd) (calcd)	1.612(8) 1.62
crystal faces	(100) (011) and (001)
crystal volume (mm³)	0.00954
radiation, wavelength (Å)	Mo Kα λ = 0.71073
abs. coefficient (cm⁻¹) Gaussian grid	8.94 16 x 12 x 8
transmission factors max. min.	0.913 0.817
detector aperture (mm) vert. horiz.	4.0 5.0 + 0.35 tanθ
crystal-detector distance (mm)	205
take-off angle (deg)	2.5
scan mode	θ-2θ at 0.75 to 2.75 deg min⁻¹
scan width (deg.)	0.70 + 0.35 tanθ
data collected	1 < 2θ < 50. 0 ≤ h ≤ 12 -17 ≤ k ≤ 0 -22 ≤ ℓ ≤ 22
standard reflections	2$\bar{3}$1 300 020 and 006

difference-Fourier synthesis. The structure determination and refinement were carried out using 3977 reflections for which $F_o > 3\sigma(F_o)$ from a set of 5085 reflections.

The refinement proceeded using block-diagonal initially followed by full-matrix least squares techniques (once all the non-hydrogen atomic parameters were being refined). The refinement minimized the function $\Sigma w(|F_o| - |F_c|)^2$ where w is the weighting factor given by $4F_o^2/\sigma^2(F_o^2)$ and F_o and F_c are the observed and calculated structure amplitudes. The scattering factors used were those of Cromer and Waber.[135] Anomalous dispersion effects were included in F_c.[163] The values for $\Delta f'$ were those of Cromer and were used for Pd, Cl, P, O, P and C atoms.

Having found and refined all 40 non-hydrogen atoms with anisotropic thermal parameters, a difference Fourier synthesis was calculated. All 25 hydrogen atoms were located in the Fourier synthesis as the 25 hydrogen atoms were located in the Fourier synthesis as the 25 highest peaks, ranging from 0.66(9) to 0.28(9) eA^{-3}. Subsequent cycles of least-squares refinement included the hydrogens in structure factor calculations with idealized geometry assumed (C-H 0.90 and 0.95 A for sp^2 and sp^3 hybridization, respectively, thermal parameters 110% of those of attached atoms). The scattering factors for the hydrogen atoms were taken from Stewart et al.[136]

The final cycle of full-matrix least-squares refinement included 361 variables (3 positional parameters

and 6 anisotropic thermal parameters for each of the 40 non-hydrogen atoms plus the overall scale factor) and 3977 unique data with $F_o > 3\sigma(F_o)$. The value of p in the final cycle was 0.05. The model converged with weighted and unweighted agreement factors of 0.025 and 0.035 respectively. The largest parameter shift/error was 0.02 for four anisotropic thermal parameters of phenyl-ring carbons. The standard deviations on an observation of unit weight was 1.01 e.

A final difference Fourier synthesis was calculated and the highest peak had a height of 0.23 e/A^3 with an estimated error based on F of 0.04 e/A^3. This peak appears at (0.305, 0.645, 0.533) and had no chemical significance.

Plots of $w(|F_o| - |F_c|)$ versus $|F_o|$, data collection order, sin theta/lambda and various classes of indices showed no unusual trends, indicating a satisfactory weighting scheme and no sign of secondary extinction.

Positional and U(equiv) thermal parameters are given in Appendix 2. Hydrogen atom parameters appear in Appendix 4.

5.6.3 Structure Description

The crystals are built up of independent molecules of $Pd(L^1)Cl(PPh_2Me)$ with the shortest intermolecular non-bonding contact being 2.54 A between HC(34) and HC(54) at (x-1, 0.5-7, 0.5+z). Ignoring the hydrogens, the shortest distance is 2.833 (3) A between F(4) and F(4) at (-x, 1-y, -z). The closest Pd-Pd approach is 5.5413 (3)

A. Therefore no significant inter- or intra- non-bonding interactions were observed.

An ORTEP drawing of the molecule showing the atom numbering scheme is given in Fig. 5.3. Selected bond distances and angles are presented in Table 5.3 while supplementary dimensions appear in Table 5.4.

The coordination geometry about the palladium atom is square-planar with cis phosphorus atoms. The weighted least-squares plane through the palladium, oxygen, chlorine and two phosphorus atoms was calculated and is given in Table 5.5. The oxygen atom deviates the most from this plane, by a distance of 0.065(2) A. Furthermore, the four angles about the palladium atom add up to 360.0(2)° indicating that the geometry is indeed planar.

The conformation of the chelate ring is that of an asymmetric envelope, that is, both carbon atoms in the chelate ring backbone lie on the same side of the coordination plane but at different distances from the plane. The carbon atom bonded to the CF_3 groups (labelled C(2) deviates much less (0.113(3)A) from the plane than the methylene carbon (0.518(3)A) labelled C(1). Torsional angles are given in Table 5.6.

The CF_3 groups are in an up-down configuration because of the small deviation of C(2) from the coordination plane. The conformation of the CF_3 groups which allows them to pack best with other molecules in the unit cell, here an up-down conformation, thus determines the deviation

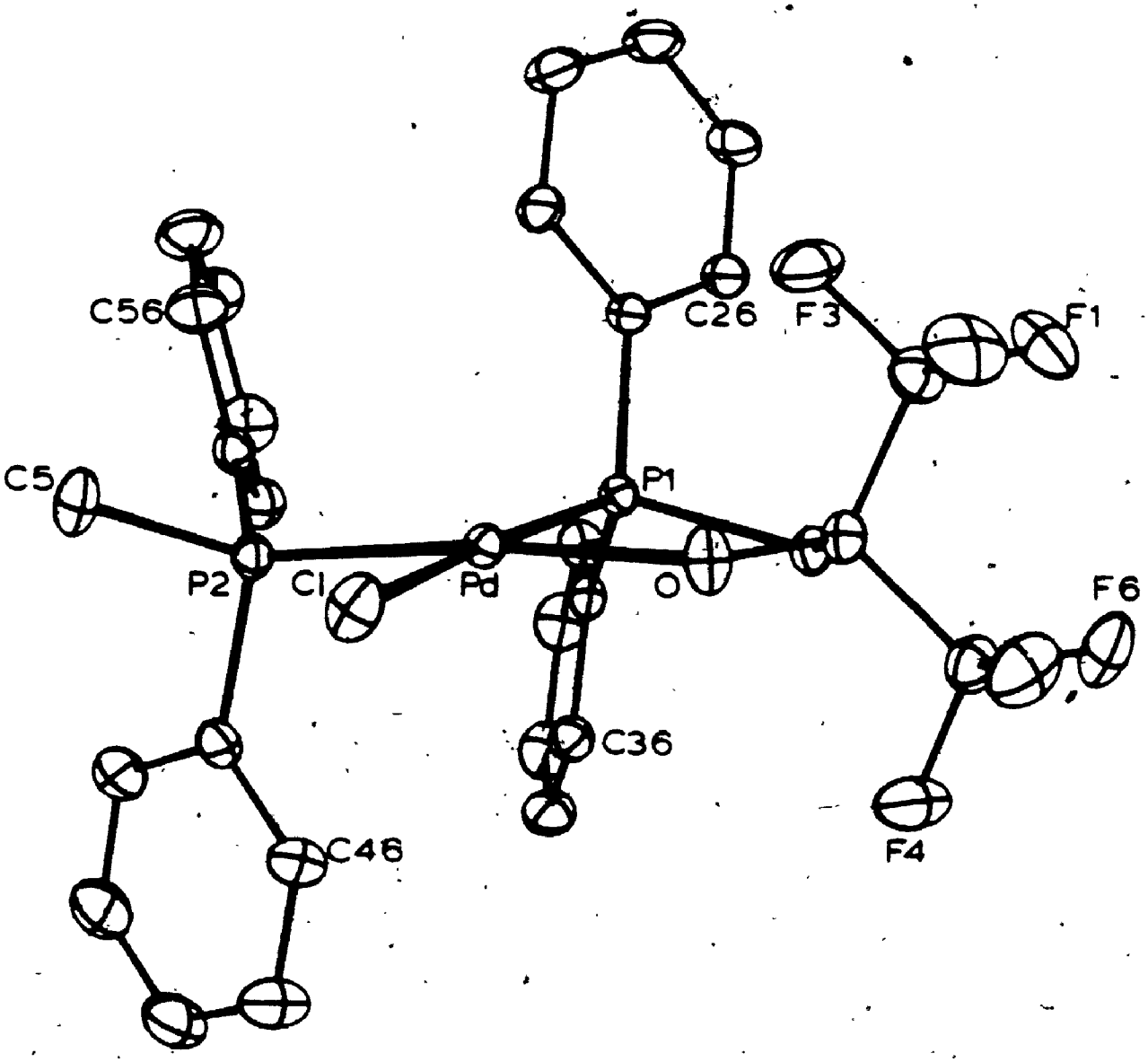

Figure 5.3 ORTEP drawing of $[Pd(PPh_2Me)(L^1)Cl]$

Table 5.3 Selected Bond Distances (Å) and Bond angles (deg.) in [Pd(PPh_2Me)(L)Cl].

Atom1	Atom2	Distance
Pd	Cl	2.339(1)
Pd	P1	2.231(1)
Pd	P2	2.259(1)
Pd	O	2.048(2)
P1	Cl	1.840(3)

Atom1	Atom2	Distance
P1	C21	1.802(3)
P1	C31	1.812(3)
P2	C8	1.818(3)
P2	C41	1.823(3)
P2	C51	1.810(3)

Atom1	Atom2	Distance
O	C2	1.365(3)
Cl	C2	1.539(4)
C2	C3	1.548(4)
C2	C4	1.540(4)

Atom1	Atom2	Atom3	Angle
Cl	Pd	P1	172.58(3)
Cl	Pd	P2	88.91(3)
Cl	Pd	O	88.23(6)
P1	Pd	P2	98.51(3)
P1	Pd	O	84.36(6)
P2	Pd	O	173.92(6)
Pd	P1	Cl	100.7(1)
Pd	P1	C21	116.43(9)
Pd	P1	C31	119.44(9)

Atom1	Atom2	Atom3	Angle
Cl	P1	C21	107.1(1)
Cl	P1	C31	102.8(1)
C21	P1	C31	108.5(1)
Pd	P2	C8	115.4(1)
Pd	P2	C41	108.7(1)
Pd	P2	C51	117.88(9)
C8	P2	C41	105.0(1)
C8	P2	C51	102.4(2)
C41	P2	C51	106.7(1)

Atom1	Atom2	Atom3	Angle
Pd	O	C2	122.7(2)
P1	Cl	C2	110.3(2)
O	C2	Cl	113.8(2)
O	C2	C3	108.7(2)
O	C2	C4	107.7(2)
Cl	C2	C3	110.8(2)
Cl	C2	C4	107.6(2)
C3	C2	C4	108.3(2)

Numbers in parentheses in this and other tables are estimated standard deviations in the least significant digits

Table 5.4 Table of Supplementary Bond Distances and Angles in [Pd(PPh_2Me)(L^1)Cl].

Atom1	Atom2	Distance
C1	H1C1	0.98
C1	H2C1	0.98
C3	F1	1.327(4)
C3	F2	1.313(4)
C3	F3	1.341(4)
C4	F4	1.318(4)
C4	F5	1.328(4)
C4	F6	1.338(4)
C8	H1C8	0.96
C8	H2C8	0.98
C8	H3C8	0.96
C21	C22	1.388(4)
C21	C26	1.396(4)
C22	C21	1.388(4)
C22	C23	1.373(4)
C22	HC22	0.98
C23	C22	1.373(4)
C23	C24	1.383(5)
C23	HC23	0.98
C24	C23	1.383(5)
C24	C25	1.388(5)
C24	HC24	0.98
C25	C24	1.386(5)
C25	C26	1.390(4)
C25	HC25	0.98
C26	C21	1.396(4)
C26	C25	1.390(4)

Atom1	Atom2	Distance
C26	HC26	0.98
C31	C32	1.388(5)
C31	C36	1.398(4)
C32	C31	1.389(5)
C32	C33	1.378(5)
C32	HC32	0.98
C33	C32	1.378(5)
C33	C34	1.369(5)
C33	HC33	0.98
C34	C33	1.369(5)
C34	C35	1.373(6)
C34	HC34	0.98
C35	C34	1.373(6)
C35	C36	1.384(5)
C35	HC35	0.98
C36	C31	1.398(4)
C36	C35	1.384(5)
C36	HC36	0.98
C41	C42	1.372(5)
C41	C46	1.389(5)
C42	C41	1.372(5)
C42	C43	1.389(6)
C42	HC42	0.98
C43	C42	1.389(6)
C43	C44	1.363(7)
C43	HC43	0.98
C44	C43	1.363(7)

Atom1	Atom2	Distance
C44	C45	1.388(7)
C44	HC44	0.98
C45	C44	1.388(7)
C45	C46	1.391(6)
C45	HC45	0.98
C46	C41	1.388(5)
C46	C45	1.391(6)
C46	HC46	0.98
C51	C52	1.383(5)
C51	C56	1.398(4)
C52	C51	1.383(5)
C52	C53	1.400(5)
C52	HC52	0.98
C53	C52	1.400(5)
C53	C54	1.383(6)
C53	HC53	0.98
C54	C53	1.383(6)
C54	C55	1.386(6)
C54	HC54	0.98
C55	C54	1.386(6)
C55	C56	1.388(6)
C55	HC55	0.98
C56	C51	1.398(4)
C56	C55	1.388(6)
C56	HC56	0.98

Table 5.4 Continued. Table of Supplementary Bond Distances and Angles in [Pd(PPh_2Me)(L^1)Cl].

Atom1	Atom2	Atom3	Angle
P1	C1	H1C1	109 3
P1	C1	H2C1	109 3
C2	C1	H1C1	109 3
C2	C1	H2C1	109 3
H1C1	C1	H2C1	109 5
F1	C3	F2	106 4(2)
F1	C3	F3	106 3(3)
F1	C3	C2	114 0(3)
F2	C3	F3	106 2(3)
F2	C3	C2	113 2(3)
F3	C3	C2	110 1(2)
F4	C4	F5	106 0(3)
F4	C4	F6	106 6(3)
F4	C4	C2	110 5(2)
F5	C4	F6	106 9(3)
F5	C4	C2	113 8(3)
F6	C4	C2	112 7(3)
P2	C5	H1C5	109 3
P2	C5	H2C5	109 3
P2	C5	H3C5	109 3
H1C5	C5	H2C5	109 7
H1C5	C5	H3C5	109 7
H2C5	C5	H3C5	109 7
P1	C21	C22	118 7(2)
P1	C21	C26	121 1(2)
C22	C21	C26	119 1(3)
C21	C22	C23	120 3(3)
C21	C22	HC22	119 8
C23	C22	HC22	119 8
C22	C23	C24	119 7(3)
C22	C23	HC23	120 1
C24	C23	HC23	120 1
C23	C24	C25	120 0(3)
C23	C24	HC24	119 8
C25	C24	HC24	119 8
C24	C25	C26	119 8(3)
C24	C25	HC25	120 1
C26	C25	HC25	120 1
C21	C26	C25	120 1(3)
C21	C26	HC26	119 9
C25	C26	HC26	119 9
P1	C31	C32	124 7(2)
P1	C31	C36	116 8(2)
C32	C31	C36	118 8(3)
C31	C32	C33	120 8(3)
C31	C32	HC32	119 7
C33	C32	HC32	119 7
C32	C33	C34	120 3(4)
C32	C33	HC33	119 8
C34	C33	HC33	119 8
C33	C34	C35	120 5(3)
C33	C34	HC34	119 8
C35	C34	HC34	119 8
C34	C35	C36	119 7(3)
C34	C35	HC35	120 1
C36	C35	HC35	120 1
C31	C36	C35	120 5(3)
C31	C36	HC36	119 8
C35	C36	HC36	119 8
P2	C41	C42	122 8(3)
P2	C41	C46	119 3(3)
C42	C41	C46	118 1(3)
C41	C42	C43	121 2(4)
C41	C42	HC42	119 4
C43	C42	HC42	119 4
C42	C43	C44	119 5(4)
C42	C43	HC43	120 3
C44	C43	HC43	120 3
C43	C44	C45	120 0(4)
C43	C44	HC44	119 6
C45	C44	HC44	119 6
C44	C45	C46	119 7(4)
C44	C45	HC45	120 1
C46	C45	HC45	120 1
C41	C46	C45	120 6(4)
C41	C46	HC46	119 7
C45	C46	HC46	119 7
P2	C51	C52	123 1(2)
P2	C51	C56	117 9(3)
C52	C51	C56	118 9(3)
C51	C52	C53	120 0(3)
C53	C52	HC52	120 0
C52	C53	C54	121 1(4)
C52	C53	HC53	119 5
C54	C53	HC53	119 5
C53	C54	C55	119 2(4)
C53	C54	HC54	120 4
C55	C54	HC54	120 4
C54	C55	C56	121 0(4)
C54	C55	HC55	119 5
C56	C55	HC55	119 5
C51	C56	C55	118 7(3)
C51	C56	HC56	120 1
C55	C56	HC56	120 1

Table 5.5 Table of Weighted Least-Squares Planes in [Pd(PPh$_2$Me)(L^1)Cl].

The equation of the plane is of the form: $Ax + By + Cz - D = 0$

where A,B,C & D are constants and x,y & z are orthogonalized coordinates

Plane No	A	B	C	D	Atom	x	y	z	Distance	Esd
1	-0 3862	0 7943	-0 4614	2 2928	----------Atoms in Plane----------					
					Pd	-0 8478	2 6787	0 2849	-0 040	0 000
					P1	-1 0699	3 6186	2 2632	-0 039	0 001
					P2	-2 6288	1 6361	-0 0186	0 084	0 001
					Cl	0 0608	1 8368	-1 7742	-0 040	0 001
					O	1 1006	3 7378	0 3811	0 066	0 002
					Chi Squared = 58424					
					----------Other Atoms----------					
					C1	0 1817	4 9587	2 2812	0 518	0 003
					C2	1 4084	4 6582	1 4276	0 113	0 003
2	0 8711	0 2006	-0 1280	-0 7101	----------Atoms in Plane----------					
					C21	-0 7767	2 5968	3 7170	-0 002	0 003
					C22	-0 8192	1 2418	3 8624	-0 004	0 003
					C23	-0 2087	0 4896	4 6618	0 004	0 004
					C24	-0 1578	1 0378	5 9100	0 003	0 004
					C25	-0 4214	2 3664	6 0854	-0 008	0 004
					C26	-0 7120	3 1588	4 9924	0 008	0 003
					Chi Squared = 17					
					----------Other Atoms----------					
					P1	-1 0699	3 6186	2 2632	0 108	0 001
3	-0 8136	-0 7678	-0 3837	-3 0944	----------Atoms in Plane----------					
					C31	-2 8169	4 8315	2 8038	-0 001	0 003
					C32	-3 3976	4 4788	3 8611	0 003	0 003
					C33	-4 8861	5 2101	3 7448	-0 002	0 004
					C34	-4 9896	6 8898	2 7021	-0 001	0 004
					C35	-4 2128	6 0698	1 8822	0 003	0 004
					C36	-3 0397	6 3427	1 4808	-0 002	0 003
					Chi Squared = 3					

Table 5.5 Continued Table of Weighted Least-Squares Planes in [Pd(PPh_2Me)(L^1)Cl].

Plane No	A	B	C	D	Atom	x	y	z	Distance	Esd
					Other Atoms					
					P1	-1 0589	3 8196	2 2632	-0 003	0 001
4	0 1086	-0 5783	-0 8090	-1 1828	Atoms in Plane					
					C41	-3 7326	2 7387	-0 9624	-0 007	0 003
					C42	-5 0900	3 0488	-1 0241	0 009	0 004
					C43	-5 9073	3 4202	-1 1828	-0 007	0 005
					C44	-5 3478	4 4888	-2 4188	0 003	0 005
					C45	-4 0070	4 8694	-2 3881	-0 001	0 004
					C46	-3 1883	3 8088	-1 6659	0 003	0 004
				Chi Squared =	14.					
					Other Atoms					
					P2	-2 6288	1 6361	-0 0188	-0 016	0 001
5	-0 6778	-0 4816	-0 5559	1 0414	Atoms in Plane					
					C51	-3 8431	1 1238	1 4871	0 008	0 003
					C52	-4 8374	1 8822	2 0350	-0 010	0 003
					C53	-5 1868	1 4437	3 1913	0 003	0 004
					C54	-4 8394	0 2748	3 7787	0 008	0 004
					C55	-3 8248	-0 4861	3 2206	-0 006	0 004
					C56	-3 1778	-0 0767	2 0862	0 000	0 004
				Chi Squared =	20.					
					Other Atoms					
					P2	-2 6288	1 6361	-0 0188	-0 038	0 001

Dihedral Angles Between Planes

Plane No	Plane No	Dihedral Angle
1	2	89 6
1	3	103 3
1	4	87 3
1	5	81 8
2	3	127 1
2	4	84 6
2	5	133 1
3	4	45 6
3	5	21 4
4	5	49 0

Table 5.6 Torsional Angles in [Pd(PPh$_2$Me)(L^1)Cl].

Atom 1	Atom 2	Atom 3	Atom 4	Angle	Atom 1	Atom 2	Atom 3	Atom 4	Angle
Cl	Pd	P1	C1	17.6	P2	Pd	O	C2	117.7
Cl	Pd	P1	C21	-97.7	Pd	P1	C1	C2	-27.7
Cl	Pd	P1	C31	128.8	C21	P1	C1	C2	94.4
P2	Pd	P1	C1	159.6	C31	P1	C1	C2	-151.4
P2	Pd	P1	C21	85.1	Pd	O	C2	C1	-18.1
P2	Pd	P1	C31	-48.4	Pd	O	C2	C3	105.7
O	Pd	P1	C1	15.0	Pd	O	C2	C4	-137.3
O	Pd	P1	C21	-100.4	P1	C1	C2	O	30.5
O	Pd	P1	C31	126.1	P1	C1	C2	C3	-92.2
Cl	Pd	O	C2	179.6	P1	C1	C2	C4	149.7
P1	Pd	O	C2	-0.7					

of C(2) from the coordination plane and hence the chelate ring conformation.

The application of the x^2 test[138] to the various bond lengths allowed some to be averaged. The C-CF_3 bond lengths could be averaged to give a mean value of 1.543(3)A. This agrees well with previous reports of structures of metal complexes of perfluoroalkoxide ligands. The C-CF_3 bond length typically falls in the range 1.519(9) to 1.60(2)[15,18,164].

In spite of the considerable thermal motion usually associated with the CF_3 groups, (Table 5.7 contains the root-mean-square amplitudes of vibration) it was possible to average the C-F bond lengths if the σ values were doubled. The mean value was found to be 1.327(3) A. In a previous structure, the C-F bond lengths were averaged to 1.327(5) A.[92]

The C-O bond length of 1.365(3) A falls within the range of previously-reported values for perfluoroalkoxide complexes of 1.33(1) to 1.362(4) A. The bond is again shorter than would normally be expected for a C-O single bond, due to the partial π bonding between carbon and oxygen removing excess electron density from the oxygen.

Within the coordination sphere, the Pd-P bond lengths to the unidentate and bidentate ligands were found to be 2.259(1) and 2.231(1)A respectively. The bond length involving the unidentate ligand agrees well with the structure of the related complex cis-dichlorobis-

Table 5.7 Root-Mean-Square Amplitudes for Thermal Vibration.

Atom	Min	Int'med	Max	Atom	Min	Int'med	Max
P0	0 154	0 181	0 191	C25	0 174	0 231	0 287
C1	0 163	0 217	0 302	C26	0 175	0 205	0 260
P1	0 157	0 181	0 189	C31	0 161	0 180	0 220
P2	0 171	0 194	0 213	C32	0 183	0 222	0 242
F1	0 205	0 302	0 346	C33	0 179	0 262	0 301
F2	0 176	0 307	0 356	C34	0 174	0 258	0 326
F3	0 206	0 249	0 367	C35	0 190	0 245	0 289
F4	0 215	0 257	0 343	C36	0 202	0 209	0 228
F5	0 187	0 282	0 339	C41	0 178	0 229	0 246
F6	0 186	0 302	0 347	C42	0 207	0 262	0 323
O	0 178	0 185	0 292	C43	0 207	0 312	0 376
C1	0 172	0 190	0 224	C44	0 212	0 293	0 383
C2	0 180	0 188	0 224	C45	0 218	0 309	0 362
C3	0 188	0 238	0 251	C46	0 208	0 259	0 281
C4	0 197	0 233	0 252	C51	0 178	0 210	0 223
C5	0 176	0 244	0 299	C52	0 215	0 236	0 248
C21	0 178	0 185	0 208	C53	0 219	0 286	0 298
C22	0 181	0 211	0 250	C54	0 206	0 288	0 331
C23	0 187	0 239	0 294	C55	0 207	0 304	0 318
C24	0 186	0 254	0 308	C56	0 218	0 243	0 277

(dimethylphenylphosphine) palladium (II) in which the Pd-P distance is 2.260(2) A[165] (λ=0.5). The Pd-P distance involving the bidentate ligand is somewhat shorter. This distortion is likely due to the effect of chelation which is also evidenced by the distortion of angles about P1 so that they form a range from 100.7 (1)° to 119.44 (9)°. The structure of bis(diphenylphosphinoacetato)palladium(II)[166] features an analogous five-membered chelate ring with phosphorus and oxygen donor atoms. The Pd-P bond length in that structure is similarly shortened to 2.236(2) and 2.234(2) A.

The remaining two bonds lengths in the coordination sphere, the Pd-Cl and the Pd-O bond lengths, were found to be 2.335(1) A and 2.046(2) A respectively.

5.6.4 Discussion of Structure

In chapter 3, the values of $^1J(P,Pt)$ for various complexes were used to show that the trans influence of a fluorinated alkoxide, $R(CF_3)_2O^-$, is greater than that of the chloride ion. Platinum-chlorine bond lengths have also been used in the past, in complexes of the type trans-$PtClXL_2$, to measure the relative trans influences of the anionic ligand X. The Pd-Cl bond length in $Pd(L^1)Cl(PPh_2Me)$ will be used to discuss the relative cis influence of the fluorinated alkoxide.

The phenomenon of the trans influence deals with the ability of a ligand to weaken the metal-ligand bond trans

to itself. Syrkin[167] suggested that a ligand with a high trans influence should strengthen the metal-ligand bonds in the cis positions. More recently Bennett showed this to be true for arylplatinum(II) complexes.[241,242]

A partial listing of anionic ligands according to this cis influence is[168]

$$CN^-, I^- > NCS^-, Br^- > NCO^-, Cl^- > N_3^- > NO_2^- > NO_3^-$$

Through the use of the Cambridge Crystallographic Database[169] (1985 edition) it is possible to obtain all structures of compounds of the type cis-PdP_2ClX (5-8) where P_2 is either two monodentate phosphines or a chelating disphosphine.

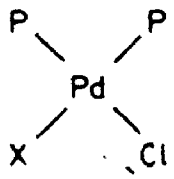

5-8

There are 15 such structures located besides $Pd(L^1)Cl(PPh_2Me)$. These are listed in Table 5.8 along with the length of the Pd-Cl bond.

One can observe the effects of changing X on the Pd-Cl bond length. Since in all of these structures, with the exception of two, X = Cl, then one may only compare the cis influence of $R(CF_3)_2O^-$ with that of the chloride ion. One may argue that since the trans influence and cis influence

Table 5.8. Pd-Cl Bond Lengths in cis-[PdP_2ClX] Complexes

X	P_2	Bond Length	Ref
Cl	$Ph_2PCH_2P(Ph)CH_2PPh_2$	2.354(3)	198
Cl	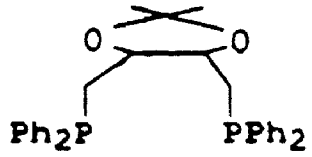	2.34 2.36	199
Cl	$Ph_2PCpFeCpPPh_2$	2.348(1) 2.347(1)	200
Cl	$(PPhMe_2)_2$	2.362(3)	165
Cl	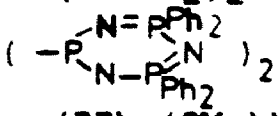	2.398(1)	201
Cl	$(PPh_2(OMe))_2$	2.358(6) 2.349(8)	202
Cl		2.350(3) 2.356(3)	203
Cl	$Ph_2PN(Et)PPh_2$	2.370(5)	204
Cl	$Ph_2PCH_2PPh_2$	2.362(1) 2.352(1)	205
Cl	$Ph_2P(CH_2)_2PPh_2$	2.361(2) 2.357(2)	205
Cl	$Ph_2P(CH_2)_3PPh_2$	2.351(1) 2.358(2)	205
Cl	$(CF_3)_2P(CH_2)_2P(CF_3)_2$	2.311(4)	206
Cl	$(PPr^n{}_3)_2$	2.398(2) 2.417(2)	207
O	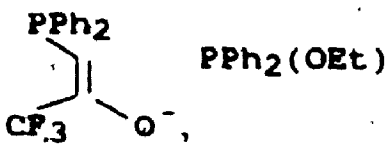	2.356(2)	208
	$(PEt_3)_2$	2.352	209

is not constant for different phosphines and the nature of P_2 is not constant throughout the series, that more than one variable is changing, and no conclusions can be drawn. However, there are some complexes in the series of structures which are highly analogous to $Pd(L^1)Cl(PPh_2Me)$ and the variance in the Pd-Cl bond length is great enough that comparisons can be made.

Perhaps the structure most analogous to $Pd(L^1)Cl(PPh_2Me)$ is that of dichloro(bis(diphenylphosphino)-ethane) palladium(II),[205] in which the Pd-Cl bond length in $Pd(L^1)Cl(PPh_2Me)$ is significantly shorter (λ = 15.6). In fact the Pd-Cl bond is consistently longer when X = Cl regardless of the identity of P_2 (with the exception of the Pd-Cl bond trans to $(CF_3)_2PR$).[206] This would suggest that the stabilizing cis influence of a fluorinated alkoxide is greater than that of a chloride ion. Syrkin's[167] proposal that a high trans influence should be accompanied by a high cis influence is borne out in the case of $R(CF_3)_2O^-$ and Cl^-; $R(CF_3)_2O^-$ has the greater destabilizing trans influence and the greater stabilizing cis influence.

The higher position of the fluorinated alkoxide in the trans influence series is believed to be due to its strongly electron withdrawing nature which withdraws electron density from the metal-ligand σ orbital trans to it via an inductive effect. However, this same electron-withdrawing nature may stabilize the bonds in the cis positions by removing electron density from the metal

centre thus making the cis ligands stronger σ donors.

The more strongly electron-withdrawing nature of a fluorinated alkoxide results in shorter Pd-Cl bond lengths in cis-$[PdP_2ClX]$ compounds when X = $R(CF_3)_2O^-$. In chapter 6 it will be noted that the Ni-P bonds are likewise shortened in trans-$[Ni(L^1)_2]$ under the influence of cis fluorinated alkoxides.

The Pd-Cl bond length is also shorter in $Pd(L^1)Cl(PPh_2Me)$ than in 5-9 where a pyrazole ligand is in the cis position.[209]

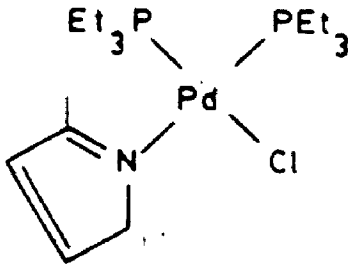

5-9

However this may be simply due to the presence of PEt_3 in the trans position. Triethylphosphine would be expected to exert a greater destabilizing trans influence than the phosphino group in L^1 since a partial trans influence series for phosphines shows[168]

$$PEt_3 > Me_2PhP > Ph_3P$$

Substitution of aryl groups for alkyl groups in tertiary phosphines appears to decrease the trans influence.

A highly analogous structure is that of

[Pd{$Ph_2PCH{=}C(O)CF_3$}($PPh_2(OEt)$)Cl][208] where the phosphorus atoms are in a cis arrangement. This structure fits into the class of cis-[PdP_2ClX] compounds where X is an enolate group. The Pd-Cl bond length is again longer (2.099(5)A) than in [Pd(L^1)Cl(PPh_2Me)] indicating that the cis influence of a fluorinated alkoxide is greater than that of an enolate. This would be expected based on the explanation given for the greater cis influence of fluorinated alkoxides over chloride ions; a fluorinated alkoxide would be more strongly electron withdrawing than an enolate as well.

The Pd-O bond length is also of note, as it too is rather short (2.046(2)A). Very few alkoxides of palladium have been reported, although comparisons can be made with analogous systems. The structure of the perfluoropinacol derivative [Pd{$OC(CF_3)_2C(CF_3)_2O$}($PEt_3)_2$][172] has been determined;[173] the Pd-O distances in this structure are 2.043 and 2.016A. This compound contains fluorinated alkoxides in a five-membered chelate ring trans to tertiary phosphines and the values for the Pd-O distances are very close to that of [Pd(L^1)Cl(PPh_2Me)]. Likewise the tetrachlorocatechol complex [Pd($C_6Cl_4O_2$)($PPh_3)_2$] contains the Pd-O bonds which are 2.028(5) and 2.038(5) A; again the values are close to that [Pd(L^1)Cl(PPh_2Me)] for this very similar compound.

Considerably shorter Pd-O bonds are found in the dinuclear complex ([F_6acac)Pd(μ-OMe)$_2$Pd(F_6acac)].[175] The

four bonds from palladium to hexafluoroacetylacetonyl oxygen average 1.993(7)A, while the four bonds to bridging methoxide average 1.996(7)A. The difference between these values and that in [Pd(L^1)Cl(PPh_2Me)] is more likely due to the greater trans influence of the phosphine in the latter. In the compound [Pd(F_6acad)$_2$(P(o-tolyl)$_3$)], the Pd-O bond trans to the phosphine is 2.084(6)A.[176]

There are two other examples of comparable Pd-O bonds. The structure of [Pd($Ph_2PCH{=}C(O)CF_3$)Cl(PPh_2OEt)][208] mentioned earlier contains a considerably longer Pd-O bond (2.099(5)A). Also the Pd-O bonds in the structure of [Pd($Ph_2PCH_2C(O)O$)][166] are long by comparison, (2.074(5)A and 2.078(5)A), consistent with the more ionic character in the Pd-O bond in the acetato complex.

The chemistry of the ligand HL^1 with palladium(II) will be compared with that of platinum(II) and nickel(II) in chapter 7 when the final conclusions are given.

Chapter 6

Solution and Solid State Studies on the Complex, $[Ni(L^1)_2]$

6.1 Introduction

The transition-metal ion, Ni(II), is considered a borderline acid on the hard-soft scale, similar to Cu(II), Co(II), and Rh(III). As a result, it forms numerous complexes with hard oxygen donor ligands such as alkoxides,[90] including a number with fluorinated alkoxides.[10,16,91,92]

Phosphine complexes of Ni(II), of the type NiL_2X_2, are also well-known. These complexes tend to be tetra-coordinate; when the tertiary phosphine contains only aryl groups, the geometry is tetrahedral for steric reasons, while trialkyl- and dialkyl-phosphines form square-planar complexes. Diarylalkyl phosphines can form complexes of either geometry, and the complexes often exist in an equilibrium between tetrahedral and square-planar. The nature of X also affects the stereochemistry, as the tendency to form tetrahedral complexes increases with decreasing ligand field strength, i.e. $Cl^- < Br^- < I^-$.[93]

In addition, Ni(II) complexes often exhibit other anomalous forms of behaviour, besides square-planar-tetrahedral isomerism. Four-coordinate complexes can become five- or six-coordinate through association[94] or by the coordination of additional ligands.[95] Also temperature-dependence of structure in Ni(II) complexes

often leads to thermochromism.[96]

We therefore decided to prepare a Ni(II) complex analogous to $[Pt(L^1)_2]$ and $[Pd(L^1)_2]$ in order to test the versatility of this new hybrid ligand with respect to coordination to metals of both hard and soft character. The stereochemistry of such a complex was also of interest, in light of the varied stereochemical preferences of Ni(II) complexes, and in order to better understand the coordination properties of L^1. One might expect the steric demands of the phenyl rings and CF_3 groups to favour a tetrahedral geometry while the high ligand-field strength of an alkoxide relative to Cl^-, Br^- or I^- would favour a square-planar arrangement. If square-planar geometry was assumed by the complex, it was of interest to see whether the stereochemistry would be cis or trans, in order to compare the relative importance of such factors as antisymbiosis and steric demands when a smaller, harder, metal ion is used.

The complex, $[Ni(L^1)_2]$, was readily prepared by the addition of HL^1 and base to an ethanolic solution of $NiCl_2.6H_2O$.

$$NiCl_2 + 2HL^1 + 2KOH \longrightarrow Ni(L^1)_2 + 2KCl + 2H_2O$$

The complex precipitated out of the reaction mixture as a green solid, and was characterized by its mass spectrum and elemental analysis.

6.2 Solution Studies on the Complex, $[Ni(L^1)_2]$

6.2.1 NMR Results

The complex, $[Ni(L^1)_2]$, is readily soluble in acetone, methylene chloride and chloroform and slightly soluble in benzene. Since the complex is diamagnetic it was possible to obtain NMR data in a variety of solvents and over a wide range of temperature. ^1H, ^{31}P, and ^{19}F spectra were obtained.

The ^{31}P spectra exhibited two peaks at +14.5 ppm and +34.7 ppm in acetone solution at 35°C. Both signals appeared as singlets in the proton-decoupled spectra; that is, no coupling to ^{19}F was observed. It was however found that the ratio of the signal intensities changed with changing temperature. For example, at 55°C in acetone the ratio of the upfield to downfield signal was 1.60 while at -5°C the ratio decreased to 0.45. Likewise a change in solvent at constant temperature effected a change in the ratio of the two signals; at 35°C the ratio was 0.49 in CH_2Cl_2, 1.60 in acetone and 4.21 in $CHCl_3$, while in C_6H_6 only the upfield signal was observed at all temperatures. It is clear from the ^{31}P NMR spectra alone that two species are present in solution in a solvent- and temperature-dependent equilibrium, with the upfield signal favoured by high temperatures and less polar solvents.

Similarly the ^{19}F NMR spectra showed two species in equilibrium. At -5°C in acetone, the signals appear as triplets at -76.7 and -76.5 ppm with coupling constants of

1.6 and 2.6 Hz respectively. Once again, changes in temperature or solvent result in shifts in the equilibrium which produce corresponding changes in the ratio of the two signals in the NMR spectrum. However, a phenomenon was observed in the ^{19}F spectrum which was not seen in the case of the ^{31}P spectrum. As the temperature is increased from -5°C the two ^{19}F signals move together, coalesce and eventually give a single resolved triplet at high temperature (see Fig. 6.1).

At coalescence, the lifetime of an exchanging species, τ, is inversely proportional to the difference in resonance frequency between the two species in the region of stopped exchange, $\nu_A^0 - \nu_B^0$, according to the equation[97]

$$\tau = \frac{\sqrt{2}}{2\pi(\nu_A^0 - \nu_B^0)}$$

Therefore the greater the separation of the peaks in the slow exchange region, the shorter must be the lifetime at coalescence, the faster the exchange rate and the higher the temperature of coalescence. For this reason, coalescence is not observed for ^{31}P due to the large value of $\nu_A^0 - \nu_B^0$ (~2030 Hz) while it is observed for ^{19}F where $\nu_A^0 - \nu_B^0$ is much smaller (~23 Hz).

The apparent triplet in the ^{19}F NMR might initially be attributed to a four-bond coupling between the fluorine atoms and the methylene protons in the chelate ring backbone. However, no coupling to ^{19}F was observed in the

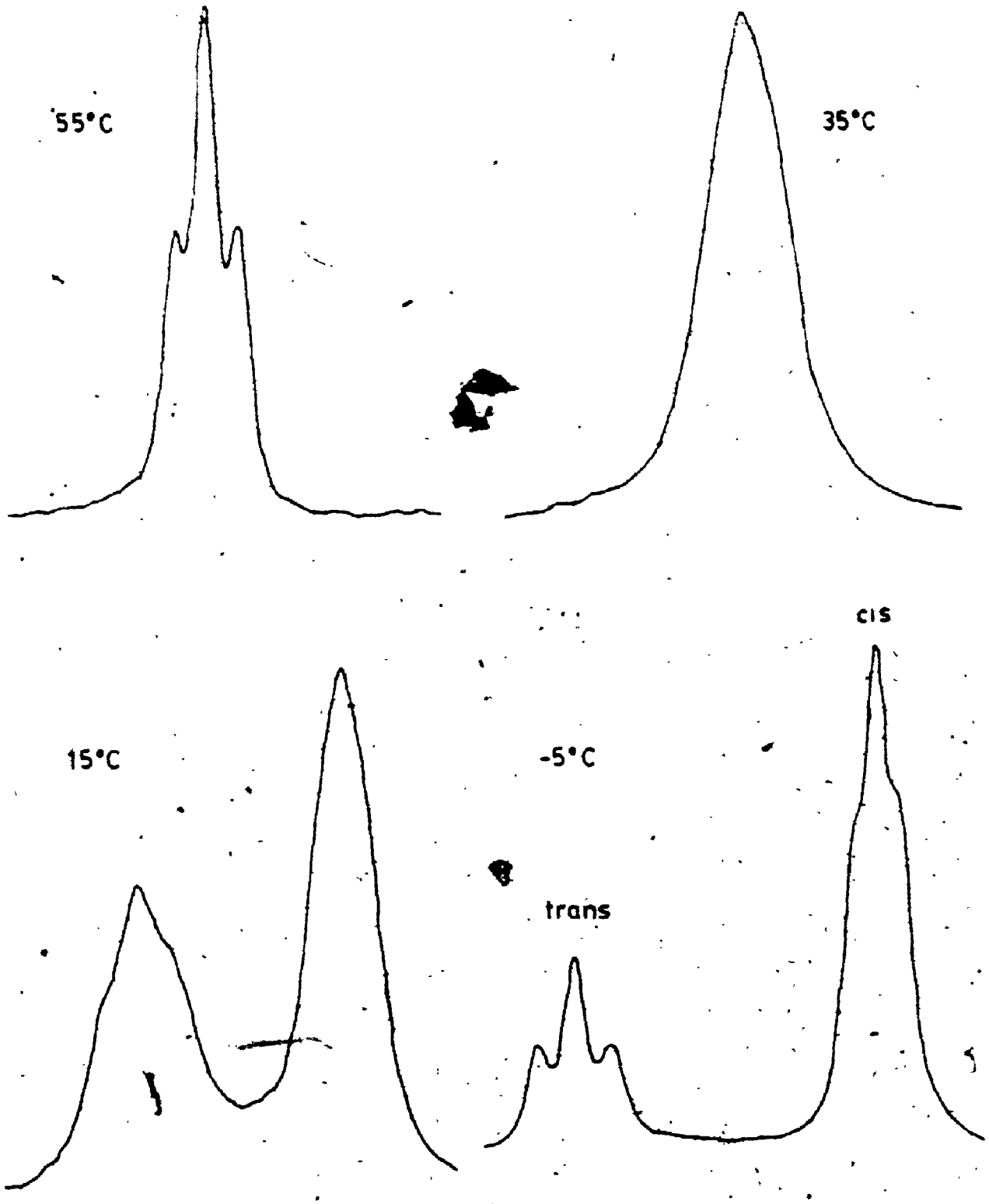

Figure 6.1 ^{19}F NMR spectra showing coalescence of signals due to CF_3 groups of cis and trans isomers

^{31}P NMR spectrum and neither was it observed in the ^{1}H spectrum. Decoupling experiments were needed to determine which nuclei the ^{19}F was coupling to. Selective ^{31}P decoupling of the ^{19}F NMR spectrum of $[Ni(L^1)_2]$ in acetone at -5°C is shown in Fig. 6.2. Clearly the downfield ^{31}P signal is coupled to the upfield signal in the ^{19}F spectrum while the upfield ^{31}P signal is coupled to the downfield ^{19}F signal.

The surprising result, that the triplet pattern in the ^{19}F NMR spectrum is due to coupling to ^{31}P rather than the methylene protons, represents an example of the phenomenon of virtual coupling. The ^{19}F nuclei would be expected to couple to the two phosphorus nuclei with differing coupling constants, if at all; the value of the coupling constant for the intraligand coupling, $^{4}J(P,P)$, should be greater than that to the phosphorus bonded through nickel, $^{5}J(P,F)$. However the appearance of the pseudo-triplet indicates that the fluorine nuclei regard the phosphorus nuclei as equivalent. Virtual coupling in such complexes results from a relatively high value of $^{2}J(P,P)$ and the effect will be discussed in more detail in section 6.2.5. The apparent coupling constants are 2.6 and 1.6 Hz for the downfield and upfield ^{19}F signals respectively. It is because of the relatively small value of the couplings that they are not observed in the ^{31}P NMR spectrum. The values of the width at half height for the downfield and upfield ^{31}P signals at -5°C in acetone are 13 Hz and 15 Hz

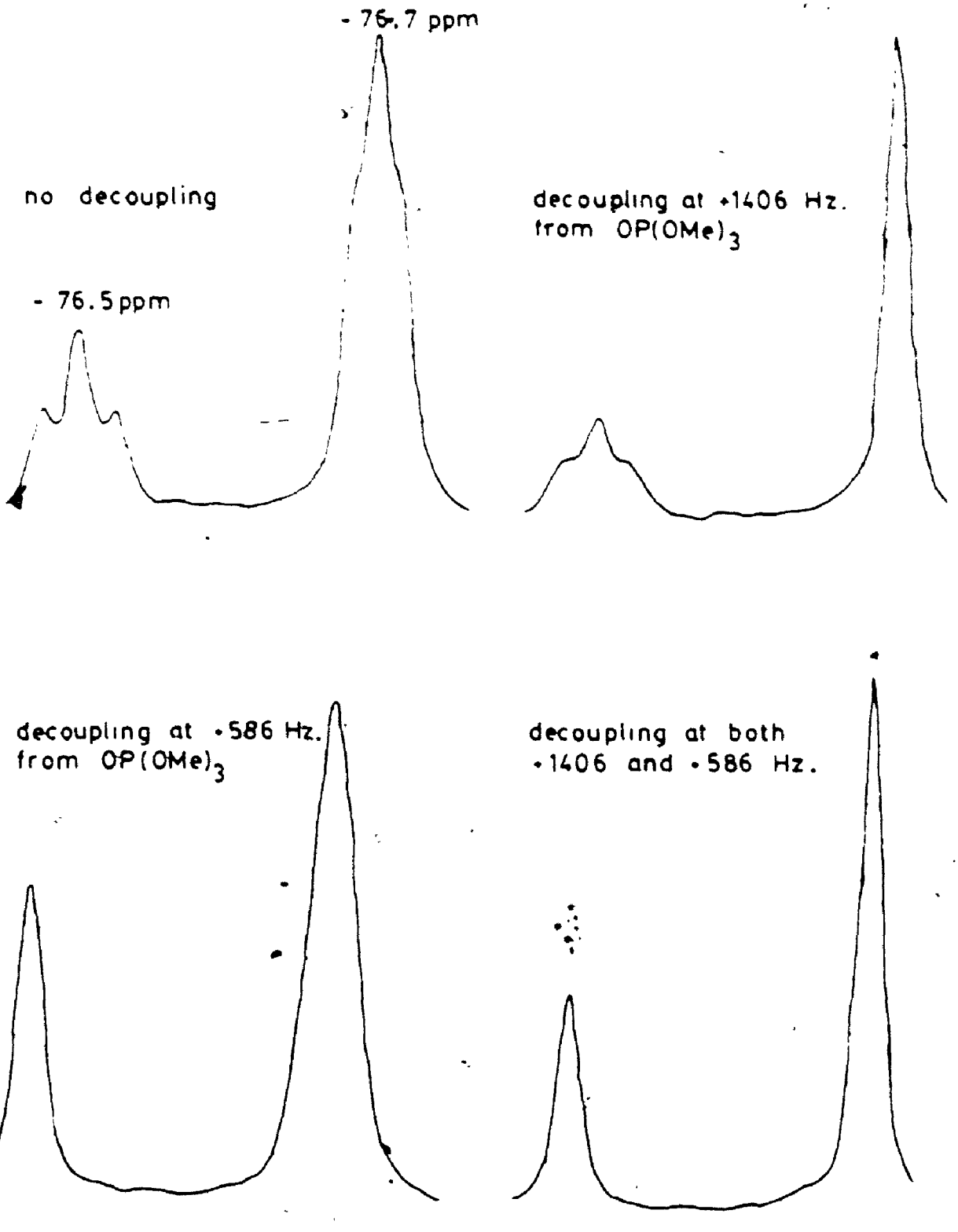

Figure 6.2 ^{31}P decoupled ^{19}F NMR spectra (at -5°C)

respectively, too great for resolution of such a small coupling.

The ^{1}H NMR displays signals due to both aromatic and methylene protons. Again, the methylene region of the spectra contains two signals due to two species in a temperature- and solvent-dependent equilibrium. At -5°C in acetone, the signals appear at 3.26 and 2.90 ppm. As in the ^{19}F NMR spectra, the methylene proton signals are not split into a doublet due to intraligand coupling to the ^{31}P nucleus but rather into a pseudo-triplet due to virtual coupling to both phosphorus nuclei. Decoupling experiments were used to determine that the downfield peak in the ^{31}P NMR is coupled to the downfield methylene protons of the ^{1}H NMR while the upfield ^{31}P and ^{1}H signals are coupled. The apparent $^{2}J(H,P)$ values are 6.5 Hz for the downfield species and 5.7 Hz for the upfield species.

As the temperature is increased, not only does the ratio of the intensities of the two methylene proton pseudo-triplets vary but also the two signals move closer together and coalesce. As in the ^{19}F NMR spectrum (but unlike the ^{31}P NMR spectrum), the value of $(\nu_A^0 - \nu_B^0)$ is sufficiently small ($\sim$37 Hz) that coalescence may be observed.

The NMR data for the complex, $[Ni(L^1)_2]$, are summarized in Table 6.1.

Table 6.1 NMR Data for $Ni(L^1)_2$[a]

Species	Solvent	$^1H(CH_2)$ δ ppm	$^2J(P,H)$ Hz	$^{19}F(CF_3)$ δ ppm	$^4J(P,F)$ Hz	^{31}P δ ppm	Δδ[b] ppm
A (trans isomer)[d]	acetone	2.90(t)	5.7[c]	-76.5(t)	2.6[c]	+14.5	+48.1
B (cis isomer)[d]	acetone	3.26(t)	6.5[c]	-76.7(t)	1.6[c]	+34.7	+68.3

a At -5°C, the region of slow exchange

b the coordination shift, $\Delta\delta = \delta_{coord} - \delta_{free}$

c apparent coupling constants, see text, 6.25

d structural assignment will be discussed in 6.2.2.

6.2.2 Visible Spectra Results

Solutions of $[Ni(L^1)_2]$ in acetone, methylene chloride, chloroform and benzene are orange in colour. There were three absorption bands identified in an acetone solution at room temperature: the most intense band was seen at 30,800 cm^{-1} with an intensity of 7200 ℓ $mole^{-1}$ cm^{-1} and was likely charge transfer in origin; a second band appeared at 23,000 cm^{-1} with an intensity of 640 ℓ $mole^{-1}$ cm^{-1}; a very weak shoulder appeared at 16,600 cm^{-1} with an intensity of 8 ℓ $mole^{-1}$ cm^{-1}.

Since the NMR results indicated clearly that two species are present in solution in a temperature- and solvent-dependent equlibrium, the effect of changing solvent and temperature on the visible spectrum was investigated. At all temperatures the solution remained orange in colour. Visible spectra were obtained at various temperatures in acetone and chloroform and no shift in the energies of the absorption bands was observed. However, the intensity of the band at 23,000 cm^{-1} as well as the shoulder at 16,600 cm^{-1} varies with temperature. For example for a 5.5 x 10^{-4} M solution of $[Ni(L^1)_2]$ in $CHCl_3$, as the temperature is increased from 21°C to 48.5°C, the extinction coefficient for the band at 23,000 cm^{-1} decreases from 704 to 673.

Similarly if one varies the solvent, the extinction coefficient for the band at 23,000 cm^{-1} changes as illustrated in Fig. 6.3. In benzene, the observed

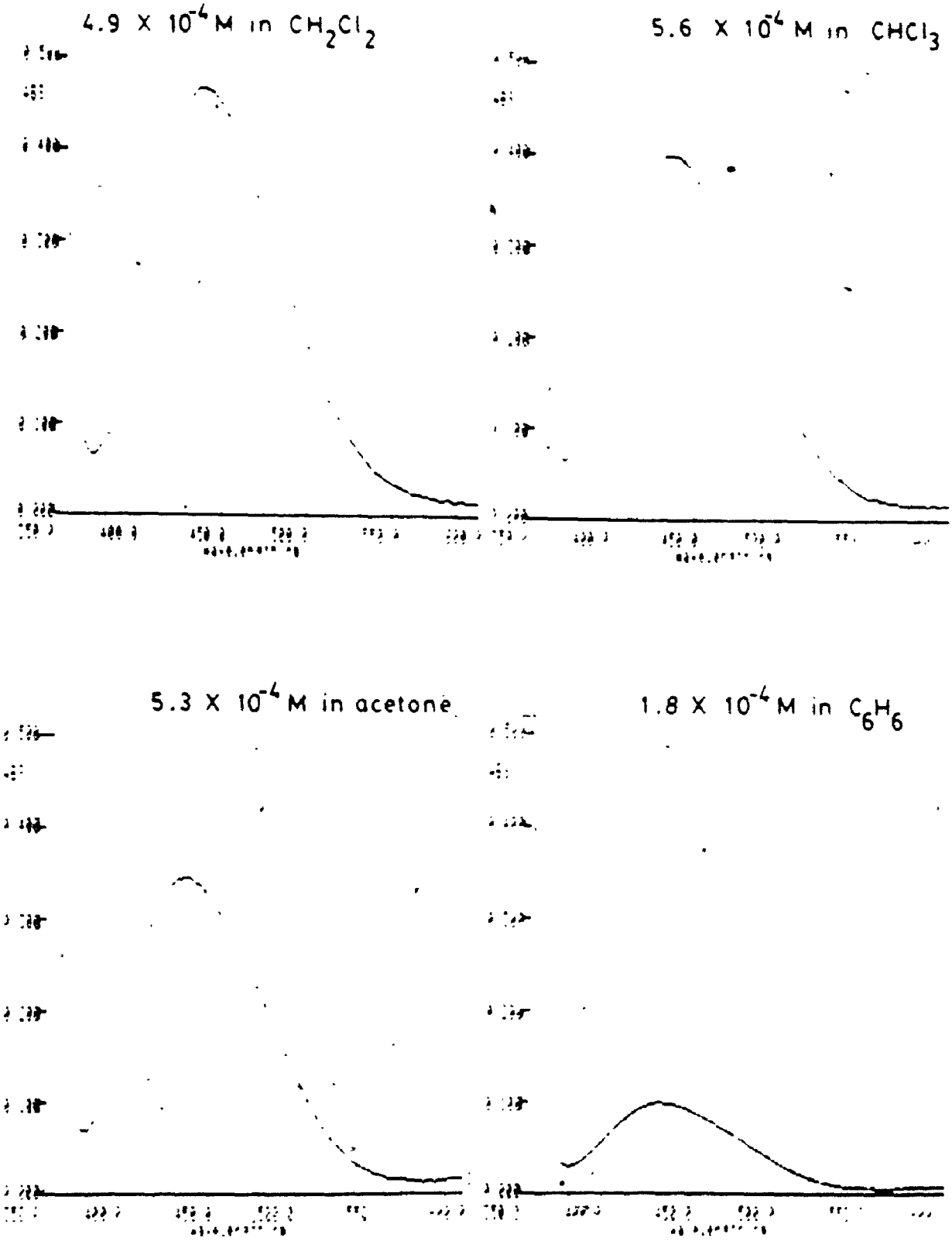

Figure 6.3 Visible spectra of solutions of $[Ni(L^1)_2]$

extinction coefficient was 550, whereas in methylene chloride the value reached 940.

In the case of $[Co(L^1)_2]$ and $[Cu(L^{1}=O)_2]$, solvation resulting in an increase in coordination number from four to five was observed. By contrast, the addition of pyridine seemed to have no effect on the visible spectrum of $[Ni(L^1)_2]$ beyond causing a shift in the equilibrium of the two species present.

The two species observed in equilibrium in the NMR studies exhibit very similar visible spectra. Both are orange in solution with absorption bands at 30,800 (CT), 23,000 cm^{-1} and a shoulder at 16,600 cm^{-1}. Only the extinction coefficients of these bands seem to differ. Since it is known from the ^{31}P NMR studies that in benzene only the upfield species exists, then the observed extinction coefficient in benzene is that of the one species A. Knowing the relative concentrations of the two species in a particular solvent at a given temperature from the NMR studies, one can calculate the value of the extinction coefficient for the absorption of species B at 23,000 cm^{-1}. The visible spectral data are given in Table 6.2.

Given the NMR and visible spectral results, it is possible to demonstrate the nature of the equilibrium observed in solution. There are two possibilities for isomerism in a nickel complex of this type: square-planar versus tetrahedral geometry, or cis-trans isomerism in

Table 6.2 Visible Spectral Data for $Ni(L^1)_2$

Species	Absorption Bands		
A	16,600	23,000(550)[a]	30,800(CT)
B	16,600	23,000(~1100)[a]	30,800(CT)

[a]bracketed numbers are extinction coefficients given in units of $\ell \cdot mole^{-1} \cdot cm^{-1}$

square-planar geometry. Square-planar versus tetrahedral isomerism has long been a known process for phosphine complexes of nickel(II) halides, $[NiP_2X_2]$.[98,99] For such systems, both the thermodynamics[98] and kinetics[100] have been thoroughly investigated. The thermodynamic studies would suggest that the planar state is the more favourable electronically, while the steric ligand-ligand interactions tend to favour the tetrahedral geometry. The NMR studies on $[Cu(L^1)(PPh_3)_2]$ indicated that the complex was partially dissociated even at low temperatures, presumably because L^1 is a sterically demanding ligand. Therefore it seemed possible that in $[Ni(L^1)_2]$ the tetrahedral geometry may be stabilized by steric interactions.

However, the possible existence of a tetrahedral species in solution can be ruled out for two reasons. Firstly, tetrahedral Ni(II) complexes are paramagnetic and therefore the formation of such a species in solution should be accompanied by pronounced changes in the NMR spectrum. However, no such trend was observed. For example, the width at half height for the ^{31}P, ^{19}F and ^{1}H NMR signals of both isomers were approximately the same; no significant line broadening was ever observed.

Secondly, were one species square-planar and the other tetrahedral, one would expect considerable differences in the visible absorption spectra. No differences in the colour of the solution (orange) or in the position of λ_{max} were observed, even when solvent or temperature changes

caused dramatic shifts in the equilibrium. The visible spectra themselves were also inconsistent with a tetrahedral geometry.

Typically, tetrahedral nickel(II) complexes are blue or green. The ground state for a d^8 ion with T_d symmetry is $^3T_1$ and the major visible band appearing near 16,000 cm^{-1} with an intensity of $\sim 10^2$ ℓ $mole^{-1}$ cm^{-1} is attributed to a $^3T_1(P) \longleftarrow {}^3T_1$ transition.[101] A near-infrared band around 8000 cm^{-1} of intensity ~ 20 ℓ $mole^{-1}$ cm^{-1}, characteristic of tetrahedral Ni(II), is assigned as a $^3A_2 \longleftarrow {}^3T_1$ transition.[101] Absorption spectral data for some typical tetrahedral complexes of Ni(II) are given in Table 6.3.

Since the spectral data, both NMR and visible, indicate that no tetrahedral Ni(II) species is present in solution, the visible spectra must be examined to see if the results are consistent with a cis-trans square-planar equilibrium.

Square-planar complexes of Ni(II) are typically yellow, orange, red or brown. The spectra of these complexes differ from those with a tetrahedral geometry in the absence of any bands of electronic origin below 10,000 cm^{-1}. Most square-planar Ni(II) complexes exhibit a strong absorption band, ν_3, in the region 23,000 - 30,000 cm^{-1} which is considered to be charge-transfer in origin.[105]

Assignment of bands to specific transitions in square-planar Ni(II) complexes has proved difficult and often conflicting. Four low-lying d orbitals each contain

Table 6.3 Absorption Spectra for Some Tetrahedral Nickel(II) Complexes.

Complex	$^3A_2 \leftarrow {}^3T_1$	$^1E \leftarrow {}^3T_1$	$^3T_1(P) \leftarrow {}^3T_1$	$^1T_2 \leftarrow {}^3T_1$	Ref
$NiCl_4^{2-}$	6550(21)	11630(6)	14250(160) 15240(160) 15950	19800	102
$Ni(Ph_3PO)_2Cl_2$	7288	12120	14290 16260	22470	102
$Ni(2,3\text{-lut})_2Cl_2$	10130		16330 18080		103
$Ni(PPh_3)_2Cl_2$	10000	13500	15000(600) 18500	21500(CT)	104

an electron pair, while the highest energy orbital is left empty. In monodentate systems, this high-energy orbital is the $d_{x^2-y^2}$ orbital, but when bidentate ligands are used, the x and y axes are drawn to bisect the ligands, making the d_{xy} orbital of highest energy. For the four remaining low-energy orbitals, there are a number of possible orderings, but they are often so close in energy that it is not possible to distinguish and assign individual transitions. As a result, the one major band is usually seen in the visible region. In such cases, one may tentatively assume that the band position approximates the $xy \rightarrow x^2-y^2$ transition whose energy is 10 Dq-C.[106] Some typical square-planar Ni(II) complexes and their absorption spectra are recorded in Table 6.4.

The visible spectra for solutions containing $[Ni(L^1)_2]$ are, by comparison with those of known square-planar Ni(II) complexes, consistent with the presence of two square-planar isomers each with the same P_2O_2 donor set. There is one major visible band at 23,000 cm^{-1} for both isomers, higher in energy than for the comparable complexes: $[Ni(PEtPh_2)_2Br_2]$ and $[Ni(PMePh_2)_2Cl_2]$. This is consistent with the expected spectrochemical series:

$$Br^- < Cl^- < R(CF_3)_2O^-$$

The visible spectra for cis and trans $[Ni(L^1)_2]$ can be compared with those of other square-planar Ni(II) fluorinated alkoxide complexes. Such a comparison is given

Table 6.4 Absorption Spectra for Some Square-Planar Nickel(II) Complexes

Complex	ν_1	ν_2	ν_3	Ref
$Ni(PEt_3)Cl_2$		20,140(450)	27,030(14,200)	99
$Ni(PEt_3)_2Br_2$		18,450(350)	25,000(6200)	99
$Ni(PMePh_2)_2Cl_2$	18,200	21,750	26,200	107
$Ni(PEtPh_2)_2Br_2$	18,000	20,600	24,300	107
$Ni(en)_2^{2+}$		21,550		108

in Table 6.5. The complexes all exhibit one major band in the range 19,000 to 23,000 cm^{-1} but there are a number of trends in the data.

First of all there is a shift to the blue in the position of λ_{max} as the imino group in the chelate ring is replaced by the phosphino group. This is consistent with the phosphines' ability as π-acceptor ligands, which allows them a higher position in the spectrochemical series than N-donor ligands. There is also a significant increase in the value of ϵ for the absorption when the phosphine donor is employed. This is because phosphines are softer, more polarizable, ligands than N-donor ligands and as such form bonds of more covalent nature with metals. This is demonstrated by the relative positions of the two ligands in the Nephalauxetic series. The more covalent the bonding, the greater the transition intensity, since the mixing of ligand p orbitals with the metal d orbitals relaxes the Laporte rule forbidding d-d transitions.

There is also a trend in the data of Table 6.5 suggesting the the transitions are more intense for complexes having a five-membered chelate ring rather than a six-membered ring. Since there is a definite relationship between complex stability and transition intensity, the six-membered rings in these complexes are likely more strained and less stable.

Finally, one may compare the cis and trans isomers for each type of complex. As mentioned, the four low-energy

Table 6.5 Absorption Spectra for Some Square-Planar Fluorinated Alkoxide Ni(II) Complexes.

	6-membered chelate ring; N,O donors[a]	5-membered chelate ring; N,O donors[a]	5-membered chelate ring; P,O donors[b]
Cis Isomer	19350 cm^{-1} (168)	20500-20800 cm^{-1} (240-260)	23000 cm^{-1} (1100)
Trans Isomer.	19100-19300 cm^{-1} (68-84)	-	23000 cm^{-1} (550)

a ref 92

b this work

d-orbitals are usually so close in energy in square-planar Ni(II) complexes that only one major band is resolved. Therefore it is not surprising that no change in λ_{max} is observed in going from the cis to the trans isomer. However, the cis isomer is of lower symmetry, having no centre of inversion, and for such complexes the Laporte parity selection rule is relaxed. This rule, which states that transitions between states of the same parity, such as d-d transitons, are forbidden, cannot be applied since it is nonsensical to consider d-orbitals being even to inversion where a centre of inversion is lacking. For this reason, cis isomers exhibit more intense transitions than those of their trans counterparts.

All the NMR and visible data are thus consistent with a cis-trans square-planar isomerism for $[Ni(L^1)_2]$ in solution. In Tables 6-1 and 6-2, species A is assigned as the trans isomer. This species was favoured by polar solvents as expected for the less polar isomer and high temperatures. In the ^{31}P and ^{1}H NMR, the signals for this species appeared further upfield as expected for the isomer where the phosphino groups are trans to a strong trans influence ligand (each other), thus serving as a poorer σ-donor and being more highly shielded. By similar arguments, the alkoxides in the trans isomer are trans to a poorer trans influence ligand and would be expected to be more deshielded than in the cis isomer. Consistent with this, the ^{19}F resonance for species A, which reflects more

the alkoxide portion of the ligand, lies downfield relative to that of species B. In the visible spectra, the higher symmetry trans isomer would be expected to have less intense d-d transitions, while the position of the absorption bands should not necessarily differ from that of the cis isomer as both have the same donor set. Again, as expected, species A has the lower extinction coefficient for the band at 23,000 cm^{-1}. Similar arguments can be used to show that the spectral results are consistent with species B being the cis-square-planar isomer.

6.2.3 Discussion of Thermodynamic Data

All the spectroscopic results were consistent with $[Ni(L^1)_2]$ existing in solution as cis- and trans-square-planar isomers in a dynamic equilibrium dependent on temperature and solvent. Since each isomer gave a distinct signal in the ^{31}P NMR spectrum, it was possible to determine the position of the equilibrium by integrating to obtain the area under each curve. The equilibrium constant, K_{eq}, is then the ratio of these two areas. Using acetone, dichloromethane, chloroform and benzene, ^{31}P spectra were run over a range of temperature, and values of K_{eq} for the cis-trans equilibrium were evaluated by integration in each case except benzene, where only the trans isomer could be detected. The equilibrium constant, K_{eq}, is related to temperature by the expression:

$$\ln K_{eq} = \left[\frac{\Delta S}{R}\right] - \left[\frac{\Delta H}{R}\right]\frac{1}{T}$$

Therefore, plots of $\ln K_{eq}$ as a function of 1/T should be linear for each solvent. Such plots for chloroform, acetone and dichloromethane are shown in Fig. 6.4 and are indeed linear. Values of ΔS and ΔH were then obtained from the intercepts and slopes respectively and are recorded in Table 6.6 for each solvent.

There are a number of factors involved in determining whether the cis or trans geometry is thermodynamically favoured in square-planar complexes of Pt(II), Pd(II) and Ni(II). Three factors contribute to the value of ΔH for the cis → trans isomerization. Firstly there is the electronic contribution of the inner bond strength. Chatt and Wilkins[109] have shown that, for complexes of the type, $[Pt(ER_3)_2X_2]$ (E = P, As, Sb; R = methyl to n-pentyl; X = Cl^-, I^-) in benzene, the cis form is actually the thermodynamically favoured isomer and that heat is absorbed in going from the cis to the trans isomer. Originally, this was explained in terms of π-bonding, but it is now attributed to the mutually destabilizing effect of two trans soft ligands; Pearson's "antisymbiotic effect".[110] Thus the contribution of the inner bond strength to ΔH favours the cis form because of antisymbiotic behaviour.

Secondly, the ΔH of solvation also favours the cis isomer, since the dipole-dipole interactions between solute and solvent are greater in the case of the more polar cis

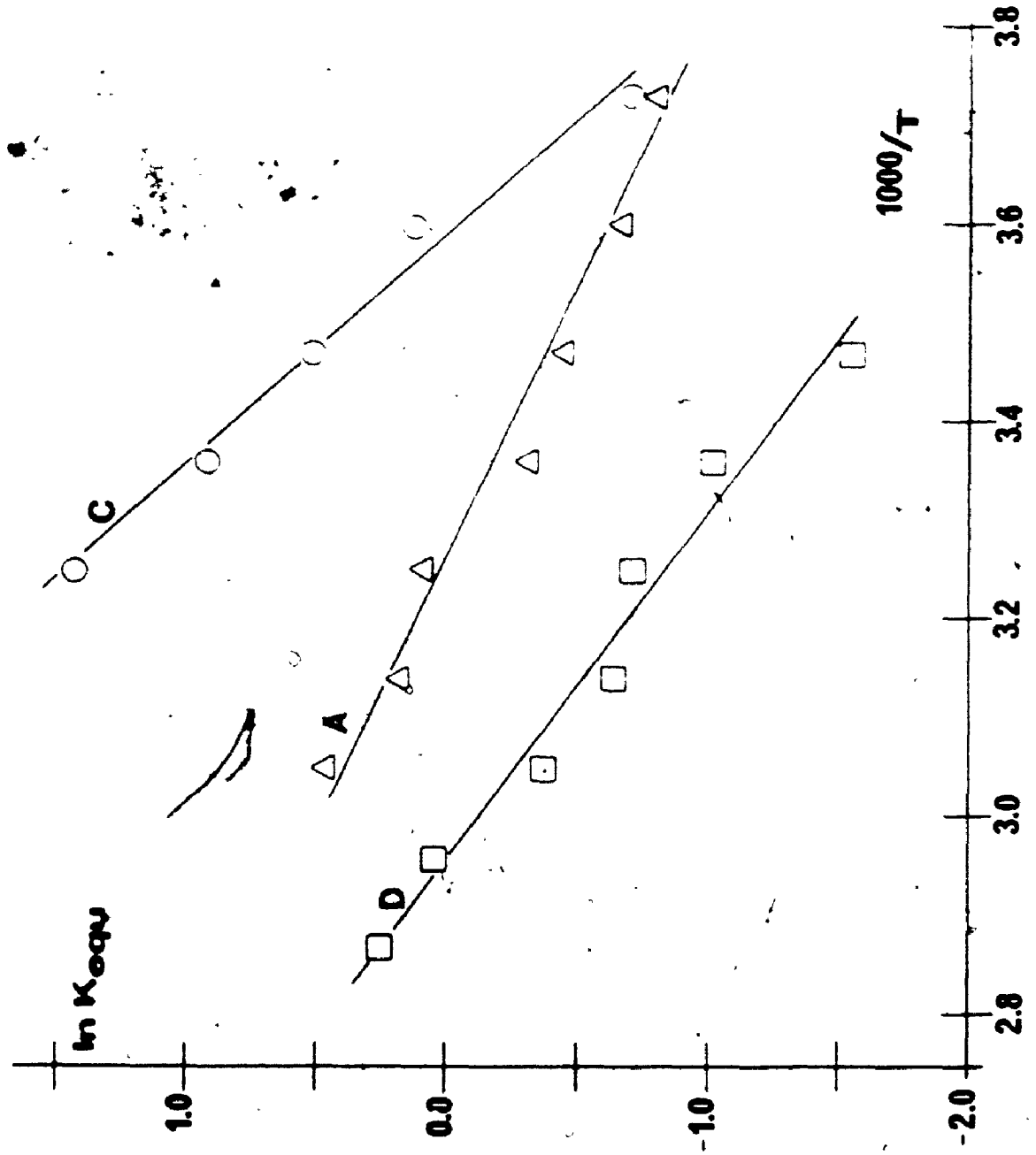

Figure 6.4 Plots of $\ln K_{equ}$ vs. 1000/T in acetone(A), chloroform(C) and dichloromethane(D)

Table 6.6. Thermodynamic Data for Cis⟶Trans Conversion of $[Ni(L^1)_2]$

Solvent	Dipole Moment, D[a]	ΔH, kJ/mol	ΔS, J/mol	ΔG, kJ/mol[b]	K_{equ}[b]
$(CH_3)_2CO$	2.88	15.7	51.3	0.41	0.85
CH_2Cl_2	1.60	23.5	69.4	2.82	0.32
$CHCl_3$	1.01	35.5	127	-2.35	2.58
C_6H_6	0.0	(only trans isomer detected at all temperatures)			

[a] "Lange's Handbook of Chemistry", Twelfth Edition, Ed. Dean, J. A., McGraw-Hill, New York, 1972.

[b] at 298 K.

isomer.

The steric interactions make a contribution to the overall ΔH in favour of the trans isomer. In the trans geometry, steric repulsions between the phenyl groups are minimized.

There are two contributions to ΔS, that of the steric effects and the ΔS of solvation. The contribution to ΔS by the steric interactions would be expected to be minimal as it only involves the loss of some vibrational and rotational degrees of freedom. The ΔS of solvation should favour the trans isomer as dipole-dipole interactions are minimized in the case of the less polar isomer. Therefore ΔH_{steric} and $\Delta S_{solvation}$ favour the trans isomer while $\Delta H_{solvation}$ and $\Delta H_{electronic}$ favour the cis isomer.

As mentioned above, it has long been shown that, in the case of Pt(II) - phosphine complexes, the cis isomer is the more thermodynamically stable isomer. This is seen in the case of $[Pt(L^1)_2]$, where only the cis isomer is observed. Similarly, $[Pd(L^1)_2]$ exists only in the cis geometry. For these soft metals where antisymbiosis is significant, the contribution to ΔH by the electronic factors predominates.

However, in the case of a complex formed with a harder acid, Ni(II), antisymbiosis is no longer as important. Also, the decrease in the ionic radius as one moves to the first-row transition metals makes the steric repulsions between the phenyl groups more significant. Therefore, the electronic contribution to ΔH decreases while the steric

contribution increases. As a result, the trans isomer is more favourable with the harder metals than with the softer metals and in fact the trans isomer is observed in solution in the case of $[Ni(L^1)_2]$. Although $\Delta H_{electronic}$ is less significant for Ni(II), nevertheless the overall value of ΔH in each solvent favours the cis isomer. Therefore even for such hard metals, the combination of $\Delta H_{electronic}$ and more importantly $\Delta H_{solvation}$ is enough to overwhelm ΔH_{steric} in solution to give a positive overall ΔH for the cis → trans isomerization.

Likewise for each solvent, ΔS is positive, favouring the trans isomer. This is expected since the only significant contributor, $\Delta S_{solvation}$, favours the trans isomer.

Since solvent interactions are at a minimum in benzene, and only the trans isomer is present in a solution in benzene, it may be concluded this solution best approximates the gaseous state and that, in isolation, the trans isomer is the more stable. Isomerization to the cis isomer occurs only as a result of interactions with the more polar solvents.

The overall ΔS favours the trans isomer while the ΔH favours the cis isomer in each solvent where values were obtained. Therefore the trans isomer is favoured at high temperatures.

Also as expected, the less polar trans isomer becomes increasingly favourable as the solvent polarity decreases;

as the solvent polarity increases, ΔG for the cis → trans isomerization increases. The results in acetone do not fit into this trend however. Acetone is more polar than dichloromethane or chloroform, but the value of ΔG for acetone solution lies between that of dichloromethane and chloroform solution. Most likely, this is due to the ability of acetone to function as a weakly coordinating solvent through the oxygen. As a result the solvent-solute interactions are greater than expected simply considering dipole-dipole interactions.

Since differences in bond strengths and intramolecular steric effects between isomers are constant, then the variations in thermodynamic values observed in Table 6.6 must arise solely from solvation effects. An increase in solvent polarity should be accompanied by an increase in solvent-solute dipole-dipole interactions. Therefore one would expect that S_{cis}, S_{trans}, H_{cis} and H_{trans} would all decrease as solvent polarity increases. The value of ΔG should increase, as was observed, but it is more difficult to predict whether ΔH and ΔS will increase or decrease. It was found that, as solvent polarity increases, both ΔH and ΔS decrease. This surprisingly suggests that the ΔH contribution has the effect of stabilizing the polar cis form to the greater extent in the less polar solvent. Therefore while H_{cis} and H_{trans} both decrease as solvent polarity increases, the effect is greater for the non-polar trans-isomer. Regardless, it is the change in ΔS which

dominates as solvent polarity is decreased so that overall the more polar cis is favoured by more polar solvents.

There have been other reports of cis-trans isomerization in square-planar Ni(II) complexes.[111-114] For the isomerization of $[NiBr_2(Cy_2PH)_2]$ in CH_2Cl_2, ΔH° = 23.6 kJ/mole and ΔS° = 75.77 J/mole[114] while for the isomerization of the bischelate complex nickel salicyladoximate in DMSO, ΔH = 18.62 kJ/mole and ΔS = 45.6 J/mole.[113] These values compare very favourably with the results reported here in dichloromethane and acetone respectively.

6.2.4 Kinetic Studies

In a system where exchange is occurring, as is the case for $[Ni(L^1)_2]$ in solution, the band shape of the NMR spectra is dependent on a number of parameters: the chemical shifts, coupling constants, relaxation times, populations of the different sites and the rate constants for exchange between the various sites. It is therefore possible to determine the value of a rate constant by adjusting these various parameters to achieve the best fit between calculated and experimental spectra. Such a calculation is called "the Complete Band-Shape method" (CBS) or "the Complete Lineshape method" (CLS). However such a calculation can be extremely involved, while a number of methods making use of various approximations are accurate enough for most determinations.

Such methods often make use of a consideration of the line shape of the resonance at the coalescence temperature. In the case of the cis-trans isomerization under examination in this study, the ^1H NMR spectra will be used. In these spectra, the two methylene signals which appear as individual virtual triplets at low temperature (in the region of slow exchange) move together with increasing temperature, merge into a single broadened peak and finally become a sharpened signal in the region of fast exchange. The coalescence temperature is therefore taken as that temperature at which these two signals form the widest single resonance.

When studying the kinetics of a chemical reaction using NMR methods, one is observing the decay in the net magnetization of the sample as the reaction occurs, a first order process.[115]

$$\frac{-d[A]}{dt} = \frac{1}{\tau_A}[A]$$

The lifetime of the nucleus in site A, τ_A, is inversely related to the width at half height of the A resonance signal. A first order rate constant, $1/\tau_A$, is always observed

$$\frac{1}{\tau_A} = -\frac{1}{[A]}\frac{d[A]}{dt}$$

If the reaction being studied is a first order process then the rate law describing the loss of A would be:

$$\frac{-d[A]}{dt} = k[A]$$

And the observed $1/\tau_A$ would equal the rate constant k.

$$k = -\frac{1}{[A]}\frac{d[A]}{dt} = \frac{1}{\tau_A}$$

By altering [A], there will be an appropriate change in the rate but not in the value of $1/\tau_A$

Alternatively, if the reaction is second order, the rate law is given by

$$-\frac{d[A]}{dt} = k[A][B]$$

If one continues to monitor the A resonance, then as [A] is varied there should again be no observed change in $1/\tau_A$ but as [B] is varied $1/\tau_A$ should likewise vary since:

$$\frac{1}{\tau_A} = -\frac{1}{[A]}\frac{d[A]}{dt} = k[B]$$

The rate law for the isomerization was therefore determined by examining the effect on the width at half height, W^*, for the coalesced methylene proton signal. For solutions having $[Ni(L^1)_2]$ concentrations of 0.052 M and 0.026 M, the value of W^* for the coalesced methylene proton resonance remained constant within experimental error, 50 Hz and 46 Hz respectively. Likewise for a sample containing $[Ni(L^1)_2]$ (.050 M) and HL^1(.016 M), the value of W^* remained 46 Hz. Since the value of W^* is independent of the concentration of complex of that of free ligand, then the rate of isomerization appears to be first order in $[Ni(L^1)_2]$ and independent of $[HL^1]$. Such a rate law would suggest that the mechanism is intramolecular.

It is also possible to determine a value for the first order rate constant k for the isomerization in each

order rate constant k for the isomerization in each direction by using the approximation method devised by Shanan-Atidi and Bar-Eli[116] and reported in Sandstrom's "Dynamic NMR Spectroscopy".[117] This method may be applied to a system undergoing exchange between sites of uncoupled spin systems with unequal populations. It can be shown that:

$$\Delta p = p_A - p_B = \left(\frac{X^2-2}{3}\right)^{3/2} \frac{1}{X}$$

where p_A, p_B are the populations of the two sites ($p_A > p_B$). X is then given by:

$$X = 2\pi\tau_C d\nu$$

where τ_C is the lifetime at coalescence and $\delta\nu$ is the difference between the resonance frequencies of the two sites. Egan and Mislow[119] have determined X for a range of selected values of Δp. The value of $\delta\nu$ can be approximated by measurement of W^* while p_A, p_B, Δp and thus X can be calculated given the thermodynamic parameters, ΔH and ΔS. The lifetime at coalescence τ_C may be expressed as

$$\tau_C = (k_A + k_B)^{-1} = p_A/k_A = p_B/k_B$$

while the rate constants are then given by

$$k_A = p_B(2\pi)W^*/X \qquad k_B = p_A(2\pi)W^*/X$$

It is this relationship which is used to evaluate the forwards and backwards rate constants in this isomerization. The value of the activation energy may then

be calculated using the Eyring equation:[118]

$$k = \chi(k_b/h)Te^{-\Delta G^{\ddagger}/RT}$$

where k is the rate constant, χ is the transmission constant and k_b is the Boltzman constant. Taking χ to be unity then this equation can be rearranged to

$$\Delta G^{\ddagger} = (1.914 \times 10^{-2})T(10.319 + \log|T/k|).$$

When a 100 MHz NMR spectrometer was used, the two methylene signals coalesced in acetone at 42°C and W^{*} was measured as 33 Hz. In acetone solution, the values of ΔH and ΔS for the cis → trans isomerization are 15.7 kJ/mole and 51.3 J/K mole. Therefore the equilibrium constant is given by

$$K_{eq} = e^{[-1893(1/T) + 6.17]}$$

Therefore at 42°C, $K_{eq} = 1.17$

$$p_{cis} = \frac{1}{K_{eq} + 1} = 0.46$$

$$p_{trans} = 1 - \frac{1}{K_{eq} + 1} = 0.54$$

$$\Delta p = 0.08$$

From the work of Egan and Mislow,[119] for $\Delta p = 0.08$

$$X = 1.6684$$

It is now possible to calculate the rate constants, k_{trans} and k_{cis} where k_{trans} refers to the trans → cis direction and k_{cis} refers to cis → trans direction

$$\text{cis} \underset{k_{trans}}{\overset{k_{cis}}{\rightleftharpoons}} \text{trans}$$

$k_{trans} = P_{cis}\, 2\pi W^*/X$ $\qquad$ $k_{cis} = p_{trans}\, 2\pi W^*/X$

$= \frac{(0.46)(2\pi)(33)}{(1.6684)\ sec^{-1}}$ $\qquad$ $= \frac{(0.54)(2\pi)(33)}{(1.6684) sec^{-1}}$

$= 57.2\ sec^{-1}$ $\qquad$ $= 67.1\ sec^{-1}$

The activation is then readily calculated

$$\Delta G^* = (1.914 \times 10^{-2})\, T(10.319 + \log_{10} k)$$

$\Delta G^*_{trans} = 66.7$ kJ $\qquad$ $\Delta G^*_{cis} = 66.3$ kJ

The most obvious source of error in such determinations involves the measurement of the temperature. Allowing for an error of ±2°C in measurement of temperature, then the final values are:

$k_{trans} = 57 \pm 3\ sec^{-1}$ $\qquad$ $k_{cis} = 67.1 \pm 0.5\ sec^{-1}$

$\Delta G^* = 66.7 \pm .6$ kJ $\qquad$ $\Delta G^*_{cis} = 66.3 \pm .5$ kJ

There are a number of possible mechanism for cis-trans isomerization in square-planar complexes. In the case of platinum(II) complexes, a catalyst such as excess ligand is required, suggesting that the mechanism is an intermolecular one involving a trigonal-bipyramidal intermediate.[120] Alternatively, an intramolecular rearrangement through a tetrahedral intermediate is

possible for complexes of metals such as Ni(II) which are known to form stable tetrahedral complexes. A third possibility involves an S_N1 process with a symmetrical trigonal planar intermediate.

The rate law for the isomerization was found to be first-order in $[Ni(L^1)_2]$ and independent of $[HL^1]$. This suggests an intramolecular mechanism rather than the intermolecular mechanism of square-planar Pt(II) complexes. The mechanism then involves either a twisting motion through a tetrahedral intermediate, or dissociation of one end of the bidentate ligand and a trigonal planar intermediate. This is consistent with results of kinetic studies on the bischelate hybrid ligand complex, 6-1, where the cis-trans isomerization was found to occur by an intramolecular process.[111]

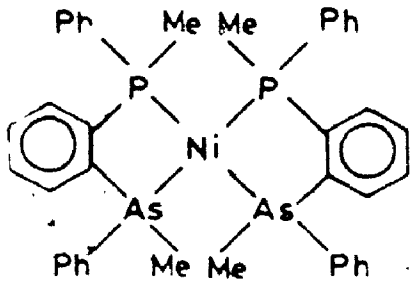

6-1

Both tetrahedral and square-planar Ni(II) phosphine complexes are known while some exist as an equilibrium distribution between the two geometries. For example, for complexes of the type, $[NiL_2X_2]$, when L is a triaryl-phosphine the complexes are tetrahedral, when L is a trialkylphosphine the complexes tend to be square-planar,

while when L is a mixed alkylarylphosphine, an equilibrium mixture often results. La Mar and Sherman[100] studied the kinetics of the tetrahedral-square-planar isomerization of a number of complexes of the type $[Ni(PPh_2R)_2X_2]$. They found that while the two geometries are very close in energy, the activation energies, ΔG^*, for the isomerization are in the range 35-45 kJ/mole. Allowing for the additional ring strain involved with the twisting of a bischelate complex, these values are not inconsistent with those determined for $[Ni(L^1)_2]$.

We therefore propose that the mechanism of cis-trans isomerization for $[Ni(L^1)_2]$ is an intramolecular twisting mechanism, through a tetrahedral intermediate. The maximum in the reaction profile lies at a configuration intermediate between tetrahedral and square-planar. The reaction profile is illustrated for the isomerization in acetone at 42°C in Fig. 6.5.

6.2.5 Virtual Coupling

Although the two ^{31}P nuclei in each of the two geometrical isomers in solution are chemically equivalent, they are not magnetically equivalent. Therefore one would expect the methylene signals in the ^1H NMR and the CF_3 signals in the ^{19}F NMR in each compound to exhibit inequivalent couplings to the two phosphorus nuclei. However for both cis and trans isomers of $[Ni(L^1)_2]$, the methylene proton and CF_3 ^{19}F resonances each appear as

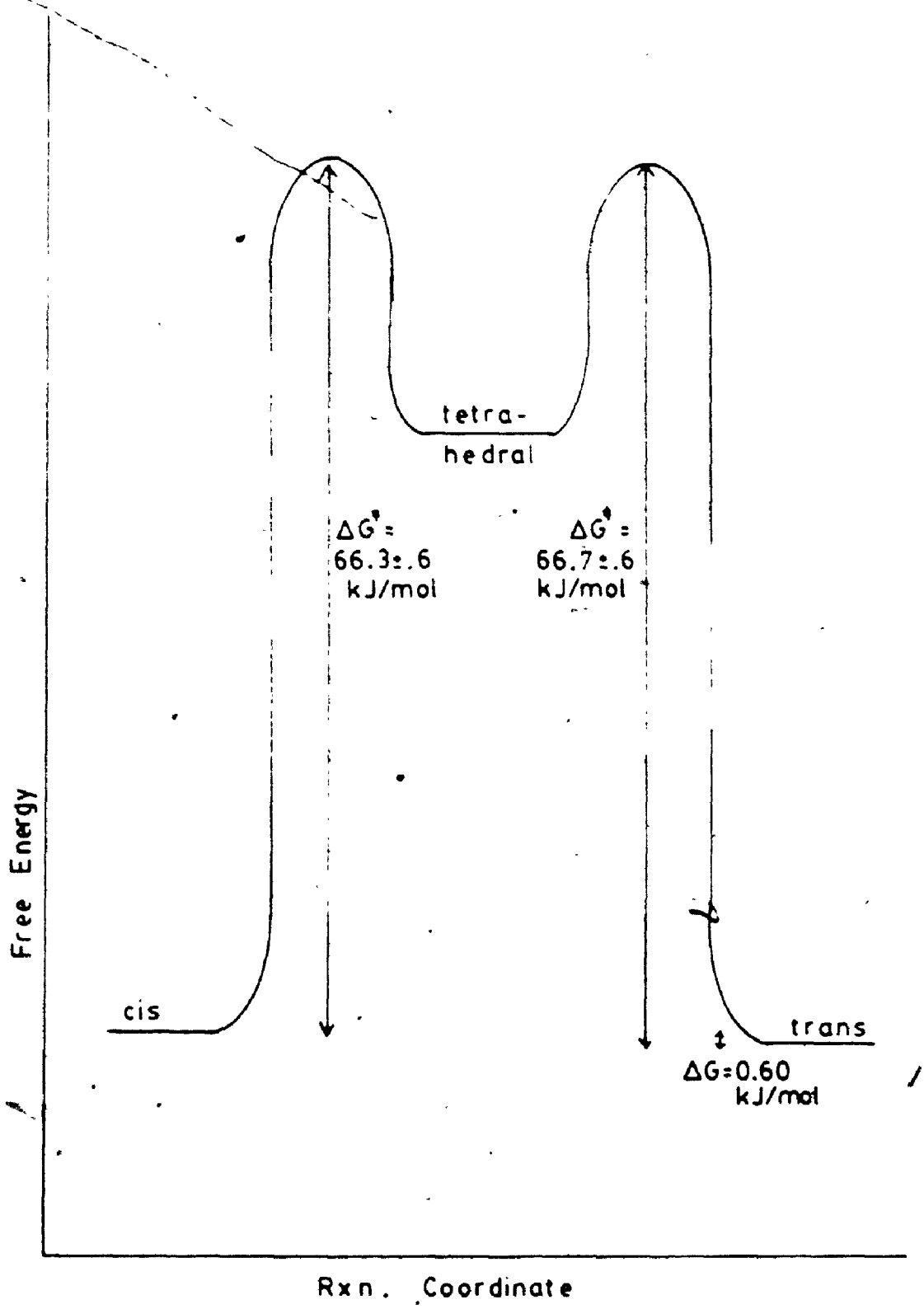

Figure 6.5 Reaction profile for isomerization of $[Ni(L^1)_2]$ (in acetone at 42°C)

triplets.

This phenomenon, called virtual coupling, is well-known, and is often observed for bisphosphine metal complexes.[121] Most often the phosphines in complexes which exhibit virtual coupling are trans; in fact for some time the existence of virtual coupling was used as evidence of trans geometry.

A theoretical consideration of the phenomenon of virtual coupling is included in the examination by Harris[122] of the X spectrum for an $X_nAA'X'_n$ nuclear magnetic system. It was found that the general description of the X spectrum consists of (2n+1) pairs of lines symmetrically placed about ν_X, with half of the total intensity lying in a doublet of separation N where $N = |J(A,X) + J(A,X')|$. The line positions and intensities of the remaining 2n pairs of lines are dependent only on the ratio $L/|J(A,A')|$ where $L = |J(A,X) - J(A,X')|$. Fig. 6.6 illustrates how the spectral appearance changes with $L/|J(A,A')|$.

One limiting case which simplifies the spectrum considerably occurs when $L/|J(A,A')|$ approaches zero. When this happens, it is as if L is approaching zero and the two A nuclei are approaching magnetic equivalence. The spectrum therefore has the appearance of a 1:2:1 triplet with the central peak falling on ν_X. If the separation of the first inner doublet is less than the effective resolution of the instrument, that is, the width at half

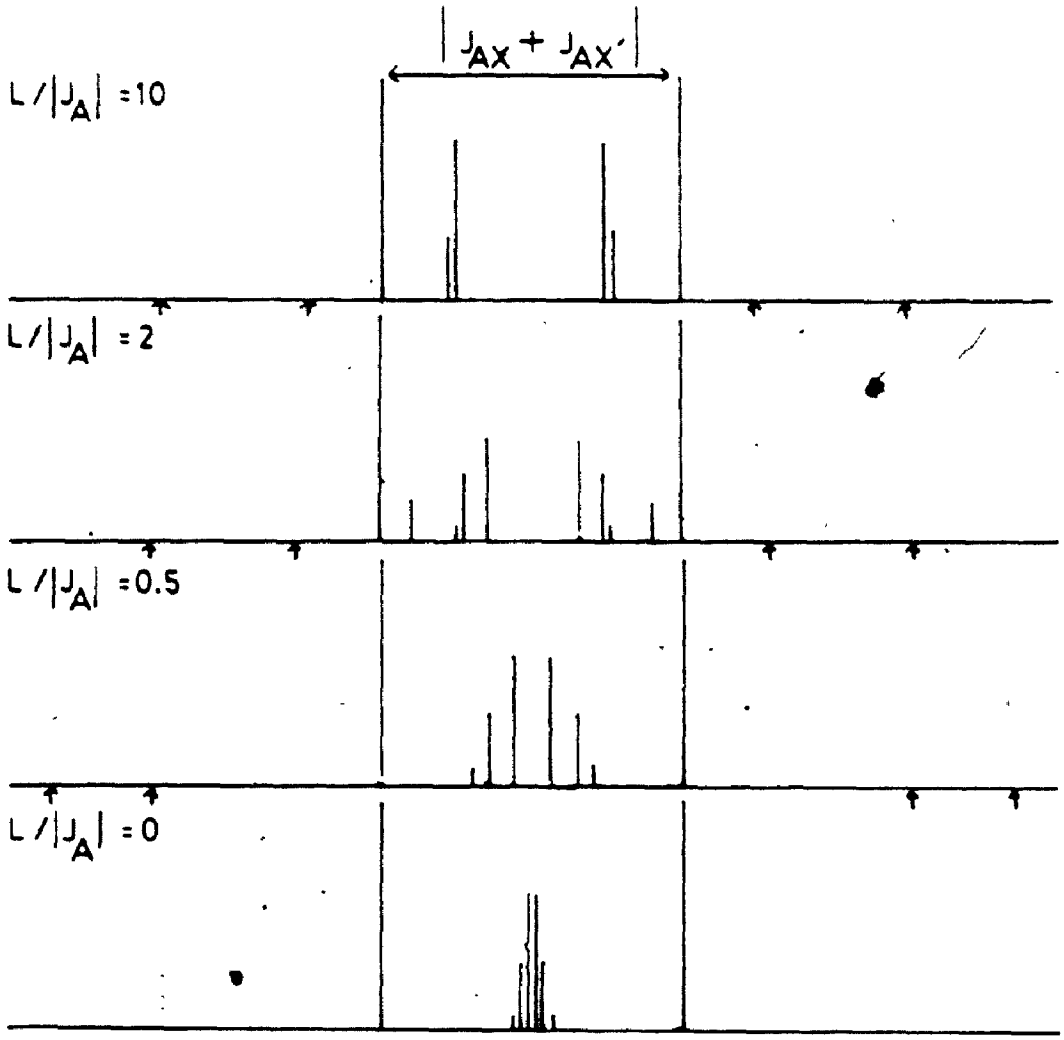

Figure 6.6 X spectra of an $X_n AA'X'_n$ spin system with changing $L/|J_A|$ (from ref. 122)

$|J_A| = |J_{AA'}|$

↑ outer lines of negligible intensity

height of a single peak, $\Delta\nu_{\frac{1}{2}}$, then the triplet will appear as a singlet. Therefore the condition for appearance of a virtual triplet is

$$L^2 < 2|J(A,A')|\Delta\nu_{\frac{1}{2}}$$

A virtual triplet can be distinguished from a true triplet where the A nuclei are actually magnetically equivalent; in a virtual triplet, the central line should be broader than the other two, and less than fully twice the height of the other two.

The only information that can be drawn from these spectra is the value of N from the separation of the two outer peaks of the triplet and from the width of middle line, the upper limit for $L^2/J(A,A')$. Although it was difficult, because of resolution limitations, to measure accurately the peak widths for some of the triplets, it is known that:

$|J(P,P) + (J(P',P)|$ = 3.2 Hz for the cis isomer

$|J(P,P) + (J(P',P)|$ = 5.2 Hz for the trans isomer

$|J(H,P) + (J(H',P)|$ = 13.0 Hz for the cis isomer

$|J(H,P) + (J(H',P)|$ = 11.4 Hz for the trans isomer

Therefore virtual coupling is <u>not</u> a result of a particular geometrical isomer, but rather the value of $^2J(P,P')$. Values of $^2J(P,P')$ in complexes containing chemically equivalent phosphines can be calculated using double resonance techniques, through computer simulation, or by using high radio-frequency power to observe the weak

outer lines described by Harris. Ogilvie, Jenkins and Verkade[123] reported $^2J(P,P')$ values for a number of complexes. Since nuclear spin-spin coupling is transmitted by electrons and electronic effects are stronger between two trans ligands than two cis ligands, one would expect the coupling constants to be greater in the trans isomers. This has generally been found to be true. Likewise, Palmer and Whitcomb[114] estimated $^2J(P,P')$ values for dicyclohexylphosphine complexes of NiX_2 as ~65 Hz for cis and ~380 Hz for trans isomers.

However, Ogilvie et al[123] caution against assigning the stereochemistry of a complex based on the appearance or nonappearance of a virtual triplet, as many cis complexes have large $^2J(P,P')$ values. In addition, a virtual triplet may appear for a complex with a small $^2J(P,P')$ value provided J(A,X) is likewise very small. Indeed, cis virtual coupling has been verified experimentally,[124-126].

Wade and Sameshima[127] reported the NMR spectra for a variety of compound $NiRR'(PR''_3)_2$ where R,R' are aromatic or vinylic ligands. The methyl proton signals in the PMe_3 complexes appear as triplets with apparent $^2J(P,H)$ values of 7-8 Hz, and as a result these complexes were assigned a trans configuration. While this assignment is likely correct, it must again be emphasized that virtual triplets are not necessarily indicative of a trans geometry.

For $[Ni(L^1)_2]$, virtual coupling is observed for the ^{19}F and methylene ^1H resonances for both cis and trans

isomers. In order to confirm virtual coupling in cis-phosphine complexes of Ni(II), the ^1H NMR spectrum of the analogous known compound $[Ni(PFP)(PMePh_2)_2]$[10] was re-examined. This unambiguously cis-complex shows a virtual triplet for the methyl proton and for the carbon-13 resonances, with apparent coupling constants of 5.5 Hz and 13.6 Hz respectively. Virtual coupling was not observed for $[Pt(L^1)_2]$ or $[Pd(L^1)_2]$ because these complexes are both cis in geometry and have much lower values of $^2J(P,P')$ as a result. This is commonly found for phosphine complexes of platinum(II) and palladium(II); for example the $^2J(P,P)$ values for cis- and trans-$[Pd(PMe_3)_2Cl_2]$ are -8.0 and +610 Hz respectively.[185] The occurrence of virtual coupling in cis Ni(II) complexes has not been reported previously, presumably because of the scarcity of such complexes.

6.3 Solid State Studies on $[Ni(L^1)_2]$

6.3.1 Introduction

The solution studies indicated that both cis- and trans-square-planar isomers of $[Ni(L^1)_2]$ are present in solution in a temperature- and solvent-dependent equilibrium. Both the visible spectra and the multinuclear NMR studies are consistent with this. In solution, both cis- and trans-isomers have the same orange colour with λ_{max} = 430 nm. However the crystals obtained from an acetone solution were green, changing progressively and reversibly to orange on heating to 200°C, while cooling to

77K produced an intensification of the green colour. A diffuse reflectance spectrum of the solid at room temperature showed the peak at 430 nm still present, but an additional absorption appeared at 600 nm. By evaporation from ethanol, a metastable orange form of the complex was obtained which slowly reverted to the green form at room temperature. As a result, attempts to isolate single orange crystals were unsuccessful.

Most square-planar Ni(II) complexes are yellow, red, brown or orange (as $[Ni(L^1)_2]$ is in solution) although some green and purple examples are known. While examples of green, diamagnetic Ni(II) complexes are known,[107,128-131] the observation that the complex changes colour on crystallization from an orange solution suggests that the green colour must be associated with a specific solid-state interaction. A blue, green or purple colour is generally associated with an octahedral or tetrahedral geometry for Ni(II) complexes. There are, therefore, a number of possibilities, consistent with the known chemical behaviour of Ni(II) complexes, which could result in such a colour change. One such possibility is the formation of a six-coordinate complex in the solid-state by solvation, but this possibility may be ruled out on the basis of the analytical data. There remain two further possibilities: a tetrahedral distortion of the coordination plane, or an increase in the coordination number of the nickel through either intra- or intermolecular association. However in

either case the interaction must be a weak one since the solid is diamagnetic.

Therefore an x-ray crystallographic structure determination was undertaken to:

a) correlate the solid-state structure with the solution behaviour of $[Ni(L^1)_2]$ as well as the structural preferences of $[Pd(L^1)_2]$ and $[Pt(L^1)_2]$,

b) determine whether an interaction such as those mentioned is responsible for the colour change on crystallization.

6.3.2 Experimental

Slow evaporation of a solution of $[Ni(L^1)_2]$ in acetone yielded the dark green crystals which were filtered off and air-dried. A single crystal was chosen for photographic analysis. Preliminary photography was undertaken and precession photographs of the 0kl, 1kl, hk0 and hk1 layers along with Weissenberg photographs of the h0l and h1l layers were obtained. The photography showed that the crystal was orthorhombic with Laue symmetry mmm.

The systematic absences observed were h00 when h is odd, 0k0 when k is odd and 00l when l is odd. From these systematic absences, the space group was therefore uniquely determined to be $P2_12_12_1$ - D^4_2 No. 19[132] (see Table 6.7). This is an acentric space group.

Preliminary measurements of the unit cell dimensions were also obtained. Then by measuring the crystal density

Table 6.7 Systematic Absences for $Ni(L^1)_2$ Structure

Class of Reflection	Condition for Non-extinction	Interpretation	Symbol
hOO	h = 2n	[100] screw axis, component a/2	2_1
OkO	k = 2n	[010] screw axis, component b/2	2_1
OOℓ	ℓ = 2n	[001] screw axis, component c/2	2_1

using the method of neutral buoyancy in cyclohexane/dibromoethane, it was found that Z = 8. The space group $P2_12_12_1$ has a maximum of four symmetry-related positions. Therefore there are two formula weights per equivalent position in this crystal structure; each unit cell contains equal numbers of two crystallographically inequivalent $[Ni(L^1)_2]$ molecules.

Another single crystal was chosen for data collection, having 20 faces with the longest dimension being approximately 0.532 mm along the a^* axis. Perpendicular to this direction, the crystal measured approximately 0.405 mm in the b^* direction and 0.422 mm in the c^* direction. The data crystal is illustrated as an ORTEP plot in Fig. 6.7.

The crystal was mounted on an Enraf Nonius/CAD-4F computer-controlled four-circle diffractometer. A polaroid rotation photograph was obtained and from it 21 intense reflections were chosen and centred. A least-squares indexing and fitting procedure of these 21 intense reflections with $26.92 < 2\theta < 32.03$ provided the lattice constants and cell volume. The cell constants were in reasonable agreement with those obtained by measuring the photographs. For the new constants, with Z = 8, the calculated density would be 1.587 g/cm^3 compared with an observed density of 1.59(1) g/cm^3.

Crystal data and conditions for data collection are summarized in Table 6.8.

It is noteworthy that CuKα radiation was used in the

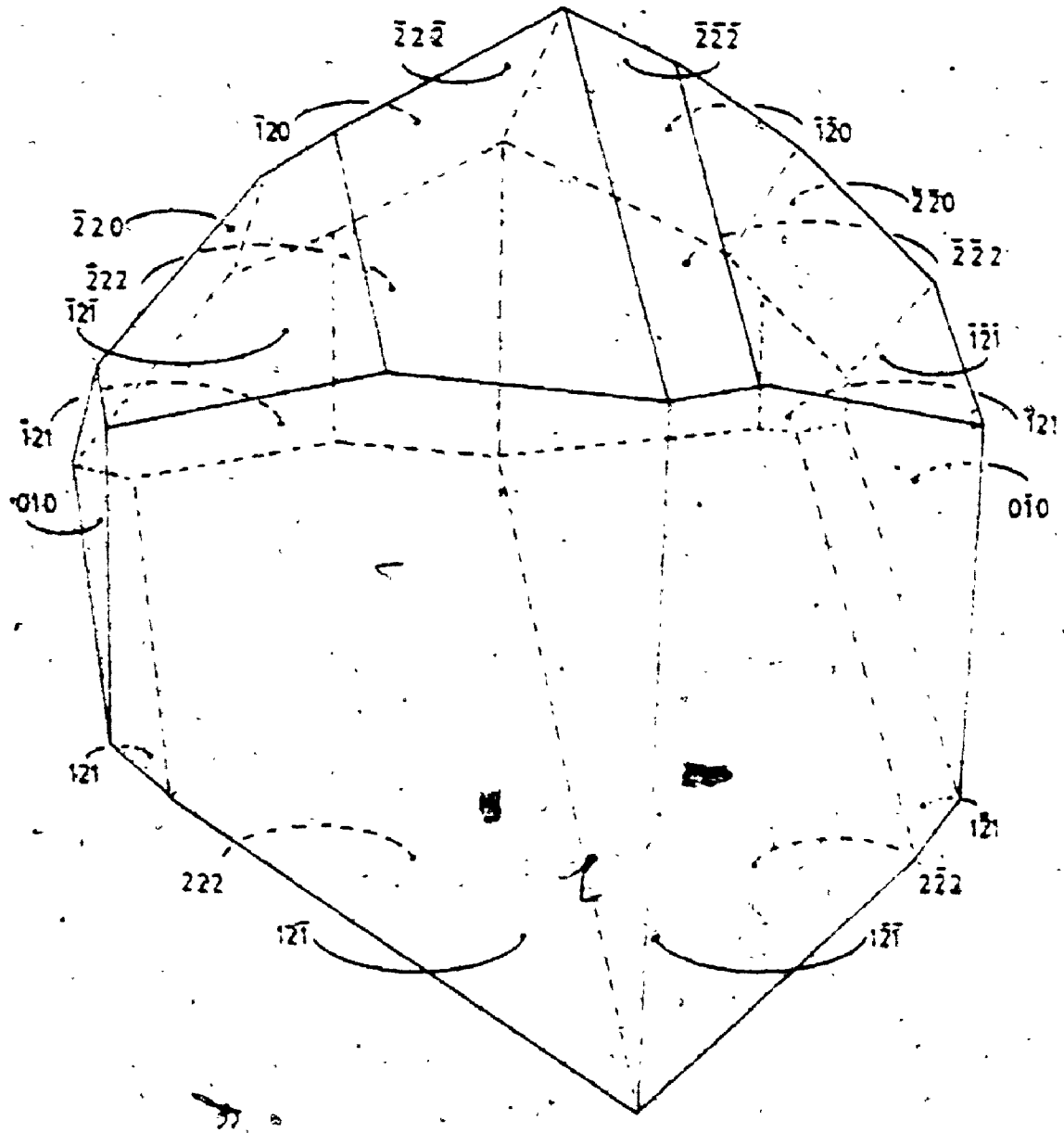

Figure 5.7 Drawing of data crystal for $[Ni(L^1)_2]$

Table 6.8

Summary of Crystal and Data Collection Parameters

Molecular formula	$C_{32}H_{24}F_{12}NiO_2P_2$
Formula weight	789.18
Crystal class	orthorhombic
a	18.145(2) Å
b	33.269(3)
c	10.945(1)
V	6607(2) $Å^3$
Z	8
d(obs)[a]	1.59(1) g cm^{-3}
d(calc)	1.587
Systematic absences:	$h00$: $h \neq 2n$
	$0k0$: $k \neq 2n$
	$00l$: $l \neq 2n$
Space group	$P2_12_12_1$
Diffractometer	Enraf-Nonius CAD4F
Temperature	22°
Radiation	CuKα, λ = 1.54185 Å
Filter	Ni prefilter, 0.015 mm
Aperture	4 mm + (4 × 0.15tanθ) mm
Exposure time	152 h
Data collected	$0 \leq h \leq 22$, $0 \leq k \leq 40$, $0 \leq l \leq 13$
θ Range	$0.50 \leq 2\theta \leq 70°$
Scan type	ω/2θ, at 0.9 - 4.0 deg min^{-1}
Scan width	0.65 + 0.15tanθ

Table 6.8 (continued)

Backgrounds	25% above and below calculated scan width
Standard reflections	6,0,0 0,12,0 0,0,2
Loss in intensity	0.01 % per hour, 1.6% overall.
Crystal dimensions	0.41 x 0.53 x 0.42 mm
Crystal Volume	0.02960 mm^3
μ (CuK_α)	26.67 cm^{-1}
Absorption correction	Gaussian, ACNOST
Range trans. coeff.	0.457 - 0.580
Crystal faces[a]	(010), ($\bar{1}21$), ($\bar{1}\bar{2}1$)
	(222), ($2\bar{2}2$), ($\bar{2}2\bar{2}$), ($\bar{2}\bar{2}\bar{2}$), ($2\bar{2}\bar{2}$), ($\bar{2}22$)
	($\bar{2}\bar{2}0$), ($\bar{2}20$), ($\bar{1}\bar{2}0$), ($\bar{1}20$)
Reflections collected	6942
No. unique data in final cycle	5922
Sigma	$I_o > 3\sigma(I_o)$
Variables, final cycle	407
Final R_1[b]	0.0716
Final weighted R_2[c]	0.0720

[a] by neutral buoyancy in cyclohexane/$C_2H_4Br_2$

[b] $R_1 = \Sigma||F_o| - |F_c||/\Sigma|F_o|$

[c] $R_2 = (\Sigma w(|F_o| - |F_c|)^2/\Sigma wF_o^2)^{1/2}$

data collection. Nickel nuclei strongly absorb CuKβ radiation. Therefore the radiation was Ni prefiltered. The longer wavelength of Cu radiation allows for better resolution of the reflections and thus prevents errors in intensity counting due to overlapped data.

The CAD-4F intensity data were processed by the program START of the Structure Determination Package,[133] in order to correct for background counts, scan time and attenuation. In this way the total count is reduced to a raw intensity value.

The data were then corrected for the Lorentz effect and polarization according to the formula, $F_{obs} = \sqrt{I_{raw}/L_p}$. The processed data file contained 6942 reflections.

The reduction in intensity of the three standard reflection was minimal; the average percentage slope per hour was -0.01%. As a result, no correction was made for decay.

The data collected were in the range $0 \leq h \leq 22$, $0 \leq k \leq 40$, $0 \leq l \leq 13$. As a result, there were no symmetry-related data and thus no estimate of agreement between such data was obtained.

The data crystal was examined under a microscope fitted with a filar eyepiece, after the data collection, in order to determine the crystal dimensions. The faces were indexed by optical goniometry, matching ρ and ϕ values observed for each face with those predicted by the SDP program CRYSTL. There were twenty faces, indexed as (010),

(1̄21), (222), (2̄2̄2), (2̄22̄), (2̄2̄2̄), (2̄22), (22̄2), (2̄2̄0), (2̄20), (1̄2̄0) and (1̄20). Included in these are the four faces adjacent to the point of mounting which were assigned as (1̄2̄0), (1̄20), (2̄22̄) and (1̄21̄). This description of the crystal was used to perform a differential absorption correction. This correlation was carried out by Gaussian numerical methods using the program AGNOST.[134] All 6942 reflections were corrected.

6.3.3 Structure Determination and Refinement

The initial stages of structure determination and refinement were carried out using a set of 5564 reflections for which $F^2 > (5\sigma)F^2$. The positions for the two nickel atoms (remembering that there are 8 formula weights per unit cell in space group $P2_12_12_1$) were determined from a three-dimensional Patterson syntheses.[133]

The Patterson vectors for the space group $P2_12_12_1$ were calculated and peaks 5, 7 and 9 appeared to correspond to three of these vectors. One nickel position was therefore calculated as (0.097, 0.125, 0.032).

Peak 3 in the Patterson peak listing was judged to represent an intermolecular Ni-Ni vector because of its high relative intensity and length (10.26Å). This peak, being still unaccounted for, was assumed to represent the vector between the independent molecules and was added to the coordinates of Ni(1) to generate another set of coordinates (0.597, 0.125, 0.468) for Ni(2).

The program PATTER calculates the expected Patterson peaks given atomic coordinates and symmetry elements. When these two calculated sets of coordinates for Ni(1) and Ni(2) were used, the program generated peaks 2, 3, 4, 5, 7, 9 and 22. It therefore seemed likely that these were the correct coordinates for the two nickel atoms.

However, the most intense Patterson peak, peak 1, was still unaccounted for. This vector was 2.08Å long, clearly too short for a Ni-Ni vector. Such a distance would be not unreasonable for a Ni-P bond length and a Ni-P vector would be expected to be so intense only if the phosphorus atoms were trans to each other in the compound. In such a geometry, the two Ni-P vectors would be summed.

A least-squares refinement of the two nickel positions, followed by a difference Fourier synthesis, supported this idea. Peaks appeared in the difference Fourier having the same coordinates as those one would obtain by adding and subtracting Patterson vector 1 from both Ni(1) and ~~Ni(2)~~ coordinates.

However when one continued with this possible solution, running another cycle of least-squares refinement followed by a difference Fourier synthesis, using the two nickel positions and four phosphorus positions derived from the Patterson synthesis, there were no further reasonable positions generated for oxygen or carbon atoms. Apparently this solution was only partially correct.

It was thought that the structure might not be easily

solved by the heavy atom method since the molecular weight is 789.2 while the heaviest atom is nickel and the second heaviest atom is phosphorus. The ratio of the number of electrons in a nickel atom to the number in a phosphorus atom is only 28/15. As a result, the nickel atoms may not be heavy enough relative to the entire compound to determine enough phases so that a Fourier map will reveal the positions of the lighter elements.

Therefore an attempt was made to solve the structure by direct methods. A system of computer programs called MULTAN[133] was used. Not surprisingly, the possible solutions produced by MULTAN all contained, among the most intense peaks, the two nickel and four phosphorus atomic positions generated by the heavy atom method. It therefore became apparent that the relationship between the nickel atom coordinates was leading to pseudo-symmetry, a condition that was to be broken only through trial and error.

Patterson peak 6, like peak 1, was unaccounted for by the two nickel atom positions. The length of this vector (2.19Å) suggested it might be a Ni-P vector as well. Therefore by adding and substracting Patterson peaks 1 and 6 from the two nickel positions, it was possible to generate four positions around each nickel. There were therefore 36 possible dispositions of the four phosphorus atoms around the two nickel atoms. This number could be decreased to 16 by assuming that the bite angle of the

bidentate ligand would be less than 90°.

A least-squares refinement and a difference Fourier synthesis were calculated for each of the 16 possible orientations of the four phosphorus atoms. Only one difference Fourier generated reasonable positions for the four oxygen atoms. This solution also had a slightly lower residual factor than any of the others after the least-squares refinement.

Thereafter the structure determination proceeded using this solution. The remaining 92 non-hydrogen atoms were located and slowly added after six cycles of least-squares refinement and difference Fourier syntheses.[133] Also, starting with the heaviest atoms, the thermal positions were slowly added to vary, first as isotropic, then as anisotropic thermal parameters.

Having found all 98 non-hydrogen atoms using the SDP on the PDP 11/23+ computer, it was necessary to refine the structure on the CYBER computer because of the large number of variables. This could be reduced somewhat by using the rigid group refinement techniques. The final cycle would involve 407 variables while the maximum number of variables in any one cycle was 435 (in cycles 7-11). The number of variables is limited by the size of the matrix. The size of the matrix is given by (NV)(NV-1)/2 where NV is the number of variables.

The refinement[134] proceeded using the full-matrix least-squares techniques on F, minimizing the function

$\Sigma w(|F_o|-|F_c|)^2$ where $|F_o|$ and $|F_c|$ are the observed and calculated structure factor amplitudes respectively. The weighting factor 'w' is given by $w = 4F_o^2/\sigma^2(F_o^2)$.

The atomic scattering factors for the non-hydrogen atoms were those of Cromer and Waber,[135] while those for the hydrogen atoms were taken from Stewart, Davidson and Simpson.[136] The $\Delta f'$ and $\Delta f''$ components of anomalous dispersion were those of Cromer and Liberman[137] and were included for the nickel, phosphorus, oxygen and fluorine atoms.

The eight phenyl rings in the structure were refined as eight idealized rigid groups (D_{6h} symmetry; C-C = 1.392Å).

The first cycle of refinement on the CDC CYBER 835 computer refined the scale factor only. For cycles 2 and 3, the thermal parameters of all non-group atoms were allowed to vary along with a single group thermal parameter for each phenyl ring.

For cycles 4 and 5, the anisotropic thermal parameters of the two nickel atoms and the four phosphorus atoms were allowed to vary. Also the phenyl ring group thermal parameters were fixed at those refined values from the cycle 3 output, and the thermal parameters of the individual atoms were initially set at zero and allowed to vary. The value of the thermal parameter for the individual carbon atom in a phenyl ring would then be equal to the fixed group thermal parameter plus the individual refined parameter.

Because of the potentially large number of variables, and restrictions in matrix size due to limitations in core, when the fluorine atom anisotropic thermal parameters were allowed to vary in cycle 6, the phosphorus anisotropic thermal parameters were fixed. Subsequently, in cycle 7 and 8, the nickel β values were fixed while the phosphorus and fluorine anisotropic thermal parameters were allowed to vary.

At this point in the refinement, a difference Fourier synthesis, using all 98 non-hydrogen atoms, was calculated. All 48 hydrogen atoms were located in the Fourier synthesis at densities ranging from 0.12(9) to 0.56(9) e A^{-3}. Subsequent cycles of least-squares refinement included the hydrogens with idealized geometry assumed.

The largest peak in this final difference Fourier appeared at the coordinates (0.3997, -0.1332, 0.6990) and had a density of 0.59(9) e A^{-3}. This peak is associated with O(2) and has no chemical significance.

Before cycle 9, the contribution of the hydrogen atoms (assumed to be in idealized positions) to the calculated intensities was first calculated and stored on tape. Then in cycles 9,10 and 11, the nickel anisotropic thermal parameters were again fixed while the phosphorus, and fluorine anisotropic thermal parameters were allowed to vary. The hydrogen atom contribution was recalled and added to the non-hydrogen contribution so that the residual

value now included contributions from all atoms in the asymmetric unit.

In cycle 12, the individual atomic B's for those carbons in the phenyl rings were fixed at the values from the output of cycle 11 and the overall group thermal parameters were once again allowed to vary. By doing so, the number of variables was decreased by five for each phenyl ring, a total of 40. This made it possible to vary the anisotropic thermal parameters of the nickel atoms.

Because the compound crystallized in the acentric space group $P2_12_12_1$, it was necessary to refine the inverse model as it was possible that either "handed" model might be correct one. Therefore, after cycle 12, the "handedness" of the structure was checked by temporarily relabelling reflections hkl as $\bar{h}\bar{k}\bar{l}$ with the sign of ΔF" unchanged. The input for this cycle (cycle 12-inverse) was the same as for the preceeding cycle 12, only omitting the hydrogen atom contribution. A second cycle was then run (cycle 13-inverse) again relabelling reflections hkl to $\bar{h}\bar{k}\bar{l}$ and using the refined values from cycle 12-inverse as input. For this cycle, the hydrogen atom contribution was calculated and included.

The weighted R-factor after this cycle had increased to 0.0884 from 0.0720 after cycle 12. In addition, some of the bond lengths had become less reasonable. For example, the C(2)-C(10) and C(4)-C(12) bonds in molecule 1, had increased from 1.52 Å and 1.54Å respectively to 1.59Å.

Also the C-F bonds, C(14)-F(18) and C(9)-F(3) changed from 1.33 Å and 1.31 Å respectively to 1.38 Å and 1.28 Å. Therefore, the first model was chosen as the correct one.

A final cycle was run using the original model with nickel, phosphorus and fluorine anisotropic thermal parameters being varied along with a single group thermal parameter for each of the phenyl groups. The model converged and final R- and weighted R-factors of 0.0716 and 0.0720 respectively were obtained. The largest shift in the final cycle was 0.272 esd for the y group positional parameter of phenyl group 5. No shift for a non-group atom (other than fluorine) was greater than 0.100. The final positional and thermal parameters are given in Appendix.

Using the program, RANGER,[134] a statistical analysis of R-factors in terms of $|F_o|$, $\lambda^{-1}\sin\theta$, Miller indices and diffractometer setting angle χ, was done after cycle 12 and showed no unusual trends. Therefore no data were dropped and no secondary extinction correction was applied.

6.3.4 Structure Description

The final positional and thermal parameters are listed in Appendix 2 while the anisotropic thermal parameters and rigid group parameters are given in Appendices 3 and 5 respectively. Appendix 4 contains the hydrogen atom positional and thermal parameters while Table 6.9 contains various selected final bond lengths and bond angles with errors assigned. ORTEP drawings of the two

molecules appear in Fig. 6.8 and Fig. 6.9 while a stereoview of the unit cell appears in Fig. 6.10.

The following line diagrams show the numbering scheme used in each molecule

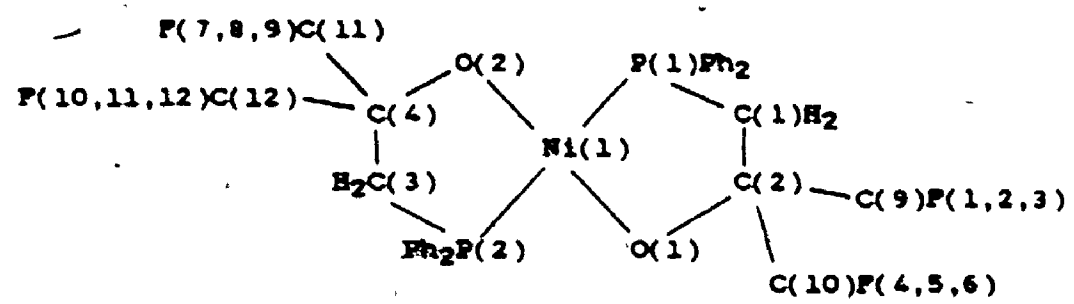

Molecule 1. Phenyl C atoms 21-26 and 31-36 are attached to P(1); phenyl C atoms 41-46 and 51-56 to P(2)

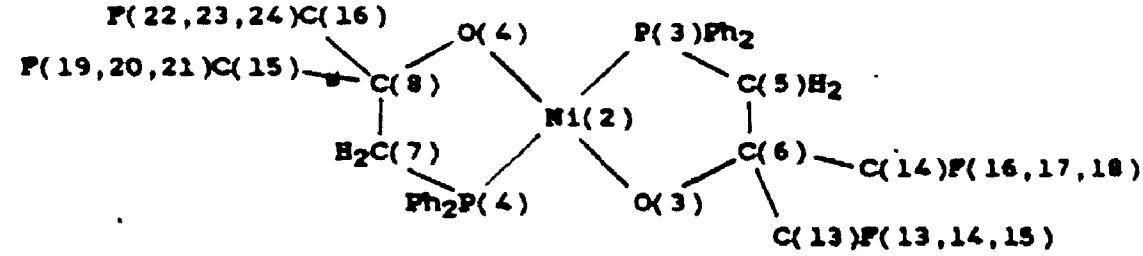

Molecule 2. Phenyl C atoms 61-66 and 71-76 are attached to P(3); phenyl C atoms 81-86 and 91-96 to P(4)

As best as can be determined, this is the first structure of a nickel compound with a P_2O_2 donor set. In the case of both molecules in this structure, the coordination geometry around the nickel atom is trans-square-planar. For each, the weighted least-squares plane through the nickel, two phosphorus and two oxygen atoms was calculated (these appear in Table 6.10). In both molecules, the average deviation from the least-squares

Table 6.9. Selected Intramolecular Dimensions

Molecule 1.		Molecule 2.	
Bond Lengths, Å			
Ni(1)–P(1)	2.195(2)	Ni(2)–P(3)	2.192(2)
Ni(1)–P(2)	2.183(2)	Ni(2)–P(4)	2.202(2)
Ni(1)–O(2)	1.838(7)	Ni(2)–O(3)	1.839(7)
Ni(1)–O(2)	1.844(7)	Ni(2)–O(4)	1.837(6)
P(1)–C(1)	1.82(1)	P(3)–C(5)	1.83(1)
P(1)–C(21)	1.813(6)	P(3)–C(61)	1.789(7)
P(1)–C(31)	1.797(7)	P(3)–C(71)	1.790(7)
P(2)–C(3)	1.85(1)	P(4)–C(7)	1.818(9)
P(2)–C(41)	1.789(7)	P(4)–C(81)	1.817(7)
P(2)–C(51)	1.807(7)	P(4)–C(91)	1.805(7)
O(1)–C(2)	1.37(1)	O(3)–C(6)	1.39(1)
O(2)–C(4)	1.37(1)	O(4)–C(8)	1.37(1)
C(1)–C(2)	1.55(1)	C(5)–C(6)	1.56(1)
C(3)–C(4)	1.55(1)	C(7)–C(8)	1.58(1)
C(2)–C(9)	1.54(1)	C(6)–C(13)	1.54(1)
C(2)–C(10)	1.52(1)	C(6)–C(14)	1.51(1)
C(4)–C(11)	1.52(1)	C(8)–C(15)	1.53(1)
C(4)–C(12)	1.55(1)	C(8)–C(16)	1.55(1)

C–P bond lengths were in the range 1.22(1) to 1.37(1) Å

Table 6.9 (continued)

Bond angles, Deg

P(1)–Ni(1)–O(1)	86.6(2)	P(3)–Ni(2)–O(3)	87.5(4)
P(2)–Ni(1)–O(2)	87.1(2)	P(4)–Ni(2)–O(4)	87.9(2)
Ni(1)–P(1)–C(1)	100.5(3)	Ni(2)–P(3)–C(5)	101.5(3)
Ni(1)–P(2)–C(3)	101.2(3)	Ni(2)–P(4)–C(7)	99.4(3)
Ni(1)–O(1)–C(2)	121.1(6)	Ni(2)–O(3)–C(6)	123.9(6)
Ni(1)–O(2)–C(4)	122.1(6)	Ni(2)–O(4)–C(8)	122.4(6)
C(1)–C(2)–O(1)	112.6(8)	C(5)–C(6)–O(3)	114.5(8)
C(3)–C(4)–O(2)	114.7(8)	C(7)–C(8)–O(4)	115.9(8)
P(1)–C(1)–C(2)	107.6(7)	P(3)–C(5)–C(6)	107.8(6)
P(2)–C(3)–C(4)	107.4(7)	P(4)–C(7)–C(8)	108.8(6)

C–C–P bond angles were in the range 105(1) to 116(1); P–C–P 103(1) to 112(1).

Table 6.10. Weighted Least-Square Planes for $[Ni(L^1)_2]$

Molecule 1		Molecule 2	
6.04x + 29.93y + 3.09z + 4.52 = 0		15.30x - 1.47y + 5.86z + 11.64 = 0	
Atom	Distance, Å	Atom	Distance, Å
Ni(1)	0.017(1)	Ni(2)	-0.009(1)
P(1)	-0.029(2)	P(3)	0.020(2)
P(2)	-0.031(2)	P(4)	0.019(2)
O(1)	0.040(6)	O(3)	-0.063(6)
O(2)	0.038(6)	O(4)	-0.075(6)
Av. Deviation	0.031	Av. Deviation	0.037
C(1)	0.17	C(5)	-0.09
C(2)	0.56	C(6)	0.18
C(3)	-0.22	C(7)	-0.26
C(4)	-0.44	C(8)	0.06

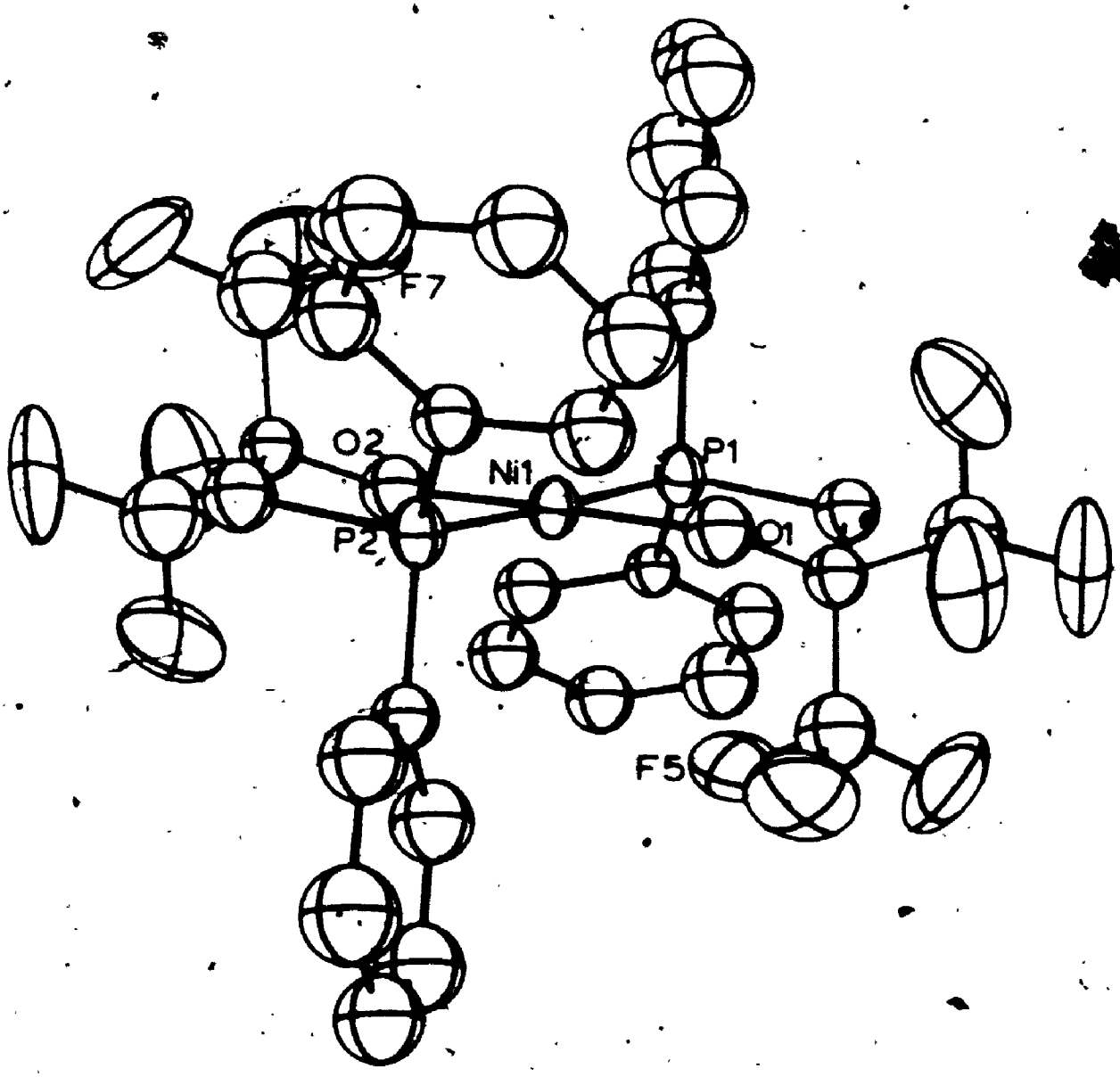

Figure 6-8 ORTEP drawing of $[Ni(L^1)_2]$ molecule 1

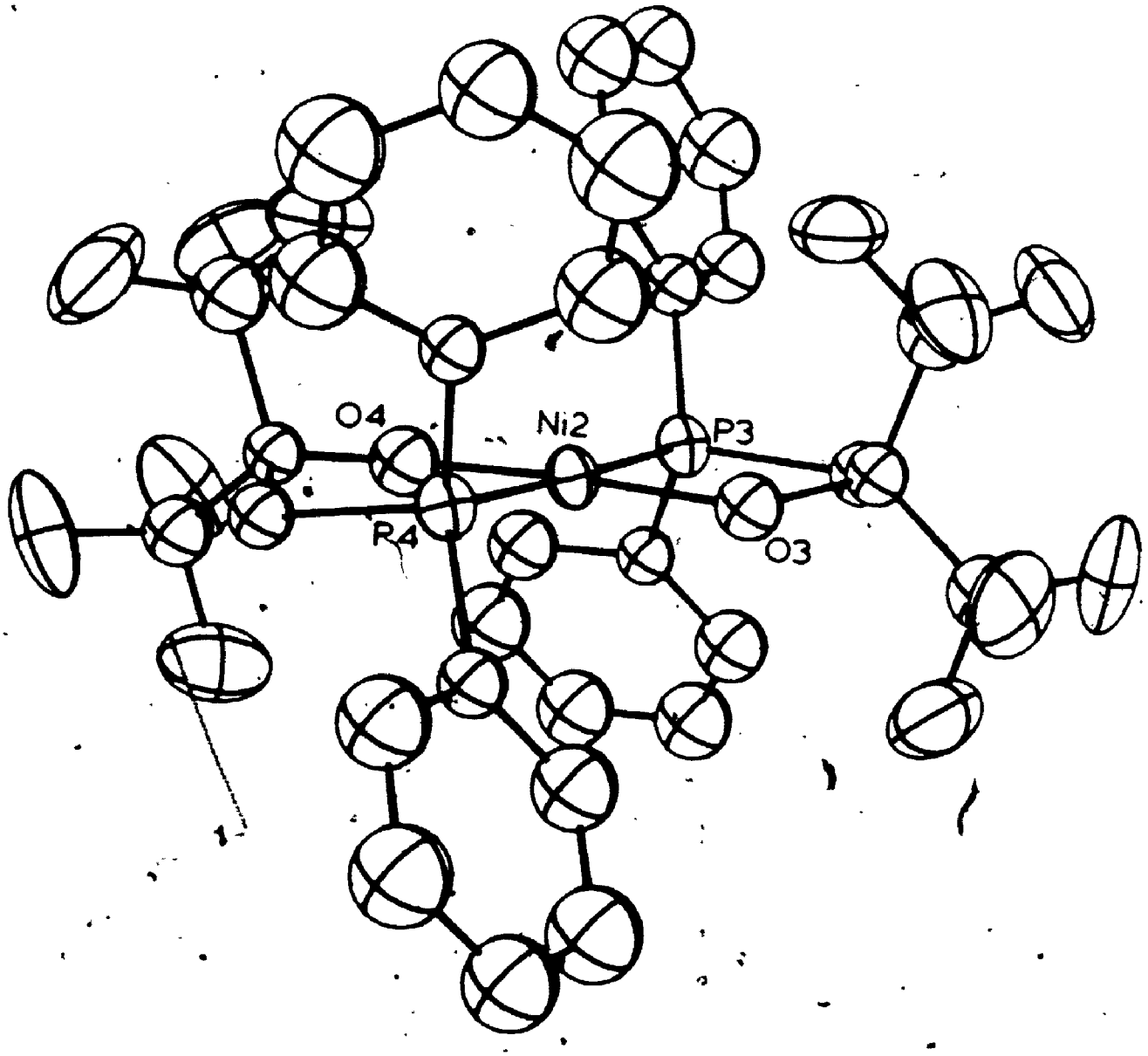

Figure 6.9 ORTEP drawing of $[Ni(L^1)]_2$ molecule 2

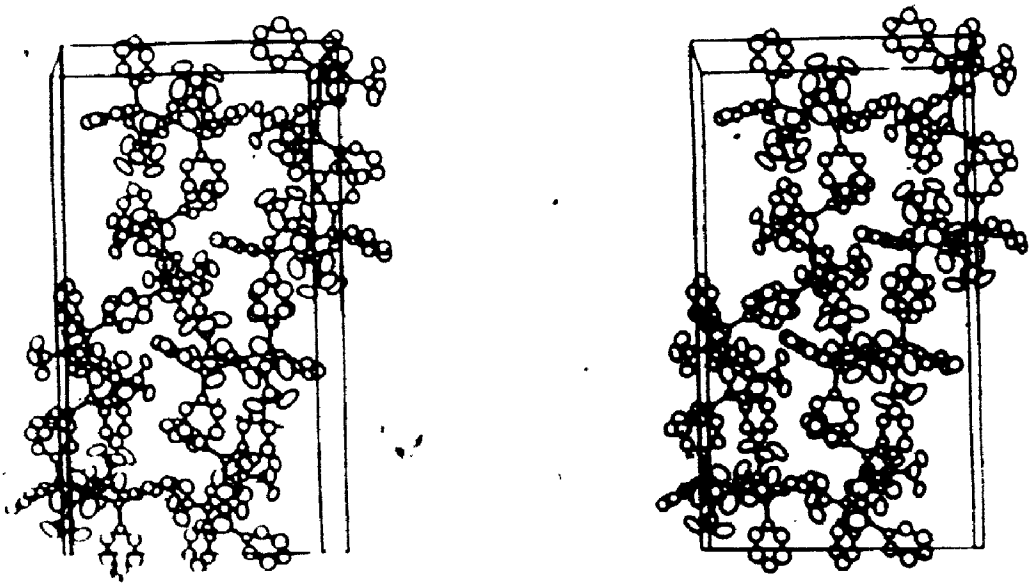

Figure 6-10 Stereoview of the unit cell of $[Ni(L^1)_2]$

plane is small (0.0310 and 0.0372 Å for molecules 1 and 2 respectively).

Furthermore, the dihedral angle between the planes formed by Ni(1), P(1), O(1) and Ni(1), P(2), O(2), (2.9(2)°) and that formed by Ni(2), P(3), O(3) and Ni(2), P(4), C(4) (4.1(3)°) indicates that there is little or no tetrahedral distortion. The coordination geometry is thus square-planar.

The structures of the two molecules per equivalent position differ in their conformation of the chelate ring particularly in the carbon atoms in the backbone of the ring. The nickel, two phosphorus and two oxygen atoms in each molecule form a plane. The differing deviations of the chelate ring carbon atoms from these planes are listed in Table 6.10.

In molecule 1, the two carbon atoms in each chelate ring lie on the same side of the plane, with the carbon atoms bonded to oxygen (C(2) and C(4)) deviating the most from the plane. The chelate ring conformation of molecule 1 is thus an asymmetric envelope. As a result, the CF_3 groups in molecule 1 are forced into a strongly axial-equatorial conformation.

In molecule 2, the two carbon atoms in each chelate ring lie on opposite sides of the coordination plane, with the carbon atom bonded to oxygen deviating a greater distance from the plane. Molecule 2 is thus in an asymmetric skew conformation. As a result, the CF_3 groups

appear in an "up and down" conformation. The differences in the arrangement of the CF_3 groups between the two molecules are illustrated clearly in Fig. 6.8 and Fig. 6.9.

The χ^2 test[138] was applied to the various final bond lengths in order to determine whether or not chemically equivalent bonds may be considered crystallographically equivalent. The four Ni-O bond lengths could be averaged to 1.839(3)A. This distance is short by comparison with the normally observed range for Ni-O bonds (1.85 - 1.93 A) in square-planar Ni(II) complexes.[139] However it is comparable to the mean Ni-O distance in a square-planar Ni(II) compound where two perfluoroalkoxy groups are coordinated to the nickel (1.842(2) A) in mutually trans positions.[92]

Likewise the O-C bonds could be averaged to 1.375(5) A. This is comparable to previously reported C-O bond lengths in a perfluoroalkoxy group coordinated to a transition metal. Previously reported values lie in the range 1.33(1) to 1.38(1) A.[15,16,92,140] As mentioned for previous structures in this study, the highly polar nature of the metal-oxygen σ-bond in a fluorinated alkoxide complex leads to C-O π-bonding and hence a shorter C-O bond. The bond length reported here is in line with such a trend, being considerably shorter than the normal C-O single bond length of 1.43(1) A.[141]

The length of the P-C bonds in the chelate ring backbone could be averaged to a mean value of 1.829(5) A.

This is in agreement with previously reported values. For trans-$[NiBr_2(PPhMe_2)_2]$, the P-CH_3 bond distances are 1.824(11) and 1.822(9) A.[142]

The C-CF_3 bond lengths could also be averaged, to an overall mean value of 1.533(3) A. However, as mentioned previously in molecule 1, the CF_3 groups are axial and equatorial while in molecule 2, the CF_3 groups are up and down. The average value of the C-CF_3 bond length in molecule 2 is 1.533(5) A. In molecule 1, the axial C-CF_3 bonds are shorter (average value, 1.520(7) A) than the equatorial bonds (average value, 1.545(7) A). In a previously-reported structure of a square-planar perfluoroalkoxide complex of Ni(II), the axial C-CF_3 bond length is 1.522(6) A compared with 1.552(5) A for the equatorial bonds.[92] However, it is not obvious why the two types of C-CF_3 bond should be different; it is more likely that the observed difference is simply an artifact of thermal motion.

The C-F bond lengths could not be averaged, but this is not surprising considering the considerable thermal motion expected of these groups. The values for this bond length fall in the range of 1.22(1) to 1.37(1) A. The mean C-F distance in a previously-reported structure of a perfluoroalkoxide complex of square-planar Ni(II) was 1.327(5) A.

It was not statistically reasonable to average the four C-C bonds in the chelate ring when σ was used. However by

using 2σ, one finds that the values can be averaged to 1.55(2) Å. This compares favourably to previously reported values of C-C bonds in compounds of the type trans-$[Ni(PR_3)_2X_2]$.[143,144]

Finally the Ni-P bond distances of 2.195(2), 2.183(2), 2.192(2) and 2.202(2) Å could not be averaged using σ in the χ^2 test. However, by using 3σ, the bond distances could be averaged to 2.193(3) Å.

The Ni-P bond distances in compounds of the type, trans-$[Ni(PR_3)_2X_2]$ are in general slightly shorter than the sum of the covalent radii, (2.34 Å).[145] This is due to the considerably greater electrostatic and steric repulsions in square-planar Ni(II) complexes than in tetrahedral species. As a result of these repulsions, greater overlap between metal and ligand orbitals is necessary to stabilize these complexes. Typical values in such compounds lie in the range of 2.25 to 2.30 Å.[142,144,146,147]

The Ni-P bond length reported in this structure of 2.193(6) Å is therefore quite short. Other short Ni-P distances in square-planar Ni(II) complexes include the values 2.151(1)[148] and 2.159[149] for cis-$[Ni(P(C_6H_{11})_2H)_2Cl_2]$ and $[NiMe(pd)P(C_6H_{11})_3]$ respectively (where pd = pentane -2,4-dionate). However in these complexes the phosphorus atom is trans to a chloride ligand and alkoxide species respectively, both of which have a considerably weaker trans influence than the phosphine present in this structure. Therefore a shorter

Ni-P distance would be expected in these examples.

There are at least two examples of Ni-P distances shorter than that determined here, for complexes with phosphines mutually trans to each other. One such complex is $[NiClN(SiMe_2CH_2PPh_2)_2]$ where the Ni-P distances are reported as 2.1975(5) and 2.2086(6) Å[150]. Another short Ni-P distance occurs in $[Ni(C{\equiv}CPh)_2(PEt_3)_2]$[143]. The bond length reported for this trans structure is 2.175 Å. This short distance is explained as resulting from increased π-back bonding. The -C≡CPh ligand is a strong σ donor due to its negative charge and relatively electropositive donor atom. As a result, the nickel atom is made electron-rich by this strong σ-donor, thus becoming a good π-donor. However, in the structure determined here, the alkoxide is too "hard" a ligand to increase the π-donor properties of the nickel atom. Rather, it is likely that the ability of the fluorinated alkoxide to withdraw electron density from the nickel enhances the σ-donor capability of the phosphine group and thus strengthens the nickel-phosphorus bond. This is further evidence of the relatively high cis-influence of fluorinated alkoxides as discussed previously in chapter 5.

Another short Ni-P bond length appears in the structure of the highly analogous compound, 6-2.[186]

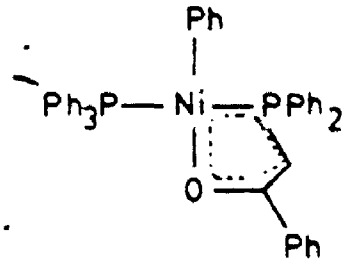

6-2

The Ni-P bond length in this compound is 2.168 A. Again the reason for the short bond is the high cis-influence of a coligand, in this case the phenyl group. This ligand also has a high-trans-influence, making the Ni-O bond (1.914 A) considerably longer than that in $[Ni(L^1)_2]$ (1.839(3) A).

Since intermolecular association increasing the coordination number at the nickel was proposed as one possible cause of the colour change observed on crystallization, a search for such interactions was carefully carried out. The crystals were built up from independent molecules with no unusual intermolecular nonbonded contacts. The shortest intermolecular distance was 2.52 A between HC(86) and HC(83) at (3/2-x, -y, z-1/2). The shortest intermolecular distances involving only one hydrogen were those between F(12) and HC(55) at (x, y, 1+z) (2.59 A) and F(18) and H[redacted] at (1+x, -y, z) (2.54 A). A similar approach of 2.57 A appears within molecule 2 between F(18) and HC(86). The shortest intramolecular nonbonding approach involving only one hydrogen, however, is 2.317 A between P(4) and either

H1C(7) or H2C(7). The shortest intermolecular approaches involving no hydrogen atoms are 2.82(1) Å between F(2) and F(10) at (x, y, z-1) and 2.99(1) Å between F(1) and F(11) at (x, y, z-1).

6.3.5 Discussion of Structure

Both $[Pd(L^1)_2]$ and $[Pt(L^1)_2]$ have cis-square-planar structures in solution and in the solid state, while $[Ni(L^1)_2]$ exists in solution in an equilibrium involving cis and trans isomers. It was suspected that the trans-isomer would be the more stable isomer in isolation in the gaseous state based on the fact that only the trans isomer is seen in the apolar solvent, benzene. The cis-isomer therefore appears in solution only as a result of interactions with the more polar solvents. The reason given for this trend in geometrical preference as one moves up the nickel triad from platinum is the effect of antisymbiosis. This effect dictates that mutually trans soft ligands will have a destabilizing effect on each other. However, this is more significant for soft metal ions. As a result as one substitutes the hard metal ion, Ni(II), for softer ones, Pd(II) or Pt(II), antisymbiosis becomes less important and the dominating factor becomes the trans-directing steric effects.

As a result, one might be tempted to predict a trans structure for $[Ni(L^1)_2]$ in the solid state, where interactions with solvent molecules have been removed.

However, these interactions have been replaced by interactions between $[Ni(L^1)_2]$ molecules; that is, packing factors. These factors are unpredictable, so while the trans geometry in the solid state is not surprising, neither does it indicate as much concerning the inherent relative stabilities of the two geometrical isomers as does the result that only the trans isomer appears in benzene solution.

The most important reason for carrying out the structure determination was to determine the cause of the colour change from orange to green on crystallization. It was suggested that the colour change was due to an interaction present only in the solid state, either a weak tetrahedral distortion or a weak association, intramolecular or intermolecular.

It was found that the green form of $[Ni(L^1)_2]$ consists of equal numbers of two types of molecules in the unit cell. In both molecules, the geometry is trans-square-planar; the departure from planarity towards a tetrahedron, measured by the dihedral angle between chelating ligands, is negligible. Therefore one can rule out the possibility of a slight tetrahedral distortion being the cause of the observed colour change.

The measurements of nonbonding close approaches between molecules likewise eliminate the possibility of an intermolecular association being the cause. This leaves an intramolecular association as the only remaining

possibility.

As mentioned, the two molecules differ in their chelate ring conformation. In molecule 1, the conformation with axial and equatorial CF_3 groups is such that two fluorine atoms, F(5) and F(7), make an unusually close approach to the metal atom from opposite sides of the coordination plane. The Ni-F distances are 3.190(8) and 3.193(7) A to F(7), and F(5) respectively. The F-Ni-F axis makes an angle of 55° with the coordination plane.

The distances are considerably less than the sum of the covalent radii for Ni (1.39 A for octahedral, 1.16 A for square-planar) and F (0.71 A). However, the van der Waals radii[151] for Ni and F are 1.50 A and 1.50 to 1.60 A respectively which supports the proposal that there may be a weak interaction between Ni and F atoms in molecule 1.

It is this weak interaction in molecule 1 that is believed to cause the addition absorption band at 600 nm to appear in the solid state visible spectrum, and hence gives the crystals their green colour. However, the interaction is not strong enough to cause the ground electonic state to change from a singlet to a triplet state, and the solid remains diamagnetic.

Such a solid-state interaction may explain other features of the behaviour of this complex. The compound is orange in solution and in the melt because this weak interaction exists only in the solid state. Also raising the temperature of the solid causes a weakening of the

interaction, thus explaining the decrease in the intensity of the green colour on heating. The metastable orange form of the solid likely consists of crystals where all molecules are similar in conformation to molecule 2, where the interaction is absent. This form could then undergo a low-energy solid-state transformation to the green form, where half the molecules in each unit cell are like molecule 1. It is extremely unlikely that the orange form is actually the cis-isomer, since the ease by which the transformation occurs at room temperature precludes such a high energy interconversion as a cis → trans isomerization.

6.4 The Possibility of Six-Coordinate Diamagnetic Ni(II) Complexes

6.4.1 Theoretical Background

The d^8 metal ion, Ni(II), will have a $(t_{2g})^6 (e_g)^2$ electron configuration in an octahedral ligand field. The ground state is then described by the term $^3A_{2g}$. Such an electron configuration and electronic state would be expected as long as the nickel atom is surrounded by six equal, strongly coordinating, ligands.

However, by drawing away the axial ligands, one moves from an octahedral field to a tetragonal field and eventually to a square-planar ligand field. As the interaction between metal and axial ligands weakens, the d_{z^2}, d_{xz} and d_{yz} orbitals are stabilized.

This perturbation, going from free metal ion to an

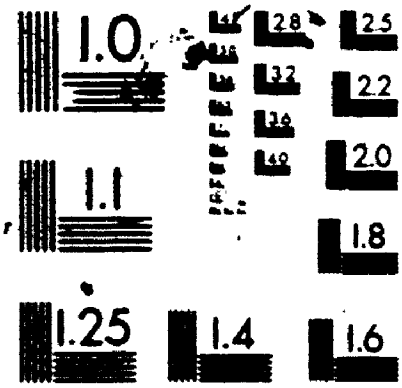

octahedral environment, to a tetragonal environment, to a square-planar environment, may be depicted in an energy level correlation diagram for the d-orbitals (Fig. 6.11).

Ballhausen and Liehr[152] have calculated the relative energies of the electronic states in such complexes. Both diamagnetic and paramagnetic species are considered possible.

In the case of a weakly tetragonal Ni(II) complex, the electronic configuration may be $(e_g)^4(b_{2g})^2(a_{1g})^2$ and diamagnetic or $(e_g)^4(b_{2g})^2(a_{1g})^1(b_{1g})^1$ and paramagnetic. Likewise for a strongly tetragonal (or square-planar) complex, the electron configuration may be $(e_g)^4(a_{1g})^2(b_{2g})^2$ and diamagnetic or $(e_g)^4(a_{1g})^2(b_{2g})^1(b_{1g})^1$ and paramagnetic. Ballhausen and Liehr were then able to calculate the conditions for diamagnetism in a) a weak and b) a strong tetragonal case.

a) Weak tetragonality

$E(^3B_{1g}) > E(^1A_{1g})$

or $\Delta_1 > 8\frac{1}{2}\ (4F_2 + 15F_4)$

b) Strong tetragonality

$E(^3A_{2g}) > E(^1A_{1g})$

or $\Delta_2 > 8\frac{1}{2}\ (35F_4)$

Taking F_2 and $10F_4$ to be $\sim$1000 cm^{-1} these conditions become a) $\Delta_1 > 15{,}000\ cm^{-1}$ (weak tetragonality)

b) $\Delta_2 > 9{,}900\ cm^{-1}$ (strong tetragonality)

Therefore six-coordinate diamagnetic nickel (II)

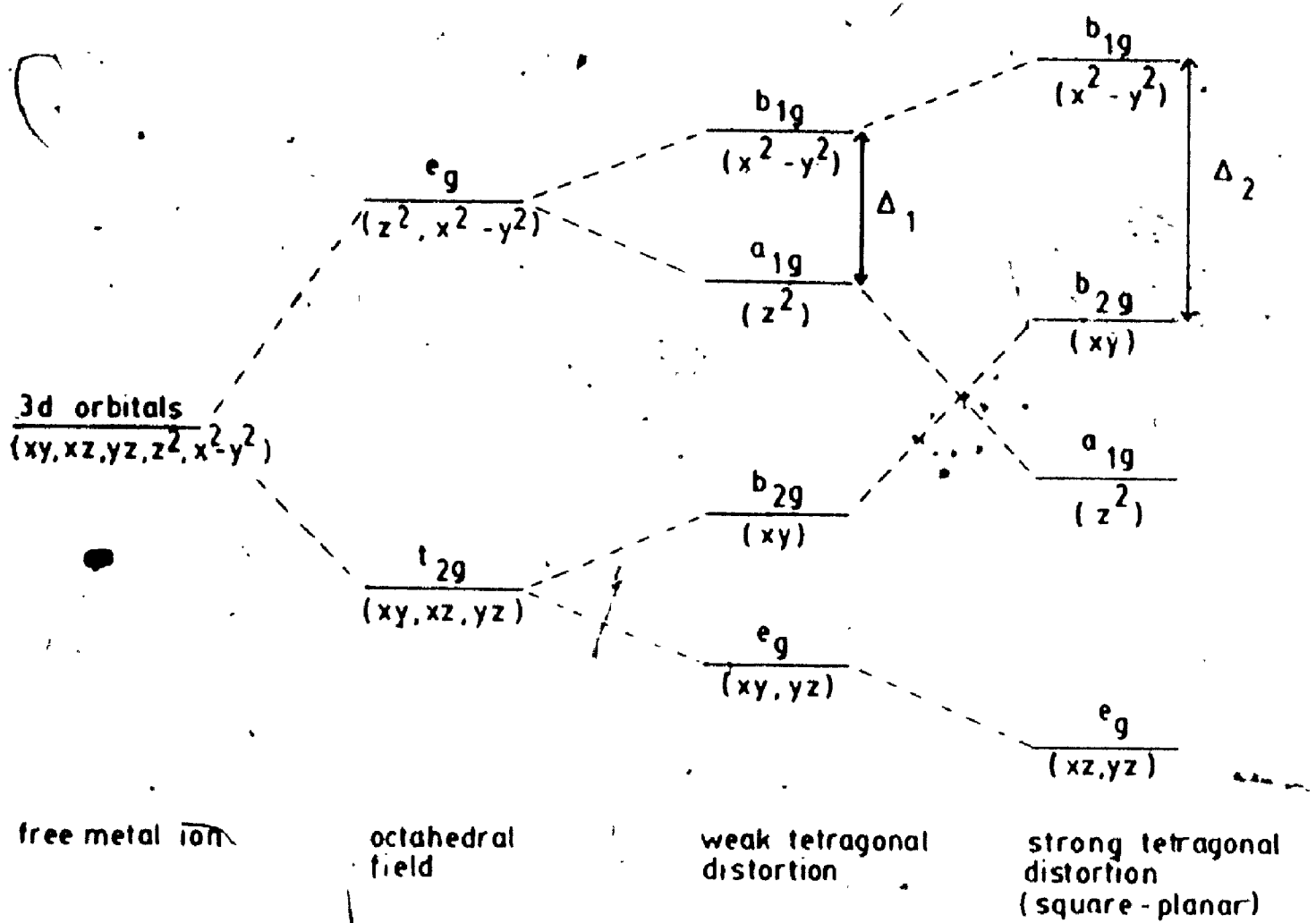

Figure 6.11 d Orbital energy level correlation diagram

complexes are theoretically possible provided:

1) the interaction between the nickel and the axial ligands is strong enough so that they may be considered bonded to the nickel
2) the interaction between the nickel and the incoming axial ligands is sufficiently weak so that Δ_1 has not decreased to the point that $E(^3B_{1g}) < E(^1A_{1g})$ and the complex becomes paramagnetic.

6.4.2 Previous Possible Examples

Goodgame and Venanzi[153] first claimed to have prepared six-coordinate diagmagnetic nickel(II) compounds. These compounds, $[NiY_2(NO_3)_2]$, $[NiY_2Br_2]$ and $[NiY_2I_2]$ were part of a series of complexes of N,N-diethylethylene-diamine, (Y), with Ni(II), some six-coordinate and paramagnetic and some four-coordinate and diamagnetic. Based on electrolytic conductance measurements that showed the conductance of these three compounds to be intermediate between the six-coordinate and four-coordinate compounds, a tetragonal structure was proposed for these three complexes. However, on closer examination the conductivity measurements in better coordinating solvents more closely resemble those of the four-coordinate compounds, rather than those of the six-coordinate compounds. It is therefore rather questionable to suggest that the axial anions are truly coordinated to the nickel since dissociation does occur in solution.

In the intervening twenty years since the original work of Goodgame and Venanzi, there have been a number of other proposals of six-coordinate diamagnetic Ni(II) complexes. These complexes are listed in Table 6.11. However for these complexes, the experimental evidence supporting the claim does not differ much from that of Goodgame and Venanzi.

Solid-state diffuse-reflectance spectra were reported for $[Ni(etu)_4I_2]$, $[Ni(detu)_4Br_2]$, $[Ni(detu)_4I_2]$, $[Ni(dpe)_2Br_2]$, $[Ni(dpe)_2I_2]$, $[Ni(pdta)_2I_2]$ and $[Ni(pdpa)_2I_2]$. In all cases, the spectra were consistent with that of a square-planar complex.

Crystal structures have been done on very few of these complexes. One structure that is known is that of $[Ni(diarsine)_2I]I$.[161] The Ni-I distance of 3.21 Å is considerably greater than the sum of the covalent radii (2.67 Å) although the anions are located in the trans positions of a tetragonal structure.

In solution, conductivity measurements were given for $[Ni(diarsine)_2I]I$, $[Ni(etu)_4I_2]$, $[Ni(detu)_4Br_2]$, $[Ni(detu)_2I_2]$, $[Ni(cyclam)I_2]$, $[Ni(dpe)_2Br_2]$, $[Ni(dpe)_2I_2]$, $[Ni(pdta)_2I_2]$ and $[Ni(pdpa)_2I_2]$. Generally, the values obtained are intermediate between a non-electrolyte and a bi-univalent electrolyte. Sandhu et al[159] concluded based on molar conductances and solution spectra that $[Ni(pdpa)_2I_2]$ and $[Ni(pdta)_2I_2]$ formed five-coordinate species in methylene chloride solution. Harris et al[154]

Table 6.11. Proposed Six-Coordinate Diamagnetic Ni(II) Complexes

Complex	Ref
$[Ni(diarsine)_2I]I$	154
$[Ni\{P(OCH_2)_3CCH_3\}_5H_2O](ClO_4)_2$	155
$[Ni(etu)_4I_2]$	156
$[Ni(detu)_4Br_2]$	156
$[Ni(detu)_4I_2]$	156
$[Ni(cyclam)I_2]$	157
$[Ni(macrocyclic)Br_2 \cdot H_2O]$	158
$[Ni(dpe)_2Br_2]$	98
$[Ni(dpe)_2I_2]$	98
$[Ni(pdta)_2I_2]$	159
$[Ni(pdpa)_2I_2]$	159
$[Ni(EtPH)_4I_2]$	159
$[Ni(EtPH)_4Br_2]$	160

diarsine = o-phenylenebis(dimethylarsine)

etu = ethylenethiourea

detu = N,N'-diethylthiourea

cyclam = 1,4,8,11-tetraazacyclotetradecane

macrocyclic = 2,12-dimethyl-3,7,11,17-tetraazabicyclo-heptadeca-1,2,11,13,15 pentaene

dpe = 1,2-bis(diphenylphosphino)ethane

pdta = o-phenylenebis(di-p-tolylarsine)

pdpa = o-phenylenebis(diphenylarsine)

reached the same conclusion for $[Ni(diarsine)_2I]I$.

Therefore it would seem that diamagnetic nickel(II) complexes do exist which have a tetragonal structure in the solid state. However the fact that these complexes at least partially dissociate in solution suggests that the interaction between the nickel atom and axial anions is a weak one and the complex may not be considered to be truly six-coordinate.

In this study, there is certainly no suggestion being made that F(5) and F(7) are coordinated to the nickel. It is merely a solid state interaction sufficient to alter the ligand field enough so that a change is observed in the visible spectrum but not great enough to cause a change in the magnetic properties.

There are previous reports of diamagnetic, green nickel(II) complexes for which a weak axial interaction may exist, although complex structural information is lacking. For example, Hayter and Humiec[107] a number of complexes of the type $[Ni(PR_3)_2X_2]$ where X = Cl, Br or I and found both square-planar (diamagnetic) and tetrahedral (paramagnetic) forms in several cases. However, for $[NiI_2(P(i\text{-}C_3H_7)(C_6H_5)_2)_2]$, they found a green, diamagnetic substance whose properties are not consistent with either geometry. Interestingly, this compound exhibits thermochroic behaviour in solution; toluene or methylene chloride solutions are dark brown when hot, greenish at room temperature and intensely green when cooled to -78°C.

Similarly, complexes of nitrogen donors such as quinoline,[128] lutidine,[129] tetramethylpyrazine[130] and quinoxaline[131] with NiI_2, give red or yellow colours in solution but change to green in the solid state or at high concentrations or low temperatures. It is noteworthy that such behaviour is most frequently observed when iodide is present. This large, easily polarizable ion is a good bridging ligand and it may be that a weak additional interaction, either inter- or intramolecular, between nickel and iodide exists in these complexes similar to that being proposed in $[Ni(L^1)_2]$ between nickel and fluorine. Clearly, additional structural investigations are needed on these interesting systems.

Chapter 7

Synthesis of HL^1 and Complexes of HL^1

7.1 Introduction

This chapter gives experimental detail on the preparation of the various compounds in this study.

The compounds were all characterized by elemental analysis. The microanalyses were determined by Guelph Analytical Laboratories, Guelph, Ontario and the results are reported in Table 7.1. Also, mass spectra were obtained where possible (some compounds disproportionated in the mass spectrometer). The mass spectra were obtained on a Varian MAT 311 instrument and the results appear in Table 7.2. In addition, in each case an infrared spectrum was obtained as a Nujol mull between NaCl plates on a Beckman IR4250 spectrometer. These spectra were used primarily to confirm the presence of the fluorinated alkoxide in the complex by the strong absorption in the region from 1160 to 1190 cm^{-1} due to C-F stretching.

NMR spectra were obtained using Varian XL100 and XL300 instruments for ^1H and ^{19}F spectra and XL100 and XL200 instruments for ^{31}P spectra. All ^{31}P spectra were proton decoupled. NMR spectroscopy was the primary method of structural characterization in this study and the spectra results are reported and discussed throughout the thesis. The chemical shifts are reported relative to Me_4Si, $CFCl_3$ and $(MeO)_3PO$ for ^1H, ^{19}F and ^{31}P spectra respectively. In the case of variable-temperature spectra, the temperature

Table 7.1. Analytical Data

Compound	Formula	% carbon		% hydrogen		% phosphorus	
		calcd	found	calcd	found	calcd	found
$Co(L^1)_2$	$C_{32}H_{24}CoF_{12}O_2P_2$	48.68	48.61	3.06	3.28	7.85	7.58
$Cu(L^{1=O})_2$	$C_{32}H_{24}CuF_{12}O_4P_2$	46.36	46.53	3.01	2.93	7.01	7.50
$Cu(Ph_3P)_2(L^1)$	$C_{52}H_{42}CuF_6OP_3$	65.51	65.53	4.44	4.70	9.75	9.98
$K[RhCl_2(L^1)_2]$	$C_{32}H_{24}Cl_2F_{12}KO_2P_2Rh$	40.74	40.96	2.56	2.58	6.57	5.76
$Pt(L^1)_2$	$C_{32}H_{24}F_{12}O_2P_2Pt$	41.52	41.69	2.62	2.70	6.69	7.71
trans-$PtCl_2(HL^1)_2$	$C_{32}H_{26}Cl_2F_{12}O_2P_2Pt$	38.49	38.16	2.62	2.64	6.20	7.78
cis-$PtCl(L^1)(HL^1)$	$C_{32}H_{25}ClF_{12}O_2P_2Pt$	39.95	40.17	2.62	2.58	6.44	7.44
trans-$PtCl(L^1)HL^1)$	$C_{32}H_{25}ClF_{12}O_2P_2Pt$	39.95	39.81	2.62	2.72	6.44	6.27
cis-$PtCl(L^1)(PPh_3)$	$C_{34}H_{27}ClF_6OP_2Pt$	47.54	47.04	3.17	3.24	7.21	7.73
cis-$PtCl(L^1)(PPhMe_2)$	$C_{29}H_{25}ClF_6O_2Pt$	43.76	43.21	3.16	3.41	7.78	7.97
cis-$PtCl(L^1)(PPhMe_2)$	$C_{24}H_{23}ClF_6OP_2Pt$	39.28	39.54	3.16	3.09	8.44	8.37
cis-$PtCl(L^1)(PMe_3)$	$C_{19}H_{21}ClF_6OP_2Pt$	34.80	33.76	3.23	2.99	9.44	9.03
trans-$PtMe(L^1)(HL^1)$	$C_{33}H_{28}F_{12}O_2P_2Pt$	42.09	41.98	3.00	3.01	6.59	6.63

Table 7.1 Continued.

Compound	Formula	% carbon		% hydrogen		% phosphorus	
		calcd	found	calcd	found	calcd	found
$PtCl_2(L^1)_2$	$C_{32}H_{24}Cl_2F_{12}O_2P_2Pt$	38.57	37.96	2.43	2.78	6.23	5.43
$Pd(HL^1)_2Cl_2$	$C_{32}H_{26}Cl_2F_{12}O_2P_2Pd$	42.24	42.36	2.88	3.09	6.81	7.66
$Pd(L^1)_2$	$C_{32}H_{24}F_{12}O_2P_2Pd$	45.92	46.99	2.90	3.05	7.40	7.34
$[Pd(L^1)Cl]_2$	$[C_{16}H_{12}ClF_8OPPd]_2$	37.90	37.24	2.39	2.75	6.11	6.30
$Pd(L^1)Cl(PPh_3)$	$C_{34}H_{27}ClF_6OP_2Pd$	53.08	52.49	3.54	3.58	8.05	8.27
$Pd(L^1)Cl(PPh_2Me)$	$C_{29}H_{25}ClF_6OP_2Pd$	49.25	48.07	3.56	3.58	8.76	8.76
$Pd(L^1)Cl(PPhMe_2)$	$C_{24}H_{23}ClF_6OP_2Pd$	44.67	44.39	3.59	3.56	9.60	10.94
$Pd(L^1)Cl(PMe_3)$	$C_{19}H_{21}ClF_6OP_2Pd$	39.13	39.23	3.63	3.82	10.73	10.62
$Pd(L^1)Cl(SMe_2)$	$C_{18}H_{18}ClF_6OPPdS$	37.98	38.22	3.19	3.27	5.44	5.53[a]
$Pd(L^1)Cl(pyr)$	$C_{21}H_{17}ClF_6NOPPd$	43.03	42.17	2.92	3.08	5.28	5.52
$Ni(L^1)_2$	$C_{32}H_{24}F_{12}NiO_2P_2$	48.70	48.61	3.07	3.08	7.85	7.99

[a] Sulfur: Calcd, 5.63. Found, 5.71%

Table 7.2 Mass Spectra Data[a]

Compound	Molecular Ion	loss of F	loss of Cl	loss of CF_3 (or 2 Cl)	loss of CF_3, F	loss of $2CF_3$	loss of HFA	loss of 2 (HFA)	loss of L^1	L^1	MP (°C)	Temp (°C)
HL^1	366	347	-	297	278	228	200	-	-	-	59-62	18
$[Co(L^1)_2]$	789	770	-	720	-	-	623	457	-	365	283	80
$[Cu(L^1{-}O)_2]$	825	806	-	756	736	687	659	-	-	365	252	150
$[Cu(PPh_3)_2(L^1)]$	852	-	-	-	-	-	786	-	-	-	166-168	80
$K[[illegible](L^1)_2Cl_2]$[c]	942	-	-	873	-	-	-	-	-	365	291	120
$[Pt(L^1)_2]$	925	906	-	856	-	787	-	-	-	365	289	160
cis-$[Pt(HL^1)_2Cl_2]$	-	-	962	928	909	859	-	-	-	365	206-207	50
trans-$[Pt(HL^1)_2Cl_2]$	-	-	962	928	909	859	-	-	-	365	214-215	50
cis-$[Pt(HL^1)(L^1)Cl]$	961	942	926	-	-	-	-	-	-	365	197	160
trans-$[Pt(HL^1)(L^1)Cl]$	961	942	926	-	-	-	-	-	-	365	197	160
$[Pt(PPh_3)(L^1)Cl]$	857	838	822	788	-	719	691	-	-	-	267	210
$[Pt(PPh_2Me)(L^1)Cl]$	795	-	760	726	-	-	-	-	-	365	277	100
$[Pt(PPhMe_2)(L^1)Cl]$[b]	-	-	-	-	-	-	-	-	-	-	270	70
$[Pt(PMe_3)(L^1)Cl]$	671	652	636	602	-	-	-	-	-	365	146	100
$[Pt(HL^1)(L^1)Me]$[d]	941	-	960	926	907	857	-	-	-	365	241	180
$[Pt(L^1)_2Cl_2]$	995	-	960	926	907	857	-	-	-	365	241	180
$[Pd(HL^1)_2Cl_2]$	-	-	-	838	819	770	-	-	-	366	227	170
$[Pd(L^1)_2]$	836	817	-	767	748	-	670	504	471	365	240-241	150
$[Pd(L^1)Cl_2]$[b]	1012	993	-	943	-	-	-	-	-	-	218	150
$[Pd(PPh_3)(L^1)Cl]$[b,e]	-	-	-	-	-	-	-	-	-	-	212	150

Table 7.2 Mass Spectra Data[a]

Compound	Molecular Ion	loss of F	loss of Cl	loss of CF_3 (or 2 Cl)	loss of CF_3, F	loss of $2CF_3$	loss of HFA	loss of 2 (HFA)	loss of L^1	L^1	MP (°C)	Temp (°C)
$[Pd(PPh_2Me)(L^1)Cl]$[b,e]	706	-	671	637	-	-	-	-	-	365	215	150
$[Pd(PPhMe_2)(L^1)Cl]$[b,e]	644	-	609	-	-	-	-	-	-	365	212	140
$[Pd(PMe_3)(L^1)Cl]$[b,e]	582	-	547	-	-	-	-	-	-	365	223	140
$[Pd(SMe_2)(L^1)Cl]$[b]	568	-	533	-	-	-	-	-	-	365	114-115	110
$[Pd(py)(L^1)Cl]$[b,e]	585	-	550	-	-	-	-	-	-	365	195	112
$[Ni(L^1)_2]$	788	769	-	719	-	-	622	-	-	-	252	150

[a] Peaks calculated using the following isotopes, ^{1}H, ^{12}C, ^{19}F, ^{16}O, ^{31}P, ^{195}Pt, ^{106}Pd, ^{58}Ni, ^{63}Cu, ^{59}Co, ^{103}Rh, ^{39}K, ^{35}Cl; observed peaks may have been ±1 due to gain/loss of ^{1}H; all spectra run at 70 eV.

[b] Also disproportionates giving $[M(L^1)_2]$ and corresponding fragmentation pattern.

[c] plus loss of CF_3, K (834); CF_3, K, HFA (668); CF_3, K, L^1 (469)

[d] plus loss of CH_3 (926); CH_3, F (907); CH_3, HFA (760); CH_3, HA, Ph (683)

[e] also loss of L', Ph.

settings were checked with a Doric Trendicator 400 Type T digital thermometer.

Volatile compounds such as hexafluoroacetone were manipulated on a vacuum line. Air- and moisture-sensitive materials were transferred using standard techniques employing serum caps and syringes.

7.2 Starting Materials

Most of the starting materials used were commercially available. Methyldiphenylphosphine was obtained from Alfa. The remaining phosphines were supplied by Fisher or Aldrich while n-butyllithium and N,N,N',N'-tetramethyl-ethylenediamine (TMED) were both obtained from Aldrich. Solvents were all reagent grade or better, and were supplied by Fisher or Baker. The tetrahydrofuran (THF) used was dried by distillation over $LiAlH_4$ and the water content was then analyzed by Karl Fischer titration. The metal halides ($PtCl_2$, K_2PtCl_4, $PdCl_2$, $NiCl_2 \cdot 6H_2O$, $CuCl_2 \cdot 2H_2O$ etc.) were supplied by Fisher, Baker and Alfa.

Other materials were prepared by known literature methods as outlined here.

7.2.1 $[Cu(PPh_3)_3Cl]$

This compound was prepared by the method of Costa, Reisenhofer and Stefani.[270] The preparation was carried out using 0.385 g (3.89 mmole) of CuCl and 2.0 g of $[Cu(PPh_3)_3Cl]$ was obtained (58% yield).

7.2.2 $[Pt(CH_3CN)_2Cl_2]$

$[Pt(CH_3CN)_2Cl_2]$ was prepared by the method of Hartley, Murray and McAuliffe[271] using 0.54 g (2.03 mmole) of $PtCl_2$. The yield of $[Pt(CH_3CN)_2Cl_2]$ was 0.52 g or 74%.

7.2.3 $[Pt(SMe_2)_2Cl_2]$

$[Pt(SMe_2)_2Cl_2]$ was prepared by the method of Cos, Saenger and Wardlaw[272] using 0.63 g (1.52 mmole) of K_2PtCl_4. The product, $[Pt(SMe_2)_2Cl_2]$, was obtained as a mixture of cis and trans isomers in 80% yield.

7.2.4 $[Pt_2Me_4(\mu\text{-}SMe_2)_2]$

This dimer was prepared by the method of Puddephatt and Scott[273] starting with 0.51 g (1.31 mmole) of a mixture of cis- and trans-$[Pt(SMe_2)_2Cl_2]$. The final product, $[Pt_2Me_4(\mu\text{-}SMe_2)_2]$, was obtained in 40% yield.

7.2.5 $[Pt(COD)Cl_2]$

$[Pt(COD)Cl_2]$ was prepared by the method of Clark and Manzer[274] starting from 0.66 g (1.59 mmole) of K_2PtCl_4. The final product was obtained in 86% yield.

7.2.6 $[Pt(COD)Me_2]$

$[Pt(COD)Me_2]$ was prepared by the method of Clark and Manzer[274] starting from 0.14 g (0.42 mmole) of $[Pt(COD)Cl_2]$. The yield of $[Pt(COD)Me_2]$ was 87%.

7.2.7 $[Pd(PhCN)_2Cl_2]$

$[Pd(PhCN)_2Cl_2]$ was prepared by the method of Kharasch, Seyler and Mayo.[275] Starting with 2.00 g of $PdCl_2$, the metal dihalide was converted to $[Pd(PhCN)_2Cl_2]$ in quantitative yield.

7.3 Preparation of the Ligand, HL^1

A 1.6 M solution of n-butyllithium in hexane (44 mL, 70 mmole C_4H_9Li) was syringed into a dry round-bottom flask under argon, followed by tetramethylethylenediamine, (TMED) (10.6 mL, 70 mmole). Methyldiphenylphosphine (14.5 mL, 70 mmole) was syringed in and the reaction mixture was left stirring under argon. After about 20 min, a bright yellow precipitate formed ($Ph_2PCH_2^-Li^+$).[56] Tetrahydrofuran (THF), dried over $LiAlH_4$, was syringed in with stirring until all the yellow precipitate was taken up in solution (~30 mL).

The reaction vessel was then removed from the vacuum line and cooled to -78°C while 12.0 g of hexafluoroacetone (72 mmole) was bubbled into the orange solution under a constant flow of N_2. After all of the HFA had been transferred into the reaction vessel, the solution was poured out into cold, (0°C), concentrated HCl (~100 mL).

This mixture was then extracted with diethyl ether (3x150 mL) and the ether extract was dried over sodium sulfate. The diethyl ether was removed by vacuum rotary evaporation and the orange oil obtained was dried over sodium sulfate. The desired product, 2-(diphenylphosphino-

methyl)-1,1,1,3,3,3-hexafluoro-2-propanol, HL^1, was then obtained by vacuum distillation of the oil as a waxy solid in 52% yield.

7.4 Preparation of Complexes

The syntheses of the various metal complexes prepared in this study are outlined here. Although many of the platinum complexes could be interconverted as outlined in chapter 3, only the principal methods of preparation for these complexes will be outlined here. The syntheses are presented in the order in which the complexes have been discussed in the thesis.

7.4.1 $[Co(L^1)_2]$

$CoCl_2 \cdot 6H_2O$ (0.325 g, 1.37 mmole) was dissolved in ethanol (100 mL) to give a deep blue solution. The ligand HL^1 (1.0 g, 2.73 mmole) was taken up in ethanol (10 mL) and added with stirring to the blue ethanolic solution of $CoCl_2$. As the ethanolic KOH (2.73 mmole) was added, the solution turned a red-orange colour and KCl was precipitated. The ethanol was removed by vacuum rotary evaporation and the resulting orange oil was taken up in CH_2Cl_2. The KCl was then centrifuged off and the CH_2Cl_2 was removed from the supernatant liquid by rotary evaporation. The orange oil was taken up in a minimal amount of $CHCl_3$ and the addition of diethyl ether caused the precipitation of an orange solid. The yield of the

product, $[Co(L^1)_2]$, was 37%

7.4.2 $[Cu(L^1{=}O)_2]$

$CuCl_2 \cdot 2H_2O$ (0.195 g, 1.14 mmole) was dissolved in ethanol (50 mL). The ligand, HL^1, (0.839 g, 2.29 mmole) was added to the solution followed by ethanolic KOH (2.29 mmole). As the solution was stirred, discolouration occurred. The KCl precipitate was centrifuged off and the ethanol was removed to give a purple oil. The oil was taken up in $CHCl_3$ and after hexane was added, blue crystals slowly formed. The yield of $[Cu(L^1{=}O)_2]$ was 44%.

7.4.3 $[Cu(PPh_3)_2L^1]$

$[Cu(PPh_3)_3Cl]$ (1.00 g, 1.13 mmole) was dissolved in $CHCl_3$ (50 mL). The ligand, HL^1, (0.50 g, 1.37 mmole) was dissolved in EtOH (10 mL) and added to the Cu(I) solution. Ethanolic KOH (1.13 mmole) was added dropwise and the solution was left stirring for 24 hrs. The ethanol was removed and the resultant oil was taken up in CH_2Cl_2. The insoluble KCl was centrifuged off and the solvent was again removed. The oil was taken up in $CHCl_3$; hexane was added and after cooling in ice, a white precipitate was collected. The yield of $[Cu(PPh_3)_2L^1]$ was 36%.

7.4.4 $K[Rh(L^1)_2Cl_2]$

$RhCl_3 \cdot 3H_2O$ (0.50 g) was suspended in ethanol (50 mL). The ligand, HL^1, (2.07 g, 5.66 mmole) was dissolved

in ethanol (20 mL) and added to the suspension of the rhodium compound. Ethanolic KOH (5.66 mmole) was added dropwise and as this was done, the $RhCl_3$ was dissolved giving an orange-yellow solution. This solution was left stirring for 24 hrs after which the solvent was removed. The KCl was again removed by dissolving the resultant oil in CH_2Cl_2 and centrifuging. The CH_2Cl_2 was then removed and an orange solid precipitated from a solution in $CHCl_3$/hexane. The yield of $K[Rh(L^1)_2Cl_2]$ was 74%.

7.4.5 $[Pt(L^1)_2]$

K_2PtCl_4 (1.00 g 2.40 mmole) was dissolved in dimethylformamide (100 mL) and HL^1 (2.00 g, 5.46 mmole) in ethanol (20 mL) was added with stirring. Ethanolic KOH (4.80 mmole) was added dropwise. The mixture was centrifuged to remove KCl, then stirred for 24 hours and centrifuged again. The DMF was removed by vacuum evaporation, leaving an oil. Addition of $CHCl_3$ to this oil precipitated a white solid. The solid was filtered off and washed with $CHCl_3$. The yield of $[Pt(L^1)_2]$ was 99%.

7.4.6 trans-$[Pt(HL^1)_2Cl_2]$

$[Pt(CH_3CN)_2Cl_2]$ (0.46 g, 1.32 mmole) was dissolved in CH_3CN (60 mL), giving a yellow solution. HL^1 (0.98 g, 2.68 mmole) was taken up in ethanol (10 mL) and added to the solution of $[Pt(CH_3CN)_2Cl_2]$. On addition of the ligand the solution immediately turned a brighter shade of

yellow. The solvent was removed by vacuum evaporation leaving a yellow oil. Addition of $CHCl_3$ to the oil caused a yellow solid to precipitate. This solid was collected by filtration and washed with $CHCl_3$. The yield of trans-$[Pt(HL^1)_2Cl_2]$ was 70%.

7.4.7 cis-$[Pt(HL^1)_2Cl_2]$

$[Pt(L^1)_2]$ (0.30 g, 0.32 mmole) was dissolved in acetone (60 mL). HCl gas was bubbled into the solution with stirring for five min., then the acetone was removed by vacuum evaporation leaving a yellow oil. Addition of $CHCl_3$ to the oil, followed by hexane, caused a creamy white solid to precipitate. The solid was collected by filtration and washed with hexanes. The yield of cis-$[Pt(HL^1)_2Cl_2]$ was 89%.

7.4.8 cis-$[Pt(HL^1)(L^1)Cl]$

$PtCL_2$ (0.40 g, 1.50 mmole) was placed in dimethyl-formamide (100 mL). HL^1 (1.50 g, 4.10 mmole) was added with stirring. As the ligand was added, most of the $PtCl_2$ was taken up into solution; the remaining undissolved $PtCl_2$ was taken up by heating the mixture gently. The yellow solution was stirred for three hours. The solvent was removed, leaving a yellow oil. The oil was dissolved in CH_2Cl_2 and the solution was filtered. Hexanes were added to the solution and white crystals of cis-$[Pt(HL^1)(L^1)Cl]$ slowly formed. The yield was 64%.

7.4.9 trans-[Pt(HL^1)(L^1)Cl]

The method of preparation was identical to that of the cis-isomer except rather than using an excess of HL^1, the $PtCl_2$ was kept in excess. To 0.30 g (1.13 mmole) of $PtCl_2$ in 60 mL of DMF was added 0.80 g (2.18 mmole) of HL^1. The work-up was identical to that of the cis-isomer, yielding yellow crystals of trans-[Pt(HL^1)(L^1)Cl]. The yield was 20%.

7.4.10 [Pt(PPh_3)(L^1)Cl]

[Pt(HL^1)(L^1)Cl] (0.20 g, 0.21 mmole) was dissolved in ethanol (25 mL) and triphenylphosphine (0.08 g, 0.031 mmole) was added. The solution was gently refluxed for three hrs after which the ethanol was removed, leaving a colourless oil. The oil was taken up in CH_2Cl_2 and addition of hexanes precipitated a white solid [Pt(PPh_3)(L^1)Cl], which was collected by filtration and washed with diethyl ether. The yield was 87%.

7.4.11 [Pt(PPh_2Me)(L^1)Cl]

The method of preparation and work-up was the same as for [Pt(PPh_3)(L^1)Cl]. The PPh_2Me (30% excess) was syringed in. The yield of white [Pt(PPh_2Me)(L^1)Cl] was 75%.

7.4.12 [Pt($PPhMe_2$)(L^1)Cl]

The method of preparation and work-up was the same as for [Pt(PPh_3)(L^1)Cl]. The $PPhMe_2$ (50% excess) was

syringed in. The yield of white [Pt(PPhMe$_2$)(L^1)Cl] was 71%.

7.4.13 [Pt(PMe$_3$)(L^1)Cl]

The synthesis of [Pt(PMe$_3$)(L^1)Cl] made use of the apparatus shown in Fig. 7.1. This apparatus was evacuated using a vacuum line and weighed. Into the 25 mL bulb was placed a small stirring bar and [Pt(HL^1)(L^1)Cl] (0.10 g, 0.10 mmole) and into the other arm, AgPMe$_3$I (0.50 g, 0.16 mmole). The apparatus was again evacuated and dry ethanol (20 mL) was transferred into the 25 mL bulb. The bulb was frozen down using liquid N_2 and the arm containing the PMe$_3$ complex was heated to 240°C using an oil bath. The PMe$_3$ complex dissociates under such conditions and as a result the phosphine was transferred over to the frozen arm. The frozen bulb was allowed to warm up to room temperature with stirring. The sample was left stirring for 12 hours and the ethanol was removed to leave a white soid, [Pt(PMe$_3$)(L^1)Cl]. The product was recrystallized from CH_2Cl_2/hexane and collected with a final yield of 57%.

7.4.14 [Pt(HL^1)(L^1)CH$_3$]

[Pt$_2$Me$_4$(μ-SMe$_2$)$_2$] (0.175, 0.30 mmole) was dissolved in CH_2Cl_2 (10 mL) and a solution of HL^1 (0.54 g, 1.5 mmole) in CH_2Cl_2 (5 mL) was added. The solution was stirred for one hour and the CH_2Cl_2 was removed leaving an oil. The oil was dissolved in $CHCl_3$ and petroleum ether was added to precipitate a white solid, [Pt(HL^1)(L^1)CH$_3$]. The solid was

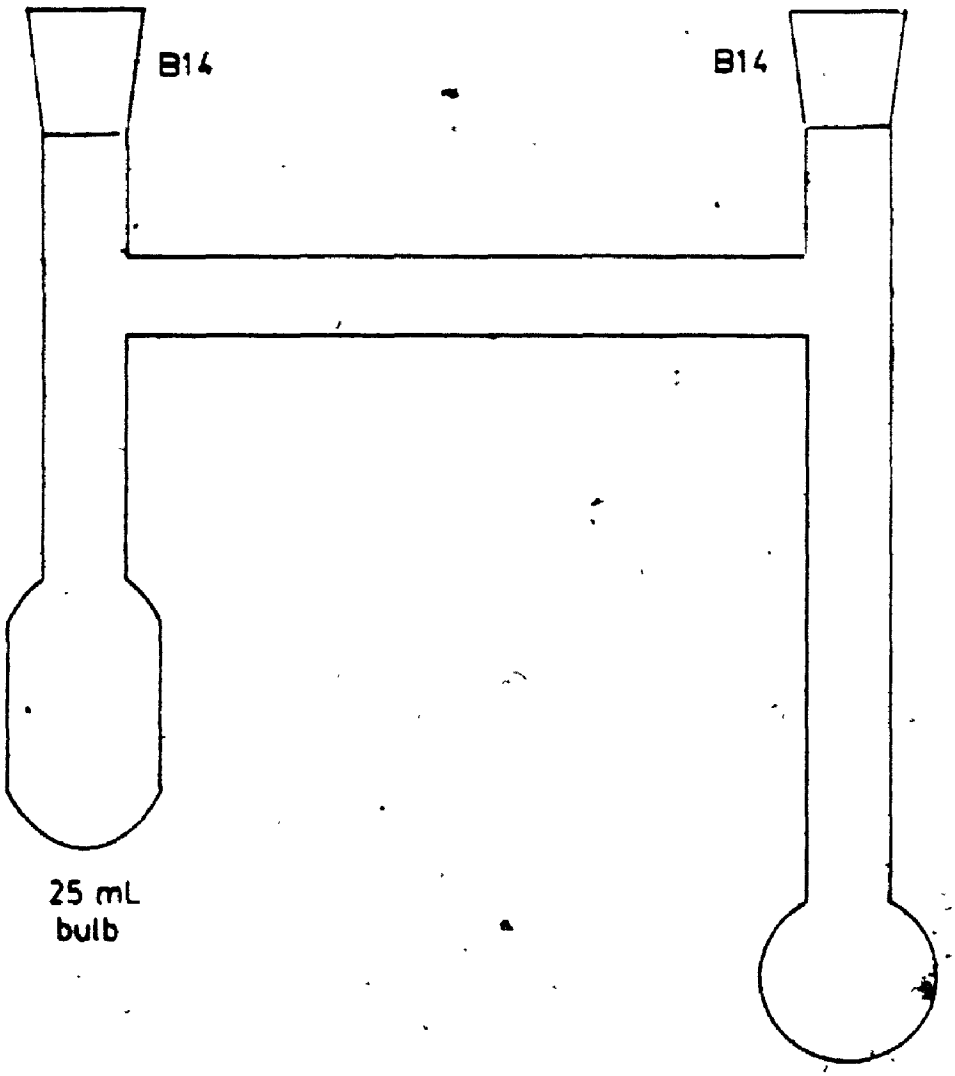

Figure 7.1 Apparatus for handling PMe_3

collected and washed with $CHCl_3$/petroleum ether; the yield was 31%.

7.4.15 $[Pt(L^1)_2Cl_2]$

$[Pt(L^1)_2]$ (0.10 g, 0.11 mmole) was suspended in benzene (25 mL). Chlorine gas was bubbled through with stirring. The solution immediately turned yellow and undissolved $Pt(L^1)_2$ was taken up into solution before a yellow precipitate appeared. The benzene was then removed, by evaporation leaving a yellow solid. This solid, $[Pt(L^1)_2Cl_2]$, was collected and washed with benzene. The final yield was 87%. Attempts to recrystallize the product resulted only in decomposition to $[Pt(L^1)_2]$.

7.4.16 $[Pd(HL^1)_2Cl_2]$

$[Pd(C_6H_5CN)_2Cl_2]$ (0.155 g, 0.40 mmole) was dissolved in $CHCl_3$ (20 mL) and a solution of HL^1 (0.30 g, 0.82 mmole) in $CHCl_3$ (10 mL) was added with stirring. Upon addition of the ligand, the deep red solution turned a yellow-orange colour. The solvent was removed and an orange oil remained. Addition of a small amount of $CHCl_3$ to this oil caused a yellow solid to precipitate. The solid was collected and washed with $CHCl_3$. The final yield of $[Pd(HL^1)_2Cl_2]$ was 75%.

7.4.17 $[Pd(L^1)_2]$

$[Pd(C_6H_5CN)_2Cl_2]$ (1.00 g, 2.61 mmole) was dissolved

in $CHCl_3$ (50 mL). The ligand, HL^1, (2.10 g, 5.73 mmole) in ethanol (20 mL) was added, followed by ethanolic KOH (5.22 mmole) dropwise. The KCl was removed by centrifuging and the solvent was removed from the supernatant liquid, leaving a yellow oil. Addition of $CHCl_3$ to the oil caused the precipitation of the white product $[Pd(L^1)_2]$, which was collected and washed with $CHCl_3$. The final yield was 93%.

7.4.18 $[Pd_2(L^1)_2(\mu\text{-}Cl)_2]$

$[Pd(L^1)_2]$ (1.00 g, 1.19 mmole) was dissolved in $CHCl_3$ containing 10% acetone (50 mL). $[Pd(PhCN)_2Cl_2]$ (0.46 g, 1.12 mmole) was dissolved in $CHCl_3$ (25 mL). The solution of $[Pd(L^1)_2]$ was heated to the point of refluxing and the $[Pd(PhCN)_2Cl_2]$ solution was added dropwise with stirring. After all of the $[Pd(PhCN)_2Cl_2]$ had been added, the solution was concentrated to ~20 mL volume by rotary evaporation and then poured into a vast excess of low-boiling petroleum ether (~200 mL). The orange precipitate, $[Pd_2(L^1)_2(\mu\text{-}Cl)_2]$ was collected by filtration and washed with petroleum ether. The yield was 91%.

7.4.19 $[Pd(PPh_3)(L^1)Cl]$

$[Pd(L^1)Cl]_2$ (0.10 g, 0.10 mmole) was dissolved in 1/1 ethanol/acetone (50 mL). Triphenylphosphine (0.06, 0.23 mmole) was dissolved in ethanol (15 mL) and added to the solution of $[Pd(L^1)Cl]_2$ with stirring. The orange solution turned a yellow colour. The solvent was removed

by rotary evaporation yielding a pale yellow solid. The solid was collected and washed with ether. The yield was 85%.

7.4.20 $[Pd(PR_3)(L^1)Cl]$; PR_3 = PPh_2Me, $PPhMe_2$

$[Pd(L^1)Cl]_2$ (0.50 g, 0.49 mmole) was dissolved in $CHCl_2$ (0.50 g, 0.49 mmole) was dissolved in $CHCl_3$ (50 mL). The phosphine, PR_3, (0.60 mmole) was syringed into the solution of $[Pd(L^1)Cl]_2$ with stirring. The solvent was removed by rotary evaporation to give a yellow oil. The oil was taken up in a minimal amount of CH_2Cl_2 and hexane was added to precipitate a yellow solid. The precipitate was collected by filtration and washed with diethyl ether. The yields were 79%, for PPh_2Me and 83% for $PPhMe_2$.

7.4.21 $[Pd(PMe_3)(L^1)Cl]$

The apparatus in Fig. 7.1 and the same method used to prepare $[Pt(PMe_3)(L^1)Cl]$ were employed here. The dimer $[Pd(L^1)Cl]_2$ (0.125 g, 0.12 mmole) was placed in the 25 mL bulb. Ethanol was transferred in and the phosphine was transferred from one arm to the other. After the reaction solution was allowed to warm up with stirring, the solvent was removed leaving a yellow solid, $[Pd(PMe_3)(L^1)Cl]$. The solid was collected and washed with ether. The yield was 81%.

7.4.22 $[Pd(py)(L^1)Cl]$

$[Pd(L^1)Cl]_2$ (0.125 g, 0.12 mmole) was dissolved in $CHCl_3$ (20mL) and pyridine (24 µl, 0.30 mmole) was syringed into the solution with stirring. The solvent was removed leaving a yellow oil. Addition of $CHCl_3$, followed by hexane to the oil precipitates a creamy-yellow solid. The solid was filtered off and washed with hexane. The final yield of $[Pd(py)(L^1)Cl]$ was 53%.

7.4.23 $[Pd(SMe_2)(L^1)Cl]$

$[Pd(L^1)Cl]_2$ (0.135 g, 0.13 mmole) was taken up in acetone (30 mL) and SMe_2 (50 µl, 0.68 mmole) was syringed in with stirring. The solvent was removed to leave a yellow oil. The oil was taken up in $CHCl_3$ and the addition of hexane caused an orange solid to precipitate. This solid, $[Pd(SMe_2)(L^1)Cl]$, was filtered off and washed with hexane. The yield was 64%.

7.4.24 $[Ni(L^1)_2]$

$NiCl_2 \cdot 6H_2O$ (0.59 g, 2.48 mmole) was dissolved in ethanol (150 mL) to give a light green solution. The ligand HL^1 (2.00 g, 5.46 mmole) was dissolved in ethanol (20 mL) and added to the solution of $NiCl_2$. The solution immediately turned yellow. Ethanolic KOH (4.96 mmole) was added dropwise and the solution turned orange. The solution was left stirring for 24 hrs. The solvent was removed by rotary evaporation, leaving a green oil.

Addition of a minimal amount of ethanol to the oil yielded a green solid which was collected and washed with ethanol. The yield of $[Ni(L^1)_2]$ was 96%.

Chapter 8

Thesis Summary and Conclusions

8.1 Summary

A new hybrid ligand was prepared which combined for the first time a soft phosphino donor with a hard fluorinated alkoxide. The synthesis of this ligand, $Ph_2PCH_2C(CF_3)_2OH$, HL^1, was accomplished by the lithiation of dimethylphenylphosphine followed by nucleophilic attack of this lithiated species on hexafluoroacetone. As with previously-studied fluorinated alcohols, the presence of the highly electronegative CF_3 groups causes the alcohol to be easily deprotonated in solution, giving a bidentate, uninegative, ligand.

The versatility of this ligand was demonstrated by its ability to form complexes with both soft and hard transition metals. Hard metals such as Rh^{3+}, Co^{2+} and Ni^{2+} gave the complexes $K[Rh(L^1)_2Cl_2]$, $[Co(L^1)_2]$ and $Ni(L^1)_2]$ respectively. In the case of Cu^{2+}, oxidation occurred giving the complex $[Cu(L^1{=}O)_2]$. Complexes of softer metals such as Pt^{2+}, Pd^{2+} and Cu^{+} were also prepared. The chemistry of the $[M(L^1)_2]$ complexes, where M = Pt^{2+}, Pd^{2+} and Ni^{2+}, were investigated further.

In the case of Pt^{2+}, it was found that the ligand could also serve, in the protonated form, as a monodentate ligand coordinated to the metal through phosphorus only. As a result, a number of interconvertible Pt^{2+} complexes were prepared having either two bidentate, one bidentate, one

bidentate and one monodentate, or two monodentate L^1 (or HL^1) ligands. The ease with which complexes of monodentate HL^1 were prepared is indicative of the preference of Pt^{2+} for soft ligands. In addition, a Pt(IV) alkoxide was prepared.

The preferred geometry of these platinum complexes appeared to depend on a subtle interplay of electronic factors (antisymbiosis, preferring a geometry with cis-soft ligands) and steric factors. The steric factors were investigated by X-ray crystallography; the structures of trans-$[Pt(HL^1)_2Cl_2]$ and cis-$[Pt(L^1)_2]$ were determined.

It was found that the fluorinated alcohol substituent in HL^1 approximates a tertiary butyl group sterically and as such causes HL^1 to be a rather sterically demanding phosphine. This explains the preferred trans-geometry in complexes with two monodentate HL^1 ligands.

However, on deprotonation to give a bidentate ligand, the steric properties of L^1 change. The small bite angle and the position of the CH_3 groups on the chelate ring backbone cause L^1 to be less sterically demanding. As a result, platinum complexes of bidentate L^1 prefer a cis-geometry.

The preference of Pd^{2+} for soft ligands also allowed a complex with HL^1 to be prepared. However, because of the greater lability of Pd^{2+} over Pt^{2+}, a chloro-bridged dimer was prepared using $[Pd(L^1)_2]$. This dimer, $[(L^1)Pd(\mu\text{-}Cl)_2Pd(L^1)]$, was then cleaved with a number of

potential ligands, L', giving mixed donor complexes $[Pd(L')(L^1)Cl]$.

The crystal structure of one of these complexes, $[Pd(PPh_2Me)(L^1)Cl]$, was determined. From the Pd-Cl bond length it was proposed that the cis influence of a fluorinated alkoxide is greater than that of a chloride ion.

The complex $[Ni(L^1)_2]$ was found to exist in solution as a cis-trans mixture in a temperature- and solvent-dependent equilibrium. Thermodynamic and kinetic data for the isomerization process were determined using NMR methods. It was concluded that the isomerization occurs by an intramolecular process, going through a tetrahedral intermediate.

In going from a solution to the solid-state, $[Ni(L^1)_2]$ changes colour form orange to green while remaining diamagnetic. The cause of this colour change was investigated by a crystal structure determination. It was proposed that a close approach to the nickel atom of two CF_3 groups, one above and one below the coordinatron plane, results in a weak interaction and causes the colour change.

8.2 Conclusions

A novel hybrid ligand has been prepared which combines, for the first time, a phosphino donor site with an alkoxide donor. This combination of donor groups results in considerable versatility, as complexes of both soft and hard transition metals have been prepared.

In addition, the strong coordinating ability of the phosphine allows the fluorinated alkoxide to be protonated and removed from the metal, giving stable complexes of a monodentate phosphine with a fluorinated alcohol substituent. Complexes have been prepared where the ligand functions as a bidentate, uninegative ligand or as a monodentate phosphine. The preferred geometry of these complexes is determined by a subtle interplay of electronic and steric effects. The steric properties of both the monodentate and bidentate forms have been investigated.

The combination of a strongly-coordinating, soft donor with the hard, fluorinated alcohol has extended the coordination chemistry of both fluorinated alkoxides and functional phosphines. Further work in this area might involve the use of a different phosphino group, thus altering the steric as well as electronic properties of the ligand. Chiral phosphino-fluorinated alcohols might also be prepared. In addition, arsines or stibines might be used in place of the phosphino group.

Appendix 1. Crystallographic Computer Programs

The following is a list of the computer programs used in the crystal structure determinations of this thesis.

1. Structure Determination Package (or SDP) - SDP is a software package marketed by Enraf Nonius for the complete determination of crystal structures. It contains programs for all steps in the determination, from data reduction to ORTEP drawings.
2. AGNOST - This program is used to apply absorption corrections to data sets. It employs both Gaussian and analytical methods and was written by D. Cahen and J.A. Ibers.
3. FORDAP - FORDAP, written by A. Zalkin, calculates Patterson and Fourier syntheses.
4. PATTER - This program calculates the Patterson peaks for a given set of atomic positions. It was writen by N.C. Payne.
5. UWOLS - This program is used for full-matrix least-squares refinement of structural parameters. It will then calculate structure factors for the refined parameters. UWOLS is a local modification of the program NUCLS, written by R.J. Doedens and J.A. Ibers.
6. NUDAP - This program calculates bond distances and angles.

7. ORFFE - ORFFE calculates interatomic distances and angles along with estimated standard deviations. It was written by W.R. Busing.
8. HYDRA - This program calculates idealized hydrogen positions. It was written by J.A. Ibers.
9. LIST - This program lists both observed and calculated structure factors. It is a local modification of a program by D. Bright.
10. RBANG - This program calculates the rigid group parameters to be input into UWOLS. It was written by S.F. Watkins.
11. RANGER - This program performs a statistical analysis of R-factors and weights based on magnitudes, $\sin\theta/\lambda$, even/odd combinations of indices and phi and chi angles. The program was written by P.W.R. Corfield and modified by N.C. Payne.
12. ORTEP - This program is used to prepare a plot of the molecule or crystal. It was written by C.K. Johnson.
13. TABLE - TABLE is written by N.C. Payne and tabulates the final crystallographic data.

Each structure determined as part of this thesis employed SDP and PATTER. The determination of the structure of $[Ni(L^1)_2]$ also made use of the remaining programs.

Appendix 2. Final Atomic Positional and Thermal Parameters.

Anisotropically refined atoms are given in the form of the isotropic equivalent thermal parameters defined as:

$$(1/6\pi^2)[a^2 \cdot \beta(1,1) + b^2 \cdot \beta(2,2) + c^2 \cdot \beta(3,3) + ab(\cos\gamma) \cdot \beta(1,2) + ac(\cos\beta) \cdot \beta(1,3) + bc(\cos\alpha) \cdot \beta(2,3)]$$

Appendix 2a) Positional ($x10^4$) and Thermal ($x10^3$) Parameters for 4-1.

Atom	x	y	z	Ueq(A2)
Pt	0	0	0	32 93(4)
Cl	469 6(8)	-1701(1)	1241(1)	55 3(3)
P	972 6(7)	1265(1)	971(1)	33 0(3)
F(1)	1368(4)	5002(4)	-2510(5)	132(2)
F(2)	331(3)	4585(5)	-1402(5)	116(2)
F(3)	1318(4)	5521(5)	-512(5)	134(2)
F(4)	2627(2)	2134(4)	-916(4)	103(1)
F(5)	2625(2)	3759(5)	-2101(4)	116(1)
F(6)	2632(3)	3980(7)	-13(5)	165(2)
O	1216(2)	2400(4)	-1942(4)	70(1)
C(1)	1108(3)	2957(5)	408(5)	39(1)
C(2)	1429(3)	3271(5)	-966(5)	46(1)
C(3)	1124(4)	4585(8)	-1373(7)	94(2)
C(4)	2346(3)	3295(7)	-1009(6)	71(2)
C(21)	610(3)	1568(4)	2624(4)	34(1)
C(22)	-67(3)	2316(5)	2772(5)	46(1)
C(23)	-370(3)	2578(6)	4000(6)	56(2)
C(24)	-4(3)	2065(7)	5082(5)	65(2)
C(25)	650(4)	1282(7)	4971(5)	62(2)
C(26)	954(3)	1031(5)	3724(5)	45(1)
C(31)	1960(3)	611(5)	1128(5)	40(1)
C(32)	2512(3)	1184(6)	1958(5)	52(1)
C(33)	3279(3)	747(7)	1987(6)	67(2)
C(34)	3499(4)	-273(6)	1197(7)	77(2)
C(35)	2959(3)	-860(6)	386(6)	65(2)
C(36)	2185(3)	-427(6)	341(6)	52(1)

Appendix 2b) Positional ($x10^4$) and Thermal ($x10^3$) for 4-2.

Atom	x	y	z	Ueq(A2)
Pt	2494 8(2)	2186 8(4)	-2459 8(2)	29 05(8)
C11	7597(3)	6223(5)	4595(3)	139(2)
C12	9027(3)	5604(8)	5034(3)	189(3)
C13	8007(4)	3962(5)	4037(3)	185(3)
P1	1715(1)	560(3)	-2698(1)	34 8(7)
P2	3512(1)	1176(3)	-2281(1)	31 7(7)
F1	970(4)	4698(8)	-1835(4)	136(3)
F2	458(4)	2948(9)	-1669(4)	138(3)
F3	1575(5)	3019(11)	-1328(4)	141(4)
F4	372(5)	2914(10)	-3807(4)	137(4)
F5	-235(4)	3120(10)	-3105(6)	145(4)
F6	412(4)	4685(8)	-3268(6)	151(4)
F7	4790(3)	5089(7)	-2111(4)	85(2)
F8	3894(3)	4802(7)	-3074(3)	80(2)
F9	3823(4)	6150(6)	-2253(4)	85(2)
F10	3713(4)	5150(7)	-1021(3)	84(2)
F11	4708(4)	4229(8)	-846(4)	90(3)
F12	3810(4)	3083(7)	-868(3)	80(2)
O1	1612(3)	3320(7)	-2678(3)	49(2)
O2	3073(3)	3878(6)	-2318(3)	42(2)
C1	952(5)	1358(11)	-2566(5)	54(3)
C2	1012(5)	2872(10)	-2570(5)	40(2)
C3	4146(5)	2550(10)	-2134(5)	42(3)
C4	3800(5)	3860(10)	-2007(5)	39(2)
C5	998(7)	3400(14)	-1847(7)	84(4)
C6	386(7)	3407(14)	-3184(7)	87(4)

Appendix 2b) Cont'd.

Atom	x	y	z	Ueq(A2)
C7	4081(6)	4996(11)	-2351(5)	59(3)
C8	4010(6)	4083(11)	-1174(6)	60(3)
C9	8246(7)	5526(14)	4312(7)	91(4)
C21	1883(4)	-917(9)	-2143(4)	32(2)
C22	2079(5)	-2054(10)	-2399(5)	48(3)
C23	2242(6)	-3211(12)	-1972(6)	69(3)
C24	2188(6)	-3147(12)	-1287(6)	68(3)
C25	2000(6)	-2016(12)	-1024(6)	67(3)
C26	1836(5)	-896(11)	-1445(5)	54(3)
C31	1414(5)	-34(10)	-3630(5)	40(2)
C32	1714(5)	449(11)	-4112(5)	52(3)
C33	1476(6)	36(12)	-4846(6)	65(3)
C34	941(6)	-846(13)	-5073(6)	72(4)
C35	625(7)	-1333(13)	-4607(6)	80(4)
C36	860(5)	-926(11)	-3887(5)	56(3)
C41	3566(4)	315(9)	-3073(4)	35(2)
C42	3572(5)	1040(11)	-3678(5)	53(3)
C43	3537(6)	395(12)	-4320(6)	68(3)
C44	3520(6)	-929(13)	-4335(6)	71(4)
C45	3515(6)	-1664(12)	-3759(6)	67(3)
C46	3528(5)	-1059(11)	-3127(5)	52(3)
C51	3872(5)	65(10)	-1513(5)	39(2)
C52	3547(5)	12(11)	-990(5)	52(3)
C53	3836(6)	-788(13)	-370(6)	73(4)
C54	4426(7)	-1519(14)	-317(7)	84(4)
C55	4762(6)	-1472(13)	-814(6)	78(4)
C56	4480(6)	-636(12)	-1414(5)	61(3)

Appendix 2c) Positional ($x10^4$) and Thermal ($x10)^4$ Parameters for [Pd(PPh_2Me)(L^1)Cl].

Atom	x	y	z	U_{eq}(Å^2)
Pd	-5464(2)	18348(1)	1555(1)	310 9(5)
Cl	-2701(8)	12574(5)	-9687(4)	548(2)
P1	-5729(6)	24792(5)	12357(4)	310(2)
P2	-24328(7)	11206(5)	-102(4)	374(2)
F1	3259(2)	3135(2)	1831(1)	842(8)
F2	3606(2)	2448(2)	894(1)	839(7)
F3	2368(2)	1854(1)	1516(1)	797(7)
F4	1069(2)	4428(2)	41(1)	766(6)
F5	2868(2)	3865(2)	50(1)	766(6)
F6	2521(2)	4606(1)	979(1)	824(7)
O	1087(2)	2560(2)	208(1)	504(6)
C1	596(3)	3396(2)	1245(2)	386(7)
C2	1564(3)	3122(2)	779(2)	390(7)
C3	2715(3)	2649(2)	1255(2)	517(9)
C4	2019(3)	4006(2)	462(2)	522(9)
C5	-2546(3)	67(2)	-539(2)	600(10)
C21	-34(3)	1778(2)	2029(2)	364(7)
C22	175(3)	850(2)	1945(2)	466(8)
C23	665(4)	319(2)	2540(2)	595(10)
C24	940(4)	711(2)	3227(2)	646(10)
C25	729(3)	1621(2)	3323(2)	552(9)
C26	260(3)	2164(2)	2726(2)	451(8)
C31	-1958(2)	3104(2)	1367(2)	356(7)
C32	-2469(3)	3065(2)	1993(2)	484(8)
C33	-3522(3)	3569(3)	2045(2)	638(10)
C34	-4087(3)	4110(3)	1475(2)	678(10)
C35	-3608(3)	4157(2)	848(2)	618(10)
C36	-2543(3)	3659(2)	792(2)	456(8)
C41	-3626(3)	1876(2)	-525(2)	480(8)
C42	-4892(3)	1746(3)	-559(2)	719(11)
C43	-5778(4)	2343(3)	-946(3)	937(13)
C44	-5386(4)	3054(3)	-1319(3)	925(13)
C45	-4142(5)	3198(3)	-1303(3)	912(13)
C46	-3253(4)	2607(3)	-910(2)	632(10)
C51	-3007(3)	770(2)	796(2)	418(8)
C52	-3819(3)	1296(2)	1111(2)	545(9)
C53	-4207(4)	989(3)	1742(2)	728(11)
C54	-3778(4)	188(3)	2063(2)	785(13)
C55	-2943(4)	-333(3)	1758(2)	785(13)
C56	-2557(3)	-53(3)	1128(2)	612(10)

Appendix 2d) Positional ($x10^4$) and Thermal ($x10^3$) Parameters for $[Ni(L^1)_2]$.

Atom	x	y	z	$U_{eq}(Å^2)$[a]
Ni(1)	1071.1(7)	1267.8(4)	306.6(13)	36(1)
Ni(2)	5932.7(7)	1236.3(4)	4677.1(13)	36(1)
P(1)	2202.2(12)	1037.9(7)	173(2)	41(1)
P(2)	-70.5(11)	1473.0(7)	393(2)	43(1)
P(3)	6015.8(12)	1893.5(6)	4674(2)	39(1)
P(4)	5866.9(12)	575.7(6)	4730(2)	39(1)
F(1)	1236(4)	1701(2)	-3631(6)	111(6)
F(2)	1536(5)	1094(3)	-3417(6)	120(7)
F(3)	2383(4)	1530(3)	-3760(6)	131(7)
F(4)	1492(5)	2184(2)	-1690(8)	127(7)
F(5)	2206(4)	1973(2)	-301(7)	99(5)
F(6)	2624(5)	2068(3)	-2066(8)	148(8)
F(7)	32(5)	538(2)	1090(8)	129(7)
F(8)	-487(5)	499(3)	2841(9)	155(9)
F(9)	656(6)	376(2)	2645(10)	155(9)
F(10)	904(5)	926(3)	4286(6)	141(8)
F(11)	539(5)	1528(3)	3949(8)	150(8)
F(12)	-244(5)	1077(3)	4415(6)	145(8)
F(13)	6984(4)	1216(2)	913(6)	101(5)
F(14)	7056(5)	1855(2)	801(6)	122(6)
F(15)	6016(4)	1572(2)	1088(6)	105(3)
F(16)	7696(3)	1563(2)	4310(6)	92(5)
F(17)	8032(3)	1836(2)	2659(7)	103(6)
F(18)	7935(3)	1203(2)	2785(7)	88(5)
F(19)	4305(4)	1301(2)	7799(7)	103(5)
F(20)	3940(4)	1006(2)	6225(7)	108(6)
F(21)	4128(4)	672(2)	7818(8)	119(6)
F(22)	5539(5)	559(3)	8511(7)	133(7)
F(23)	5677(5)	1195(2)	8516(6)	117(6)
F(24)	6382(4)	833(2)	7412(7)	98(5)
O(1)	1171(4)	1421(2)	-1299(6)	56(2)
O(2)	977(4)	1126(2)	1929(6)	58(2)

Appendix 2d) continued

Atom	x	y	z	U_{eq}(Å^2)
O(3)	6450(3)	1240(2)	3234(6)	50(2)
O(4)	5360(4)	1245(2)	6063(6)	57(2)
C(1)	2452(5)	1211(3)	-1354(9)	54(3)
C(2)	1847(5)	1507(3)	-1782(9)	46(2)
C(3)	-339(6)	1304(3)	1940(10)	60(3)
C(4)	304(5)	1050(3)	2453(9)	45(2)
C(5)	6503(5)	1985(3)	3235(9)	52(2)
C(6)	6814(5)	1576(3)	2778(8)	45(2)
C(7)	5207(5)	516(3)	5968(8)	46(2)
C(8)	5176(5)	902(3)	6690(8)	43(2)
C(9)	1757(7)	1472(4)	-3180(12)	73(3)
C(10)	2051(7)	1942(4)	-1504(12)	75(3)
C(11)	126(9)	606(4)	2302(15)	92(4)
C(12)	375(9)	1175(5)	3808(14)	93(4)
C(13)	6724(6)	1550(4)	1380(11)	63(3)
C(14)	7623(6)	1551(4)	3077(11)	65(3)
C(15)	4395(6)	972(3)	7162(10)	60(3)
C(16)	5697(7)	881(4)	7814(11)	68(3)
C(21)	2892(3)	1202(2)	1264(5)	40(1)
C(22)	2676(3)	1225(2)	2483(6)	59(1)
C(23)	3180(4)	1345(2)	3370(4)	72(1)
C(24)	3899(4)	1442(2)	3039(6)	72(1)
C(25)	4115(3)	1418(2)	1820(7)	89(1)
C(26)	3611(4)	1298(2)	933(5)	67(1)
C(31)	2260(4)	499(2)	108(7)	49(1)
C(32)	1771(4)	301(3)	-665(7)	96(1)
C(33)	1787(4)	-117(3)	-749(7)	109(1)
C(34)	2292(6)	-336(2)	-61(9)	91(1)
C(35)	2781(5)	-137(3)	711(8)	126(1)
C(36)	2765(4)	280(3)	795(6)	94(1)
C(41)	-177(4)	2008(1)	432(8)	47(1)
C(42)	-818(3)	2200(2)	50(7)	75(1)
C(43)	-875(4)	2616(2)	131(8)	99(1)
C(44)	-291(5)	2840(1)	594(8)	82(1)

Appendix 2d continued

Atom	x	y	z	U_{eq}(Å^2)
C(45)	350(4)	2648(2)	976(7)	87(1)
C(46)	407(3)	2232(2)	895(7)	78(1)
C(51)	-723(3)	1298(2)	-735(6)	48(1)
C(52)	-1359(4)	1083(2)	-450(5)	68(1)
C(53)	-1832(3)	959(2)	-1377(7)	80(1)
C(54)	-1671(4)	1050(2)	-2589(6)	76(1)
C(55)	-1036(4)	1265(2)	-2874(5)	84(1)
C(56)	-562(3)	1389(2)	-1947(7)	71(1)
C(61)	5173(3)	2173(2)	4636(7)	44(1)
C(62)	4736(4)	2152(2)	5679(5)	66(1)
C(63)	4066(4)	2354(2)	5720(6)	90(1)
C(64)	3832(3)	2578(2)	4717(8)	87(1)
C(65)	4269(4)	2599(2)	3674(6)	88(1)
C(66)	4940(4)	2396(2)	3633(5)	72(1)
C(71)	6540(3)	2123(2)	5871(5)	48(1)
C(72)	6904(4)	1880(1)	6714(7)	56(1)
C(73)	7311(4)	2054(2)	7653(6)	86(1)
C(74)	7356(4)	2470(2)	7749(6)	85(1)
C(75)	6992(5)	2713(2)	6906(8)	96(1)
C(76)	6585(4)	2539(2)	5967(6)	71(1)
C(81)	6708(3)	306(2)	5662(7)	42(1)
C(82)	6749(4)	-2(2)	5962(6)	85(1)
C(83)	7414(5)	-199(2)	6165(7)	103(1)
C(84)	8039(4)	-89(3)	5507(8)	82(1)
C(85)	7998(3)	219(3)	4647(8)	110(1)
C(86)	7333(4)	416(2)	4444(6)	84(1)
C(91)	5482(4)	323(2)	3418(6)	47(1)
C(92)	5398(4)	-93(2)	3396(7)	81(1)
C(93)	5064(5)	-278(2)	2398(8)	93(1)
C(94)	4815(4)	-47(3)	1422(7)	85(1)
C(95)	4899(4)	369(2)	1444(6)	93(1)
C(96)	5233(4)	554(2)	2442(7)	75(1)

Appendix 3. Anisotropic Thermal Parameters.

The form of the thermal ellipsoid is given by:

$$\exp\{-(\beta_{11}h^2 + \beta_{22}k^2 + \beta_{33}l^2 + 2\beta_{12}hk + 2\beta_{13}hl + 2\beta_{23}kl)\}.$$

$U_{ij} = \beta_{ij} / (2\pi^2 a_i^* a_j^*)$ Å^2.

Appendix 3a) Anisotropic Thermal Parameters ($x10^3$) for 4-1.

Name	U(1,1)	U(2,2)	U(3,3)	U(1,2)	U(1,3)	U(2,3)
Pt	372 4(9)	337 9(9)	276 9(8)	29(2)	-65 5(7)	-13(1)
Cl	560(7)	488(7)	607(7)	-1(6)	-196(6)	185(6)
P	363(5)	353(5)	273(5)	26(5)	-36(4)	-14(5)
F(1)	165(4)	121(3)	112(3)	66(3)	75(2)	80(2)
F(2)	100(3)	113(3)	135(4)	46(2)	29(3)	62(3)
F(3)	250(6)	42(2)	110(4)	5(4)	18(4)	1(3)
F(4)	62(2)	121(3)	128(3)	31(2)	34(2)	57(3)
F(5)	81(2)	156(4)	110(3)	15(3)	42(2)	72(2)
F(6)	91(3)	283(6)	121(4)	-88(3)	2(3)	-63(4)
O	81(3)	82(3)	47(2)	1(2)	6(2)	-11(2)
C(1)	49(2)	34(2)	34(2)	1(2)	5(2)	-1(2)
C(2)	48(3)	51(3)	39(2)	5(2)	7(2)	2(2)
C(3)	100(4)	93(4)	92(4)	42(4)	53(3)	45(4)
C(4)	54(3)	92(5)	67(4)	2(3)	15(3)	20(4)
C(21)	37(2)	37(2)	29(2)	-6(2)	-1(2)	-2(2)
C(22)	43(2)	57(3)	39(2)	5(2)	1(2)	1(2)
C(23)	48(3)	61(3)	59(3)	4(3)	16(2)	-0(3)
C(24)	73(3)	81(4)	41(2)	-18(4)	17(2)	-2(3)
C(25)	71(3)	79(4)	37(3)	4(3)	1(3)	10(3)
C(26)	53(3)	51(3)	32(2)	-1(2)	2(2)	4(2)
C(31)	39(2)	44(2)	37(2)	2(2)	-3(2)	7(2)
C(32)	45(3)	58(3)	51(3)	-3(3)	-6(2)	4(3)
C(33)	47(3)	93(5)	59(3)	-10(3)	-15(3)	12(4)
C(34)	45(3)	98(4)	87(4)	28(3)	3(3)	42(3)
C(35)	63(3)	59(3)	73(4)	25(3)	17(3)	9(3)
C(36)	53(3)	53(3)	51(3)	9(3)	8(2)	1(3)

($x10^4$ for Pt, P and Cl atoms)

Appendix 3b) Anisotropic Thermal Parameters ($x10^3$) for 4-2.

Name	U(1,1)	U(2,2)	U(3,3)	U(1,2)	U(1,3)	U(2,3)
Pt	271(1)	269(2)	359(1)	23(2)	143(1)	12(2)
C11	154(3)	125(4)	141(3)	48(3)	54(3)	34(3)
C12	105(3)	309(8)	133(4)	-37(4)	13(3)	42(4)
C13	344(7)	93(3)	130(3)	17(4)	97(3)	-16(3)
P1	30(1)	33(1)	45(1)	-1(1)	16 5(8)	-3(1)
P2	28(1)	27(1)	43(1)	3(1)	15 7(8)	1(1)
F1	175(6)	94(5)	178(5)	-32(5)	111(4)	-74(4)
F2	171(4)	125(7)	188(4)	-34(5)	53(3)	-57(4)
F3	146(7)	217(10)	57(4)	-39(7)	29(4)	-21(5)
F4	142(8)	194(8)	79(5)	-28(7)	-26(5)	15(5)
F5	34(4)	129(7)	261(10)	13(5)	34(5)	26(7)
F6	77(5)	87(6)	235(10)	24(5)	-7(6)	60(6)
F7	46(3)	86(5)	125(5)	-26(3)	29(3)	15(4)
F8	87(4)	80(5)	78(3)	-10(4)	33(3)	29(3)
F9	97(4)	35(4)	133(5)	-1(3)	52(3)	18(4)
F10	113(5)	67(4)	67(3)	27(4)	27(3)	-12(3)
F11	66(4)	109(6)	70(4)	-11(4)	-9(4)	-19(4)
F12	133(5)	67(4)	54(3)	0(4)	47(3)	5(3)
O1	35(3)	45(4)	74(3)	6(3)	29(2)	3(3)
O2	38(3)	25(4)	67(3)	-1(3)	22(2)	7(3)

($x10^4$ for Pt atom)

Appendix 3c) Anisotropic Thermal Parameters ($x10^3$) for $[Pd(PPh_2Me)(L^1)Cl]$.

Atom	U(1,1)	U(2,2)	U(3,3)	U(1,2)	U(1,3)	U(2,3)
Pd	3853(8)	3049(9)	2816(9)	-101(9)	848(7)	-486(8)
Cl	821(5)	485(4)	409(3)	-120(4)	294(3)	-140(3)
P1	328(3)	307(3)	297(3)	8(3)	67(3)	-62(3)
P2	408(4)	361(4)	344(3)	-63(3)	54(3)	-42(3)
F1	60(1)	107(2)	74(1)	4(1)	-15(1)	-14(1)
F2	48 5(9)	105(2)	106(1)	27(1)	34 1(9)	12(1)
F3	60(1)	63(1)	120(2)	17(1)	28(1)	33(1)
F4	73(1)	78(1)	83(1)	17(1)	24(1)	34(1)
F5	70(1)	78(1)	96(1)	-4(1)	49 6(9)	13(1)
F6	100(1)	55(1)	95(1)	-35(1)	23(1)	-14(1)
O	43(1)	62(1)	50(1)	-1(1)	20 5(8)	-22(1)
C1	36(1)	35(1)	45(1)	-1(1)	9(1)	-9(1)
C2	35(1)	40(1)	44(1)	-4(1)	11(1)	-7(1)
C3	38(1)	56(2)	62(2)	-4(1)	12(1)	-2(2)
C4	46(2)	60(2)	63(2)	-6(1)	17(1)	2(2)
C5	72(2)	50(2)	61(2)	-20(2)	18(2)	-21(2)
C21	40(1)	36(1)	33(1)	4(1)	6(1)	-2(1)
C22	58(2)	37(1)	43(2)	3(1)	4(1)	-6(1)
C23	82(2)	39(2)	56(2)	11(2)	8(2)	5(2)
C24	85(2)	56(2)	47(2)	13(2)	-1(2)	12(2)
C25	70(2)	59(2)	32(1)	10(2)	-1(1)	-4(1)
C26	57(2)	40(1)	36(1)	5(1)	3(1)	-7(1)
C31	31(1)	32(1)	44(1)	-4(1)	8(1)	-9(1)
C32	44(1)	55(2)	49(2)	-1(1)	16(1)	-5(1)
C33	50(2)	73(2)	77(2)	2(2)	33(1)	-13(2)
C34	40(1)	64(2)	104(3)	9(2)	26(2)	-10(2)
C35	43(2)	56(2)	84(2)	11(2)	7(2)	12(2)
C36	41(1)	44(2)	52(2)	0(1)	9(1)	0(1)
C41	52(2)	51(2)	36(1)	-2(2)	-2(1)	-6(1)
C42	52(2)	72(2)	82(3)	-4(2)	-11(2)	9(2)
C43	60(2)	96(3)	109(3)	8(2)	-24(2)	4(3)
C44	94(3)	82(3)	83(3)	18(2)	-28(2)	5(2)
C45	114(3)	77(3)	74(3)	7(3)	-8(3)	25(2)
C46	71(2)	63(2)	51(2)	2(2)	1(2)	10(2)
C51	37(1)	44(1)	44(1)	-8(1)	7(1)	-1(1)
C52	55(2)	56(2)	54(2)	-6(2)	15(1)	1(2)
C53	77(2)	86(3)	83(2)	-3(2)	30(2)	-2(2)
C54	94(3)	86(3)	59(2)	-18(2)	26(2)	14(2)
C55	101(3)	69(2)	67(2)	1(2)	18(2)	24(2)
C56	88(2)	61(2)	57(2)	7(2)	19(2)	11(2)

Values for Pd x 10^5, for Cl and P x 10^4

Appendix 3d. Anisotropic Thermal Parameters ($x10^3$) $Å^2$ for $[Ni(L^1)_2]$.

Atom	U(1,1)	U(2,2)	U(3,3)	U(1,2)	U(1,3)	U(2,3)
N11	29(1)	45(1)	34(1)	4(1)	3(1)	4(1)
N12	36(1)	34(1)	38(1)	2(1)	9(1)	-2(1)
P1	35(1)	47(1)	39(1)	7(1)	5(1)	3(1)
P2	33(1)	54(1)	43(1)	6(1)	6(1)	1(1)
P3	40(1)	34(1)	44(1)	3(1)	8(1)	0(1)
P4	39(1)	36(1)	43(1)	2(1)	5(1)	-1(1)
F1	114(6)	173(8)	46(4)	54(6)	-5(4)	40(5)
F2	149(8)	149(8)	63(5)	19(6)	-28(5)	-30(5)
F3	117(6)	214(10)	63(4)	46(7)	48(5)	44(6)
F4	189(9)	72(5)	120(7)	43(6)	-14(7)	19(5)
F5	137(7)	75(4)	86(5)	-27(4)	-8(6)	-20(4)
F6	176(9)	149(8)	118(7)	-97(7)	43(7)	20(6)
F7	170(9)	113(6)	105(6)	-40(6)	-4(7)	-43(5)
F8	165(9)	133(7)	167(9)	-95(7)	35(8)	24(7)
F9	197(10)	82(6)	187(10)	24(6)	-20(9)	43(7)
F10	141(8)	230(10)	53(4)	40(8)	-9(5)	-3(6)
F11	181(10)	138(8)	130(8)	-52(7)	6(7)	-84(7)
F12	117(7)	256(11)	63(5)	10(7)	52(5)	-3(6)
F13	119(6)	123(6)	62(4)	4(5)	30(4)	-31(4)
F14	154(8)	115(6)	67(5)	-11(6)	46(5)	27(4)
F15	92(5)	160(7)	62(4)	18(6)	-11(4)	-7(5)
F16	61(4)	132(6)	83(5)	13(4)	-20(4)	-5(5)
F17	56(4)	109(6)	144(7)	-20(4)	17(5)	31(5)
F18	51(4)	89(5)	122(6)	20(3)	30(4)	4(5)
F19	84(5)	100(5)	125(6)	-12(4)	54(5)	-57(5)
F20	65(4)	131(6)	128(7)	27(5)	-17(5)	-30(6)
F21	91(5)	109(6)	158(8)	-20(5)	76(6)	13(6)
F22	180(9)	139(7)	79(5)	-5(7)	-36(6)	46(5)
F23	164(8)	123(6)	64(5)	15(6)	-35(5)	-36(5)
F24	66(4)	133(6)	95(5)	7(4)	-16(4)	-20(5)

Appendix 4. Hydrogen Atom Positional and Thermal Parameters.

Appendix 4a) Hydrogen Atom Positional ($x10^4$) and Thermal ($x10^3$) Parameters for 4-1.

H0	1420	1545	-2024	83
H1C1	1460	3353	1016	43
H2C1	605	3360	461	43
HC22	-326	2653	2016	51
HC23	-825	3106	4092	61
HC24	-205	2254	5928	71
HC25	891	918	5729	69
HC26	1402	485	3636	50
HC32	2359	1882	2508	57
HC33	3656	1147	2550	73
HC34	4030	-572	1215	84
HC35	3117	-1567	-149	71
HC36	1811	-835	-221	58

Appendix 4b) Hydrogen Atom Positional ($x10^4$) and Thermal ($x10^3$) Parameters for 4-2.

Atom	x	y	z	Ueq(A2)
HC9	8305	5979	3910	100
H1C1	922	1086	-2112	59
H2C1	535	1096	-2947	59
H1C3	4287	2642	-2550	46
H2C3	4550	2366	-1720	46
HC22	2107	-2067	-2875	53
HC23	2382	-4000	-2149	75
HC24	2286	-3915	-990	75
HC25	1981	-2000	-544	74
HC26	1692	-116	-1264	59
HC32	2089	1073	-3950	57
HC33	1690	375	-5177	72
HC34	782	-1131	-5566	80
HC35	247	-1947	-4778	89
HC36	641	-1260	-3541	62
HC42	3599	1976	-3653	58
HC43	3526	883	-4740	74
HC44	3512	-1367	-4768	78
HC45	3501	-2600	-3792	73
HC46	3511	-1572	-2725	57
HC52	3131	513	-1048	57
HC53	3627	-820	0	81
HC54	4609	-2089	90	93
HC55	5174	-1988	-757	85
HC56	4717	-554	-1760	67

Appendix 4c. Hydrogen Atom Positional ($x10^4$) and Thermal ($x10^3$) Parameters for [Pd(PPh_2Me)(L^1)Cl].

Atom	x	y	z	Ueq(A^2)
H1C5	-3388	-152	-617	73
H2C5	-2314	186	-994	73
H3C5	-1994	-377	-277	73
H1C1	1020	3501	1733	42
H2C1	178	3941	1052	42
HC22	-22	580	1473	51
HC23	813	-314	2479	65
HC24	1281	342	3637	71
HC25	904	1879	3798	61
HC26	136	2800	2790	50
HC32	-2087	2688	2389	53
HC33	-3860	3540	2477	70
HC34	-4815	4454	1514	75
HC35	-4006	4530	452	68
HC36	-2206	3696	359	50
HC42	-5168	1238	-313	79
HC43	-6649	2255	-951	103
HC44	-5991	3454	-1593	102
HC45	-3878	3701	-1559	100
HC46	-2382	2703	-903	70
HC52	-4114	1866	899	60
HC53	-4780	1348	1949	80
HC54	-4046	-13	2491	86
HC55	-2629	-891	1985	87
HC56	-1988	-418	923	67

Appendix 4d. Hydrogen Atom Positional ($\times 10^4$) and Thermal ($\times 10^3$) Parameters for $[Ni(L^1)_2]$.

Atom	x	y	z	U(Å^2)
H1C22	2211	1163	2697	64
H1C23	3041	1360	4158	78
H1C24	4225	1519	3612	78
H1C25	4580	1480	1606	98
H1C26	3750	1283	145	74
H1C32	1444	442	-1110	105
H1C33	1471	-245	-1248	119
H1C34	2303	-606	-115	100
H1C35	3108	-279	1157	138
H1C36	3081	409	1295	103
H1C42	-1196	2055	-250	82
H1C43	-1290	2740	-117	108
H1C44	-327	3109	646	89
H1C45	728	2793	1275	95
H1C46	822	2107	1142	85
H1C52	-1463	1024	334	74
H1C53	-2243	820	-1192	87
H1C54	-1977	970	-3188	83
H1C55	-931	1324	-3657	92
H1C56	-151	1528	-2131	77
H1C62	4887	2007	6327	72
H1C63	3783	2341	6395	98
H1C64	3399	2709	4744	96
H1C65	4118	2744	3026	96
H1C66	5222	2410	2959	78
H1C72	6875	1611	6652	61
H1C73	7546	1897	8198	94
H1C74	7619	2583	8356	93
H1C75	7021	2983	6968	105
H1C76	6350	2696	5422	78
H1C82	6345	-73	6387	93

Appendix 4d Cont'd Hydrogen Atom Positional ($\times 10^4$) and Thermal ($\times 10^3$) Parameters (continued)

Atom	x	y	z	U(Å²)
H1C83	7440	-398	6720	112
H1C84	8469	-236	5638	89
H1C85	8402	290	4222	121
H1C86	7306	615	3889	92
H1C92	5559	-242	4028	88
H1C93	5010	-546	2384	102
H1C94	4599	-166	776	93
H1C95	4738	519	812	101
H1C96	5288	823	2456	83
H1C1	2915	1343	-1331	59
H2C1	2478	989	-1897	59
H1C3	-425	1529	2452	66
H2C3	-774	1145	1897	66
H1C5	6173	2093	2647	56
H2C5	6896	2169	3364	56
H1C7	4734	458	5641	50
H2C7	5357	302	6485	50

Atoms H1C7 and H2C7 are bonded to C7, and so forth.

Appendix 5. Phenyl Ring Rigid Group Parameters for $[Ni(L^1)_2]$.

Group	x_g	y_g	z_g	δ	ϵ	η	B
Ph20	3395(3)	1321.8(11)	2152(4)	1.982(6)	2.370(4)	1.381(6)	4.79(9)
Ph30	2276(3)	82(2)	23(5)	0.021(5)	-3.075(5)	-2.415(5)	6.73(12)
Ph40	-234(3)	2423.9(14)	513(4)	-3.067(4)	3.078(5)	-0.395(5)	5.94(11)
Ph50	-1197(3)	1174.1(12)	-1662(4)	-1.124(6)	-2.325(4)	1.448(7)	5.28(10)
Ph60	4503(3)	2375.3(13)	4677(5)	-2.077(4)	3.110(5)	1.192(4)	5.49(10)
Ph70	6948(3)	2296.7(15)	6810(4)	2.234(7)	2.311(4)	2.615(7)	5.32(10)
Ph80	7373(3)	108.4(15)	5304(5)	1.073(5)	2.982(5)	2.369(5)	6.18(11)
Ph90	5149(2)	138(2)	2420(5)	-0.778(7)	-2.239(5)	0.774(7)	5.71(11)

x_g, y_g, and z_g are the fractional coordinates ($x10^4$) of the group origin, and δ, ϵ and η (radians) the group orientation angles, and B the overall group thermal parameter, see ref. 20. Carbon atoms C21 through C26 form ring Ph20, and so forth.

Appendix 6. Observed and Calculated Structure Factors

($10|F_o|$ vs. $10|F_c|$ in electrons, on enclosed microfiche)

REFERENCES

1. C. Ettling, Ann. Chem. Pharm. (1840) 35, 241.
2. J.V. Dubsky and A. Sokól, Collection Czech. Chem. Commun. (1931) 3, 548.
3. S. Ahrland, J. Chatt and N.R. Davies, Quart. Rev. (London) (1958) 12, 265.
4. R.G. Pearson, J. Am. Chem. Soc. (1963) 85, 3533.
5. M.E. Redwood and C.J. Willis, Can. J. Chem. (1965) 43, 1893.
6. M.E. Redwood and C.J. Willis, Can. J. Chem. (1967) 45, 389.
7. D.A. Johnson, J.C. Taylor and A.B. Waugh, J. Inorg. Nucl. Chem. (1980) 42, 1271.
8. P.G. Eller and P.J. Vergamini, Inorg. Chem. (1983) 22, 3184.
9. R. Puller and R. Schure, J. Org. Chem. (1967) 32, 1217.
10. W.S. Cripps and C.J. Willis, Can. J. Chem. (1975) 53, 809.
11. M. Allan and C.J. Willis, J. Am. Chem. Soc. (1968) 90, 5343.
12. C.J. Willis, J. Chem. Soc. Chem. Commun. (1972) 944.
13. R.T. Boeré and C.J. Willis, Inorg. Chem. (1985) 24, 1059.
14. J.W.L. Martin and C.J. Willis, Can. J. Chem. (1977) 55, 2459.
15. S.J. Loeb, J.R. Richardson and C.J. Willis, Inorg.

Chem. (1983) 22, 2736.

16. E. Konefal, S.J. Loeb, D.W. Stephan and C.J. Willis, Inorg. Chem. 23, 538.

17. a) R.T. Boeré and C.J. Willis, Can. J. Chem. (1985) 63, 3530, b) R.T. Boeré and C.J. Willis, Can. J. Chem, (in press), c) R.T. Boeré, N.C. Payne and C.J. Willis, Can. J. Chem. (in press).

18. R.T. Boeré, W. M. Brown, D.W. Stephan and C.J. Willis, Inorg. Chem. (1985) 24 , 593.

19. R. Uriarate, T.J. Mazanec, K.D. Tau and D.W. Meek, Inorg. Chem. (1980) 19, 79.

20. J.P. Farr, M.M. Olmstead and A.L. Balch, J. Am. Chem. Soc. (1980) 102, 6654.

21. D.M. Roundhill, R.A. Bechtold and S.G.N. Roundhill, Inorg. Chem. (1980) 19, 284.

22. B.D. Dombek, J. Organomet. Chem. (1979) 169, 315.

23. G.K. Anderson and R. Kumar, Inorg. Chem. (1984) 23, 4064.

24. J.C. Jeffrey and T. Rauchfuss, Inorg. Chem. (1979) 18, 2658.

25. E.M. Miller and B.L. Shaw, J. Chem. Soc., Dalton Trans. (1974) 480.

26. C.E. Jo[redacted].L. Shaw and B.L. Turtle, J. Chem. Soc., Dalton Trans. (1974) 992.

27. K.H.P. O'Flynn and W.S. McDonald, Acta Cryst. (1977) B33, 194.

28. H.D. Empsall, B.L. Shaw and B.L. Turtle, J. Chem.

Soc., Dalton Trans. (1976) 1500.

29. H.D. Empsall, E.M. Hyde, C.E. Jones and B.L. Shaw, J. Chem. Soc., Dalton Trans. (1974) 1980.

30. H.D. Empsall, E.M. Hyde and B.L. Shaw, J. Chem. Soc., Dalton Trans (1975) 1690.

31. H.D. Empsall, P.N. Heys, W.S. McDonald, M.C. Norton and B.L. Shaw, J. Chem. Soc., Dalton Trans. (1978) 1119.

32. T.B. Rauchfuss, J. Am. Chem. Soc. (1979) 101, 1045.

33. H.D. Empsall, S. Johnson and B.L. Shaw, J. Chem. Soc., Dalton Trans. (1980) 302.

34. C.J. Moulton and B.L. Shaw, J. Chem. Soc., Dalton Trans. (1980) 299.

35. H.D. Empsall, E.M. Hyde, D. Pawson and B.L. Shaw, J. Chem. Soc., Dalton Trans. (1977) 1292.

36. P. Braunstein, D. Matt, Y. Dusausoy, J. Fischer, A. Mitschler and L. Ricard, J. Am. Chem. Soc. (1981) 103, 5115.

37. P. Braustein, D. Matt and Y. Dusausoy, Inorg. Chem. (1983) 22, 2043.

38. A.F. Borowski, D.J. Cole-Hamilton and G. Wilkinson, Nouv. J. Chim. (1978) 2, 137.

39. T. Jarolim and J. Podlahová, J. Inorg. Nucl. Chem. (1976) 38, 125.

40. J. Podlahová, J. Loub and J. Ječný, Acta. Cryst. (1979) B35, 328.

41. J. Pangrác and J. Podlahová, Collection Czech. Chem.

Commun. (1981) 46, 1222.

42. A. Jegorov, B. Kratochvil, V. Langer and J. Podlahová, Inorg. Chem. (1984) 23, 4288.

43. J. Ludvik and J. Podlahová, J. Inorg. Nucl. Chem. (1978) 40, 1045.

44. J. Podlahová, B. Kratochvil and V. Langer, Inorg. Chem. (1981) 20, 2160.

45. D. Nosková and J. Podlahová, Polyhedron (1983) 2, 349.

46. M. Etienne, R. Choukroun and D. Gervais, J. Chem. Soc., Dalton Trans. (1984) 915.

47. G.W. Parshall, "Homogeneous Catalysis", John Wiley and Sons: New York, (1980) p. 58.

48. R.S. Bauer, H. Chung, P.W. Glockner and W. Keim. U.S. Patent 3,655,563 (1972); R.M. Mason. U.S. Patent 3,737,475 (1973).

49. W.S. Knowles and M.J. Sabacky. U.S. Patent 3,849,480 (1974).

50. B.D. Vineyard, W.S. Knowles, M.J. Sabacky, G.L. Bachman and D.J. Weinkauff, J. Am. Chem. Soc. (1977) 99, 5946.

51. C.G. Krespan and W.J. Middleton, Fluorine Chem. Rev. (1967) 1, 145.

52. D.P. Graham and V. Weinmayr, J. Org. Chem. (1966) 31, 2047.

53. I.S. Chang, J.T. Price, A.J. Tomlinson and C.J. Willis, Can. J. Chem. (1972) 50, 512.

54. R. Fillen and R.M. Schure, J. Org. Chem. (1967) 32,

1217.

55. R.T. Boere, Ph.D. thesis, University of Western Ontario (1984).

56. D.J. Peterson, J. Organomet. Chem. (1967) 8, 199.

57. G.G. Eberhardt and W.A. Butte, J. Org. Chem. (1964) 29, 2928.

58. D.J. Peterson and J.H. Collins, J. Org. Chem. (1966) 31, 2373.

59. D.J. Peterson and H.R. Hays, J. Org. Chem. (1965) 30, 1939.

60. D.P. Craig, A. Maccoll, R.S. Nyholm, L.E. Orgel and L.E. Sutton, J. Chem. Soc. (1954) 332.

61. F. Ramirez, C.P. Smith, J.F. Pilot and A.S. Gilati, J. Org. Chem. (1968) 33, 3738.

62. J.P. van Linthadt, E.V. van den Berghe and G.P. van der Kelen, Spectrochimica Acta (1979) 35A, 1307.

63. J.B. Hendrickson, M.L. Maddox, J.J. Sims and H.D. Kaesz, Tetrahedron (1964) 20, 449.

64. F.A. Cotton and G. Wilkinson, "Advanced Inorganic Chemistry: A Comprehensive Text", 4th Ed., Interscience Publishing, New York (1980) p. 769.

65. A.B.P. Lever, "Inorganic Electronic Spectroscopy", 2nd Ed., Elsevier, Amsterdam (1984) p. 496.

66. A.A.G. Tomlinson, C. Bellitto, O. Piovesana and C. Furlani, J. Chem. Soc., Dalton Trans. (1972) 76, 350.

67. H.F. Wasgestian, J. Chem. Phys. (1972) 76, 1947.

68. M. Goodgame, D.M.L. Goodgame and F.A. Cotton, Inorg.

Chem. (1962) 1, 239.

69. L. Sacconi, I. Bertini and F. Mani, Inorg. Chem. (1967) 6, 262.

70. H.V. Rahman and W.A. Runciman, J. Phys. C: Solid St. Phys. (1971) 4, 1576.

71. A. Muller, P. Christophliemk and I. Tossidis, J.Mol. Struct. (1973) 15, 289.

72. D.P. Rillema, J.F. Endicott and E. Papaconstantinov, Inorg. Chem. (1971) 10, 1739.

73. F.L. Urbach, R.D. Bereman, J.A. Topich, M. Harihan and B.J. Kalbacher, J. Am. Chem. Soc. (1974) 96, 5063.

74. A.B.P. Lever, "Inorganic Electronic Spectroscopy", Elsevier, Amsterdam (1968) p. 328.

75. H. Sigel and D.B. McCormick, Acc. Chem. Res. (1970) 3, 201.

76. D.D. Axtell and J.T. Yoke, Inorg. Chem. (1973) 12, 1265.

77. G. Ondrejovic, D. Makanova, D. Valigura and J. Gazo, Z. Chem. (1973) 13, 193.

78. F. Leh and K.M. Chan, Bull. Chem. Soc. Jap. (1972) 45, 2709.

79. G. Costa, A. Camus and N. Marisch, J. Inorg. Nucl. Chem. (1965) 27, 281.

80. T. Tsuda, T. Hashimoto and T. Saegusa, J. Am. Chem. Soc. (1972) 94, 658.

81. G.M. Whitesides, J. Sadowski and J. Lilburn, J. Am. Chem. Soc. (1974) 96, 2829.

82. H. Schmidbauer, J. Aldkofer and K. Schwirten, Chem. Ber. (1972) 105, 2985.

83. S.J. Lippard and J.J. Mayerle, Inorg. Chem. (1972) 11, 753.

84. J.T. Gill, J.J. Mayerle, P.S. Welcker, D.F. Lewis, D.A. Ucko, D.J. Barton, D. Stowens, S.J. Lippard, Inorg. Chem. (1976) 15, 1155.

85. D.D. Axtell and J.T. Yoke, Inorg. Chem. (1973) 12, 1265.

86. B.E. Mann, C. Masters, B.L. Shaw, R.M. Slade and R.E. Stainbank, Inorg. Nucl. Chem. Letters (1971) 7, 881.

87. G. Bracher, D.M. Grove, L.M. Venanzi, P. Bachechi, P. Mura and L. Zambonelli, Helv. Chim. Acta. (1980) 63, 2519.

88. P.E. Garrou, Inorg. Chem. (1975) 14, 1435.

89. B.E. Mann, C. Masters and B.L. Shaw, J. Chem. Soc., Dalton Trans. (1972) 704.

90. R.C. Mehrotra, Adv. Inorg. Chem. Radiochem. (1983) 26, 287.

91. W.S. Cripps and C.J. Willis, Can. J. Chem. (1975) 53, 817.

92. J.W.L. Martin, N.C. Payne and C.J. Willis, Inorg. Chem. (1978) 17, 3478.

93. D. Nichols, "Comprehensive Inorganic Chemistry" Vol. 3, J.C. Bailar, H.J. Emeléus, R. Nyholm and A.F. Trotman-Dickenson, Editors, Pergamon Press, Oxford (1973) pp. 1142-43.

94. C.S. Chamberlain and R.S. Drago, Inorg. Chim. Acta (1979) 32, 75.

95. F.L. Urbach and D.H. Busch, Inorg. Chem. (1973) 12, 408.

96. J.R. Ferraro and A.T. Sherren, Inorg. Chem. (1978) 17, 2498.

97. R.S. Drago, "Physical Methods in Chemistry" W.B. Saunders Co., Philadelphia (1977) p. 255.

98. G.R. Van Kecke and W.D. Horrocks, Jr., Inorg. Chem. (1966) 5, 1968.

99. C.R. Coussmaker, M.H. Hutchinson, J.R. Mellor, L.E. Sutton and L.M. Venanzi, J. Chem. Soc. (1961) 2705.

100. G.N. La Mar and E.O. Sherman, J. Am. Chem. Soc. (1970) 92, 2691.

101. A.B.P. Lever "Inorganic Electronic Spectroscopy" 2nd Ed., Elsevier Amsterdam (1984) p. 530.

102. M. Goodgame, D.M.L. Goodgame and F.A. Cotton, J. Am. Chem. Soc. (1961) 83, 4161.

103. M.I. Ban, J. Czaszar and M. Hegyhati, J. Mol. Struct. (1973) 19, 455.

104. P.J. Stone and Z. Dori, Inorg. Chim. Acta (1971) 5, 434.

105. A.B.P. Lever, "Inorganic Electronic Spectroscopy", Elsevier, Amsterdam (1968) p. 343.

106. A.B.P. Lever, "Inorganic Electronic Spectroscopy", 2nd Ed., Elsevier, Amsterdam (1984) pp. 534-542.

107. R.G. Hayter and F.S. Humiec, Inorg. Chem. (1965) 4,

1701.

108. A.B.P. Lever, J. Lewis and R.S. Nyholm, J. Chem. Soc. (1963) 2552.

109. J. Chatt and R.G. Wilkins, J. Chem. Soc. (1952) 273 and 4300.

110. R.G. Pearson, Inorg. Chem. (1973) 12, 712.

111. G. Salem and S.B. Wild, Inorg. Chem. (1984) 23, 2655.

112. O. Steltzer and E. Unger, J. Chem. Soc. (1973) 1783.

113. J.R. Majer and K. Al-Kuwarty, Proc. Analyt. du. Chem. Soc. (1978) 15, 98.

114. R.A. Palmer and D.R. Whitcomb, J. Mag. Resonance (1980) 39, 371.

115. R.S. Drago "Physical Methods in Chemistry", W.B. Saunders Co., Philadelphia (1977) pp. 257-259.

116. H. Shanan-Atida and K.H. Bar-Eli, J. Phys. Chem. (1970) 74, 961.

117. J. Sandstrom, "Dynamic NMR Spectroscopy", Academic Press, New York, (1982) pp. 81-84.

118. H. Eyring, Chem. Revs. (1935) 17, 65.

119. W. Egan, Thesis, Princeton University (1971).

120. F. Basolo and R.G. Pearson, "Mechanisms of Inorganic Reactions", Wiley Interscience, New York (1958) p. 252.

121. J.M. Jenkins and B.L. Shaw, J. Chem. Soc. A (1966) 770.

122. R.K. Harris, Can. J. Chem. (1964) 42, 2275.

123. F.B. Ogilvie, J.M. Jenkins and J.G. Verkade, J. Am.

Chem. Soc. (1970) 92, 1916.

124. W.R. Cullen, J.R. Sams and J.A.J. Thompson, Inorg. Chem. (1971) 10, 843.

125. L.M. Haines, Inorg. Chem. (1971) 10 1685 and 1693.

126. G.M. Bancroft and E.T. Libbey, Can. J. Chem. (1973) 51, 1482.

127. M. Wada and K. Sameshima, J. Chem. Soc., Dalton Trans. (1981) 240.

128. D.M.L. Goodgame and M. Goodgame, J. Chem. Soc. (1963) 207.

129. S. Buffagni, L.M. Vallarino and J.V. Quagliano, Inorg. Chem. (1964) 3, 480.

130. A.B.P. Lever, J. Lewis and R.S. Nyholm, J. Chem. Soc. (1963) 5042.

131. A.B.P. Lever, J. Inorg. Nucl. Chem. (1965) 27, 149.

132. International Tables for X-ray Crystallography, Vol. I, Kynoch Press, Birmingham (1962) p. 105.

133. Structure Determination Package, 4th Ed. (1981) Copyright 1982; B.A. Frenz & Associates Inc., College Station, Texas and Enraf/Nonius, Holland.

134. The computer programs used in the refinement include local modifications of the following: full-matrix least-squares, J.A. Ibers' NUCLS; Patterson and Fourier synthesis, A. Zalkin's FORDAP; function and errors, W.R. Busing, K.O. Martin and H.E. Levy's ORFFE; crystal structure illustrations, C.K. Johnston's ORTEP; absortpioncorrection by Gaussian

numerical methods in the program AGNOST as modified by D. Cohen and J.A. Ibers, J. Appl. Crystallogr. (1972) 5, 298.

135. D.T. Cromer and J.T. Waber, Acta. Cryst. (1965) 18, 104.

136. R.F. Stewart, E.R. Davidson and W.T. Simpson, J. Chem. Phys. (1965) 42, 3175.

137. D.T. Cromer and J. Liberman, J. Chem. Phys. (1970) 53, 1891.

138. W. Mendenhall, "Introduction to Statistics", Wadsworth, Belmont, Cal., (1963) pp. 197-205.

139. M.R. Fox, E.C. Lingafelter and L. Sacconi, Acta Cryst. (1964) 17, 1159.

140. S.J. Loeb, D.W. Stephan and C.J. Willis, Inorg. Chem. (1984) 23, 1509.

141. R.T. Boeré, N.C. Payne and C.J. Willis, Can. J. Chem. (in press).

142. S.K. Stalick and J.A. Ibers, Inorg. Chem. (1970) 9, 453.

143. G.R. Davies, R.H.B. Mais and R.G. Owston, J. Chem. Soc. (1967) 1750.

144. V. Scatturum and A. Turzo, J. Inorg. Nuc. Chem. (1958) 8, 447.

145. D.E.C. Corbridge, "The Structural Chemistry of Phosphorus", Elsevier, Amsterdam (1974) p. 309.

146. D.J. Watkin, J. Chem. Soc., Dalton Trans. (1976) 1803.

147. A.T. McPhail and J.C.M. Steele, J. Chem. Soc. A (1972)

2680.

148. R.A. Palmer, H.F. Giles and D.R. Whitcomb, J. Chem. Soc., Dalton Trans. (1978) 1671.

149. B.L. Barnett and C. Kruger, J. Organomet. Chem. (1972) 42, 169.

150. M.D. Fryzuk, P.A. MacNeil, S.J. Rettig, A.S. Secco and J. Trotter, Organometallics (1982) 1, 918.

151. A. Bondi, J. Phys. Chem. (1964) 68, 441.

152. C.J. Ballhausen and A.D. Liehr, J. Am. Chem. Soc. (1959) 81, 538.

153. D.M.L. Goodgame and L.M. Venanzi, J. Chem. Soc. (1963) 616.

154. C.M. Harris, R.S. Nyholm and D.J. Phillips, J. Chem. Soc. (1960) 4379.

155. J.G. Verkade and T.S. Piper, Inorg. Chem. (1963) 2, 944.

156. S.L. Holt and R.L. Carlin, J. Am. Chem. Soc. (1964) 86, 3017.

157. B. Bosnich, M.L. Tobe and G.A. Webb, Inorg. Chem. (1965) 4, 1109.

158. J.L. Karn and D.H. Busch, Nature (1966) 211, 160.

159. S.S. Sandhu, S. Baiveja and S.S. Parmer, Transition Met. Chem. (1980) 5, 299.

160. K. Issleib and G. Doll, Z. Anorg. Allgem. Chem. (1960) 305, 1.

161. N.C. Stephenson and G.A. Jeffrey, Proc. Chem. Soc. (1963) 173.

162. "International Tables for X-ray Crystallography" Vol. 1, Kynoch Press, Birmingham (1962) p. 99.

163. J.A. Ibers and W.C. Hamilton, Acta. Cryst. (1964) 17, 781.

164. S.J. Loeb, D.W. Stephan and C.J. Willis, Inorg. Chem. (1984) 23, 1509.

165. L.L. Martin and R.A. Jacobson, Inorg. Chem. (1971) 10, 1795.

166. S. Civiš, J. Podlahová, J. Loub and J. Ječný, Acta Cryst. (1980) B36, 1395.

167. Y.K. Syrkin, Bull. Acad. Sci. U.S.S.R. (1948) 69.

168. F.H. Allen and S.N. Sze, J. Chem. Soc. Part A (1971) 2054 and references therein.

169. Cambridge Crystallographic Database, 1985 edition, Crystallographic Data Centre, University Chemical Laboratory, Lensfield Road, Cambridge, England.

170. A.J. Carty, S.E. Jacobson, R.T. Simpson and N.J. Taylor, J. Am. Chem. Soc. (1975) 97, 7254.

171. H.D. Empsall, E.M. Hyde, E. Mentzer and B.L. Shaw, J. Chem. Soc., Dalton Trans. (1977) 2285.

172. H.D. Empsall, M. Green and F.G.A. Stone, J. Chem. Soc., Dalton Trans. (1972) 96.

173. B.R. Penfold, Personal communication.

174. C.G. Pierpont and H.H. Downs, Inorg. Chem. (1975) 14, 343.

175. A.R. Siedle and L.H. Pignolet, Inorg. Chem. (1982) 21, 3090.

176. S. Okeya, T. Miyamoto, S. Ooi, Y. Nakamura and S. Kawaguchi, Inorg. Chim. Acta (1980) 45, L135.

177. G. Booth, Adv. Inorg. Radiochem. (1964) 6, 1.

178. G.E. Coates and C. Parkin, J. Chem. Soc. (1963) 421.

179. A. Pidcock, Chem. Commun. (1968) 92.

180. R.G. Goodfellow, Chem. Commun. (1968) 114.

181. S.O. Grim and R.L. Keiter, Inorg. Chim. Acta, (1970) 4, 56.

182. R.G. Goodfellow, J.G. Evans, P.L. Goggin and D.A. Duddell, J. Chem. Soc. A (1968) 1604.

183. J. Chatt and R.G. Wilkins, J. Chem. Soc. (1951) 2537.

184. D.A. Redfield and J.H. Nelson, Inorg. Chem. (1973) 12, 15.

185. R.J. Goodfellow and B.F. Taylor, J. Chem. Soc., Dalton Trans. (1974) 1676.

186. W. Keim, F.H. Kowaldt, R. Goddard and C. Kruger, Angew. Chem. Int. Ed. Engl. (1978) 17, 466.

187. H.F. Klein and H.H. Karsh, Chem. Ber. (1973) 106, 1433.

188. H.C. Clark and A.B. Goel, J. Organomet. Chem. (1979) 178, C27.

189. H.D. Empsall, M. Green and F.G.A. Stone, J. Chem. Soc., Dalton Trans. (1972) 96.

190. R.T. Boeré and C.J. Willis, J. Fluorine Chem. (1982) 21, 18.

191. P.S. Pregosin and R.W. Kunz "^{31}P and ^{13}C NMR of Transition Metal Phosphine Complexes",

Springer-Verlag, Berlin (1979) pp. 54-55.

192. C.H. Lindsay, L.S. Brenner and A.L. Balch, Inorg. Chem. (1980) 19, 3503.

193. J. Chatt and L.M. Venanzi, J. Chem. Soc. (1957) 2351.

194. R.J. Goodfellow, P.L. Goggin and L.M. Venanzi, J. Chem. Soc. A (1967) 1897.

195. M. Okunaka, G. Matsubayashi and T. Tanaka, Bull. Chem. Soc. Japan (1977) 50, 907.

196. Z. Kanda, Y.Nakamura and S. Kawaguchi, Inorg. Chem. (1978) 17, 910.

197. H. Alper and J.K. Curnoe, J. Organomet. Chem. (1979) 168, 369.

198. M.M. Olmstead, R.R. Guimerans, J.P. Farr and A.L. Balch, Inorg. Chim. Acta (1983) 75, 199.

199. V. Gramlich and G. Consiglio, Helv. Chim. Acta (1979) 62, 1016.

200. T. Hayashi, M. Konishi, Y. Kobori, M. Kumada, T. Huguchi and K.Kirotsu, J. Am. Chem. Soc. (1984) 106, 158.

201. A. Schmidpeter, K. Blaack, H. Hess and H. Riffel, Angew. Chem. Int. Ed. Engl. (1980) 19, 650.

202. D.R. Powell and A. Jacobson, Cryst. Struct. Commun. (1980) 9, 1023.

203. J.J. Macdougall, J.H. Nelson, F. Mathey and J.J. Mayerle, Inorg. Chem. (1980) 19, 709.

204. J.A.A. Mokuolu, D.S. Payne and J.C. Speakman, J. Chem. Soc., Dalton Trans. (1973) 1443.

205. W.L. Steffen and G.J. Palenik, Inorg. Chem. (1976) 15, 2432.

206. L. Manojlovic-Muir, D. Millington, K.W. Muir, D.W.A. Sharp, W.E. Hill, J.V. Quagliano and L.M. Vallarino, Chem. Commun. (1974) 999.

207. N.W. Alcock, T.J.Kemp, F.L. Wimmer and O. Traverso, Inorg. Chim. Acta (1980) 44, L245.

208. N.J. Taylor and A.J. Carty, J. Chem. Soc., Dalton Trans. (1976) 799.

209. G.W. Bushnell, K.R. Dixon, D.T. Eadie and S.R. Stobart, Inorg. Chem. (1981) 20, 1545.

210. J. Chatt and L.M. Venanzi, J. Chem. Soc. (1955) 3858.

211. P.L. Goggin et al, J. Chem. Soc., Dalton Trans. (1974) 523.

212. W.A. Henderson and S.A. Buckler, J. Am. Chem. Soc. (1960) 82, 5794.

213. J.J. Macdougall, J.H. Nelson and F. Mathey, Inorg. Chem. (1981) 21, 2145.

214. B.E. Mann, C. Masters, B.L. Shaw, R.M. Slade and R.E. Stainbank, Inorg. Nucl. Chem. Letters (1971) 7, 881.

215. T.G. Appleton, H.C. Clark and L.E. Manzer, Coord. Chem. Rev. (1973) 10, 335.

216. A.J. Cheney, B.E. Mann, B.L. Shaw and R.M. Slade, J. Chem. Soc. A (1971) 3833.

217. J. Chatt, J. Chem. Soc. (1951) 652.

218. J. Chatt and L.M. Venanzi, J. Chem. Soc. (1955) 2787.

219. R.D.W. Kemmitt, D.I. Nicholls and R.D. Peacock, J.

Chem. Soc. A (1968) 2149.

220. M.A. Bennett, G.B. Robertson, P.O. Whimp and T.J. Yoshida, J. Am. Chem. Soc. (1973) 95, 3028.

221. M.A. Bennett and T. Yoshida, J. Am. Chem. Soc. (1978) 100, 1750.

222. Y. Yoshida, T. Okana and S. Otsuka, J. Chem. Soc., Dalton Trans. (1976) 993.

223. R.A. Michelin, M. Napote and R. Ros, J. Organomet. Chem. (1979) 175, 239.

224. F.G.A. Stone, Pure Appl. Chem. (1972) 30, 551.

225. P.J. Hayward and C.J. Nyman, J. Am. Chem. Soc. (1971) 93, 617.

226. S.O. Grim, R.L. Keiter and W. McFarlane, Inorg. Chem. (1967) 6, 1133.

227. N. Muller, P.C. Lauterbur and J. Goldenson, J. Am. Chem. Soc. (1956) 78, 3557.

228. G. Singh and G.S. Reddy, J. Org. Chem. (1979) 44, 1057.

229. F.A. Cotton and R.A. Schunn, J. Am. Chem. Soc. (1963) 85, 2394.

230. S.O. Grim, D.A. Wheatland, and W. McFarlane, J. Am. Chem. Soc. (1967) 89, 5573.

231. P.L. Goggin, R.J. Goodfellow, J.R. Knight, M.G. Norton and B.F. Taylor, J. Chem. Soc., Dalton Trans. (1973) 2220.

232. G. Mavel, Prog. NMR Spectr. (1966) 1, 251 and references therein.

233. S.L. Manatt, G.L. Juvinal and D.D. Elleman, J. Am. Chem. Soc. (1963) 85, 2664.

234. J. Apel, R. Bacher, J. Grobe and D. Le Van, Z. Anorg. Allg. Chem. (1979) 453, 39.

235. E. Vincent, L. Verdonck and G.P. van der Kelen, Spectrochim. Acta (1980) 36A, 699.

236. T.G. Appleton, M.A. Bennett and I.B. Tomkins, J. Chem. Soc., Dalton Trans. (1977) 261.

237. A. Pidcock, R.E. Richards and L.M. Venanzi, J. Chem. Soc. A (1966) 1707.

238. F.H. Allen and A. Pidcock, J. Chem. Soc. A (1968) 2700.

239. J.L. Ruddick and B.L. Shaw, J. Chem. Soc. A (1969) 2801.

240. T.G. Appleton, M.A. Bennett and I.B. Tomkins, J. Chem. Soc., Dalton Trans (1976) 439.

241. D.P. Arnold and M.A. Bennett, Inorg. Chem. (1984) 23, 2117.

242. T.G. Appleton and M.A. Bennett, Inorg. Chem. (1978) 17, 738.

243. O.M. Ivanova and A.D. Gellman, Zhur. Neorg. Khim. (1958) 3, 1334.

244. P.K. Monaghan and R.J. Puddephatt, Inorg. Chim. Acta (1958) 3, 1334.

245. P.K. Monaghan and R.J. Puddephatt, Organometallics (1984) 3, 444.

246. P.S. Pregosin and R.W. Kunz, ^{31}P and ^{13}C NMR of

Transition Metal Phosphine Complexes", Verlag-Springer, Berlin (1979) p. 20.

247. G.G. Mather, A. Pidcock and G.J.N. Rapsey, J. Chem. Soc., Dalton Trans. (1973) 2095.

248. F.R. Hartley "The Chemistry of Platinum and Palladium", .Wiley, New York (1973) pp 292-323 and references therein.

249. Ibid p. 339.

250. P. Haake and R.M. Pfeiffer, J. Am. Chem. Soc. (1970) 92, 4996.

251. A.R. Rossi and R. Hoffmann, Inorg. Chem. (1975) 14, 365.

252. J. Karle and H. Hauptman, Acta. Cryst. (1956) 9, 635.

253. J.A. Ibers and W.C. Hamilton, Acta Cryst. (1964) 17, 781.

254. A. Del. Pra and G. Zanotti, Inorg. Chim. Acta (1980) 39, 137.

255. G.G. Messmer and E.L. Amma, Inorg. Chem. (1966) 5, 1775.

256. F.C. March, R. Mason, K.M. Thomas and B.L. Shaw, Chem. Commun. (1975) 584.

257. P.B. Hitchcock, B. Jacobson and A. Pidcock, J. Organomet. Chem. (1977) 133, 273.

258. C.J.Cardin D.J. Cardin, M.F. Lappert, K.W.Muir, J. Chem. Soc., Dalton Trans. (1978) 46.

259. L. Manojlovic-Muir, K.W. Muir and T. Solomun, J. Organomet. Chem. (197) 142, 265.

260. G.B. Robertson and P.A. Tucker, Acta. Cryst. (1983) 39C, 858.

261. F. Cariati, R. Mason, G.B. Robertson and R. Ugo, Chem. Commun. (1967) 408.

262. A. Modinos and P. Woodward, J. Chem. Soc. Dalton Trans. (1975) 2134.

263. R.S. Nyholm, J. Chem. Soc. (1950) 843.

264. J. Chatt, J. Chem. Soc. (1950) 2301.

265. J.E. Huheey, "Inorganic Chemistry: Principles of Structure and Reactivity" 2nd Ed., Harper and Row: New York (1978) p. 847.

266. T. Koritsanszky and G. Menczel, Acta. Cryst. (1982) 38B, 1617.

267. G.A. Jeffrey and A. Robbins, Acta. Cryst. (1978) 34B, 3817.

268. G.A. Jeffrey and M.S. Shen, J. Chem. Phys. (1972) 57, 56.

269. W.P.J. Gaykema, J.A. Kanters and G. Roelofsen, Cryst. Struct. Commun. (1978) 7, 463.

270. G. Costa, E. Reisenhofer and L. Stefani, J. Inorg. Nucl. Chem. (1965) 27, 2581.

271. F.R. Hartley, S.G. Murray and C.A. McAuliffe, Inorg. Chem. (1979) 18, 1394.

272. E.G. Cox, H. Saenger and W. Wardlaw, J. Chem. Soc. (1934) 183.

273. J.D. Scott and R.J. Puddephatt, Organometallics (1983) 2, 1643.

274. H.C. Clark and L.E. Manzer, J. Organomet. Chem. (1973) 59, 411.

275. M.S. Kharasch, R.C. Seyler and F.R. Mayo, J. Am. Chem. Soc. (1938) 60, 882.

276. PROFILE is a U.W.O. program, written by D.H. Farrar (1978).

277. G. Ferguson, P.J. Roberts, E.C. Alyea and M. Kahn, Inorg. Chem. (1978) 17, 2965.

278. C.A. Tolman, Chem. Rev. (1977) 77, 313.

279. E. Vincent, L. Verdonck and G.P. Van Der Kelen, Inorg. Chim. Acta (1980) 36A, 699

280. J.E. Huheey, J. Phys. Chem. (1965) 69, 3284.